A STUDY OF CRACK INITIATION IN CORROSION-FATIGUE OF A.I.S.I. 316 STAINLESS STEEL BY DYNAMIC MEASUREMENT OF CORROSION CHARACTERISTICS AND CORROSION CURRENT TRANSIENTS.

by

J. W. MARTIN

Submitted for the degree of

Doctor of Philosophy

Brunel University

Metallurgy Department

April 1980

ACKNOWLEDGEMENTS

I would like to thank Mr. D.E.J. Talbot for advice and encouragement during the course of the work and Professor C.Bodsworth for the provision of laboratory facilities.

Special thanks are due to Mr. G.C. Ford of the Electronic Construction Facility at Brunel University, for assistance in the design and construction of the ancilliary electronic equipment.

I would also like to acknowledge the award of a studentship by the Science Research Council.

Finally, I would like to thank Mrs. D.I.L. Martin, for typing the thesis.

1. ABSTRACT

A technique has been developed and applied to monitor corrosion current transients, in phase with a cyclic stress applied in reverse bending at 24 Hz to AISI 316 stainless steel plate immersed in selected aqueous media. The amplitude and waveform of this fluctuating current component, together with the measurement of the corrosion characteristics during fatigue, yield information on the nature of the stress-environment interaction.

In conditions where the metal surface was passive, a mechanism is proposed, which involves the repeated transient depassivation of the surface at persistent slip bands, leaving ultimately to premature crack initiation. In conditions where the metal surface was active (transpassive) a mechanism is proposed, which involves the preferential dissolution at slip steps with resultant enhancement in plastic strain and premature crack initiation.

CONTENTS

2. CORROSION-FATIGUE - INTRODUCTION AND REVIEW

2.1 Introduction

The effect of environmental influences in reducing the fatigue lives of metals has been recognised for a long time. The first reference to such a phenomena was made during the First World War, when it was recognised that fatigue failure of steel minesweeper paravane cables was exacerbated by the presence of sea water. Haigh (1) published a paper in 1917 in which he reported the corrosion enhanced fatigue of brass in an aggressive ammonia environment. McAdam (2) first coined the term "corrosion-fatigue" in 1926 to describe this phenomena, defining it as the damage resulting from the simultaneous action of corrosion and cyclic stresses. It is only in the past decade, however, with the advances in technology in directions typified by offshore oil and gas installations, power generation and chemical plant that the full implication of corrosion fatigue in design has been appreciated. Corrosion-fatigue as a subject for intense scientific study is therefore of quite recent origin.

Even a casual review of published work reveals no shortage of mechanisms proposed to account for the observed effects. These include the following acting singly or in concert:-

(i) Stress intensification at local corrosion damage.

(ii) Reduction of surface energy by the absorption of species from the environment.

(iii) Mechanisms involving localised dissolution due to plastic deformation.

(iv) Mechanisms involving the rupture of protective surface films during fatigue.

(v) Hydrogen assisted cracking.

(vi) Wedging action by corrosion products.

(vii) The prevention of crack rewelding by environmental interactions.

The principle difficulty lies in validating these mechanisms and assigning relative significance to them for appropriate circumstances. This arises because the approaches hitherto adopted are not particularly suited to the task. One general line of approach has been to adapt standard fatigue tests to permit testing in selected environments e.g. to produce stress versus cycles-to-failure data. The other general approach has been to develop simulative tests yielding electrochemical information which is assumed to apply to normal corrosion-fatigue conditions.

The real need is for means to measure electrochemical parameters during the course of a standard fatigue test. The present work was conceived to exploit a test first utilised by Journeaux (3) with which he demonstrated that in principle it is possible to monitor the transient corrosion currents flowing when a sample is subjected to fatigue in an aqueous environment. At the outset it was apparent that the technique was inadequately developed to realise its full potential for reasons to be discussed later. Of necessity, therefore, the present work followed two parallel and complementary lines. The main objective of obtaining electrochemical information was pursued and the experience gained from this work was continuously applied to the development of the technique. This cross-fertilisation steadily improved the reliability and significance of the results obtained as the work progressed.

A rewarding feature of this dual approach is that the ultimate benefits of the work were not only a contribution toward the advancement of theory, but also an addition to the range of techniques generally applicable to the assessment of corrosion-fatigue properties.

By its very nature corrosion-fatigue is an inter-disciplinary study requiring expertise drawn from diverse fields. The following sections review briefly all aspects of corrosion-fatigue

and the relevant principles of the component disciplines into which it can be resolved. In this task those topics of particular relevance to the present work are, of course, discussed in detail, but certain other topics, notably the use of fracture mechanics, are also reviewed to give perspective to the present, rather specialised, approach in the general attack on the problem.

2.2 Methods of Fatigue and Corrosion-Fatigue testing and the presentation of results

2.2.1 Fatigue testing

Fatigue tests must take into account many variables, the most important being as follows:-

(1) The magnitude and form of the stress cycle. Stresses can be applied by axial, torsional or plane bend loading modes, or by a combination of two or more of these. The fatigue stress wave-form can also be varied, for example sinusoidal, square wave or saw tooth wave forms can be used as depicted in figure (2.1). Figure (2.2) shows in detail the other parameters of the stress cycle which can be varied such as mean stress and frequency.

(2) The shape and size of the test-piece.

(3) The metallurgical condition of the test-piece, i.e., its hardness, grain size, microstructure etc.

(4) The surface condition of the test-piece, i.e., whether it has been shot peened, whether it has a surface coating etc.

(5) The nature of the environment.

(6) The test temperature.

Fatigue test machines can be broadly grouped into five categories according to the basic type of straining or loading system used. These are:-

(i) Rotating-Bending - this was the original fatigue test developed by Wohler (4) and hence most of the early fatigue data was produced using this method. In this test the test-piece is rotated under a bending load so that each point on the surface is alternately stressed in tension or

compression as shown in figure (2.3). The stress amplitude is given by the elastic beam theory:-

$$Sa = \frac{M\,y}{I} \quad \text{.....(1)}$$

Where Sa is the stress amplitude

M is the bending moment at the test section

I is the moment of inertia at the test section

y is the distance from the neutral axis to the extreme fibre at test section

(ii) Plane Bending - In these tests the test-piece can be loaded as a cantilever, a centrally loaded beam or a four-point loaded beam as shown in figure (2.3). Again elastic beam theory is used to calculate the stress amplitude.

(iii) Axial loading - Here the whole test section of the test-piece is uniformly stressed in tension or compression or in each alternately, as shown in figure (2.3). The stress amplitude is given by the equation:-

$$Sa = \frac{\text{Load}}{\text{Cross Sectional Area of the test section}} \quad \text{.....(2)}$$

(iv) Torsional loading - The maximum stress in this case occurs in the test-piece surface because the test-piece is twisted alternately about the neutral axis as shown in figure (2.3). The stress amplitude is again given by elastic stress consideration. Hence

$$S_{shear} = \frac{T\,y}{J} \quad \text{.....(3)}$$

Where S_{shear} is the shear stress amplitude

T is the applied torque

y is the distance from the neutral axis

to extreme fibre at the test section

J is the polar moment of inertia at the test section.

(v). Combined Stressing - This can be any combination of the four loading methods previously described, for instance, applied combined torsional and bending loads as illustrated in figure (2.3).

In any of these five categories the test can be displacement, strain or load controlled and the load can be applied by mechanical, electromagnetic, hydraulic or pneumatic means. Detailed descriptions of some of these methods can be found in the books by Forrest (5), Weibull (6), and in the ASTM manual on fatigue testing (7).

All of these tests are general purpose methods of investigating fatigue in as much as a constant cyclic stress is applied to a test-piece and the time to failure measured. This information is usually presented graphically as a plot of the alternating stress amplitude (S) versus the logarithm of the number of cycles to failure (N); these are commonly known as S/N diagrams and a typical example is shown in figure (2.4)

Although S/N diagrams are useful in such basic studies as the effect of particular factors on fatigue, it takes no account of the fact that fatigue is a two stage process consisting of initiation and propagation (see section 2.7). Furthermore, in applying such data to predicting the fatigue lives of structures, S/N diagrams take little or no account of the fact that some structures contain flaws and that the crack propagation rate is the important parameter in these situations, although notched test-pieces have been used to study the effect of stress

concentration. In recent years these considerations have stimulated the development of methods used to measure crack propagation rates. Such methods depend on the measurement of a parameter which is proportional to crack length, as described in more detail in section 2.3.

2.2.2. Corrosion-fatigue testing

Corrosion-fatigue tests are usually based on the types of fatigue test described in the previous section, suitably modified to allow the required environment to be maintained around the test-piece. The variables involved in such tests are the same as those for fatigue tests and their effect on corrosion-fatigue is described in section 2.2.3.

There are many methods of maintaining an aqueous environment around the test-piece. The most important ones are:-

(i) Complete immersion of the test-piece in the solution, in this case the solution can be deaerated if required.

(ii) Directing a drip or flow on to the test-piece during the fatigue test.

(iii) Spraying the solution on to the test-piece during the fatigue test.

(iv) Applying a pad moistened with the solution to the test-piece.

(v) Keeping a wick saturated with solution near the test-piece so that a liquid film is maintained on the test-piece by capillary action.

2.2.3 Effect of variables on corrosion-fatigue testing

(1) The magnitude and form of the stress cycle

It is generally true to say that the fatigue life increases as the stress is decreased; for some materials

there is a critical stress below which failure will not occur and this is known as the fatigue limit. This phenomenon very rarely, if ever, occurs in aqueous media. Much work has been done on the effect of the mode of stressing on fatigue life, but this work is out of the scope of this brief review. Barsom (8) and more recently, Atkinson and Lindley (9) have studied the effect of wave form on crack propagation. Barsom concluded that:-

(i) air-fatigue crack growth rates are independent of wave form.

(ii) environmental effects in corrosion-fatigue occur only during the loading part of the cycle.

The second of these conclusions was confirmed by Atkinson and Lindley.

The effect of frequency is equally complex, being closely allied to the time-dependance of corrosion. Stephenson (10) reviewed the subject in 1958 and found that increasing the frequency generally produces a corresponding increase in the number of cycles to failure but reduces the time to failure. Endo and Miyao (11) studied the effect of frequency on carbon steel in tap water and in salt water and found that at low stress amplitudes the corrosion-fatigue life depended practically on time alone and was independent of frequency in the range 4.08 - 42.5 Hz. More work is needed on this aspect which has, up to now, been virtually ignored.

(2) Size and shape of the specimen

The results obtained in fatigue and particularly in corrosion-fatigue tests, are critically dependent on the size and shape of the test-pieces. It is, therefore,

difficult to correlate experimental results obtained for dissimilar test-pieces and virtually impossible to give reliable estimates for the fatigue lives of large structures using the results of standard laboratory tests.

(3) Metallurgical condition of the test-piece

Comparison of the longitudinal and transverse fatigue strengths of steels show considerable differences even if the tensile strength is the same in both directions. This is due to the shape of inclusions and the preferred orientation of grains induced by working. Apart from such directional effects, the endurance limit of steels can be fairly closely related to tensile strength, so any factor which increases tensile strength usually leads to a corresponding increase in the endurance limit In corrosion-fatigue, increases in corrosion resistance also tend to increase the endurance limit although the situation becomes complex if improvements of corrosion resistance are made at the expense of mechanical strength. The presence of inclusions in steels reduce fatigue strength to a degree dependent on the exact nature of the inclusion. This effect has been found to be more pronounced for higher strength steels by Atkinson (12) and Epremian and Mehl (13).

(4) Surface condition of the test-piece

Notches are sometimes introduced into fatigue test-pieces to study the effect of stress concentrations. This is a very wide and highly complex sphere of investigation and is out of the scope of this brief review. For further information, the ASTM manual on

fatigue testing (7) is a useful starting point. Summarising briefly, notches can influence the corrosion-fatigue strength of metals by virtue of two effects:-

(a) the effect of the fatigue notch factor of the material in question.

(b) the effect of the physico-chemical state of the material in the presence of the corrosive agent (e.g. whether the metal is electro-chemically active or passive)

With regard to the second factor, Spahn (14) has suggested that the effect of notches is more pronounced when the metal is electro-chemically passive and at low frequencies.

The surface conditions of test-pieces is also well known to be an important factor and hence great care must be taken in the preparation of fatigue test-pieces, to prevent any cold working or overheating of the surface. Spahn (15) has shown for AISI 304 stainless steel, that roll polishing can lead to an increase in corrosion-fatigue strength, due to the production of compressive residual stresses in the surface. Other treatments which induce compressive stresses in the surface also increase the corrosion-fatigue strength, but are effective only as long as these zones are not dissolved away by corrosion. Such compressive stresses can be induced in many ways, e.g. shot peening, nitriding, electroplating (15).

The effect of surface coatings is also very important in corrosion-fatigue. Some treatments which

can increase the corrosion resistance under normal static conditions, can give rise to destructive bimetallic corrosion effects in fatigue, and lower the corrosion-fatigue strength. For example, the microcracking of a chromium plated or anodised surface during fatigue leads to the exposure of small regions which are anodic to the rest of the surface so that rapid dissolution occurs at these areas leading to premature failure.

(5) The nature of the environment

This is obviously the dominant factor in corrosion-fatigue and will be comprehensively reviewed in section 2.9. Meanwhile it is sufficient here to remark that only in vacuum can fatigue be considered a purely mechanical phenomenon and all environments will affect the fatigue properties of the material to a greater or lesser degree.

(6) Test Temperature.

Temperature can affect corrosion-fatigue properties in two ways. Firstly, if the temperature is particularly high it can induce structural changes of the material and hence change the mechanical properties. Secondly it can enhance or reduce the chemical activity of the environment.

Gould (16) working on mild steel in water, found that in the temperature range 15 - 45° C, increasing temperature decreased the corrosion-fatigue life, whereas the air-fatigue life was unaffected. Cornet and Golan (17), however, working on steel in 2.5% Na Cl, in the temperature range 27-82° C, found an increase in corrosion-fatigue life with increasing temperature. They

attributed this to the differences in pitting attack, and differences in the ratio of anodic to cathodic areas.

2.3 Fracture mechanics and their application to corrosion-fatigue

2.3.1 Basic Theory

Before describing its application to corrosion fatigue it is worth considering the basic theory of fracture mechanics. The purpose is to define the conditions under which a crack will propagate in terms of the free energy change in the system. Inglis (18) was the first to consider the stress concentration around an elliptical through crack in a stressed body and he succeeded in calculating it and analysing the stress field around the crack. His main conclusions can be summarised as:

(i) the stress distribution near the crack tip is of the form shown schematically in figure (2.5)

(ii) The maximum tensile stress is given by:

$$(\sigma_{yy})_{max} = \sigma_{applied}\left(1 + 2\sqrt{\frac{c}{p}}\right) \quad \ldots\ldots\ldots(4)$$

where σ_{yy} is the tensile stress normal to the plane of the crack

2c is the crack length

p is the tip radius

Griffith (19, 20) developed these ideas in 1920, to explain the discrepancy between the predicted and actual strength of glass. He used the information to calculate the EXTRA strain energy which could be stored in a stressed plate containing a through crack of length 2c. It is unnecessary to give details of Griffith's treatment here but his final result is expressed in the equation:

$$\text{Extra Strain Energy} = \frac{\pi \sigma^2 c^2}{E} \quad \ldots\ldots\ldots\ldots(5)$$

where σ is the applied stress

E is Young's modulus of the material

The general statement of the energy balance is:

$$U\ (\text{Total Energy}) = \begin{matrix}\text{Strain Energy Stored} \\ \text{in uncracked plate}\end{matrix} + \text{extra strain energy} + \begin{matrix}\text{Surface Energy} \\ \text{of the crack}\end{matrix} \quad \ldots\ldots\ldots(6)$$

Applying this concept to a plate of area A and thickness t, this equation becomes:

$$U = \frac{\sigma^2}{2E} At + \frac{\pi \sigma^2 c^2 t}{E} + 4\gamma c t \quad \ldots\ldots\ldots(7)$$

where γ is the surface energy per unit length of crack.

Stress-strain curves under elastic loading of a cracked plate yield a lower value for the effective Young's modulus (E^1) than the true Young's modulus for the uncracked plate (E) as illustrated in figure (2.6). Thus the cracked plate is more compliant than the uncracked plate, defining compliancy as the reciprocal of the Young's modulus. The effective Young's modulus E^1 can be calculated from the stored strain energy, i.e.:

$$\text{Stored Strain Energy} = \frac{\sigma^2}{2E} At + \frac{\pi \sigma^2 c^2}{E} = \frac{\sigma^2}{2E^1} At \quad \ldots\ldots(8)$$

This yields:

$$E^1 = \frac{E\ At}{At + 2\pi c^2 t} \quad \ldots\ldots\ldots\ldots(9)$$

For the plane stress condition and a small extension of the crack dc, the work done in producing the extension is $\sigma d\epsilon\ At$ where ϵ is the applied strain which can be obtained from $E^1 = \sigma/\epsilon$, so that:

$$\text{Work Done} = \sigma \frac{\partial(\sigma/E^1)}{\partial c} dc\ At = \frac{4\pi c \sigma^2 t}{E} dc \quad \ldots\ldots(10)$$

This work goes to provide extra strain energy in the cracked plate and to create the new surfaces. Therefore:

$$\frac{4\pi c \sigma^2 t}{E} dc = \frac{2\pi \sigma^2 ct}{E} dc + 4\gamma t\, dc \quad \ldots\ldots(11)$$

Fracture will occur if:

$$\frac{2\pi \sigma^2 ct}{E} > 4\gamma t$$

The Griffith fracture stress (σ_f) is the boundary case for this relationship i.e.:

$$\sigma_f = \left(\frac{2E\gamma}{\pi c}\right)^{\frac{1}{2}} \quad \ldots\ldots\ldots\ldots(12)$$

A similar result can be obtained for the case of plane strain i.e.:

$$\sigma_f = \left(\frac{2 E \gamma}{\pi (1 - \nu)^2} a \right) \quad \text{.....(13)}$$

where ν is Poisson's ratio which is defined as the ratio of lateral contraction to longitudinal extension.

It is apparent from equation (12) that $\frac{2\pi\sigma^2}{E}$ increases with crack length (c) whereas 4γ does not. Hence as the crack propagates under either plane stress or plane strain conditions, more strain energy becomes available to extend the crack so that crack propagation can accelerate catastrophically. This is known as UNSTABLE FRACTURE.

The application of these criteria for fracture are limited by the assumptions made in their derivation, the most important being that the material is totally brittle so that only elastic strain energy is considered.

Hence the Griffith theory had to be extended to explain the fracture strength of materials for which ductility cannot be ignored, particularly steel. For such materials, account must be taken of the significant plastic deformation which occurs before and during fracture.

The fracture of ductile materials leads to the development of a plastic zone ahead of the crack tip as depicted below.

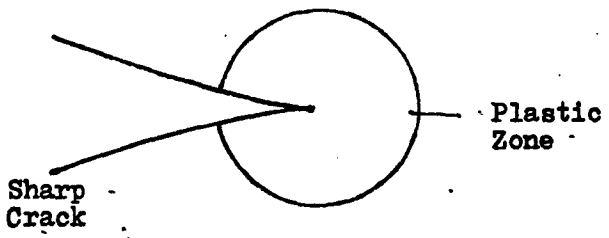

This increases the work required for crack propagation and also causes a change in the effective length of the crack. Thus the term γ in equations (12) and (13) must be replaced by the term G (21) which takes account of plastic work. Hence equation (12) becomes:

$$\sigma_f = \left(\frac{2EGc}{\pi c}\right)^{\frac{1}{2}} \qquad \text{.....(14)}$$

Where Gc is the critical value of G for fracture.

This equation has taken no account of the effective change in the crack length caused by the plastic zone. For a plastic zone of length r_y as measured from the crack tip it is found that the effective crack length is equivalent to $(c + r_y)$. Hence equation (14) becomes:

$$\sigma_f = \left(\frac{2EGc}{\pi (c + r_y)}\right)^{\frac{1}{2}} \qquad \text{.....(15)}$$

There are three ways that the crack might spread, illustrated in figure (2.7)

A suffix next to the quantity G indicates which of these modes of fracture it applies to. Hence G_I, G_{II}, and G_{III} are for type I, II and III cracking respectively.

This can be supplemented by the additional subscript c to show that the critical value of G which is being considered, e.g. G_{Ic} refers to the critical work rate for unstable fracture in the crack opening mode.

This quantity G can be used as a measure of a material's resistance to fracture, although great care must be taken in its use as its value depends critically on experimental testing conditions. This presents experimental difficulty in determining values for G. Hence a quantity more often used to quantify a material's resistance

to fracture, known more generally as the "Fracture Toughness" is the value K, the stress intensity factor, defined by the equation:

$$K = \sigma (\pi c)^{\frac{1}{2}} \quad \text{.....(16)}$$

The units of K are MN $m^{-3/2}$

The parameter K can also have the suffixes denoting the different mode of fracture i.e. K_I, K_{II} and K_{III} as depicted in figure (2.7). The solution to any particular problem can be considered as the sum of the separate solutions found by considering the three component fracture modes; this is not true of G values. A compendium of basic solutions is given by Paris and Sih (22) The suffix c once again denotes the critical value of K i.e. the value of K at the threshold of instability. This can be found from the equation:

$$K_c = \sigma_f (\pi c)^{\frac{1}{2}} \quad \text{.....(17)}$$

This concept is currently quite widely used because it is a factor which characterises the INTENSITY of the stress field ahead of the crack. For any crack length and any combination of applied forces, it is known that the local stress diminishes as the inverse of the square root of the distance, and K gives the precise magnitude of the stress by taking into account both the crack geometry and the net contribution of the applied forces.

It can be shown that the relationship between K and G for tensile loading (Mode I) is:

$$K^2 = GE \quad \text{for plane stress} \quad \text{.....(18)}$$

$$K^2 = \frac{GE}{(1-\nu^2)} \quad \text{for plane strain} \quad \text{.....(19)}$$

Some care must be taken when reading the literature on K - values, because American workers refer to K - values as $\pi^{\frac{1}{2}} \sigma c^{\frac{1}{2}}$ whereas some English workers omit the factor $\pi^{\frac{1}{2}}$. There seems to be no good reason for omitting the $\pi^{\frac{1}{2}}$ factor

and it should be included in calculating K - values if confusion is to be avoided.

The principal limitation of K - values is that insufficient allowance is made for the plastic zone present if the material is very ductile. This can be improved if use is made of equation (15). Equation (17) then becomes:

$$K_c = \sigma_f \left(\pi (c + r_y)\right)^{\frac{1}{2}} \quad \ldots\ldots\ldots\ldots\ldots\ldots (20)$$

It has been conventional to suppose, as a first approximation, that for plane stress:

$$r_y = \frac{K^2}{2\pi \sigma_y^2} \quad \ldots\ldots\ldots\ldots\ldots\ldots (21)$$

where σ_y is the yield stress of the material. Hence equation (20) becomes:

$$K_c = \sigma_f \left(\pi c \left(1 + \frac{\sigma_f^2}{2\sigma_y^2}\right)\right)^{\frac{1}{2}} \quad \ldots\ldots\ldots (22)$$

A more accurate value for K_c can be found if the Dugdale Solution (23) is used. Then:

$$K_c = \sigma_f \left(\pi c \left(1 + \frac{\sigma_f^2 \pi^2 c}{16\sigma_y^2}\right)\right)^{\frac{1}{2}} \quad \ldots\ldots (23)$$

The general approach for the plane stress condition is that equation (17) may be used if $(\sigma_f/\sigma_y) < 0.4$ and that equation (22) or better still equation (23) should be used if $(\sigma_f/\sigma_y) > 0.4$. The use of results for $(\sigma_f/\sigma_y) > 0.8$ should be treated with extreme caution.

2.3.2. The measurement of fracture toughness

(1) K - value tests

Essentially the determination of fracture toughness is based on application of the Griffith equation to the elastic-plastic case. Pre-cracks are introduced into suitable specimens which

are then loaded until they break and, if the fractures are macroscopically brittle, the fracture loads can be used to calculate the toughness or K_{Ic} value. Great care must be taken in the design of fracture toughness specimens, especially with regard to their thickness, because if they are too thin plastic deformation occurs, producing shear lips. The effect of plate thickness is illustrated in figure (2.8).

It is found in practice that to produce flat macroscopically brittle fractures, the required plate thickness (t) is given by:

$$t \geqslant 2.5 \left(\frac{K_{Ic}}{\sigma_y} \right)^2 \text{ inches} \quad \ldots\ldots\ldots\ldots (24)$$

For tough materials this result implies that very large specimens are needed. In attempting to use smaller specimens some investigators groove the face of the specimen at the point of cracking and the triaxiality produced helps to restrict the shear lips. Furthermore to reduce the loads required, which can be quite large for tough materials, bend or cantilever specimens have been used, although the stress system for these specimens is much more complex than for a simple axial loading system. It is not necessary to discuss fracture toughness testing in detail here, because it is well documented in B.S. 5447 (24), "Fracture Toughness Testing", in A.S.T.M. STP 381 (25) and the practical application of such information is discussed in some detail in reference 26.

Another difficulty in fracture toughness testing is to avoid stress relaxation in propagating cracks in specimens of finite size. Thus fracture toughness measurements are often restricted to the determination of the first sign of unstable

fracture which is then arrested by the inherent characteristics of the testing process and not by the material under investigation. This is known as the 'pop-in' measurement and is illustrated in figure (2.9).

(2) Crack opening displacements

The search for an approach capable of accommodating realistic amounts of plastic deformation has lead to the development of the Crack Opening Displacement (C.O.D.) method. This considers the plastic zone at the crack-tip when instability is just reached, and was developed independently by Cottrell (27) and Wells (28). It was found experimentally that just prior to fracture a crack tends to become 'square-fronted' as illustrated in figure (2.10). The parameter δ describing displacement normal to the direction of crack propagation can be measured using a clip or paddle gauge and it has been shown (29) that δ is related to G by the equation:

$$G = \delta \sigma_y \quad \ldots\ldots\ldots\ldots\ldots\ldots (25).$$

Hence if a value for δ_c can be found, an alternative method for calculating G_c and K_c is possible. The methods of practical measurement are described by Knott (29).

(3) The J-integral test

This is the most recently developed method for assessing the toughness of a cracked body which cannot be regarded as elastic. It relies on the determination of an energy term (J) which expresses the change in potential energy when a crack is extended by an amount dc and is analagous to the value G, but is developed for a non-linear elastic body (30).

It is possible to define (31) the line integral J on any curve Γ surrounding the notch tip starting from the lower surface and ending on the upper surface of the notch as shown in figure (2.11) using the equation:

$$J = \int_{\Gamma} \left(W dx_1 - T \frac{\partial u}{\partial x_2} ds \right) \ldots\ldots (26)$$

Where W is the strain energy density,

x_1 and x_2 define the two-dimensional stress field as shown in figure (2.11):

T is the traction vector on Γ

u is the displacement of the loading points

s is the arc length of Γ

The easiest method of evaluating J is from its definition as the rate of change of potential energy with crack length (32). This and other methods are described by Knott. (29)

It has been suggested (29) that a critical value of J, J_{Ic} represents a characteristic failure criterion in situations where fracture is preceded by substantial amounts of yielding ; this is quite a new method, however, and requires more work to establish it firmly.

To summarise, the K_{Ic} tests consider an essentially brittle fracture, and make plastic zone corrections, whereas C.O.D. and J_{Ic} tests attempt to characterise ductile fracture events. The C.O.D. focuses attention on the crack tip region whereas J_{Ic} relates to macroscopic work terms or to the crack tip conditions depending on the Γ contour chosen.

The primary application of such fracture mechanics is to aid in design and engineering by answering the following questions:

(1) What is the critical flaw size in a structure at the operational stress level.

(2) What maximum initial flaw size is likely to exist in the structure prior to service and will the operational stress levels cause these to grow to the critical size in the life of the structure.

The main disadvantages of such tests have been summarised by Boyd (33) as follows:

(1) They are essentially geometric in nature, taking little account of the actual physical behaviour of the metal i.e. its real response to loading in terms of plastic deformation, shear fracture and decohesive fracture.

(2) They are essentially two-dimensional in character, whereas the processes of breakdown and fracture must be three-dimensional.

(3) They are essentially static in character and take little or no account of the effect of different rates of application and duration of loading.

(4) They do not allow for changes in the character of the metal due to the interaction of strain and temperature.

(5) They assume that fracturing , or the extension of an existing crack is a simple continuous process, and hence take no account of its known discontinuous character.

2.3.3 Application of fracture mechanics to fatigue

Up to now we have been considering crack propagation under the action of statically applied loads. It is now appropriate to describe the application of fracture mechanics to cyclically applied loads, showing how linear elastic fracture mechanics and related small-scale crack-tip plasticity have provided the basis for describing the phenomenom of fatigue crack propagation (34).

In the experimental study of the rate of fatigue-crack propagation one of the most common tests is to use sheet specimens with a slit acting as a stress raiser to initiate and localise fatigue cracks. A typical test arrangement together with a schematic representation of how the results are presented are given in figure (2.12).

There are many different types of propagation test-piece used, these can be broadly grouped into four categories:-

(a) plane stress or plane strain test-pieces

(b) Tensile-test specimens

(c) Bend-test specimens

(d) Single-edge-notched (SEN) or
Wedge-opening-load (WOL) Specimens

Further details of these specimens are given by Knott (29).

The experimental techniques are mainly concerned with the control and measurement of ΔK, which is defined as the difference between the maximum and minimum stress intensities encountered during each cycle, and with the measurement of crack growth rate under controlled conditions. This crack growth rate is measured as the increment of crack growth per cycle, and is given the symbol da/dN where a is the linear crack extension and N is the number of cycles.

Several techniques for crack growth measurement have been employed, these include:-

(a) Optical methods

(b) D.C. potential drop methods

(c) Compliance measurements

(d) Clip gauge measurements

Further details of these methods are available in the literature, e.g. by Knott (29).

Paris and Erdogan (35) originally suggested that the quantities da/dN and ΔK, the cycle range of stress intensity, could be related by the simple equation:-

$$\frac{da}{dN} = C (\Delta K)^{m} \quad \text{.....(27)}$$

Where C and m are material constants. The more important parameter is m as it determines the stress range dependance of growth rate.

Many investigators have confirmed the validity of this law for growth rates in the range 10^{-8} to 10^{-6} m/cycle. If a plot is made of ΔK versus da/dN, however, it is typically of the form shown in figure (2.13). From this curve three regimes can be recognised:-

(i) Regime A. In this regime m (the slope of the curve) increases with decreasing ΔK and diminishing fatigue-crack growth rates are obtained leading to a threshold value of ΔK (ΔK_{TH}) below which crack propagation cannot be detected (36).

(ii) Regime B. This is the linear part of the curve for which the Paris-Erdogan (35) relationship in equation (27) applies, failure in this regime normally occurs

by a transgranular ductile striation mechanism (37,38). In this regime m is normally between 2 and 4 for most materials (39).

(iii) Regime C. In this regime K_{max} rapidly approaches the K_{IC} value and m will exceed 4 as instability is approached. Failure in this regime is by a mixed mode of striation growth and static fracture modes, such as cleavage, intergranular and fibrous fracture (40).

It is obvious from these observations that equation (27) will hold only in Regime B. In Regime A equation (27) will tend to over-estimate the propagation rate and in Regime C it will under-estimate the propagation rate; great care must thus be used in its application.

Many factors can affect the shape of these curves, these include the specimen geometry and size, the R-ratio, which is the ratio of minimum to maximum stress, K_{max}, environment etc. The effect of these variables in the case of corrosion-fatigue will be discussed in more detail in section 2.3.4.

2.3.4 The application of fracture mechanics to corrosion-fatigue

It is only in the past several years that a quantitative approach to corrosion-fatigue crack propagation has been made, using fracture mechanics, hence this approach has not yet been extensively developed. As has already been stated in 2.3.3 , fatigue crack growth can be described using fracture mechanical methods, as the rate of crack growth da/dN is governed by the cyclic range of stress intensity ΔK and this has led to the classic fatigue crack growth curve illustrated in figure (2.13). The simplest fracture mechanical approach to corrosion-fatigue is hence to find the effect of environments on the fatigue crack growth-rate curves. From such

curves Austen and Walker (41) have identified two distinctly different forms of corrosion-fatigue crack growth behaviour. Before considering these, however, it is worthwhile reviewing briefly the use of fracture mechanics in stress-corrosion crack growth. Here the crack growth rate, $^{da}/_{dt}$, is related to the stress intensity factor K as shown in figure (2.14). The important features of this curve are that there is a threshold stress intensity, K_{ISCC}, below which any crack formed will not propagate catastrophically, there is then a K-dependent region up to a stress intensity factor of Kp at which the crack growth rate reaches a plateau, finally there is a region in which the crack propagation rate increases until the stress intensity factor reaches the critical value K_{IC}.

Returning now to Austen and Walker's two forms of corrosion-fatigue crack growth. They defined these as:-

(a) True Corrosion-Fatigue (TCF) - This identifies the behaviour where fatigue crack growth rates are enhanced by the presence of an aggressive environment through a synergistic action of corrosion and cyclic loading, this is referred to as 'below K_{ISCC}' behaviour (42,43) and applies to materials where $K_{ISCC} > K_{IC}$.

(b) Stress Corrosion Fatigue (SCF) - This describes static load stress-corrosion under fatigue conditions and occurs where the stress intensity factor is above K_{ISCC} and hence is referred to as 'above K_{ISCC}' behaviour (42,43).

These two types of behaviour are illustrated schematically in Figure (2.15). Figure (2.15a) illustrates True Corrosion Fatigue. The slope of the straight line portion of the curve m is independent of the corresponding value found for non-interacting environments.

Stress Corrosion-Fatigue is illustrated in figure 2.15b. It is characterised by a deviation in the curve containing a plateau during which crack growth rate is invariant with the stress-intensity factor as observed for stress corrosion-crack growth. A third possible type of corrosion fatigue crack growth, and the most common, occurs for material/environment systems which exhibit SCF above K_{ISCC} and TCF at all K-values, as illustrated in figure 2.15c.

Fracture mechanics in corrosion-fatigue has not yet developed to the stage where accurate predictions of the fatigue lives of structures in service can be made, but its use has made a contribution to the assessment of corrosion-fatigue crack propagation mechanisms and will undoubtedly make a more positive contribution in the future.

2.4 Physical Metallurgy of Stainless Steels

This subject has recently been reviewed very well by Pickering (44) upon whose paper this brief review is largely based. Four basic types of stainless steel are produced as described in the following sections.

2.4.1 Martensitic Steels

These steels contain 12-17% Chromium, 0-4% Nickel 0.1 - 1.0% Carbon, and sometimes also Molybdenum, Vanadium, Niobium, Aluminium and Copper. They are austenitic between 950-1000° C but on cooling, transform to martensite. These steels are usually tempered for strength, ductility and toughness, and may be precipitation hardened. The main applications of these steels are in industrial plant (e.g. chemical plant), gas turbine engines, aircraft, tools etc.

2.4.2 Controlled Transformation Steels

These steels contain 14-17% Chromium, 0-7% Nickel with Molybdenum, Aluminium, Titanium, Copper etc. They are austenitic at the solution-treatment temperature. The M_s temperature can be altered, however, to promote the formation of metastable austenite or martensite at room temperature. Cold working can be performed on these steels in the metastable austenitic form, transformation to martensite requiring subsequent tempering. The main application is in the aerospace and aircraft industries for aircraft skins etc.

2.4.3. Ferritic Steels

These are steels of low carbon content containing 15-30% Chromium, together with Molybdenum, Niobium, Titanium as required. They have quite good formability, high corrosion resistance, exhibit little tendency to transformation and are relatively inexpensive compared with austenitic steels. Thus the

main applications are in conditions imposing less demands on the corrosion resistance of the material, e.g. kitchenware.

2.4.4 Austenitic Steels

These are steels of low carbon content containing 18-25% Chromium, 8-20% Nickel together with Molybdenum, Niobium, Titanium additions as required. They are predominantly austenitic at all temperatures although some residual delta ferrite may be present. These steels are very widely used for general corrosion resistant applications.

Since an austenitic steel was selected for study in the present work, it is worth considering the constitution of austenitic steels in some detail.

2.4.4.1 - Constitution of Austenitic Stainless Steels

The addition of Nickel to an 18% Chromium steel has two main effects. First it increases the amount of austenite at the solution-treatment temperature and second it decreases the M_s temperature, e.g. for 8% Ni with 0.1% C the M_s temperature is reduced to such a value that austenite is stable at room temperature. Figure(2.16)shows the effect of Nickel and Chromium content on the constitution of 0.1% C steels.

Other alloying elements either increase or decrease the tendency to form delta-ferrite at solution treatment temperatures, depending on whether they are austenite or ferrite forming elements. Figure(2.17)reproduces the well-known Schaeffler diagram which shows the effect of Nickel and Chromium equivalents on the constitution of stainless steels. The Chromium and Nickel equivalents are calculated using the equations:-

$$\text{Chromium equivalent} = (Cr) + 2(Si) + 1.5\,(Mo) + 5(V) + 5.5\,(Al) + 1.75\,(Nb) + 1.5\,(Ti) + 0.75\,(W) \quad \ldots\ldots\ldots\ldots\ldots\ldots (28)$$

$$\text{Nickel equivalent} = (Ni) + (Co) + 0.5\,(Mn) + 0.3\,(Cu) + 25(N) + 30\,(C) \quad \ldots\ldots\ldots\ldots (29)$$

where the brackets indicate the wt - % of the alloying addition. In steels containing undissolved carbonitrides of titanium or niobium, correction factors must be used. (44)

2.4.2.2. Structure - Property Relationships

The tensile strength and 0.2% proof stress have been related (47,48) to composition and microstructure, giving the relationship:-

$$0.2\%\ \text{proof stress}\ (MN\ m^{-2}) = 15.4 \left\{ 4.4 + 23(C) + 1.3\,(Si) + 0.24\,(Cr) + 0.94\,(Mo) + 1.2\,(V) + 0.29\,(W) + 2.6\,(Nb) + 1.7\,(Ti) + 0.82\,(Al) + 32\,(N) + 0.16\,(\delta\text{ - ferrite}) + 0.46 d^{-\frac{1}{2}} \right\} \quad \ldots\ldots\ldots (30)$$

$$\text{Tensile strength}\ (MN\ m^{-2}) = 15.4 \left\{ 29 + 35(C) + 55(N) + 2.4(Si) + 0.11\,(Ni) + 1.2\,(Mo) + 5.0\,(Nb) + 3.0\,(Ti) + 1.2\,(Al) + 0.4\,(\delta\text{-ferrite}) + 0.82\, t^{-\frac{1}{2}} \right\} \ldots\ldots (31)$$

Where (δ-ferrite) is the percentage of δ-ferrite:-

d is the mean linear intercept of the grain diameter (mm)

t is the twin spacing (mm)

and the brackets indicate the alloying addition in wt % .

The stacking fault energy controls the work-hardening rate. A low stacking fault energy leads to a high work-hardening rate and small twin spacing, or high twinning frequency, hence its importance in determining the Tensile strength but not the proof stress because the stacking fault energy has little effect at the low strains for which the proof stress is measured. The role of delta ferrite in increasing the proof stress and tensile strength is to give a dispersion-strengthening effect. Solid-solution strengthening effects are greatest for the interstitial solutes (Carbon and Nitrogen), followed by the ferrite forming substitutional solutes (W, Mo, V, Si) and least for the austenite-forming

substitutional solutes (Mn,Co) which have very little influence (49)

During ductile fracture the role of non-metallic inclusions is important. It has been found (50) that increasing the volume fraction of inclusions causes an exponential decrease in the total strain at fracture. Austenitic steels have lower total ductility than other steels. Pickering (44) ascribes this to the angular shape of the non-metallic inclusions which are geometrically favourable for strain concentration and rapid void formation, Ti(CN) and Nb(CN) particles behave in a similar way.

2.4.4.3 Embrittlement

If austenitic steels are heated in the temperature range 700-950°C, a brittle intermetallic compound known as the sigma phase can be formed. The tendency to sigma-phase formation becomes more severe with increasing chromium content. Molybdenum, titanium and silicon also increase this tendency. The precipitation of sigma-phase reduces ductility and toughness but in a fully austenitic structure it forms slowly. If delta-ferrite is present, however, it rapidly transforms to sigma-phase plus austenite because of the excess chromium in delta-ferrite; manganese is therefore often added to heat resisting steels to stop delta-ferrite formation.

The austenitic stainless steel selected for this research was to the specification AISI 316. This steel has 2-3% Molybdenum added to improve the corrosion resistance, together with an increase in Nickel content to 10-14% to counteract the ferrite-forming tendency of molybdenum. Typical properties for a standard AISI 316 stainless steel in the solution treated condition are 571 MN m^{-2} tensile strength, 247 MN m^{-2} 0.2% proof stress, 50% elongation.* These steels work harden rapidly in response to the low stacking fault energy. They are also non-magnetic.

* For an undisclosed gauge length (44).

2.5 Electrochemical Principles

2.5.1 Basic principles of electrochemistry and corrosion

The theoretical basis of corrosion is well-established and documented in standard text books (51) (52) (53) (54) so that a detailed description is not required here, but it is worth restating some of the essential principles as an aid in discussing the corrosion-fatigue mechanisms (section 2.9).

The corrosion of metals in aqueous media occurs by electrochemical processes and so the principles of electrochemistry apply. If an electrode is polarised to a potential more noble than its single electrode potential (E) it acts as an anode, producing electrons. On the other hand an electrode polarised to a less noble potential than its single electrode potential acts as a cathode and consumes electrons. Consider two different electrodes connected together (figure (2.18), such that a metal/metal-ion system (M/M^{z+}) is the more base electrode and the system X/X^- is the more noble (not necessarily metallic). The metal electrode (M/M^{z+}) (anodically) produces electrons and the system X/X^- (cathodically) consumes electrons. Hence there are two complementary reactions:-

$$M \rightleftharpoons M^{z+} + ze \quad \text{(anodic reaction)} \qquad \ldots\ldots\ldots(32)$$

$$X + e \rightleftharpoons X^- \quad \text{(cathodic reaction)} \qquad \ldots\ldots\ldots(33)$$

and the net reaction is:-

$$M + zX \rightleftharpoons M^{z+} + zX^- \qquad \ldots\ldots\ldots(34)$$

which is the spontaneous process forming the basis of electrochemical corrosion and consequent metal wastage. The reaction assumes a steady state in which the current produced by the metal dissolution process is equal to the current consumed by the cathodic process.

(a) Cathodic Processes

The two most common cathodic reactions complementing the anodic dissolution reaction in the corrosion of metals in aqueous media are:-

(i) The reduction of hydrogen ions:-

$$2H^+ + 2e \rightleftharpoons H_2\ (g) \quad \ldots\ldots\ldots(35)$$

and (ii) The reduction of oxygen:-

$$O_2 + 2H_2O + 4e \rightleftharpoons 4OH^- \quad \ldots\ldots\ldots(36)$$

(i) The reduction of Hydrogen ions

This reaction predominates in acidic media, the overall reaction (35) proceeds in two stages:-

$$H^+ + e \rightleftharpoons H\ (ads) \quad \ldots\ldots\ldots\ldots(37) \quad \text{(Stage 1)}$$

and either $$2H\ (ads) \rightleftharpoons H_2\ (g) \quad \ldots\ldots\ldots\ldots(38) \quad \text{(Stage 2a)}$$

or $$H^+ + H\ (ads) + e \rightleftharpoons H_2\ (g) \quad \ldots\ldots\ldots(39) \quad \text{(Stage 2b)}$$

in most cases stage (1) is found to be rate determining. For platinum and palladium, however, stage (2a) is thought to be the rate determining reaction when these metals are cathodically polarised to a sufficiently base potential.

It is worth considering in passing that the evolution of hydrogen from neutral and alkaline media which accompanies the dissolution of very strongly electropositive metal, occurs by the alternative reaction:-

$$2H_2O + 2e \rightleftharpoons H_2 + 2OH^- \quad \ldots\ldots\ldots\ldots(40)$$

This reaction is of course thermodynamically equivalent to reaction (35) with appropriate changes in standard state but is kinetically quite different and is not activated by the less electropositive metals.

The role of hydrogen in reduction is exemplified by iron corroding in sulphuric acid where the overall reaction:-

$$Fe + H_2SO_4 \rightleftharpoons FeSO_4 + H_2 \quad \ldots\ldots\ldots(41)$$

occurs by

$$Fe \rightleftharpoons Fe^{2+} + 2e \quad \ldots\ldots\ldots(42)$$

$$2e + 2H^+ \rightleftharpoons H_2 \quad \ldots\ldots\ldots(43)$$

(ii) Reduction of Oxygen

This reaction predominates in solutions where hydrogen ions are available only in limited supply, i.e. neutral or alkaline solutions and in films of condensed moisture hygroscopically adsorbed from the air.

The overall reaction (36) occurs as follows:-

Oxygen molecules diffuse to the metal surface where they are adsorbed.

The reaction can now proceed by:-

$$O + H_2O + 2e \rightleftharpoons 2OH^- \quad \text{.....(44)}$$

A more favourable path, however, is:-

$$O_2 \text{ (ads)} + H^+ + e \rightleftharpoons HO_2 \text{ (ads)} \quad \text{.....(45)}$$

$$HO_2 \text{ (ads)} + H^+ + e \rightleftharpoons H_2O_2 \text{ (ads)} \quad \text{.....(46)}$$

$$H_2O_2 \text{ (ads)} + 2e \rightleftharpoons 2OH^- \quad \text{.....(47)}$$

The rate determining reaction in this sequence is probably reaction (45).

In deaerated neutral solutions the oxygen reduction reaction is of course impossible and the hydrogen reaction, reaction (35), can occur only slowly as the hydrogen ion activity is small (10^{-7}).

In neutral solutions in equilibrium with atmospheric air, the single potential for the oxygen reduction reaction is more positive than that for hydrogen evolution (52).

i.e.

$$E_e \; O_2/OH^- = + 1.23 - 0.059 \; pH \quad \text{.....(48)}$$

$$E_e \; H^+/H^2 = 0.00 - 0.059 \; pH \quad \text{.....(49)}$$

$$E_e \; O_2/OH^- - E_{H^+/H^2} = + 1.23V \quad \text{.....(50)}$$

At the same pH

Thus the oxygen reduction reaction is more favourable thermodynamically. However, kinetically, the exchange current density

for oxygen is very low as the electrode kinetics are dependent on the electrical conducting properties of the oxide film present. Thus the exchange current density is comparatively high for the hydrogen evolution reaction so the predominating cathodic reaction will be dependant on pH.

This situation is exacerbated because the cathodic reactant for the hydrogen evolution reaction (H^+_{aq}) is readily available from solvent water molecules, whereas the solubility of oxygen in water is low (0.8g dm^{-3} at 25°C)(54),also the oxygen reduction reaction is dependant on replenishment of the surface contaminants by the diffusion of oxygen,which is several hundred times slower than that for hydrogen ions.

There are other less common but important cathodic reactions including:-

(iii) Nitric acid reduction

This is an autocatalytic reaction whereby:-

$$HNO_3 \longrightarrow NO_2 \quad \text{.....(51)}$$

(iv) Bacterial reduction of sulphates to sulphides

$$SO_4^{2-} + 8H^+ + 8e \overset{\text{Bacteria}}{\rightleftharpoons} 4H_2O + S^{2-} \text{.....(52)}$$

(b) <u>Anodic Reactions</u>

Besides the anodic reactions which cause metal dissolution, such as:-

$$Fe \rightleftharpoons Fe^{2+} + 2e \quad \text{.....(53)}$$

there are other possible anodic reactions producing a solid product on the metal surface. Examples are:-

$$2Fe + 3H_2O \rightleftharpoons Fe_2O_3 + 6H^+ + 6e \text{ .....(54)}$$

$$Fe + 2H_2O \rightleftharpoons Fe(OH)_2 + 2H^+ + 2e \text{ .....(55)}$$

$$3Fe + 4H_2O \rightleftharpoons Fe_3O_4 + 8H^+ + 6e \text{ .....(56)}$$

Under other circumstances dissolution may occur by the production of soluble anions. e.g. The following has been proposed (55):-

$$Fe + 4H_2O \rightleftharpoons FeO_4^{2-} + 8H^+ + 6e \text{ .....(57)}$$

(c) Electrode Potentials.

For a metal/solution electrode on open circuit the reaction causes either an excess or deficiency of electrons to build up in the metal. The electrode thus acquires a potential of such a value that the Gibbs free energy of the reaction is balanced by the electrical energy the ions require to traverse the adverse electric field (i.e. double layer). This is the equilibrium condition for which no net reaction occurs. The value of this potential is termed the "single potential" and is given by the Nernst equation derived from the Van't Hoff reaction isotherm:-

$$E = E^{\ominus} - (RT/zF) \ln Q \quad \ldots\ldots\ldots (58)$$

where $E^{\ominus}$ is the standard electrode potential of the reaction, i.e. the equilibrium potential for unit activity of the dissolved species ,
Q is the activity quotient for the interacting species.

R, T, z and F have their usual significance.

The equilibrium potential for a reaction cannot be measured on an absolute scale, but only with reference to a second arbitarily chosen electrode system to give a relative potential difference. The electrode system usually chosen is the "standard hydrogen electrode". This utilises the reaction:-

$$2H^{+}(aq) + 2e \rightleftharpoons H_2(g) \quad \ldots\ldots\ldots\ldots (59)$$

which is assigned the value zero for unit activity of hydrogen ions (e.g. as present in 1.2 molar HCl) at one atmosphere hydrogen pressure and 298K.

By international convention, an electrochemical reaction is written in the direction of reduction, i.e. with electrons appearing on the left hand side, and a positive value of electrode potential implies that the reaction proceeds spontaneously from left to right when coupled with a standard hydrogen electrode.

(d) Polarisation.

Corrosion occurs when a metal dissolution process is sustained by a complementary cathodic process, the net driving force being provided by the difference between the equilibrium potentials of the reactions for the existing conditions.

Corrosion rates are discussed in terms of the polarisation characteristics of the constituent electrode processes, i.e. the potential-current relationships.

Polarisation is the shift in potential from the equilibrium value when a net current flows across an electrode surface. The measured value of the polarisation, η, is known as the "overpotential" and its sign is dependent on the direction of the net current. For many electrode reactions the total polarisation is the sum of several contributions, the most important being activation, concentration and resistance polarisation.

Activation polarisation arises from the activation energies of the component steps of an electrode process. If it is assumed that there is a single rate-determining step and reverse currents can be neglected, which is a valid assumption for significant potential displacements, the activation polarisation characteristics can be expressed using the Tafel equation, a derivation of the Arrhenius relation expressed in electrical terms:-

$$\eta = a \pm b \log i \quad \text{.....(60)}$$

where i is the net current and

a and b are constants.

The $+^{ve}$ or $-^{ve}$ signs are used, depending on whether the overpotential (η) is anodic (+) or cathodic (-).

Concentration polarisation refers to departure from the linear Tafel plot of E against log i, due to an accumulation or depletion of the dissolved species at the electrode surface producing

a "diffusion layer" as reaction proceeds. The diffusion layer may reach a thickness of 100-500μm depending on concentration, agitation and temperature.

Resistance polarisation can contribute further to the total polarisation and is due to the potential drop across the ohmic resistance of the electrolyte path. In highly conductive solutions, this resistance is very small so that resistance polarisation is negligible.

2.5.2. Electrochemical methods of corrosion testing.

Electrochemical corrosion testing has the following three purposes:-

(a) The investigation of corrosion mechanisms, and possible preventive methods.

(b) The measurement of corrosion rate

(c) Provision of accelerated tests to evaluate material/media combinations.

Detailed description of the numerous methods available are not required for the present purpose. It is sufficient to indicate the general approach by briefly reviewing the more important methods.

(i) Electrode Potential Measurements

This is the simplest application of electrochemical measurement to corrosion testing. The variation of the corrosion potential is measured as a function of time against a standard reference electrode, e.g. standard hydrogen or calomel electrodes. In general, if the corrosion potential is found to approach more active values with time then corrosion is expected. Conversely an approach towards more noble values, indicates that corrosion is being stifled, either by the formation of a protective solid corrosion product, or by passivation. This kind of test cannot give

information on corrosion rates, but yields valuable information on the behaviour of test condition/material couples and the associated corrosion mechanisms. Such potential measurements can yield additional useful information, if used in conjunction with Pourbaix diagrams (55).

The interpretation of variations in corrosion potential give only a rough guide, particularly for galvanic or mixed metal couples, because differences in hydrogen potential can significantly influence the corrosion potential and reactions.

(ii) Cathodic Polarisation Curves

This method is applicable in situations where only one cathodic reaction is possible and where the process is under cathodic control by virtue of a large cathode to anode surface area ratio. The metal electrode is allowed to attain the rest potential and then cathodically polarised by small steps, either galvanostatically or potentiostatically. The corrosion rate can be evaluated from the potential-current relationship thus obtained by extrapolating the Tafel region (i.e. the straight part of the curve found at large negative potentials see figure (2.19)) of the cathodic curve back to the rest potential, applying the equation:-

$$Ec = -\beta \frac{\log i_c}{i_{o,H}} \qquad \text{.....(61)}$$

Where Ec is the corrosion potential

i_c is the corrosion current density

$i_{o,H}$ is the exchange current density for hydrogen evolution on the metal

β is the Tafel constant

The value of $i_{o,H}$ is found by extrapolating the curve back to the hydrogen potential as illustrated in figure (2.19).

This method is simple to use, but is subject to various inaccuracies.

(iii) The Polarisation Break Method

This method, devised by Schwerdtfeger and McDorman (56) is a much more accurate method for measuring the corrosion rate (i_c). It is based on the observation that anodic and cathodic polarisation curves exhibit well-defined changes in slope at critical current densities. In applying the method to a corroding system, both anodic and cathodic polarisation characteristics are determined and plotted as illustrated in figure (2.20). The currents at which the changes in slope occur are determined graphically. If the values obtained are i_p for the cathodic curve and i_q for the anodic curve, the corrosion current can be calculated using the equation:-

$$i_c = \frac{i_p \times i_q}{i_p + i_q} \qquad \text{.....(62)}$$

as derived by Pearson (57). If i_p is much greater than i_q the reaction is anodically controlled and the value of i_c is approximately the same as that of i_q and vice versa. The disadvantages of this method are difficulty in accurately assessing the currents i_p and i_q and unsuitability for use with aggressive media, (e.g. acids) which give inaccurate results.

(iv) The Linear polarisation method

This method is based on the fact that within 10-20 mV of the corrosion potential the applied current density varies linearly with the electrode potential or overvoltage. The corrosion current can be calculated using the Stern-Geary equation (58):-

$$i_c = \frac{\beta a \, \beta c}{2.3 \, (\beta a + \beta c)} \times \frac{\Delta i}{\Delta E} \qquad \text{.....(63)}$$

where βa is the anodic Tafel slope

βc is the cathodic Tafel slope

$\Delta i/\Delta E$ is the reciprocal slope of the potential versus current line (admittance).

Stearn and Weisart (59) have found for a large majority of metal/electrolyte systems that βa varies between 0.06 V/decade and 0.12V/decade and βc is greater than 0.06V/decade. Within these limits corrosion rates can be estimated to within a factor of two when only approximate values for the Tafel slopes βa and βc and for $\Delta i/\Delta E$ are available.

In using this method the corroding electrode may be polarised either potentiostatically or galvanostatically provided that the potential does not differ by more than 10mV from the corrosion potential.

This technique has certain advantages in that it is a very fast method and is capable of measuring very low corrosion rates easily.

In one method employing this principle, the current i_q is measured between two pieces of the same metal (measuring element) when held at potentials differing by 10mV. The polarity is then reversed and the current i_b measured. The mean of these two currents is calculated and converted into a corrosion rate using calibration curves.

This technique is particularly useful in studying the application of inhibitors and localised corrosion.

(v) Galvanostatic Method

This method employs a controlled current source arranged to polarise test samples in a suitable cell as shown in figure (2.21).

The current is increased either in steps or continuously (Galvanokinetic method) and the potential acquired by the sample is measured. This technique can be used to determine both anodic and cathodic polarisation characteristics. The results yield plots

of the form illustrated schematically in Figure (2.22).

When the overpotential exceeds about 50mV, the Tafel equation applies, provided that the current density is not too high, so that there is a linear relation between the overpotential and the logarithm of the current density:-

$$\eta = \pm \beta \ln (i/i_o) \quad \text{.....(64)}$$

where η is the overpotential

β is the gradient of the line (Tafel constant)

i is the applied current density

i_o is the exchange current density at the reversible potential

Deviation from Tafel behaviour can occur at high current densities, due to the onset of concentration and resistance polarisation.

The corrosion current at the rest potential can be assessed by extrapolating the Tafel line back to the rest potential E_c, but this has two main disadvantages. Firstly data to plot a curve takes a long time to accumulate and secondly the high polarisations used can disturb the system, distorting the measurements.

(vi) Potentiostatic Method

This method has largely superceded the galvanostatic method and is a very valuable technique for electrochemical corrosion studies. It is designed to determine a complete corrosion rate profile for any metal/electrolyte system, whether or not it exhibits anodic passivation.

The potentiostat is an electronic device incorporating an operational amplifier with high-impedance inverting and non-inverting input modes, followed by a power amplifier with a low-impedance input. This arrangement allows the potentiostat to control the potential of an electrode at a pre-selected value with respect to a reference electrode. The input signal to the potentiostat is developed from the potential difference between the working electrode and the reference electrode. The preselected potential (E_c) is applied to the non-inverting (+) input of the operational amplifier (OPA) as in figure (2.23) and is then compared with the existing potential (E_e) of the inverting input (-). If these two values differ, an output current (i_a) is supplied by the power amplifier (PA) between the working electrode and an auxiliary counter electrode until the potential of the working electrode is restored to the required value. As the output current required is equal to the net current sustaining processes occurring at the working electrode, a plot of the current-potential (i-E) relationship for the electrode constitutes the polarisation characteristics.

Potentiostatic polarisation can be performed using the potentiostat in one of three ways:

(a) the electrode can be held at a single potential and the current can be measured as a function of time.

(b) the potential can be stepped, i.e. raised by equal increments at regular time intervals and the resultant

current measured just prior to each step (potentiostatic method),

(c) the potential can be continuously varied and the current measured (potentiokinetic method).

The results obtained from the second two methods are of the form illustrated in figure(2.24),(i.e. they reveal the true polarisation characteristics of the system). Thus these methods can give information for a passive region which is not obtainable using the galvanostatic method.

Anodic polarisation curves obtained using potentiostat can therefore characterise the electrochemical corrosion properties of metal/electrolyte systems very precisely. Comparison of the values of the critical current densities for passivating systems or corrosion currents flowing at any particular potential for non-passivating systems provide a basis for rapidly assessing the susceptibility to corrosion. The effects of changes in environmental and material conditions can also be evaluated.

2.5.3 Passivation of Stainless Steels

Stainless steels owe their corrosion resistance to the development of a passive surface condition in appropriate conditions of service. This feature must, of course, be combined with suitable properties in other respects. The potential range over which the passive condition may be expected is indicated by the anodic polarisation characteristics of the material. Figure (2.25) illustrates the essential features of a typical anodic polarisation curve for an 18% Cr - 8% Ni steel tested in 0.5M sulphuric acid (60).

Two passive ranges are evident but only the lower range confers corrosion resistance of practical significance.

The desirable features of an anodic polarisation curve for a stainless steel are:

(i) The critical current density for passivation ($i_{critical}$) should be low.

(ii) The current density in the passive range ($i_{passive}$) should be low.

(iii) The passivation potential (E_F) and the transpassive breakdown potential (E_B) should be widely separated.

(iv) The rest potential should not be markedly more negative than the hydrogen evolution potential, so that corrosion damage is limited if the steel is exposed to an environment producing the active state.

(a) Influence of alloy components on Anodic Polarisation Chromium is the essential element in a stainless steel producing a low passivation potential. Binary iron-chromium alloys can be passivated like pure chromium. The effect of chromium content on the passivation potential and critical density is shown in figures (2.26)[283] and (2.27)[283]. Figure (2.26) shows that as the chromium content rises above 12% there is a marked shift in the passivation potential to more negative values and the minimum value to which it can be reduced lies near that found for pure chromium. Figure (2.27) shows that the critical current

density also markedly decreases with increasing chromium content.

The effect of adding nickel to binary iron-chromium alloys is to decrease the critical current density without affecting the passivation potential (61,62).

Molybdenum markedly decreases the critical current density and raises the rest potential to more positive values as illustrated in figures (2.28) and (2.29) taken from Rochel's work (63). The influence of molybdenum on the polarisation characteristics is therefore greater in the active than in the passive range.

In a neutral medium, the active range is entirely absent so that the influence of alloying elements is less evident (except for solutions containing halide ions as discussed in a later section).

(b) Nature of Passivating Films

The passive state on stainless steel surfaces is undoubtedly due to the presence of films but their precise physical nature has not yet been established.

From anodic polarisation studies Olivier (64) deduced that a film about 2 nm thick can be present on iron-chromium alloys passivated in sulphuric acid. In contrast, King and Uhlig (65) and Kolotyrkin (66) considered that an adsorbed oxygen monolayer is sufficient to passivate the metal surface. These apparently opposing views are not necessarily irreconcileable. Aronwitz and Hackerman (67) suggested the initial formation of an oxygen monolayer which is subsequently penetrated by cations to form an overlying amorphous oxide layer. Frankenthal (68) concluded from his studies of the effect of applied potential on passivation that the thickness, composition and electrochemical properties of passivating films are all potential-dependent, so that

whereas a monolayer is formed at the passivating potential, thicker films are formed irreversibly at higher potentials, increasing the degree of passivity. From extensive observations on the structure of passive films formed on 18% Cr - 8% Ni steels, Okamoto[69] proposed a model, illustrated schematically in Figure(2.30)in which a passive film is considered to exist as a gel-like hydrated oxide layer.

Alloying elements which improve the corrosion resistance of stainless steels are naturally expected to influence the composition and structure of the passivating films. Limited evidence is available for the effects of chromium and molybdenum but little is known of the effect of nickel.

The role of chromium is of greatest interest because it is the element primarily responsible for low passivation potentials. Using an electron diffraction technique, McBee and Kruger[70] identified a spinel structure in passivating films formed on iron-chromium alloys of low chromium content but found amorphous films if the chromium content were increased. Holliday and Frankenthal[71] observed that the ratio of the chromium content of passivating films to that in the underlying metal increased abruptly as the chromium content increased beyond 12%. Okada et al [72], using Auger analysis, observed that the Chromium concentration in passivating films could be increased by increasing the anodic overpotential, increasing the time allowed for development of the film and increasing the chromium content of the steel. Yahalom and Ives [73], using electron-microscopical methods also found that the chromium content of the films increases with the chromium content of the alloy and that chromium is the predominating component of the oxide.

Molybdenum is also of particular interest because of its use as an alloying element to increase the resistance of steels to attack due to local breakdown of passivity as in pitting and crevice corrosion. Some segregation of this element to passivating films might therefore be expected and Yahalom and Ives' work [73] appears to support this view, but their results do not agree with those of other investigators. Lumsden and Staehle[74], using Auger analysis, found that films formed on austenitic steels were in fact depleted in molybdenum relative to the underlying metal, so that they discounted arguments attributing to the beneficial effect of molybdenum to modified film compositions. Okada et al. [72] provided evidence to show that the molybdenum content of passivating films is increased if chloride ions are present in the environment. With this information they proposed a mechanism, illustrated in Figure (2.31) to account for the increased resistance to depassivation which molybdenum confers. It assumes that dissolution of molybdenum from the metal provides MoO_4^{2-} ions which adsorb on active sites resulting from local breakdown of passivity, where they assist repassivation.

The effect of nickel on passivating films has received little attention. Yahalom and Ives[73] could not detect nickel in films formed on austenitic stainless steels and hence attributed improved corrosion resistance to the FCC structure of the substrate. Shimodaira [75] suggested that although nickel does not itself enter the film it could still influence the film composition indirectly by excluding iron, thereby enriching it in chromium.

There is obvious scope for further direct study of the nature of passivating films. They are clearly different from those formed on pure iron and a reasonable provisional assumption is that they are essentially complex non-stoichiometric oxides[76]. Some

further insight into the nature of the films is given by observations concerning the breakdown of passivity induced by halide ions, as discussed later in Section 2.6.

2.5.4 Corrosion of Stainless Steels

Corrosion failure of stainless steels is associated with complete loss or partial breakdown of the passive surface condition. Several characteristic forms of attack are recognised according to the circumstances in which loss of passivity occurs.

(i) Uniform Attack

Uniform attack implies that the steel is exposed to an environment in which it is wholly outside its passive range, a condition seldom experienced in service. Uniform attack is, however, induced in pickling as a surface treatment during manufacture. De-aerated sulphuric and hydrochloric acids may be used to ensure that the steel is at a potential in the active range or alternatively hydrofluoric/nitric acid mixtures or aqua regia may be used to promote transpassive attack. The non-oxidising acids produce blackish deposits on the surface which must be dissolved subsequently in nitric acid. General corrosion of this kind is expressed as rate of mass loss from unit surface, using the unit mg dm^{-2} day^{-2} (mdd).

(ii) Bimetallic Corrosion

Two dissimilar metals in electrical contact can constitute a galvanic cell, promoting corrosion of the less noble metal. Table 1 gives the table drawn up by LaQue and Cox (77) on the basis of a practical EMF series for artificial seawater.

1. Magnesium alloys
2. Zinc
3. Aluminium (99%)
4. Iron and Steel
5. 18% Cr/8% Ni Steel (active)
6. Lead
7. Nickel (active)
8. Brass
9. Bronze
10. Nickel (passive)
11. 18% Cr/8% Ni Steel (passive)
12. Silver
13. Graphite
14. Gold
15. Platinum

TABLE 1

EMF Series of various metals and alloys in seawater arranged in order of increasing potential (LaQue and Cox (77)).

In view of the relative nobility of 18% Cr/8% Ni stainless steel, it is normally the more noble metal in a galvanic couple and can stimulate attack on other metals including stainless steels of lower chromium content.

(iii) Differential Aeration and Crevice Corrosion.

Stainless steels are particularly susceptible to attack by differential aeration because inadequately aerated areas can become active anodic dissolution sites through loss of passivity. Rapid attack occurs by local action cells formed between the active sites and the remaining passive surface.

The attack is particularly intense when the depassivation is the result of oxygen starvation in crevices because the ratio of cathodic to anodic area is very large. Molybdenum additions to stainless steels are found to reduce the effect of crevice corrosion[78].

(iv) Intergranular Corrosion.

Intergranular corrosion refers to selective attack at the grain boundaries due to grain boundary networks of chromium carbides precipitated as a result of unfavourable heat-treatments. There is some controversy over the mechanism of the selective attack and the following three theories have been postulated:

(a) The stress theory[79]. This theory attributes the selective attack to the internal stresses caused by carbide separation.

(b) The local cell theory[80]. This theory assumes that the chromium carbides act as cathodes and promote dissolution of the matrix.

(c) The chromium depletion theory[80]. This theory has received most recognition because it can explain the dependence of intergranular corrosion on both the heat-treatment and on the potential of the metal. The basis of the theory is that selective attack occurs in a thin continuous zone of the matrix depleted in chromium by the precipitation of chromium carbides at the grain boundaries. Direct evidence of chromium depletion has been found using electron-probe microanalyser techniques[81,82] showing that the chromium content in the depleted zone can fall from an initial value of 18% to values as low as 5-15%.

Chromium carbides in austenitic stainless steels are dissolved if the steel is heated to temperatures above 1000°C. Rapid cooling (e.g. by water-quenching) suppresses reprecipitation of the carbides so that the steel is not then sensitised, i.e. susceptible to intergranular corrosion.

(v) Pitting Corrosion.

Pitting corrosion occurs when stainless steels are exposed to aqueous environments containing unsolvated halide ions, notably chloride and bromide ions and occasionally also chlorate ions (ClO_4^-). Fluoride ions, which are solvated, do not induce pitting. The effect observed is intense local attack at numerous small, isolated areas of the metal forming the pits, i.e. small deep craters or depressions. In thin sections failure is by perforation. The local breakdown of passivity which precedes pitting is concerned with effects which are especially relevant to the present research and is discussed in detail in Section 2.6 following.

2.6 Local Passivity Breakdown on Stainless Steels

In evaluating possible corrosion fatigue mechanisms for stainless steels, one essential task is to examine the circumstances in which local breakdown of passivity may be expected as a contributing cause of crack initiation and propagation. Two factors of particular relevance are the depassivating effect of halide (usually chloride) ions if present in the environment and the mechanical rupture of films on metal strained after passivation.

Extensive information on the influence of chloride ions is available from research concerned primarily with pitting corrosion. The mechanical rupture of passive films has been considered in detail with special reference to its application in stress-corrosion cracking.

This work and its implications is discussed in the following sections.

2.6.1 Experimental Study of Passivity Breakdown Preceding Pitting

The experimental study of pitting corrosion in stainless steels is based primarily on the observation first reported in 1937 by Brennert[83], that for any particular system of steel and halide medium there exists a critical potential which must be exceeded to induce pitting. The usual practice is to assess the initiation and growth of pits from changes in the current flowing when pits are synthesised in steel samples held at controlled, externally applied potentials. Two common variants of the technique are employed, held potential tests and the determination of critical potentials from anodic polarisation characteristics:

(a) Held Potential Tests.

Held potential tests yield values of current as functions of time for constant applied potentials. Figure(2.32)illustrates schematically the nature of the results obtained from such tests, showing the marked increase in anodic current associated with the

onset of pitting if the applied potential, E, is more positive than the critical potential, E_c . Such results indicate that pitting is a multistage process, usually considered to occur through the stages, induction, nucleation and growth. The induction period, τ , first observed by Hoar[84] is easily identified from results of the form illustrated in Figure (2.32). Its value decreases with increasing anodic polarisation [84,85,86,87], with increasing temperature[84] and with increasing activity of the aggressive anion [84,86,87,88]. For chlorides the activity-dependence yields the empirical quantitative relation:

$$\log (\tau/\text{sec}) = A + B \log (C_{Cl}/ C^{\bullet}_{Cl}) \quad \ldots \quad (65)$$

where: τ is the induction period

C_{Cl} is the chloride ion concentration

$C^{\bullet}_{Cl}$ is a standard value of chloride ion concentration

A and B are constants with B negative.

At the end of the induction period the nucleation and pit growth stages are manifest by a sharply increasing current and the appearance of visible pitting.

(b) Determination of Critical Potentials.

The values of critical potentials are obtained from the anodic polarisation characteristics of stainless steel samples tested in pitting media, usually by the potentiostatic method in which the applied potential is increased (or decreased) in small steps at regular time intervals. The results obtained are illustrated schematically in Figure 2.33 in which a critical potential is evident. The experimental determination of a critical potential yields one or other of two different values depending on the direction in which the potential is scanned [89,90]. The higher value is that corresponding with the marked increase in current

during anodic scanning and is called "the potential of pit nucleation, E_{np}". The lower value corresponds with the re-establishment of the passive current during subsequent cathodic scanning and is called "the critical potential of pitting, E_{cp}". The significance of E_{np} and E_{cp} in relation to an applied potential, E, is:

$E > E_{np}$ ... ... pits nucleate

$E_{cp} < E < E_{np}$ ... existing pits propagate but no new pits nucleate.

$E < E_{cp}$ ... ... the metal remains passive.

For practical purposes the value usually measured is E_{np} because it is the most convenient to measure and has the most significance. The results have comparative value only if the experimental procedures are standardised. For example, hysteresis using anodic scanning leads to values for E_{np} more positive than the true values and the error is acceptable only if made small and reproducible by using a slow, standardised scanning rate. With this proviso, the potentiostatic method is considered to be one of the most reliable methods for assessing pitting potentials [87,89,91]. Pitting potentials depend both on the metal composition and on the nature of the environment. They become more positive as the nickel and chromium contents of the steel increase [92] and more negative as the concentration of aggressive ions in the environment increases [87,89] or the temperature rises [87,93]. Leckie and Uhlig [94] found that the pitting potential is a linear function of the logarithm of the relative chloride ion concentration. The variation of pitting potential with temperature is linear. Kolotyrkin [92] has suggested that pitting will not occur below a critical value of the chloride ion concentration but this view is not generally accepted [87].

2.6.2 Theoretical Models of Passivity Breakdown in Pitting

Models proposed to explain the breakdown of passivity preceding pitting must account for the following features:

1. The existence of a critical potential
2. The role of the aggresive ion
3. The induction period before passivity breakdown and active pit growth.
4. The highly localised nature of passivity breakdown.

Three kinds of theoretical model have been proposed for passivity breakdown on homogeneous metal surfaces, i.e. surfaces free from non-metallic inclusions etc.[95] as follows:

(a) Adsorbed Ion Displacement Models.

Two such models have been proposed. The first is due to Kolotyrkin[96] and Uhlig[94,97,98] and supported by Rosenfeld[99] and Wilde[100]. It assumes that the passive film is an adsorbed monolayer of oxygen ions which can be displaced by the damaging ions, e.g. chloride ions, thereby partially breaking down the passivity. This model has several attractive features. The ions inducing pitting are assumed to adsorb more strongly than oxygen but to lose their ability to passivate the surface at a lower potential, i.e. at the critical potential for pitting. Ions which inhibit pitting, e.g. Nitrate[101] and hydroxyl[102] ions are assumed to exert their effect by competing with the pitting ions for the available sites. The localised nature of pitting is explained by preferential adsorption of the pitting ions at surface hetrogenieties, e.g. defect sites. The induction period is more difficult to explain; although its dependance on pitting ion concentration follows from the basic assumption, the relation between film thickness and induction period[103] cannot be explained using a model assuming a passivating monolayer.

The second model was proposed by Hoar and Jacob [34]. They suggested that three or four halide ions adsorb as a cluster on the passive layer around a lattice cation. This transitional complex requires a high activation energy for formation and hence the probability of formation is small. Once formed, however, the halide ion clusters can readily remove the cation from the lattice, thinning the film at this site. Another cation migrates through the film to replace the dissolved cation where in its turn it meets more halide ions, forms a complex with them and enters solution. Subsequently the process is repeated and accelerated because of the increasing electrostatic field. Hence once localised breakdown starts, the process proceeds very rapidly. As for the first model, the critical potential can be identified as the potential required for anion adsorption. The model explains the role of the aggresive anion, the localised nature of passivity breakdown and the existence of an induction period. Since it is assumed that the rate-determining step is the formation of the transitional complex, the induction period must depend on the anion concentration, the temperature and the applied potential, as is in fact observed.

The model cannot, however, explain Kruger's observation, that chloride ions are incorporated into the passive layer [104].

(b) Ion Migration or Penetration Models.

In these models, it is assumed that the aggressive anions penetrate the passive film and that breakdown occurs when the anions reach the metal film interface. There are several such models which differ mainly with respect to the proposed mode of penetration. For example, in one of the models it is suggested that the damaging ions migrate through the lattice via defects, or by an ion exchange process. Hoar [105] suggested that anions can enter without exchange and produce

"contaminated" passive films which act as sites of high conductivity inducing high cation currents and hence pitting. Kruger[103] has suggested an ion exchange of O^{2-} or OH^- ions with the damaging ion, as represented by the following equations:

$$Cl^-_{(soln)} + \square_{O^{2-}} + 2OH^-_{(lattice)} \rightleftharpoons Cl^-_{(lattice)} + 2\square_{OH^-} + 2OH^-_{(soln)} \quad \ldots (66)$$

In such a process anion vacancies are also produced which can enhance the migration of the damaging anions to the metal/film interface. In such models the critical potential can be explained as the potential required for adsorption, the induction time as the time required for the migration of damaging anions to the metal/film surface, and the localised nature of attack as migration via discreet defects.

In an alternative approach, it is assumed that the passive film contains defects such as pores which allow the aggressive ions to permeate the film and promote localised corrosion. This theory was originally suggested by Evans [106] but it lost favour because it could not be used to explain the existence of the induction period. Richardson and Wood [107] have recently revived the idea and amended it to account for the induction period. Thus although the theory predicts that pits are initiated at the instant the damaging anions reach the metal surface, the local corrosion currents at the onset of pitting are very small and become significant only as the pits grow.

(c) Chemico - Mechanical Models

These are the most recently developed models. The first is due to Hoar [108] and assumes that adsorption of the aggressive anions progressively lowers the surface free energy of the film/solution interface until the film is "peptized", leading to rupture and hence local corrosion.

Sato [109] proposed a model on similar lines but assuming that film rupture is caused by electrostriction pressures. Using this argument he considered that the critical potential for pitting corresponds with the potential above which the electrostriction pressure exceeds the compressive fracture strength of the film. The model accounts for the localised nature of the attack but does not easily explain either the role of specific aggresive ions or the induction period.

Videm[110] has recently introduced the idea of a dynamic balance between passive film breakdown and reformation, in which the critical potential is determined by the relative rates of the two processes.

Above the pitting potential, breakdown is the dominating factor and pits formed propagate, but below this potential repassivation is the dominant feature and any pits initiated are repassivated.

Experimental evidence has recently been produced to support such a theory. At potentials just below the critical pitting potential, investigators have found current transients [111,112]. Bond and Lizlov [111] found that very small depressions formed on the metal surface at such potentials, but holding these potentials did not cause the depressions to propagate. Ambrose and Kruger [113] have further developed this theory, suggesting that breakdown results from the penetration of aggressive anions to the metal/film interface where localised film rupture occurs due to the stress induced by the production of low density corrosion product, similar to that produced during active pit growth. The special influence of the aggressive anion is to influence the repassivation rate. The critical potential is determined by several factors, including the adsorption energy of the aggressive anion, the rate of repassivation and the mechanical properties of the film. The induction period is due to the time

taken by aggressive anions to penetrate the film. Finally, the attack occurs at localised sites due to the "penetration" element in the mechanism.

It is evident that these models have elements in common such as the adsorption step. In reality it is probable that no single model can explain all the observed effects, but that the particular conditions determine which mechanism dominates in any particular situation.

As was stated earlier, the above analysis of pitting takes no account of the heterogeniety of the metal surface which is very important in the pitting of commercial alloys. One of the most important factors in the pitting of commercial stainless steel alloys is the presence of non-metallic inclusions in the metal surface. Szlarska - Smialowska and Janik-Czachor [114,115,116], using electron-microprobe techniques, found that in commercially produced stainless steels, pits form predominantly at sulphide inclusions, and also to some degree, at chromium oxide inclusions. They observed that sulphide inclusions usually occur as shells around oxide particles, which act as nuclei for sulphide crystallisation during solidification. They suggested that those shells are dissolved in pitting media, producing narrow holes or crevices providing sites for pit initiation. Furthermore the dissolution of the sulphide inclusions locally activates the metal accelerating the development of pits. Wranglen and Ekland [117,118] have offered the following alternative explanation; the sulphide inclusions are less noble than the passivating film and act as anodes in local active/passive cells aided by chloride ions preferentially adsorbed at these sites [119]. The current density is greatest at the edges of the inclusions leading to the production of micro-crevices and hence pitting.

2.6.3 Pit Growth Following Passivity Breakdown

When a pit has reached a critical size it can grow by an autocatalytic mechanism, Rosenfeld and Danilov [99], suggested that pit growth is a particular form of crevice corrosion where the electrochemical behaviour of the metal is due to the differential access of the corrosion medium and removal of corrosion products. Hence pit growth is expected to be a diffusion controlled process and this has been confirmed by many investigators [87, 117, 120]. It has been observed that pits synthesised under potentiostatic control can have a surface covering [90]. This information provides a basis on which to explain pit growth mechanism, illustrated in figure (2.34)

The chloride ions penetrate the surface metal layer and the corrosion processes occur in the closed zone so that high concentrations of chloride accumulate in the pit. Mankowski and Szlarska - Smialowska [120] found values of chloride ion concentration of up to 12M in pits grown on 18Cr - 12Ni - 2Mo - Ti austenitic stainless steels tested in 0.5M sodium chloride. They also found that the pH of the solution within the pits was reduced but ascribed this effect to the high chloride ion concentrations observed. Although at an early stage in propagation the pits are hemispherical, they later develop into spherical cups [120] or cones [87], i.e. they grow in depth but not in radius. This is probably due to unequal distribution of the chloride ion concentration in the pits.

Wranglen [117] has expanded his views on pitting producing the following summary, which refers especially to carbon steels but which evidently applies, with modifications, to stainless steels: see figure (2.35)

> "From the bottom and side walls of the pit iron is dissolved anodically as Fe^{2+} ions, which migrate and diffuse outwards, whereas anions, e.g. chloride ions, migrate into the pit with the corrosion current.

On their way outwards, the Fe^{2+} ions are partly hydrolysed to $FeOH^{+}$ ions with the formation of an acid pit solution. At the mouth of the pit, the Fe(II) ions are oxidised by dissolved oxygen to Fe(III) ions, which are still further hydrolysed with the precipitation of magnetite and red rust, often forming a crust above the pit. Hydrogen evolved inside the pit causes occasional bursting of the blister."

The propagation of pits in stainless steels should proceed in a similar manner, the principal difference being that the greater stability of the oxide film covering the pits induces them to become pear-shaped with narrow openings.

2.6.4 Mechanical Rupture of Passive Films on Strained Metal

The mechanical breakdown of passive films is recognised as an important factor in several phenomena including stress-corrosion cracking, wear, fretting corrosion and corrosion fatigue because it can cause localised corrosion of metal exposed to aqueous environments. Film rupture and its consequences depend on the nature of the film itself and of the underlying metal.

The formation and composition of passive films have been considered in Section 2.5.3, where it was shown that the compositions of both the alloy and the environment have a marked influence on the characteristics of passive films, notably the morphology, stoichiometry, crystal and defect structures, distribution of chemical species and density[121]. These differences cause variations in the resistance the film offers to slip of the substrate, in ductile/brittle transitions and in the rate of film reformation after rupture.

Another important factor is the surface deformation characteristics of the metal, in particular the height of surface slip steps, which depends on the grain size of the metal and on interactions between the slip process and the passive film. Yamamoto[122] found that the slip step height increases with increasing grain size. Latanison and Staehle[123] found that for nickel in sulphuric acid, interaction of the slip process with the passive film distributes the slip more widely over the surface. The effect of slip height on film perforation is illustrated in Figure(2.36) taken from Staehle's paper, from which it is evident that single coarse slip perforates the film more easily than multiple fine slip.

Perforation of the passive film by the slip process leads to the formation of freshly exposed metal layers which can react with the environment. Hoar [124,125] originally suggested that dynamically-strained substrates are notably more reactive due to the increased number of reactive sites and the lower activation energy of dissolution for atoms involved in the slip process. Despic et al [126] found, however, that although elastic straining increases the reactivity of the metal, the effect is small and is mostly due to a change in the rate of hydrogen evolution. Thus it is the formation of slip steps and the resultant piercing of the passive film which is more important. This newly formed surface repassivates and many investigations have been carried out to characterise the repassivation process. The methods used include straining electrode techniques [127], scratching or rubbing electrode techniques[128 to 130] and fractured surface electrode techniques [131]. Staehle [121] has found that additions of Nickel and Chromium to iron reduce the total reaction , consistent with the greater stability of the oxide expected from the presence of the alloying elements in the oxide. He also found that chlorides in the environment reduce the rate of reformation of films and that

nitrates, acetates and iodine reduce the total reaction. The dominant mechanical factor was found to be not the strain rate as might be expected but the area of new surface exposed.

The mechanical rupture of passive films has featured prominantly in the development of theories of stress-corrosion cracking (SCC). In fact Okada et al[132] consider that the mechanical rupture of passive films is the most significant factor in SCC. A brief review of these theories is instructive in view of their relevance to the related phenomenon of corrosion fatigue.

Theories of SCC based on the idea of alternating film rupture and repassivation have led to the use of a rapid straining electrode technique to characterise particular features of SCC. Galvele et al [133] demonstrated the use of such a technique to determin the susceptibility of an 18% Cr 9% Ni steel (AISI 304) to SCC in hydrochloric acid and on the basis of further work [134] advocated its use to evaluate:

1. The potential ranges in which stainless steels are susceptible to SCC.
2. Crack penetration rates.
3. Crack morphology
4. The comparative aggressive nature of different aqueous media.

Ohtami and Hayashi [135] developed a mechanochemical model of SCC based on film rupture and used it to formulate the crack propagation period for a given system in terms of the applied stress, the tensile strength and plasticity of the metal and the activation energy for anodic dissolution; predictions made with this model were in good agreement with their experimental results.

Okada et al [132], Staehle[136] and Matsushima [137], have suggested that theories based on mechanical film rupture can be

extended to explain intergranular SCC in sensitised stainless steels in particular environments. This view is based on four important experimental observations these being:

(i) the excellent correlation between Strauss (132) test results, which evaluate the corrosion resistance of the chromium depleted zone, and the susceptibility to SCC.

(ii) the existence of strain-induced current transients as reported by Matsushima (138) upon low stress application, which was not observed for unsensitised steels.

(iii) the absence of preferential grain boundary corrosion without applied stress.

(iv) the location of the corrosion potential within a range where preferential dissolution of grain boundary carbides is not expected.

Theories based on mechanical rupture of passive films probably provide only a partial explanation of stress-corrosion cracking and must be considered together with other mechanisms which have been proposed. The most significant of these are:

(a) The influence of pre-existing active paths in the metal, e.g. as stimulated by inclusions anodic or cathodic to the matrix.

(b) Strain-generated active path mechanisms, e.g. preferential dissolution of emergent slip steps.

(c) Mechanisms due to specific adsorption at sub-critically stressed sites. The adsorbed species most usually considered is hydrogen which by subsequent influx into the metal may contribute to SCC by causing decohesion of the lattice or the formation of brittle hydrides.

Some of these ideas have their counterparts in theories of corrosion fatigue and are referred to again later where appropriate.

2.7 Mechanisms of Fatigue

The failure by fatigue of a metal in air is the culmination of a sequence of events which are now briefly reviewed.

Fatigue failure occurs under the action of alternating or fluctuating stresses of lower magnitudes than the stresses causing failure under static loads. Fatigue is usually considered to be a three-stage process. The first stage is crack nucleation caused by localised cyclic plastic flow in locations such as surfaces and notches. The second stage is a crack propagation stage defined by Forsyth (139) as stage I cracking where cracks propagate along crystallographic directions by an unslipping or reverse glide mechanism, forming ever-deepening surface crevices. The last stage, defined by Forsyth as stage II cracking is characterised by crack propagation in planes normal to the maximum tensile stress.

2.7.1 Crack Nucleation

The most significant aspect of crack nucleation is the formation of persistent slip bands, (PSB's), i.e. intense slip bands formed by cyclic straining persisting more or less unchanged throughout the major part of low strain-amplitude fatigue, and which also persist if a sample is removed before crack initiation and the surface of the metal is polished and re-strained (140).

Persistent slip bands have been studied in detail, notably by Winter (141) and Laird (142). They develop from instabilities which create local channels for easy dislocation motion within previously existing and uniformly distributed dipole arrays. In the PSB the dislocation dipoles are arranged in 'ladder'or 'wall' structures. Brown (140) proposed a 'two-phase' model to explain

the relationship between the formation of PSB's and fatigue properties. This approach leads to the relationship between stress amplitude and plastic strain amplitude, illustrated in Figure (2.37) The model predicts that if the strain amplitude $< Em$, no PSB's are formed, if it is between Em and E_b the proportion of the surface covered by PSB's is a linear function of the strain amplitude, and if it is above E_b the crystal surface is completely covered with PSB's. This applies to a constant plastic strain amplitude test. For a constant stress test no PSB's are formed below a stress of σ_c. This model thus gives a possible explanation for the existence of fatigue limits and predicts that all materials should exhibit fatigue limits in vacuum, an idea also supported by Laird [143].

There now follows a transition from PSB's to the formation of cracks. It is generally accepted [140] that the cracks (stage I cracks) are initiated at the intersection of the PSB's with the crystal surface, following the formation of intrusions and extrusions. The simplest way in which this can occur is by random walk of atoms on the surfaces of the PSB's [140], so that the surface roughens during fatigue until intrusions develop into cracks and propagation can begin. A diagrammatic summary of the important features of slip band extrusion and intrusion is given in figure (2.38).

2.7.2 Stage I Crack Propagation

As already mentioned, stage I cracks continue to grow along the planes of the persistent slip bands so that the exact transition from crack initiation to stage I crack propagation is difficult to define. Lynch [144] has suggested that the crack-tip regions often consist of series of tunnels which penetrate to various depths into the PSB's, subsequently linking up as illustrated in figure (2.38). The mechanism of stage I crack propagation is still not fully understood

but it may be simply an extension of the initiation mechanism of the Wood random-walk slip process [145] into the PSB's.

The stage I crack propagation mode can persist for a greater or lesser proportion of the fatigue life depending upon the prevalent conditions.

2.7.3 Stage II crack propagation

The transition from stage I to stage II crack propagation usually occurs at grain boundaries. The criterion for this transition is uncertain but stage II cracking occurs when stress conditions favour duplex slip. Under these conditions plastic deformation in the material around the tip becomes important. Many materials exhibit fracture striations, i.e. ridges produced on the surface of the fracture during Stage II cracking . The effect is discussed in detail in Section 2 . 10 where evidence is produced. It is thought that each striation represents the crack advance during one loading cycle [139,146]. From this it is apparent that stage II crack growth is a repetitive process which has lead to a now generally accepted model, known as a repeated plastic blunting process [147]. The tensile half of the load cycle induces large plastic strains at the crack tip, causing localised slip on the planes of maximum shear. When the load is reversed the crack faces are forced together but the crack increment produced in tension is not fully rehealed by reverse slip. The compressive slip occurs on new planes giving the crack tip a "folded" appearance. After the compressive half-cycle the crack tip is resharpened and the sequence is repeated as illustrated in figure (2.39).

This mechanism responds to the greatest tensile stress across the crack tip, so that the crack path changes direction at the beginning of stage II, and the crack propagates in the plane having the greatest tensile stress across it.

The above model is not the only proposed, others include the intersecting slip process [148,149] and the fracture-deformation sequence [150], although the above mechanism is now the most widely accepted [143].

Final fracture of the metal may be either brittle or ductile, according to the characteristics of the metal and it occurs when the residual cross-section is insufficient to support the stress acting across it.

2.8 Fatigue in Gaseous Environments

Fatigue failure is determined, not by the properties of a metal alone, but by the nature of the metal/environment system. Although it is customary to refer to fatigue in air simply as "fatigue" it is well-known that fatigue life is less in a gaseous atmosphere than it is in vacuum, to a degree depending on the nature of the gas [151]. Whether the influence is predominantly during crack initiation or crack propagation is uncertain and is the subject of controversy.

Several models have been devised to explain possible effects of air on fatigue crack nucleation. Thompson et al.[152] proposed that oxygen is adsorbed on the slip steps, interfering with reverse slip as illustrated in figure (2.40). Shen et al.[153] considered that oxide films strengthen surfaces in which they form acting as barriers to dislocation movement. In contrast, it has been suggested that oxide films may be more brittle than the substrate so that premature fatigue cracks may nucleate as the result of cracks in the oxide propagating into the metal.[154] Atmospheric water vapour is cited as an important factor in crack nucleation. It is a potential source of hydrogen, leading to hydrogen embrittlement, a topic currently attracting growing interest as discussed in detail in a later section. An alternative view is that water vapour may accelerate the oxidation of emerging slip steps, blocking reverse slip[155] and on the same theme Grosskreutz and Bowles[156] have proposed a mechanism whereby water vapour modifies the mechanical properties of the oxide film.

In seeking experimental evidence to support these various ideas an obvious approach is to examine the influence of the environment on the formation of PSB's. Unfortunately, little information from work of this kind has been reported except for the simplest, oxide-free crystals [157]. Wadsworth and Hutchings [158]

found no significant differences in the intrusions, extrusions and microcracks formed in vacuum and in air for the same sequences of cyclic stressing. From this and other evidence, Laird and Smith [159] Achter [160], Latanison and Westwood [161] and others concluded that the significant environmental effect is during the crack propagation stages rather than during nucleation. Definitive experiments to resolve this dilemma are very difficult because, as Laird and Duquette [151] pointed out, it is scarcely possible in practice for a crack to nucleate in the complete absence of an oxidising environment. Even in nominal high vacuo a monolayer of oxygen is very rapidly adsorbed on newly-created surfaces. A further problem is that in defining a crack nucleus, some investigators probably do not differentiate clearly between crack initiation and the early stages of propagation.

2.9 Fatigue in Aqueous Environments

There is general agreement that aqueous environments can strongly influence both fatigue crack nucleation and fatigue crack propagation. This matter is not disputed as it is for gaseous environments but there is continuing discussion on how the effects are produced. In view of the differences between crack nucleation and propagation already referred to in Section 2.7, the influence of the environment on these two stages of fatigue failure must be considered separately.

2.9.1 Crack Nucleation

Four theoretical approaches have been developed to explain accelerated crack initiation in aqueous environments. These are based on concepts of (1) stress-intensification at local corrosion damage (2) stress-enhanced dissolution and dissolution-enhanced plastic strain (3) local destruction of protective films and (4) the reduction of surface energy by adsorbed species. These various approaches will now be considered in turn and finally some attempt will be made to view them in a general context.

2.9.1.1 Stress Intensification at Local Corrosion Damage

This is one of the earliest mechanisms proposed and it was originally cited by McAdam [162] to explain the reduction of fatigue life of metals in aqueous environments. In McAdam's observations fatigue cracks usually emanated from corrosion pits at the metal surface, indicating that the pits acted as stress raisers thereby lowering the applied stress required to initiate fatigue cracks. The idea is supported by the results of pre-corrosion experiments in which samples are exposed to the corrosive environment before fatigue testing in air. In his own experiments with steel exposed to various aqueous environments before testing, McAdam [163] found that the fatigue limit was depressed progressively with increasing pre-exposure time towards a limiting value.

This mechanism can apply, of course, only to premature crack initiation in a metal exposed to media which induce pitting or equivalent features. It does not extend to corrosion fatigue phenomena in media in which pitting dues not occur and for which other explanations must be sought. Furthermore, the application of the idea even when pits are observed is not as straightforward as it might appear. Laird and Duquette [164] expressed the view that the stress concentration factor associated with corrosion-induced pits may not be large because they are usually hemispherical and have gone so far as to suggest that pitting is a consequence rather than a cause of fatigue cracking. They based their arguments on Duquette and Uhlig's metallographic observations [165] on low carbon steels tested in neutral 3% sodium chloride solution which exhibited deep "pit-like" configurations developing progressively at the heads of stage I cracks as a result of local accelerated corrosion following crack initiation. This cannot always be true because, as the results of pre-corrosion fatigue tests show, pits can act as very potent crack initiators. It shows rather that pitting is one manifestation of phenomena which, according to circumstances, may be more or less complex.

2.9.1.2 Stress-enhanced Dissolution and Dissolution-enhanced Plastic Strain.

These concepts have developed from Evans and Simnad's early work [166] on electrochemical aspects of fatigue in aqueous solutions for mild steel. They used a two-stage test to determine the residual air-fatigue life of samples taken from tests in aqueous solutions interrupted at various stages. The essential finding was

that the air-fatigue life was reduced only if the period of exposure to the preliminary test in aqueous solutions exceeded a critical value. This critical value was reduced by increasing the fatigue stress. Complementary measurements revealed a difference in corrosion rate during fatigue between tests in neutral salt solutions and tests in acid solutions. In neutral salt solutions the corrosion rate increased with the applied stress but was constant throughout the fatigue life. In acids, the corrosion rate was independent of applied stress but increased sharply just before fracture, indicating that the mechanical damage enhanced the corrosion rate. Simnad [167] attributed the enhanced corrosion rate in acids to (a) cathodic and anodic depolarisation, (b) decreased resistance between anodes and cathodes and (c) a shift of the anodic polarisation curve to more negative values due to distortion of the metal lattice. Arguments based on these considerations suggest a mechanism whereby premature fatigue cracks are initiated as a consequence of preferential attack at sites where intense slip has occurred, e.g. persistent slip bands, which are assumed to be anodic to undeformed metal. Lihl[168], Glikman and Suprun [169] and Spahn [170] all support this principle.

The ideas were extended by Rollins et al [171] to account for results obtained for a high carbon steel tested in sodium chloride solution, using the same experimental approach as that used by Evans and Simnad [166] and supplemented by examination of the fracture surfaces. Their interpretation assumed that the stress-raising effect of local corrosion damage, i.e. pitting, is required to initiate the strain-assisted dissolution mechanism and that an early growth of a crack is by resistance-controlled dissolution at its tip. Thus failure was envisaged as the result of the following sequence of events (1) pitting (2) anodically-controlled strain-

assisted dissolution at pit sites (3) resistance-controlled dissolution at the crack tips (4) mechanical fatigue (5) brittle final fracture. The pits were assumed to grow independently of the applied cyclic stress until they attained a critical size which Pyle et al [172] identified as that required to concentrate the applied stress sufficiently to induce local yielding at the bases of the pits. From this point interaction of emergent slip planes with the surface produces changes in the local topography as illustrated schematically in Figure (2.41). In the author's words, "if rapid dissolution occurs at the exposed slip steps such as BC and DE, it is possible that removal of the atoms from these faces will contribute to propagation of the crack when reversal of the slip process drives the slip back into the surface, Figure (2.41d). Because the step is formed continuously and dissolution can only occur at that part of the step face exposed to the electrolyte, the step will take the line B'C', Figure (2.41c). The length of BB' will depend upon the rate of dissolution and the cycling speed".

Other causes of electrochemical heterogeniety have been cited to explain premature fatigue crack initiation, Lihl [168] for example suggested that cyclic deformation induces the precipitation of impurities with low dissolution overpotentials in the slip bands thus increasing the reactivity of the sites where they

intersect the surface. This suggestion receives support from Uhlig and Foroulis' [173] work on iron-carbon alloys and is consistent with Greene and Saltzmann's [174] observation that potential shifts for pure iron require very severe deformation.

Some doubt has been cast on the Evans and Simnad [166] mechanism by Duquette and Uhlig [175] from their evaluation of cathodic protection applied to carbon steel specimens subjected to fatigue at stresses above and below the air fatigue limit in neutral and in acid solutions. They found that for stresses below the air fatigue limit protection was afforded by a suitable cathodic potential whose value was independent of the strain amplitude and with this information they could not accept yielding as the cause of enhanced corrosion. Vedenkin and Sinyavski [176] took a similar view and attributed the observed potential shifts to pH changes in the vicinity of local anodes.

To allow for deficiencies in the stress-enhanced dissolution model, an alternative or additional approach is possible using the closely related concept of dissolution-enhanced plastic strain. The idea was originally put forward by Duquette and Uhlig [165,175] to explain their view that the effect of the environment is important only if a critical corrosion rate is exceeded. They drew this conclusion from the experimental observation that a fatigue limit similar to that for air could be restored for specimens tested in 3% sodium chloride solution or water by deaeration. In subsequent experimental measurements [175] they found that the critical corrosion rate for a 0.18%C steel corresponded to the removal of about 10^4 atom layers per stress cycle, indicating that the initiation of corrosion fatigue cracks is determined by the behaviour of the extreme surface of the metal. Other investigators, including Lee and Uhlig [177], Revie [178] and Asphahani [179] have since confirmed the concept of a critical corrosion rate.

Duquette and Uhlig (175) considered that the role of the corrosion process is to stimulate plastic flow under the existing stress, facilitating the formation of the intrusions and extrusions which lead to the initiation of fatigue cracks. Such an effect could be produced by dissolution of piled-up dislocations which would otherwise impede motion along slip planes as illustrated in Figure (2.42) or alternatively by the injection of imperfections which could aid the slip motion. These processes are assumed to operate only when the critical corrosion rate is exceeded, establishing a steady state as the corrosion rate increases further. Lee and Uhlig (177) used these ideas to explain why cathodic protection prevents corrosion fatigue. By eliminating dissolution of the disturbed surface it was assumed to restrict the growth of surface plastic zones to a very small size insufficient to initiate fatigue cracks.

The foregoing discussion has introduced the concepts of stress-enhanced dissolution and dissolution-enhanced plastic strain as independent concepts developed by different groups of investigators to explain specific experimental observations. As ideas develop it may be more appropriate to adopt a unified approach and regard them as complementary aspects of a complex dissolution process.

2.9.1.3 Local Destruction of Passive Films

If a passive film protecting a metal is ruptured by slip planes intersecting the surface, a local anode is created on which local dissolution is stimulated by the large surrounding cathodic area until the film is repaired by repassivation. In this way, progressive slip on the same planes produces a notch which may develop into a crack. Such a mechanism for crack initiation in stress-corrosion cracking is well supported by experimental evidence but, as Evans and Simnad (180) have remarked, it is obviously restricted

to passivated surfaces and cannot be applied to account for premature crack initiation in metal-environment systems in which the surfaces are active.

Laute [181] explained the corrosion fatigue behaviour of stainless steels on this basis as early as 1933. This application of the model leads to certain predictions concerning the behaviour and life of the material subject to fatigue stressing. For example, the electrochemical characteristics of the material may be expected to change as fatigue cracks nucleate and develop. Moreover, longer fatigue lives may be expected for high frequencies than for low because of the effect on the time available for film repair during the cyclic relief of the applied stress. Subsequent investigators have produced evidence for such effects and used it in support of film rupture models to explain their results, as illustrated in the following discussion.

Spahn [182] found that chromium-containing steels were susceptible to corrosion fatigue throughout the passive range and that the fatigue strength was adversely affected by reduction of the pH of the environment and of the chromium content of the metal, two factors which tend to reduce the stability of the passive surface condition. He expressed his concept of the film rupture model as follows:

> "The oxide film covering the material in the passive state cracks under mechanical stress when slip intersects the surface. In the case of fatigue this occurs only after repeated stress and occurs later for smaller stress amplitudes. Under passivity-producing conditions such a spot is repassivated. A certain current flows during such a passivating process and metal is thus dissolved. At such a spot an immeasurably small notch is formed at the

base of which the mechanical stress is somewhat higher than in the environment. Therefore further slips very probably occur. The passive film is again cracked and the repassivation starts anew. This interplay continues with increasing intensity. The surface area which is active owing to the slipping becomes larger and larger".

The proposed mechanism is supported by the experimental results given in Figure (2.43), showing that for material subjected to corrosion fatigue under potentiostatic control, the corrosion current increases at first slowly and then more rapidly, following an incubation period.

Ryabchenkov [183] found that the electrode potential for a stainless steel became markedly more negative during fatigue tests, the rate of change being greater for higher stresses. He accounted for this effect in terms of the film rupture model, assuming that the protective film is damaged progressively as more and more microcracks open. He also observed that for a grooved specimen subjected to fatigue-stressing, the bottom of the groove was anodic to the side of the groove and the specimen surface.

Rollins and his co-workers [172,184,185,186] have studied directly the enhanced corrosion of metal specimens exposed to aqueous media immediately following the application of a strain. The effect is manifest as transient dissolution currents with lifetimes such that they may be monitored conveniently in the intervals between the applications of alternate tensile and compressive strains generating a square wave form of frequency 0.3 Hz. When carried out on samples of metal held at prescribed potentials under potentiostatic control, measurements of this kind are of value in assessing the conditions under which passive film rupture may be expected. Transient currents were observed for stainless steels held at potentials in both the active and passive ranges and at the active/passive transition.

The values of the transient currents depended not only on whether the surface was active or passive but also on the nature of the passivating film if present. Pyle et al [172] ascribed the transient currents in the active range to stress-enhanced dissolution as discussed in the preceding section but for the passive range they preferred to attribute the effect to rupture of the protective film. From the results of this work, together with the results of a subsequent study [185] of the influences of pH and potential on the transient currents observed for mild steel, they deduced that transient local dissolution at a passive surface depends critically on the nature of the passivating film. Very strongly passivated surfaces bear films which resist rupture. They proposed two alternative mechanisms to explain this effect, as illustrated in Figure (2.44). The first assumes that the film gradually thickens as a continuous surface layer until its mechanical strength is adequate to contain the imposed surface strains. They were inclined to dismiss this idea because there was no visible evidence of such a layer and it is doubtful whether it would be sufficiently ductile. The second assumes that the volume of metal removed from the surface of an emergent slip step by dissolution is replaced by film and that during reverse slip the protected slip step is drawn into the metal surface with the film intact. If cyclic slip continues on the same plane, the protected slip step emerges later in the cycle, maintaining the integrity of the passivated surface so that no dissolution is associated with the process. Such models can account for observed decreasing values of transient currents for strongly passivated surfaces on repeated application of cyclic strains and also for Pyle's further observation that the fatigue properties of mild steel in strongly alkaline solution (pH 12) are similar to those in air. For conditions in which the

stability of passive films is less, the films are thinner and thus more likely to rupture and repassivation is slower so that the material is more susceptible to dissolution by active/passive cells at emergent slip steps. This explains the maxima observed for transient currents at the active/passive transition for stainless steels and at the perfect passivity/imperfect passivity transition for mild steel.

The disruption of the oxide film may be caused not only by slip band perforation but by fatigue failure of the film itself, so that the mechanical properties of the film must also be considered. Grosskreutz [187] found that in the presence of water vapour, the shear modulus of the oxide film on aluminium is about a third of that of the substrate but in vacuum it is about five times as great. Hence water vapour must play a very large role in the corrosion fatigue failure of aluminium.

From the foregoing discussion, it is apparent that although the basic idea of localised attack at ruptures in passive films is very simple, the assessment of conditions under which it actually applies presents a difficult problem providing scope for much more work on the influence of environmental and alloy factors. The difficulties are compounded by uncertainties in the general principles of passivation as discussed in Section 2.5.3. Payer and Staehle [188] considered the general problem of localised attack on moving dislocations and summarised the factors determining the attack quantitatively as follows:

1. The nature of any protective film which may be present on the metal.
2. The environment to which the metal is exposed.
3. The morphology of slip with respect to the size of slip packets.

4. The influence of alloy and environmental chemistry on the rate of processes occurring during dissolution and film repair following film rupture.

2.9.1.4 Reduction of Surface Energy by Adsorbed Species in the Aqueous Environments.

This concept was first suggested by Rebinder and his co-workers [189,190] and has become popularily known as the Rebinder mechanism. They originally proposed that a surface active agent is preferentially adsorbed in pre-existing microcracks, thus creating a high pressure reducing the applied stress required to propagate them. This was later extended to take account of the effect of the reduction in surface energy due to the adsorbed species facilitating the production of slip bands at the metal surface. This approach is analogous to that used to explain the accelerated creep rates of metals coated with surface-active agents.

Kramer [191] has further modified the Rebinder mechanism in view of his observation that metal-soap complex can be detected in test solutions. He suggested that the weakening effect is associated with a chemical adsorption process, in which the rate of removal of the entire metal surface by dissolution of the metal-soap complex is the controlling process, the dissolution either removing or unlocking dislocation pile-ups thus inducing further slip.

Karpenko [192,193] interpreted his results using the Rebinder mechanism on the basis of a two stage process, the first being crack initiation associated with environmental adsorption and the second a corrosion process occurring within the initiated crack. The suggestion is that adsorption occurs at microcracks oriented normal to the applied stress axis causing them to multiply and propagate . He also found that applied anodic currents did not affect crack initiation and suggested that initiation is due solely to surface adsorption processes and not to surface corrosion.

These results are in conflict with the work of other investigators such as Duquette and Uhlig [175], however, who found a marked effect of very low applied anodic currents on the fatigue behaviour in deaerated salt solutions.

Although the Rebinder mechanism is attractive it fails to explain, for example, why crack initiation in passivated steels in neutral aqueous solutions is influenced by deaeration, even when strongly adsorbing ions such as Cl^- are present. Such observations have reduced the popularity of this concept in recent years.

Another very important factor often cited to explain the premature crack initiation in corrosion fatigue is hydrogen embrittlement. Although some aspects of hydrogen embrittlement are related to the Rebinder mechanism, it is a distinct phenomenon and is discussed in some detail in a later section.

2.9.1.5 Resumé of Theoretical Approaches

As has been shown in section 2.7, the initiation of fatigue cracks has been associated with the formation of persistent slip bands and their subsequent development. It is obvious that any environmental interactions which can affect the formation and development of PSB's will be important in the acceleration of fatigue crack initiation. Although many of the mechanisms can explain how such effects can occur few direct observations have been reported on the influence of environments on PSB's. Pelloux et al.[194] have reviewed what information has been obtained. Howard and Pyle[195] found that as the electrochemical dissolution rate decreases so does the PSB spacing. Pelloux et al.[194] suggested that this could be due to an oxide film on the metal surface acting as a barrier to slip when the dissolution rate is low so that the PSB spacing is close because slip localisation is inhibited. Conversely, at high dissolution

rates the oxide film is thinner and the barriers to slip reduced so that a wider PSB spacing is expected.

This can be used to explain premature crack initiation because as the PSB spacing becomes wider the local plastic strain each PSB must carry increases.

Pelloux et al. (194) have also suggested that the environment can alter the stability of the near-surface matrix dislocations and cause them to be transferred more easily into PSB's, further accelerating PSB formation.

An alternative theory to this is that PSB's form independently of any environmental effects and that the environmental role is to accelerate the process by which PSB's lead to fatigue crack initiation through intrusion-extrusion formation by the four basic mechanisms already discussed. As with PSB formation, however, nobody has been able to show definitively which environmental interaction controls the PSB intrusion-extrusion processes.

It is evident from this resumé that no single mechanism can explain fully the effect of aqueous environments on fatigue crack initiation for all metal and alloy systems in all environments. It is more likely, therefore, that there is no generally applicable mechanism, but that more than one mechanism can operate with different mechanisms predominating according to the particular conditions. Investigators have attempted to define the circumstances under which particular mechanisms predominate. Karpenko (193) for example has suggested that the applied stress determines the relative importance of the various mechanisms. At high stresses he attributes crack initiation to hydrogen adsorption at cathodic areas leading to hydrogen embrittlement. At intermediate stresses he suggests a combined adsorption-electrochemical theory where environmental adsorption occurs at highly stressed anodic areas in the sample causing premature

crack initiation by a surface energy reduction. At low stresses premature crack initiation is explained by the destruction of the protective oxide film due to a lowering of the electrode potential in highly stressed anodic areas.

Alternatively, Spahn [182,196] has defined the operative mechanism in terms of the electrochemical condition of the metal surface. When the metal is in an active state he suggests an enhanced dissolution/enhanced plastic strain model which he summarized as follows:

> "The first or initial stage consists in the formation of slip steps at the surface which are electrochemically the more efficient the rougher the slipping and the higher the width of a slip step. The electrochemical activity of such slip steps results in a shift of the electrode potential towards less noble values or, under potentiostatic conditions, in current transients. In the second stage the corrosion begins to localise more and more. This is effected, as indicated by the potential shift and the current transients in the first stage, by a preferential dissolution of metal ions on slip steps thus giving rise to the formation of micro-grooves. Due to their notch effect the mechanical stress is increased at the root of such grooves which in turn leads to an increase in the anodic dissolution rate. Thus in a mutual increase of mechanical stress and dissolution rate the groove proceeds and the root becomes more and more acute until a corrosion fatigue crack is formed".

In the passive condition Spahn [196] prefers a film rupture mechanism where the film is ruptured by slip steps piercing it as described earlier.

Spahn [196] also recognised the important principle that other environment-sensitive cracking processes and corrosion-processes may be superimposed on the corrosion fatigue phenomena and enhance the effect. Such effects may be stress-corrosion cracking, intergranular corrosion, pitting etc.

2.9.2. Crack Propagation

Several approaches have been made to explain the mechanisms of corrosion fatigue crack propagation. The fracture mechanical and fractographic approaches are discussed in detail elsewhere, i,e, in Sections 2.3 and 2.10 respectively. In this section phenomenological aspects of the subject and their relevance to the possible mechanisms involved are discussed.

Crack propagation rates have been studied extensively and in particular a considerable volume of pioneering work has been done by Bradshaw and Wheeler [197] and by Wei and his co-workers [198]. Most of the work prior to 1970 has been reviewed by Wei [198]. There is general agreement in the published papers that the environment influences the crack propagation rate but in a manner very dependent upon the experimental conditions. A detailed discussion of the results obtained is beyond the scope of this discussion, but it is pertinent at this point to discuss the various theories proposed.

Pelloux et al [194] have classified these theories into the following three categories:

(1) theories assuming accelerated dissolution of metal at the crack-tip.

(2) theories concerning essentially mechanical crack-tip effects.

(3) theories assuming changes in the local deformation character of the material at the crack-tip.

The dissolution theories are very similar to those proposed to explain corrosion fatigue crack initiation, except that the site of

chemical/mechanical interaction is restricted to the crack-tip region where the local strains are highest, i.e. much higher than in the surface PSB's. Ford and Hoar [199] applied such a theory to crack propagation in Al/Mg alloys in chloride and sulphate solutions. They considered that the increase in propagation rates can be entirely accounted for by the loss of material dissolved at the crack-tip but this may not always be true.

Pyle et al. [172] have extended the application of the mechanism to embrace crack development from corrosion pits. The dissolution is assumed to occur at step faces formed by plastic deformation at the pit surfaces so that the important parameters in determining propagation rates are the rate of dissolution from the step face and the height of the step produced on the metal surface.

The mechanical crack-tip theories assume that the environment can affect the mechanical properties of the oxide reducing its ductility [200] until it is so brittle that microcracks can be formed in the oxide layer during straining, increasing the local stress concentration and hence the crack propagation rate. In contrast Gell and Duquette [201] have suggested that thick oxide layers could lead to a lowering of the crack propagation rate because they consider that application of the plastic blunting theory predicts that oxide forming on the crack surfaces prevents the crack being resharpened to the same degree as in vacuum. Furthermore Pelloux et al [194] have suggested that thick oxides can wedge the crack open, reducing the effective stress intensity factor and hence reducing the crack propagation rate.

Thompson et al.[152] explained higher propagation rates in air over nitrogen for copper in terms of rewelding of the crack surfaces in nitrogen during the compressive part of the cycle, whereas in air the oxide formed on the crack surfaces would prevent it.

The weight of experimental evidence is against such a mechanism [160] and in any event it probably does not apply in aqueous environments. Environmentally-induced changes in the deformation characteristics of material at the crack-tip could arise in several ways. Grosskreutz [202] in a review of metal fatigue considered that "corrosion attack at a new surface will inhibit the reversibility of slip in the compressive cycle of the plastic blunting mechanism, thereby increasing the advance per cycle". Tyson and Alfred [203] have extended the Rebinder mechanism to crack propagation by suggesting that adsorbed species on the crack-tip can reduce the cohesive strength of the material sufficiently to promote a cleavage mode of fracture but Pelloux et al.[194] have pointed out that such a mechanism is unlikely in F.C.C. metals as the very low ratio of critical shear to critical cleavage stress should result in deformation by slip and not cleavage. Pelloux et al [194] prefer another theory assuming that the distribution of slip at the crack-tip is altered by the diffusion of some species into the plastic zone ahead of the crack-tip. Finally Gell and Duquette [201] have suggested that coherent oxide films can disperse the planar slip at the fresh metal surface of the crack-tip, reducing the propagation rate.

Crack propagation is probably as complex as crack initiation in that no single mechanism adequately explains all the observed phenomena. In the words of Pelloux et al [194] "It is difficult, if not impossible, to isolate which of the mechanisms controls the corrosion fatigue behaviour of an alloy in a given environment". The situation can be further complicated by the superimposition of other phenomena, e.g. intergranular corrosion, stress-corrosion cracking, hydrogen embrittlement etc.

2.10 Fractographic studies of Fatigue and Corrosion Fatigue

The advent of electron microscopy stimulated major advances in this field by taking advantage of the higher magnifications , higher resolution and greater depths of field available as compared with optical microscopy. Many good reviews on electron fractography are available, notably by Plumbridge and Ryder [204], McMillan and Hertzberg [205] and Broek [206] and also by McCall [207] who dealt particularly with the associated techniques. For the present purpose it is sufficient to consider only the application of fractography to fatigue and corrosion fatigue and the use of such studies to develop an understanding of the mechanisms involved in crack propagation.

Fatigue cracks propagate in two stages Stage I and Stage II as described in section 2.7.

It is convenient to consider the fractographic aspects of these two stages separately.

2.10.1 Stage I Crack Growth

Stage I fracture surfaces are dependent on test conditions and are either featureless or show parabola-like features and dimples [208]. Nageswararao and Gerold [208] compared stage I crack growth with cleavage-crack propagation with the important distinction that crack-tip plasticity increases with crack velocity. From the fractographic evidence a model [208] has been suggested for stage I crack growth as follows; cracks nucleate in the plastic zone of a stage I crack and while of microscopic dimensions they grow preferentially in favoured slip directions, but the growth of macroscopic cracks is governed by the crack propagation geometry. The features observed on the fracture surface are hence a direct result of the linking of the secondary microscopic cracks with the main macroscopic crack. Figure (2.45) shows the proposed sequence

of events [208] which leads to the linking of secondary cracks with the main crack, for two situations. In situation (a) the primary slip direction coincides with the macroscope crack propagation direction and the fracture face appears relatively smooth. In situation (b) the primary slip direction is at right angles to the macroscopic crack propagation direction and the fracture face appears significantly rougher. Gell and Leverant [209] studying stage I fatigue fracture in a high strength nickel alloy found that the fracture surfaces exhibited features not normally observed on ordinary stage I fracture faces. The most important were slip markings and striations and "tongues" as illustrated in Figure (2.46) which shows fracture steps. In the regions between the steps a series of parallel markings at 60° to the steps can be seen which correspond to the trace of the (111) planes in the fracture facet. These step traces are also sometimes observed in a herringbone pattern. Gell and Leverant [209] attributed them to slip after fracture during the relaxation of the stress field. They also observed striations on the fracture face with some of the features characteristic of stage II striations to be described later. These striations were well defined as illustrated, Figure (2.47) Striations of this particular form have also been observed on aluminium alloys [210] and thoriated nickel [211]. Laird [147] concluded from their presence that a tensile stress component is essential for stage I cracking and that there is no real distinction between stage I and stage II cracking. Plumbridge and Ryder [204] have pointed out, however, that there is a gradual change from stage I to stage II cracking and striations might be formed on the fracture surface during the transition. The "tongues" observed by Gell and Leverant [209] are common in b.c.c. cleavage [212] and result from the local deviation of the crack front on to another

crystallographic plane. These tongues are triangular and are formed on a 111 plane other than that of the main fracture.

In a more recent study Lynch (144) examined Al/Zn/Mg specimens during fatigue and found that stage I cracks normally form at intrusions. He attributed the subsequent crack-propagation to the progressive development and linking up of a series of holes penetrating to different depths in the persistent slip bands. The electron fractographs showed that troughs on one fracture surface were frequently matched by much shallower troughs on the mating fracture surface and Lynch used this as evidence of his theory.

The appearance of the features observed on stage I fractures mentioned above depend on the precise conditions in which they are formed. This implies that the prevalent mechanism of stage I fatigue crack growth is also dependent on the conditions. Little work has been done on the effect of environment on stage I crack growth, because stage I cracks normally extend just a few micrometres or one grain diameter from the surface in most materials. Duquette and Gell (213) studied the effect of environment on stage I crack growth in single crystals of a high strength nickel alloy in which the transition to Stage II cracking is delayed so that crack growth is predominantly stage I. They found that in air at low stresses the fracture surface had a cleavage appearance whereas in vacuum and in air at high stresses it had a dimpled appearance, and was unaffected by atmospheric humidity. From these observations Duquette and Gell surmised that gaseous oxygen rather than water vapour is adsorbed at the fracture surface giving the cleavage appearance by lowering the surface energy during crack growth.

2.10.2 Stage II Crack Growth

In the first studies of fatigue fractures optical microscopy was employed using magnifications of up to X1500 to

examine stage II fracture surfaces because this usually constitutes by far the largest proportion of the total. Zappfe and Worden [214] using such techniques were the first to observe "striations" on fracture surfaces, i.e. parallel markings normal to the direction of propagation. With the advent of the improved depth of focus available with electron-optical techniques, it was shown that striations represent the successive position of the crack front during propagation. This is demonstrated in Figure (2.48) which is an electron fractograph of a fatigue test-piece subjected to a programmed-loading fatigue test. This proved that each striation was produced by one load cycle. Hence each striation spacing represents the advance of the crack in one load cycle. However, every load cycle does not necessarily produce a striation because the crack-tip stress intensity during some cycles may be insufficient to advance the crack. Forsyth [215] identified two types of striation, ductile and brittle as illustrated in Figure (2.49).

Brittle fatigue striations were first reported by Forsyth and Ryder [216] for a high strength aluminium alloy tested in 3% aqueous sodium chloride. They lie on fan-shaped crystallographic facets which are separated by numerous "river markings". Since this discovery, brittle striations have been observed in many other systems. The mechanism by which these form is still disputed, Stubbington [217] suggested that the fracture may be a result of the reduction in surface energy due to chemisorption. More recently Stoltz and Pelloux [218] have proposed a quasi-cleavage model for materials exhibiting planar slip in which planar slip constraints confine cracking to certain crystal planes. Wanhill [219] working on high strength aluminium alloys developed the following concept; during the tensile part of the load cycle the material can fracture by adsorption-induced cleavage in localised regions which, until fracture, are relatively undamaged.

The cleavage crack thus produced is then arrested because it cannot run into material unaffected by the environment, where the stresses required for cleavage are too high, and the crack is blunted by dislocation movement into the tip. This crack blunting together with interference with the cleavage process by second phases and/or coarse slip results in the observed morphologies of brittle striations.

Ductile striations are more common than brittle striations and have therefore attracted more attention. Each ductile striation consists of a light and a dark band lying on irregular non-crystallographic plateau. Three basic mechanisms have been proposed for ductile striation formation and these are illustrated in Figure (2.50).

(1) Forsyth[215,216] and his co-workers favoured the mechanism illustrated in Figure (7.C). Here plastic deformation generates a point of triaxial stress ahead of the crack-tip. As the resultant weak point grows, the volume of metal between it and the crack-tip decreases. Fracture occurs with associated deformation creating a rippled fracture surface.

(2) Laird and Smith[220] proposed a mechanism in which crack propagation occurs by plastic blunting which they refer to as "plastic relaxation" of the crack-tip during the tensile part of the cycle followed by re-sharpening of the tip during the compression part of the cycle.

(3) Matting and Jacoby [221] suggested a mechanism by which crack propagation occurs in slip planes as a result of cross slip or duplex slip. This mechanism was supported by Meyn [222] who found that no striations were identified on fractures produced in vacuum, an observation subsequently confirmed by many workers.

Pelloux [223] used these ideas to explain ductile striation formation by alternating shear as depicted in Figure (2.51) for aluminium alloys. In this mechanism, under increasing load the

crack grows as a geometrical consequence of the slip displacements on two active slip systems, simultaneously blunting the crack-tip. Under a diminishing load, slip takes place in the opposite direction resharpening the crack-tip and thus preparing it for propagation in the next cycle. Hence the fatigue striation consists of slip steps on the fracture surface and the fracture advances by slip plane decohesion. This model predicts peak to peak matching of mating fracture faces and this is usually observed [224] although the other mechanisms described are not necessarily precluded.

Quantitative data has been obtained more from the measurement of fatigue striations than from any other fracture surface feature. In fact the striation spacing S has been related to the stress intensity factor ΔK by the equation:

$$S = C (\Delta K)^{n} \quad \ldots\ldots\ldots\ldots\ldots\ldots (67)$$

where C and n are constants dependent on the material, which can be calculated by analysing the striation spacing in relation to the length of the crack.[225,226] Wareing and Vaughan [227] working on AISI 316 stainless steel found that the striation spacing increased with increasing crack length and for notched specimens devised the equation:

$$S = A\,l \quad \ldots\ldots\ldots\ldots\ldots\ldots (68)$$

where A is a constant dependent on the applied strain range and l is the crack length including the notch depth.

Similarly for smooth, un-notched specimens:

$$S = A^{1}\,l \quad \ldots\ldots\ldots\ldots\ldots\ldots (69)$$

where A^{1} is again a constant related to the applied strain range. They further found that the macroscopic crack growth rate $\frac{d\,l}{d\,N}$ can be related to the instantaneous crack length l by the equation:

$$\frac{d\,l}{d\,N} = B\,l \quad \ldots\ldots\ldots\ldots\ldots (70)$$

where B is a constant related to the plastic strain range. Using this data they showed that for plastic strain ranges in excess of $\sim$ 0.002 there is close agreement between the macroscopic growth rate $\frac{d\,l}{d\,N}$ and the striation spacing S. Below this strain range they found that the striation spacing exceeded the growth rate per cycle. In view of this they modified equation to the form:

$$\frac{d\,l}{d\,N} = S = \alpha B l \quad \ldots\ldots\ldots\ldots (71)$$

where α is a crack shape parameter whose value is 0.5 for semi-elliptical and 1 for straight-fronted unrestrained cracks.

The implication of their work is that for strain levels above 0.002 a one-to-one relationship exists between S and $\frac{d\,l}{d\,N}$ but for strain levels below this several cycles are associated with each striation as noted by Bathias and Pelloux [228]. The reason for the discrepancy at low strain levels is still open to question. Two theories have been proposed. Bathias and Pelloux [228] considered that the crack length is not a continuous process and new crack surface is not formed during every stress cycle. As an alternative Tomkins [229] pointed out that striations merely delineate the crack-tip opening displacement which can remain constant for several cycles in which the growth per cycle is some fraction of the crack-tip opening displacement.

As has already been discussed striation formation can be significantly influenced by the environment. Hartman et al. [230] found that fatigue crack propagation is appreciably faster in wet air than in dry argon or oxygen and the fracture faces exhibited fewer striations for the specimens tested in dry environments.

2.11 Hydrogen assisted Cracking and its Role in Corrosion-Fatigue

Hydrogen assisted cracking (HAC) was first recognised in steels by Johnson [231] in 1873 and it has now become generally accepted as one of the mechanisms contributing to stress corrosion cracking. There are two main requisites for HAC:

(i) Hydrogen must be taken up by the metal and migrate to some specific site.

(ii) Hydrogen must play a specific role in weakening the metal.

Broome and Nicholson [232] first suggested that a HAC mechanism could occur in corrosion fatigue and since then these ideas have been developed. Hydrogen in metals [233] and particularly its effect on mechanical behaviour [234,235] has been discussed in many recent international conferences.

Before considering these ideas further it is convenient to begin by referring briefly to the nature of H_2 occlusion in metals.

2.11.1 Hydrogen solution in metals

Size factors determine that the diatomic gas must dissociate on dissolution:

$$H_2 \text{ (gas)} \rightleftharpoons 2H \text{ (solution)} \quad \ldots\ldots\ldots\ldots (72)$$

Geometric and valency considerations preclude the accommodation of hydrogen in substitutional solution so that the simplest assumption is that the solute is accommodated as non-interacting atoms, all occupying equivalent interstitial sites. For dilute solutions, Henry's Law applies and if also ideal behaviour is assumed for the gas, equilibrium is described by:

$$K = \frac{a_H^{\,2}}{a_{H_2}} = \frac{N^2 p}{p} \quad \ldots\ldots\ldots\ldots (73)$$

where a_H is the activity of the solute referred to the atomic fraction

at infinite dilution as the standard state

a_{H_2} is the activity of the gas referred to the pure gas at a pressure $p^{\ominus}$ as the standard state and N is the atomic fraction of solute in equilibrium with an arbitrary gas pressure p

Equation(73) yields:

$$\frac{N}{N^{\ominus}} = \left(\frac{p}{p^{\ominus}}\right)^{0.5} \qquad \text{.....(74)}$$

Where $N^{\ominus}$ is the atomic fraction of solute in equilibrium with the standard pressure $p^{\ominus}$, assuming that $N^{\ominus}$ lies within the range of composition for which Henry's Law applies.

Equation (74) gives the relation between solute concentration and pressure in the gas phase and is known as 'Sievert's Law'.

2.11.2 Adsorption of hydrogen by chemical reaction

Metals can adsorb hydrogen produced by chemical reaction at their surface. The driving force injecting hydrogen into the metal is ultimately the free energy change of an overall reaction written formally as, for example:

$$3\,Fe + 4H_2O \rightleftharpoons Fe_3O_4 + 4H_2 \qquad \text{.....(75)}$$

for which

$$\log\left(\frac{P_{H_2}}{P_{H_2O}}\right) = \frac{1538}{T} - 1.312 \qquad \text{.....(76)}$$

assuming ideal behaviour of the gases.

For unit activity of water vapour and a temperature of 298K, equation (76) becomes:

$$\log P_{H_2} = \frac{1538}{298} - 1.312 \qquad \text{.....(77)}$$

This yields a value of P_{H_2} = 7,064 atmospheres.

The exceedingly high value obtained in calculations of this kind [236,237] are useful but must be applied with caution in interpreting real phenomena.

Clearly in practice such pressures cannot be developed because the equilibrium solution predicted by equation (74) would contain a greater molar fraction of hydrogen than metal.

In any event the pressures required to disrupt a metal are orders of magnitude less than the theoretical pressures obtainable. On the other hand taking the view that whatever pressure is theoretically obtainable in a closed system, the pressure actually developed does not exceed atmospheric because at the point of hydrogen generation the gas is in free communication with the atmosphere, it is not possible to sustain any theory of embrittlement induced by pressure because the hydrogen concentration in equilibrium with one atmosphere of hydrogen at an external interface providing the source of hydrogen cannot exert any disruptive influence at an internal interface. If indeed hydrogen embrittlement occurs through the exertion of a gas pressure, the answer is to be found in the kinetics of the reaction, making available some fraction of the activity of hydrogen that the reaction is capable of generating.

It is apparent from these arguments, however, that the corrosion reactions which can occur in aqueous corrosion circumstances are a potent source of hydrogen. The problem now is the entry of hydrogen into the metal and its migration to specific sites. It is well known that there are specific sites in metals to which hydrogen can migrate. These are known as "traps" and can be classified into chemical and physical traps.

Chemical Traps

In contrast to such metals as Fe, Ni, Cu, Al, some metals can form a metal hydride at quite low hydrogen activities, e.g. metals in group IVa (Ti, Zr, Hf) and group Va (V, Nb, Ta) [238]. Precipitation

of hydrogen within these metals can induce HAC, In addition the presence of these metals as impurities in another metal e.g. steel can induce it to adsorb more hydrogen at sites containing the impurities. A good example of this is Ti atoms and clusters, and possibly Titanium nitrocarbides in iron which Bernstein et al [239] have cited as chemical traps. Elements present as impurities or alloying additions may also react with hydrogen to liberate gases within the structure; an example of this is the formation of steam by the reaction of hydrogen with internal reducible oxides in copper [240].

Physical Traps

The simplest physical trap is a 'molecular trap'. One obvious example is a defect in which the gas phase accumulates until the pressure is in equilibrium with the adjacent solute hydrogen. Another example is the result of a spontaneous precipitation of hydrogen within the solid metal [240], producing a widespread dispersion of very small spherical pores.

The other kind of physical trap is an 'atomic trap' at a lattice defect in the metal where hydrogen atoms can be accumulated. There is some evidence that dislocations can act as such sites, Foster[241] found such evidence for hydrogen in aluminium and Wriedt and Darken[242] for nitrogen in steel.

2.11.3 Mechanisms of Hydrogen Assisted Cracking

The mechanism by which hydrogen can cause a weakening effect in the metal is a continuing source of controversy. In the following discussions some of the more important mechanisms which have been proposed are described and their applicability to S.C.C. and corrosion fatigue considered.

The mechanisms proposed can be divided into six categories as follows:

(1) Dissolved hydrogen can reduce the cohesive strength of the lattice

causing premature failure. This was probably the first explanation offered for HAC and was suggested by Pfeil [243] in 1926 and later modified by Troiano [244] and by Oriani [245].

(2) Hydrogen can precipitate as a gas at internal defects exerting a pressure supplementing the applied stress and in effect lowering the fracture stress. This mechanism was first proposed by Zapffe[246] in 1941 and has since been modified many times, for instance by Louthan.[247]

(3) Hydrogen adsorption reduces the surface energy required to form a crack thus lowering the fracture stress. This model, initially proposed by Petch and Stables[248] has since been modified by Williams and Nelson[249] and Van Leeuwen [250].

(4) Hydrogen adsorption can increase the ease of dislocation motion and generation, hence enhancing the local plasticity of the material and causing easier failure. This theory was first presented by Beachem [251].

(5) Hydrogen-rich phases can form having different mechanical properties to the matrix which lower the fracture stress and produce a preferred fracture path. This model has been reviewed by Westlake [252].

(6) Hydrogen can adsorb on dislocations preferentially and can thus produce localised areas of high hydrogen concentrations which can embrittle the lattice or restrict dislocation motion.

Bastion and Azou [253] first proposed such a mechanism and this has since been supported by others [254,255].

The cohesive strength mechanism has been severely criticised by Bernstein et al [239] and by Bernstein and Thompson (256) since, although they considered that it is possible for dissolved hydrogen to reduce the cohesive energy of the lattice, they could not see how this could be done with the necessary sensitivity, precision and selectivity or to be capable of wide variations in different alloys of different crystal structures, stacking fault energies and electronic properties.

Thus for most alloy systems they consider this process will not be the dominant one. Oriani [257], however, has supported and modified the idea suggesting that in a region of a few atomic distances from the crack-tip dissolved hydrogen accumulates in non-Hookean regions where elastic stresses attain significant fractions of the elastic modulus. If accumulated hydrogen can here lower the cohesive strength below the value of the local tensile strength then fracture will occur. Rice [258] and Van Leeuwan [259] also support these ideas. Although such a mechanism is obviously feasible no clear concept of the manner in which hydrogen can reduce cohesive strength has been proposed. These ideas are very similar to those proposed to explain liquid metal embrittlement[260,261]. This mechanism has been criticised further because hydrogen-assisted cracks normally exhibit microscopic ductility [262].

The pressure exertion model found much support in earlier investigations. Gerberich et al.[263] working on high strength steel, Cox and Gudas [264] working on titanium alloys and Tetelman [265], supporting a combination of a lowering of cohesion and pressure build up in microcracks, have all lent support to such a mechanism. Louthan [247] modified the mechanism slightly suggesting that hydrogen could be transported by dislocations and the interaction of dislocations could form a microcrack, into which their hydrogen atmosphere would be released. This, he proposed, can create localised hydrogen pressures well over 10^6 atmospheres for low carbon and austenitic steels, producing stresses in excess of the fracture stress. Some criticism of this mechanism has been made by Johnson [266] since HAC can occur in low pressure hydrogen. Louthan [267] also considers that the theory fails to explain re-initiation of HAC by small changes in external hydrogen pressure which have been observed. It is worthwhile here restating that some of the hydrogen pressures calculated to occur in microvoids such as 10^6 atmospheres in austenitic steel[247]

are only theoretical values which will probably not occur in practice since the back pressure which would be exerted would be enough to obtain the diffusion of hydrogen out of the metal, steels having quite fast diffusion rates, 9×10^{-9} mm ^{2}/sec at room temperature [268]. This however, does not invalidate the mechanism if we consider that much lower pressures will aid crack propagation in metals.

The surface energy mechanism has been cited as a necessary but insufficient cause of HAC [248]. It has also been criticised by Louthan [267] as inconsistent with the inhibition of embrittlement by oxygen which is more readily adsorbed than hydrogen and should hence lower the surface energy more.

The increased plasticity model is a fairly recent one and has gained support from fractographic evidence [251,262]. Louthan [267] objects to it, however, because of observations that delayed fracture can occur under conditions where little or no macroscopic strain precedes fracture.

The hydride formation model is obviously appropriate for alloy systems in which hydrides can be formed e.g., zirconium alloys [269] and uranium alloys [270]. It cannot, however, be considered a general mechanism because HAC occurs in other systems. Furthermore Bernstein et al. [239] have found that titanium as an alloying addition can reduce susceptibility to HAC by acting as a chemical trap and reducing the amount of hydrogen available for cracking.

The dislocation transport mechanism has gained much support [255,271,272,273]. The theory is often modified to supplement one of the other five mechanisms because it cannot be considered a mechanism for HAC in its own right. This said, however, there is much evidence that dislocations and other structural defects act as hydrogen trap sites. Laurent et al [274] using autoradiographic techniques with pure iron and a maraging steel, have shown that structural defects such

as grain boundaries, sub grain boundaries, carbides and carbonitude interfaces and dislocations are active trapping sites.

Louthan [267] noted that there are well over 3,000 references concerned with HAC so that it has been possible here to review just a small fraction of the available literature. It is evident, however, that no mechanism suggested up to the present time can completely explain HAC behaviour. It is thus likely that no universal mechanism applies and the dominant mechanism depends on the conditions. Finally it is instructive to quote a statement Thompson [275] made in a conference discussion:

> "I want to make two comments. First, the fact that different test techniques tend to emphasize different effects means that at least some of the conflict in the literature is more apparent than real. Second, at least some of the published mechanism-oriented studies have been by authors with an axe to grind, so that the conclusions may be less than general if not open to downright suspicion".

The use of HAC mechanism have been extended by some workers to explain corrosion-fatigue [151,188,233]. Although conditions can be envisaged in which HAC can dominate corrosion-fatigue behaviour it must be recognised that HAC does not require a cyclic stress and so its involvement in corrosion-fatigue must be considered an exacerbating factor rather than a prime cause, as with intergranular corrosion, pitting etc.

3. EXPERIMENTAL PROCEDURES

3.1. Material

The material used throughout this project was an austenitic stainless steel made to the specification AISI 316. This material consisted of three batches, two of plate of different thicknesses SS1 and SS2 and one of round bar SS3, all supplied in the fully annealed and pickled condition with the chemical compositions and dimensions as given in table 3.1. The differences in chemical composition were not significant in the present work because each batch was used for a self-contained series of experiments.

3.1.1. Material Characterisation

Samples were taken in the rolling direction for mechanical testing, yielding the mechanical properties given in table 3.2. A typical microsection of the material is illustrated in figure 3.1, which shows the expected structure.

3.2 Rotating-Bending Fatigue Experiments

The purpose of these experiments was to confirm the effect of local corrosion damage, exemplified by pits, on the fatigue properties of the material. The following sections describe the procedures used.

3.2.1. Test-pieces

Prior to machining into rotating-bending fatigue test-pieces, the bar stock material (SS3) was straightened and given a de-sensitising heat-treatment by soaking for one hour at 1050^{o} C and water quenching. The type of test-piece used was as shown in Figure (3.2), commonly referred to as type K70B. The machining procedure was as follows:

(i) The bar was turned down to a cylinder 7mm diameter

(ii) The 38mm radiused profile was cut leaving the minimum test-piece diameter 0.127mm oversize

(iii) The test-piece was turned to final size with three cuts,

the first two 0.025mm deep and the last 0.013mm deep.

(iv) The turned test-piece was polished transversely with 240 grit emery cloth in the lathe.

(v) The rough polished test-piece was polished longitudinally with successively fine emery papers down to 1200# by hand.

(vi) The test-piece was finally polished with a fine metal polish, making sure that no transverse machining or polishing marks were visible.

3.2.2. Rotating-bending fatigue test machine

The basic machine is illustrated in Figure (3.3). It consists of a ¼ H.P. motor running at 3000 revolutions per minute (50 Hz) which carries a chuck on its shaft. A second chuck is connected by a loading arm to a fork, which is attached to a balanced lever carrying a jockey weight by which the required bending stress can be applied. The elapsed time of the test is recorded by a meter and is converted to cycles of stress. The motor and meter are switched off automatically by a micro-switch operated when the test-piece fractures.

3.2.3. Fatigue Test Procedure

The following procedure was followed in setting up a test in the fatigue machine.

(i) The minimum diameter of the critical section of the test-piece was measured and the required reverse bending stress to be applied was selected and used to calculate the jockey weight setting.

(ii) The jockey weight was set to zero and lightly clamped.

(iii) The test-piece was fitted into the chuck on the loading arm, pushed home and the chuck tightened.

(iv) The other end of the test-piece was fitted into the chuck on the motor shaft, pushed home and the chuck carefully tightened, ensuring no bending of the test-piece.

(v) With the lower end of the fork steadied, the motor was switched on and the jockey weight moved to the required position and clamped.

(vi) The reading on the meter was noted at the beginning and end of the test so that the cycles to failure could be ascertained.

Two air fatigue S/N curves were determined using this method, one for polished test-pieces and the other for test-pieces pre-pitted as described in the following section 3.2.4.

3.2.4. Pre-pitting treatment

The test-pieces were pre-pitted under potentiostatic control; to allow for mounting in a standard potentiostat sample holder, a 6mm deep hole was drilled and tapped into one end. Before pre-pitting the test-pieces were masked with 'Lacomit' lacquer, exposing only the gauge length to the solution, to prevent spurious local corrosion elsewhere.

A 3% aqueous solution of sodium chloride was used. As a preliminary a full anodic polarisation curve was determined by the method described in Appendix A. This curve was used to select a fixed potential such that pitting would occur and the fatigue test-pieces were held at this potential in the solution for a fixed time prior to fatigue testing. For this purpose a potential of +300mV vs. SCE was chosen. After the pre-pitting treatment the test-pieces were thoroughly washed in distilled water, cleaned in an ultrasonic bath and finally thoroughly degreased ensuring that as far as possible no salt or grease was left on the test -piece which could affect the subsequent fatigue result.

TABLE 3.1

Chemical Analysis of Material

Material Designation	Dimensions	C	Si	Mn	P	S	Cr	Mo	Ni	B	Co	Cu	Nb	Ti	N
SS1	4mm thick plate	0.043	0.35	1.66	0.037	0.018	16.8	2.44	11.6	0.003	0.26	0.25	<0.1	0.024	0.036
SS2	3mm thick plate	0.038	0.41	1.51	0.028	0.011	16.7	2.35	11.8	0.001	0.20	0.27	0.01	0.03	0.052
SS3	12mm diameter bar	0.041	0.28	1.62	0.024	0.013	17.07	2.66	13.04	0.002	0.17	0.31	0.10	0.05	0.018

TABLE 3.2

Mechanical properties of the Material

Material Designation	Ultimate Tensile Stress ($MN\ m^{-2}$)	0.2% Proof Stress ($MN\ m^{-2}$)	Per cent elongation *
SS1	640	320	59
SS2	630	310	61
SS3	610	300	60

* For a 50mm gauge length

3.3 Reverse Bend Corrosion-Fatigue Test Rig

The test rig was designed and built at Brunel University for flat-plate test-pieces using a reverse bend loading mode. This mode was selected to enable the use of a simple machine operation typical of most reverse-bend fatigue rigs and to take advantage of easy determination of life to failure at different stress levels and in different liquid environments.

Figure 3.4 is a photograph of the fatigue rig set up for an air fatigue test.

The mode of operation is as follows:
The electric motor rotates the flywheel which incorporates an adjustable eccentric bearing. This bearing is in turn attached to a connecting rod which converts the rotation into the reverse bend motion applied to the test-piece, bending it backwards and forwards about a mean position.

The deflection applied to the test-piece can be varied by adjusting the eccentricity thus determining the stresses applied to the test-piece. These stresses depend upon the material and test-piece configuration so that calibration is required for every batch of samples. This was accomplished by measurement of deflections resulting from the direct application of known loads to a representative test-piece yielding a deflection versus load curve. From the known applied load the actual stress on the critical section of the test-piece can be calculated giving a direct correlation between stress and deflection. It is this stress which is normally quoted in recording results from reverse bend tests. It must be noted, however, that these tests are constant strain tests and the nominal applied stress refers strictly to only the first bend of the test-piece.

The range of deflection for the test rig described is $\pm$ 25mm, but in practice such large deflections were not used, the maximum

being of the order of $\pm$ 12mm. The adjuster on the connecting rod enables any required mean stress value to be imposed, and also allows for minor adjustments to accommodate slight variations in test-pieces.

The electric motor has a rated power of 2.25 KW, operating on a three phase supply at a fixed speed of 24 Hz and is protected against overloadfng by a centrifugal clutch coupling which engages only when the motor has attained its constant speed; this enables the inertia of the system to be overcome allowing smooth starting. There is the added advantage that if for any reason the test-piece is unable to bend, this clutch slips, protecting the motor from damage.

The number of revolutions of the motor shaft and hence the number of bend cycles is recorded by the counter, actuated by the main drive shaft via a 100 : 1 reduction gear and a toothed drive belt.

When the test-piece breaks,elastic bands (not shown) separate the two broken halves of the test-piece and the micro-switch is actuated, stopping the motor with the counter registering the number of cycles to failure.

For corrosion-fatigue tests the test-piece is surrounded by any required liquid environment contained in the test-cell shown in position in Figure 3.5. Figure 3.6 illustrates the design of the test cell. It is surrounded by a water bath which can be used to control the temperature of the test environment. A rubber 'O' ring (1) is used to make the seal between the test cell and the bottom mount by tightening a washer (2) via a screw arrangement (3). The test cell can be readily filled with a liquid medium when in position and emptied by syphoning at the end of the test. The water bath is completely sealed from the test cell and it is unnecessary to empty it between every test. The test cell is large enough to allow for the insertion

of probes and electrodes required for electrochemical experiments during a corrosion-fatigue test. It is essential in such electrochemical experiments that the test-piece be completely isolated electrically from the other metal parts of the test rig to avoid galvanic effects. This isolation was provided by "Tufnol" washers inserted between the test-piece and the mounting brackets and clamping plates, also "Tufnol" bushes were inserted into the bolt holes in the test-piece. It was also necessary to isolate the bottom mount from the rest of the machine using a resilient nylon material, to prevent interference with the electrochemical measurements.

The setting up procedure for test-pieces is somewhat complicated and is described in section 3.7.

3.4. Reverse-Bend Fatigue Test-Pieces

Test-pieces were machined from the rolled sheet material to the drawing given in Figure (3.7). The sheet was first cut to suitable rectangular coupons with the rolling direction longitudinal. The edges of these coupons were milled down to the final dimensions, 139.7 x 50.8mm and the "waist" was formed using a 38.1mm radius milling cutter. A specially built jig was used for drilling the eight holes which were finished by reaming. Care had to be taken not to mark the test-piece surface and not to generate excessive heat in the machining operations.

The test-piece surfaces were abraded with four successive grades of emery paper, 180, 320, 400 and 600 #. The abrasion with the 180# paper was in a direction parallel to the longitudinal axis and was used to remove the rough pickled surface and any other surface markings. Abrasion with subsequent paper grades was carried out in differing directions, with the final polish in the longitudinal direction. The sides of the test-pieces were also polished by this method and the sharp edges slightly smoothed. The test-piece was thoroughly washed

in water between each grade of paper to avoid carrying coarse grit over to finer polishing operations.

After polishing, the test-piece was thoroughly washed in a liquid detergent solution and water with a final rinse in distilled water, followed by alcohol after which it was allowed to dry in air. This treatment was to ensure that the test-pieces were well degreased.

3.5. Testing Environments for the reverse-bend Fatigue Experiments

3.5.1. Air

The air fatigue tests were performed in ordinary laboratory air with an ambient temperature generally in the range 16° C to 25° C.

3.5.2. Sodium Chloride Solution

'Analar' grade sodium chloride was dissolved in distilled water to give a concentration of 30g dm^{-3} (0.51M). This concentration was chosen because it is approximately equal to that in seawater.

3.5.3. Sodium Sulphate Solution

Analar grade sodium sulphate was dissolved in distilled water to give a concentration of 30g dm^{-3} (0.21M). The conductivity of this solution is similar to that of the sodium chloride solution, but the sulphate ion is innocuous being neither aggresive nor passivating.

3.5.4. Potassium Dichromate Solution

Analar grade potassium dichromate was dissolved in distilled water to give a concentration of 30g dm^{-3} (0.1M). The dichromate ion is passivating.

All these solutions are approximately neutral with pH $\sim$ 7. They were not deoxygenated and the temperature was held constant at 25° C.

3.6. System for Electrochemical Control and Measurement during Corrosion-Fatigue

As already stated in the introduction , the concept underlying the present work depended on the application of equipment for electrochemical control and measurement not available at the outset. Many difficulties were encountered during the development of a suitable system. This section, therefore, describes both the equipment in its original form and its progressive development throughout the course of the work.

3.6.1. Application of the Potentiostat

The potentiostat has rapidly become standard equipment in corrosion studies but the vast majority of investigations have been concerned with static test-pieces. The development of the present fatigue rig included provision for measurements under potentiostatic control during the course of the fatigue tests. Severe practical difficulties were experienced due to difficulties of earthing the apparatus,mains induced hum, extraneous interference and interference from within the system. These were overcome by various means,as follows:-

(i) A screened reference electrode lead was used, with its sheathing connected to the counter electrode terminal of the potentiostat to prevent the lead acting as an "aerial" picking up interference.

(ii) The counter electrode lead was also screened, the outer sheathing being connected at one end to the test-piece and at the other end to a common earth terminal.

(iii) All auxiliary equipment was disconnected from the line mains earth and connected to a common earth terminal, grounded via the potentiostat line mains.

(iv) A slave circuit, was incorporated into the microswitch so that it carried only

a small current, reducing the chance of mains-induced hum.

(v) The water-bath was surrounded by a faradaic cage enveloping three sides of the bath, the side towards the potentiostat being left open. This provided good screening from the motor and the three phase supply.

As well as the normal potentiostatic tests, e.g. the determination of anodic polarisation characteristics or held potential runs, the equipment was required for the detection and measurement of the transient behaviour of the corrosion during fatigue and for this reason the hum had to be kept to an absolute minimum. By the methods described above it was found that the interference could be substantially reduced, but not sufficiently to allow the measurement of the expected current transients. It was thus apparent that greater attention was required in reducing hum. Nevertheless it was found by experiment that a fluctuation of the D.C. potential difference between the counter and working electrode (with a good signal to noise ratio) could be observed during fatigue cycling. This signal had the same frequency as the fatigue cycling (24Hz). Its precise significance will be dealt with in more detail in the discussion, but suffice it here to say that although the signal undoubtedly proved that it was possible to distinguish and measure the transient changes in corrosion properties for test-piece during fatigue, more development was needed to extract for measurement a parameter of more direct significance.

The parameter usually measured in a potentiostatic test is the corrosion current so it is more logical to try to measure the transient changes in this parameter during a corrosion-fatigue test. As has already been mentioned the principle difficulty in measuring such a parameter was the level of main-induced hum interference at 50 Hz. A considerable reduction in the hum level was achieved by the simple expedient of moving the reference electrode away from the vicinity

of the working electrode and enclosing it in its own faradaic cage; this also reduced problems which had been experienced due to the vibration of the reference electrode stimulated by the cyclic loading which interferred with the current transient signal and made it difficult to measure.

The residual hum, however, was still too great to allow the measurement of the current transient signal and it was apparent that a completely new technique of reducing interference had to be developed and this will be discussed in the appropriate context in Section (3.6.3).

3.6.2. Measurement of the fluctuation in Potential

This was the original method employed and it presented the least experimental difficulties. The test-piece was made the working electrode in the test cell filled with the selected solution and was arranged in a circuit with a reference electrode and a counter electrode connected to a potentiostat in the normal manner. Measurements could then be made for prescribed values of potential and sample lifetime. An oscilloscope display was used for the detection and measurement of the potential transients occurring between the counter and working electrode during fatigue cycling, using the circuit shown in Figure (3.8).

A simple magnet/reed-switch triggering circuit as shown in Figure (3.8), synchronised the scanning rate of the oscilliscope with the operating frequency of the fatigue machine.

3.6.3. Measurement of the Fluctuation in Corrosion Current

This method required the insertion of a known resistor in the working electrode lead to act as a shunt for measurement of the corrosion current. Thus an important consideration was to choose a resistor which would not interfere with the normal operation of the potentiostat. The transient signal produced across the resistor

was found to be very small requiring amplification for display on the oscilliscope. In selecting a suitable amplification technique it is important to remember that the transient it is required to amplify is an A.C. signal superimposed on a D.C. signal which can be relatively large. The original circuit devised and built is shown in Figure (3.9). The main feature of this circuit is two field emission transistor operational amplifiers which amplify the A.C. component of the D.C. signal. It was found necessary to have floating earth inputs but with an earthed output for the oscilloscope, This method proved to be totally unsatisfactory for measuring the current transients because the oscilloscope, coupled as it was into the potentiostat measuring circuit, caused earth loop problems which were reduced by the use of the common earth system described earlier but not completely resolved. In addition, the circuitry of the amplifier and associated equipment acted as a large "aerial" picking up much interference and effectively masking the current transient signal.

A method thus had to be found of preventing this interference by electrically separating the potentiostat circuit from the oscilloscopic current transient circuit while still allowing the transfer of the required information to the oscilloscope. For this purpose an opto-isolation circuit was designed to insert an optical link into the circuit. To complete the required electrical separation the optoisolator and associated amplifiers were independently powered with dry cells. The optoisolator is an infra red light emitting diode coupled with a silicon photo transistor as shown in Figure (3.10a). This allows high speed transfer of the signal with excellent noise immunity. The original circuit which employed such a device, illustrated in Figure (3.10b), worked very well although some disadvantages attended its use necessitating the improvements discussed in detail later in this section. The technique proved, however, that it was indeed possible to extract, display and measure the corrosion current

transients occurring in fatigue.

The procedure for the use of this original circuitry was as follows:

(i) The potentiostat was set-up in the usual manner so that the corrosion current could be measured during the course of electrochemical experiments

(ii) A suitable current shunt was selected in the optoisolator circuit and the value noted.

(iii) The various batteries powering intermediate equipment were connected

(iv) The offset adjustment provided, shown in Figure (3.10b) was set to bring the signal within the operating range of the optoisolator.

(v) The fluctuating signal was displayed on the oscilloscope and appropriate measurements were made during the course of electrochemical experiments.

The disadvantages of this system were:

(i) The offset adjustment was difficult and uncertain because no means were provided to ensure that the signal applied to the optoisolator was within its linear operating range.

(ii) The unsteady oscilloscope trace was amenable neither to accurate measurement nor to detailed studies of waveform.

(iii) Observations required the continuous presence of an operator so that the development of the transient signal could not be adequately monitored during the longer tests.

These disadvantages were resolved by the circuit improvements together with the replacement of the standard oscilloscope with digital storage oscilloscope as illustrated in Figure (3.11).

These improvements required a modified operating procedure as follows:

Steps (i) and (ii) of the procedure are the same as for the original equipment.

(iii) The optoisolator was switched on and the condition of the batteries checked by selecting the appropriate switch positions.

(iv) By suitable adjustment of the input and amplifier A1 offset potentiometers, the value across the diode of the opto-isolator was set to + 1.15V, a value within the linear operating range of the optoisolator. This condition is reached when the level indicator shows a half scale deflection.

(v) Amplifier A2 was used, when required, to amplify the signal still further so that it was suitable for display on the oscilloscope.

(vi) The offset of amplifier A2 was adjusted, when necessary, such that the signal was in the range of the oscilloscope. It should be noted that this offset adjustment varies the D.C. level of the signal and not the magnitude of the fluctuating signal.

(vii) The signal was displayed on the storage oscilloscope and samples of the fluctuating signal were printed out on the pen recorder as required during electrochemical tests.

(viii) If continuous monitoring was required the automatic record system was activated with the drum timer set to take samples of the fluctuating signal at the required time intervals during electrochemical tests.

3.7 Experimental Programme for Reverse-Bend Fatigue Rig

3.7.1. Stressing Pattern

All reverse-bend fatigue experiments were conducted at a constant frequency of 24Hz, with a zero mean stress level and a sine wave stress configuration. Tests were carried out for nominally constant, pre-selected stress levels. Complete S/N curves were determined for the material in air and 0.51M aqueous sodium chloride solution to determine appropriate stress levels to be used for the tests under potentiostatic control.

3.7.2. Determination of Cycles to Failure (N_F)

The results obtainable using the fatigue test machine alone are limited to the Life-to-Failure of fatigue test-pieces at prescribed stresses. The additional information obtained in the course of such experiments, by application of the new electrochemical facility, is given later in Section 3.7.3. Tests were terminated if the test-piece sustained 5×10^7 Hz without fracture, which occurs in about three weeks. This limit was necessary as only one fatigue test machine was available for the tests.

The procedure for setting-up a test-piece was as follows:

(i) The test-piece was first prepared as described in Section 3.4.

(ii) Tufnol bushes were placed into the eight bolt-holes of the test-piece.

(iii) The test-piece was firmly bolted to the bottom mount using four bolts and the clamping plate with the bevelled edges. Tufnol washers were placed between the test-piece and both the bottom mount and clamping plate prior to clamping.

(iv) The water bath, with a tight-fitting polythene tube around the test cell to contain splashing and reduce evaporation, was lowered around the test-piece and bottom mount. The rubber 'O' ring was then placed into position around the bottom mount and compressed, using a washer and specially designed nut to effect a water-tight seal.

(v) A "zeroing plate" to determine the position of the neutral axis of the test-piece was then clamped to the top of the test-piece using a clamping plate, tufnol washers and four bolts.

(vi) A dial gauge with a magnetic base was then positioned so that it was zeroed against the zeroing plate at a mean point within its range. Engraved on the zeroing plate was a cross line corresponding to the axis of the pin through the yoke to provide the correct point of reference for zeroing.

(vii) The zeroing plate was removed, taking care not to disturb the dial gauge, and the yoke was bolted into place, taking care to replace the insulating washers and, once again, not to disturb the dial gauge.

(viii) The amount of deflection in each direction measured via the dial gauge was equalised by adjustments to the length of the connecting rod so that a mean stress value of zero was obtained.

(ix) The deflection required was ascertained from the calibration curve in figure A1. By loosening the clamping ring on the fly wheel and adjusting the eccentric wheel, this deflection was set via

the dial gauge and the clamping ring was then retightened.

(x) The dial gauge was removed.

(xi) The microswitch was bolted into position and the elastic bands were attached.

(xii) If required, the water bath was filled with water and the water heater placed in position.

(xiii) The test cell was filled with a prescribed aqueous environment, if required, and the surface was covered with croffles to reduce evaporation and splashing. The top of the polythene tube was secured around the test-piece to further reduce these effects.

(xiv) The microswitch slave circuit was switched on the counter set to zero and the test started.

Obviously for air fatigue tests the water bath was omitted because it was unnecessary.

The arrangements for tests in an aqueous environment and in air are shown in the photographs given in Figures 3.5 and 3.4 respectively.

3.7.3. Electrochemical Tests

Test-pieces upon which electrochemical tests were to be performed were masked so that only a known surface area on one side of the test-piece was exposed to the aqueous environment. To achieve this, all of the test-piece was given two coats of "Lacomit" lacquer except an area 2 x 2cm on the surface facing the Luggin probe, at a distance of 6.5cm from the top of the test-piece. The first and second coats were allowed to air dry for 15 and 60 minutes respectively. The exposed area of the test-piece was thoroughly degreased using detergent solution, water and alcohol washes in sequence before the experiment. The setting up procedure was then carried out as described

in section 3.6.2, with slight modifications appropriate to the electrochemical tests. Before securing the polythene bag the reference electrode, salt bridge, luggin capillary and counter electrode were positioned. The complete arrangement is shown in Figure (3.12). Various electrochemical experiments were then conducted on the test-pieces according to the following brief descriptions:

(a) Determination of Anodic Polarisation Characteristics

Anodic polarisation characteristics were determined for test-pieces under both static and dynamic (i.e.fatigue) conditions for all three of the standard aqueous environments described, using the ASTM recommended method given in Appendix A. During dynamic anodic polarisation runs the magnitude and form of the transient corrosion behaviour were recorded. For comparison, anodic polarisation characteristics were also determined in a normal potentiostatic test cell using specimens of standard shape and dimensions, i.e. cylinders of 4 cm^2 surface area, but in non-deaerated solutions.

(b) Fixed Potential Runs

The potential of the test-piece was set at a constant predetermined value. The corrosion current was recorded as a function of time for dynamic (i.e. fatigue) conditions and the effect of applied potential on fatigue life noted. During these runs the magnitude and form of the transient corrosion behaviour was recorded.

(c) Free Potential Runs

The test-piece was allowed to attain its free corrosion potential which was monitored during the fatigue life.

3.8 Presentation of Results

3.8.1. S/N Curve

This is a well-established method of presenting fatigue data in which the number of cycles to failure (N_F) is plotted as a function of peak stress (S). The curves are plotted on log-linear paper, N_F values being plotted on the logarithmic axis for convenience. The scatter of fatigue results can be large so that experiments must usually be repeated about five times and an average value taken. This would have been far too time consuming for the present work using one fatigue machine, because to obtain a typical S/N curve would have taken about six months. For this reason only three results were taken for every value of applied stress, the logarithmic mean value (N_F) being calculated from these three values (N_1, N_2, N_3) i.e. using the equation:

$$\log N_F = \frac{\log N_1 + \log N_2 + \log N_3}{3} \quad \ldots\ldots\ldots\ldots 78$$

3.8.2. Electrochemical Experiments

Many types of electrochemical experiments were conducted. These measurements are novel and the method of presentation is most conveniently described when the results are given in the next section.

3.9 Examination of Fractured Test-Pieces

3.9.1. Macrofractography

The features noted from a visual examination of the fracture were:

(a) Shape - The main feature here was the direction of fracture with respect to the stress axis. The angle of the fracture to the stress axis was recorded, i.e. 0° and 90° cracks are parallel and normal to the stress axis respectively.

(b) Multiple Cracking - Cracks secondary to that which has propagated to cause final fracture may be observed in some test-pieces. The number and extent of such cracks were recorded.

(c) Branching - Limited observation of crack branching can be made by inspecting the side of the test-piece and this effect was noted where it occurred.

3.9.2. Microfractography

Many fractures were examined using the scanning electron-microscope. This technique was chosen in preference to transmission electron-microscopy of replicas taken of the fracture surface, because it reveals all of the essential information with minimal sample preparation and the whole fracture surface can be examined at the same time. Samples for examination in the scanning electron-microscope were prepared by the following procedure:

(i) The whole fracture of interest was sawn off the broken test-piece,

(ii) If necessary, the fracture sample was stripped of any corrosion product using an inhibited chemical bath consisting of 6M HCl + $2g/dm^3$ hexamethylene tetramine. The sample was immersed in the bath for 1 - 15 min. and lightly brushed. Short periods (5 secs.) in an ultrasonic cleaner were found to assist the stripping action. Before applying the procedure for stripping the corrosion product the samples were viewed in the electron-microscope and details recorded.

(iii) The fracture sample was mounted on the specimen stub.

It was generally found that coating the samples with

gold prior to examination was not advantageous so that observations were made on uncoated specimens.

Many features were noted in the course of examination in the electron-microscope, as fully described in the results section.

4. EXPERIMENTAL RESULTS

4.1. The effect of Pre-pitting on Fatigue Life

Figure 4.1, gives S/N curves for material S.S.3 in air determined by rotating bend tests comparing un-pitted and pre-pitted test-pieces. At least triplicate results were obtained for each stress level.

4.1.1. Un-pitted test-pieces

As is characteristic for stainless steel, the curve exhibits a definite fatigue limit in air at 300 MN m^{-2}, i.e. at about 50% of the ultimate tensile strength (610 MN m^{-2}).

4.1.2. Pre-pitted test-pieces

At all stress levels the pre-pitted test-pieces have lower endurance than the un-pitted test-pieces, and exhibit no fatigue limit.

4.2. Reverse-Bend S/N Curves

Figure 4.2, gives S/N curves for alloy S.S.2 in air and 3% (0.5M) aqueous sodium chloride solution determined using reverse-bend fatigue tests.

4.2.1. Air

As before the air S/N fatigue curve exhibits a fatigue limit at 340 MN m^{-2}, i.e. at about 50% of the ultimate tensile stress (630 MN m^{-2}). It is evident that the scatter in replicate results increases as the fatigue limit is approached.

4.2.2. 3% (0.5M) Sodium Chloride

At all stress levels the endurance in sodium chloride solution is less than that in air. This curve exhibits no fatigue limit, although the fatigue life increases with decreasing stress. The reduction in fatigue life as compared with air becomes much less pronounced as the applied stress is increased. There is generally more scatter in the results for sodium chloride solution than for air.

4.3 Static and Dynamic Rest Potentials

During the course of the more extensive electrochemical experiments the values of the steady-state corrosion potential (E_R) of the test-pieces, both static and dynamic (i.e. in fatigue) were recorded, referred to the Standard Calomel Electrode Scale (S.C.E.) these are quoted in Table 4.1.
The essential features of these results are:

(a) the static rest potential, E_R, is progressively more noble in the sequence, sulphate, chloride, dichromate and varied for different test-pieces.

(b) at the onset of fatigue E_R shifted in every case to a new constant value, reached after about 20 minutes, corresponding to the imposition of about 30,000 stress cycles. Despite the variation for different test-pieces, the shift was always in the same sense for a given solution.

4.4. Polarisation Characteristics for Static and Dynamic Conditions

Anodic polarisation characteristics were determined for fatigue test-pieces under both static and dynamic (i.e. fatigue) conditions in the three test solutions without deaeration.

4.4.1. 3% (0.5M) sodium chloride solution

Figure 4.3, shows the anodic polarisation characteristics determined for both static and dynamic conditions. The results for the dynamic conditions were obtained after the imposition of 2×10^6 cycles. The anodic polarisation curve for static conditions exhibits the expected behaviour. There is a passive range from the rest potential to +150 mV during which a small passive current flows which increases as the applied potential becomes more positive.

TABLE 4.1

Comparison of Rest Potential, E_R for test-pieces both static and fatigue

Environment	Test potential, E_R mV(SCE)			
	Static Test-pieces		Dynamic Test-pieces 250 MN m^{-2} 24 Hz	
	Average	Range	Average	Range
0.5M Chloride Solution	-160	-100 to -200	-180	-120 to -290
0.2M Sulphate Solution	-270	-240 to -300	-170	-100 to -120
0.1M Dichromate Solution	+20	0 to +40	+350	+290 to +410

Above +150 mV there is a rapid increase in current corresponding with the onset of pitting.

The anodic polarisation characteristic for dynamic condition shows the same general form as the static condition but with the following significant points of difference:

(i) The value of the rest potential (E_R) is more negative

(ii) The current flowing in the passive region is greatly increased.

(iii) The pitting potential at which the passive range is terminated is less distinct but is at significantly less noble values.

Figure 4.4. shows a family of anodic polarisation characteristics for dynamic conditions determined after different numbers of cycles during a fatigue test; the number of cycles quoted denotes the elapsed life at which every anodic polarisation test was commenced. For comparison the result of a determination of the anodic polarisation characteristics for static conditions, before commencing the fatigue test, are indicated.

The same basic differences are apparent between the curve for static conditions and those for dynamic conditions, but the following additional information is apparent:

(i) During the fatigue life the current in the passive range first increases then decreases again.

(ii) As the number of elapsed cycles increases, the pitting potential becomes so indistinct that no value can be defined for it.

(iii) The rest potential remains virtually constant throughout.

It is very important to note that all these experiments were performed at a low stress i.e. $\pm$ 250 MN m^{-2} for which the

test-pieces would fail only after relatively long fatigue lives. Figure 4.5 shows the anodic polarisation characteristic determined during the fatigue life at a higher stress, i.e. $\pm$ 320 MN m^{-2} which is sufficient to cause failure in a short time i.e. after approximately 5 x 10^5 elapsed stress cycles, in this case the pitting potential decreased and the passive current increased throughout the fatigue life. The rest potential again remains fairly constant, becoming only slightly less noble.

4.4.2. 3% (0.2M) Sodium Sulphate Solution

Figure 4.6 shows the anodic polarisation characteristics determined under static and dynamic conditions for a stress of $\pm$ 250 MN m^{-2}. The polarisation characteristics under static conditions exhibit an extensive passive range from the rest potential to about + 800 mV, this corresponding with the onset of transpassivity. The polarisation characteristics under dynamic conditions are essentially of the same form but with the following significant differences:-

(i) The rest potential is shifted to more noble values.

(ii) The current flowing in the passive range is increased.

(iii) The potential at which passivity is terminated (i.e. at the onset of transpassivity) is decreased.

Figure 4.7 shows the anodic polarisation characteristic under static and dynamic conditions at a stress level of $\pm$ 320 MN m^{-2}. The same general characteristics are apparent.

4.4.3. 3% (0.1M) Potassium Dichromate Solution

Figure 4.8 shows the anodic polarisation characteristics for static and dynamic conditions at $\pm$ 250 MN m^{-2}. The curve for static conditions exhibits very small passive currents throughout an extensive passive range extending from the rest potential up to + 1,000 mV i.e. at the onset of transpassivity.

Under dynamic conditions the characteristics are essentially the same with the following significant differences:

(i) The rest potential is increased to more noble values

(ii) The anodic current flowing in the passive range is increased.

(iii) The potential at which the passive range is terminated is much less distinct and is significantly less noble

Figure 4.9 shows the anodic polarisation characteristics under both static and dynamic conditions at $\pm$ 320 MN m^{-2}. The same features are evident as for $\pm$ 250 MN m^{-2}.

4.5 Measurement of Potential Fluctuations during Fatigue

This was the original method employed to measure cyclic changes in corrosion characteristics during fatigue, manifest by fluctuations in the potential difference between the counter and working electrode. This fluctuating signal was approximately sinusoidal with a frequency of 24 Hz, matching that of the loading cycle. Its amplitude, i.e. the peak to trough height, was measured as a function of the applied potential during anodic polarisation runs in the three aqueous environments at a stress level of $\pm$ 250 MN m^{-2}.

4.5.1. 3% (0.5M) Sodium Chloride Solution

Figure 4.10 gives the amplitude of the fluctuating potential as a function of the applied potential determined after 180,000 elapsed cycles. The anodic polarisation characteristic for dynamic conditions determined simultaneously is included to aid in interpretation. The following important features are apparent from this figure:

(i) On the initial application of anodic polarising potentials the fluctuating potential falls, at first rapidly and then more gradually up to a potential of about + 100 mV.

(ii) At the onset of pitting, i.e. about + 100 mV, the

fluctuating potential falls rapidly to a constant value at about + 300 mV.

Figure 4.11. shows a family of such curves determined after different numbers of elapsed cycles. It is evident from these curves that the value of the fluctuating potential in the passive range increases generally with the number of cycles.

4.5.2. 3% (0.2M) Sodium Sulphate Solution

Figure 4.12. gives the amplitude of the fluctuating potential as a function of the applied potential determined after $2x10^6$ elapsed cycles, together with the anodic polarisation for dynamic conditions determined simultaneously. This figure shows that on initial application of the anodic polarising potential the fluctuating potential falls rapidly and then assumes an approximately constant value until the applied potential exceeds about + 800 mV. It then decreases as the potential is still further increased ultimately reaching a constant value.

4.5.3. 3% (0.1M) Potassium Dichromate Solution

Figure 4.13. give the amplitude of the fluctuating potential as a function of applied potential determined after 100,000 elapsed cycles, together with the anodic polarisation characteristics for dynamic conditions determined simultaneously. This figure shows that the fluctuating potential amplitude falls rapidly from the rest potential to an approximately constant value and at about + 800 mV it then decreases again, reaching a constant value at about + 1,000 mV.

4.6. Measurement of Corrosion Current Fluctuations during Fatigue

The results given in this section were obtained by methods which superceded the measurement of potential fluctuation for the reasons given in Section 5.3.3 of the discussion.

4.6.1. Results from Preliminary Experiments

Figures 4.14 and 4.15 present results to compare the use of fluctuating potential and fluctuating current as parameters to evaluate the cyclic corrosion behaviour of test-pieces under fatigue. The results for fluctuating current signals were obtained using the original circuit design illustrated in Figure 3.10b. In both Figures 4.14 and 4.15 the two types of fluctuating signal are given as functions of applied potential for test-pieces undergoing fatigue in 0.51 M sodium chloride solution at a stress of $\pm$ 250 MN m^{-2}. The two figures refer to different numbers of elapsed cycles. As before, the figures also include the relevant anodic polarisation curves for comparison. It is apparent from these figures that there is generally good correlation between the fluctuating potential and fluctuating current results except in the following respects:

(i) There is not such a large initial decrease in the fluctuating current as in the fluctuating potential on the application of a polarising potential.

(ii) The decrease of the fluctuating current in the passive region is more significant than the decrease in the fluctuating potential.

(iii) There is not such a large decrease in fluctuating current on the termination of passivity as for fluctuating potential.

4.6.2. Anodic Polarisation Runs

These results were obtained using the improved circuitry for measuring the fluctuating current depicted in Figure 3.11.

(a) 3% (0.5M) Sodium Chloride

Figure 4.16. shows the form of the fluctuating current signal for applied potentials in both the passive region and the pitting region.

The time zero indicates the triggering point of the signal, which corresponded with the maximum tensile stress of the exposed area of the test-piece. It is evident that for both applied potentials the signal has a 24 Hz frequency, is approximately sinusoidal and the maximum corrosion current coincides with the maximum tensile stress.

Figure 4.17 shows the variation of amplitude of the fluctuating current with applied potential, as usual including the relevant anodic polarisation curve determined simultaneously for comparison. It is apparent from this figure that the amplitude of the fluctuating current signal decreases as the sample is anodically polarised, with a slight inflection at about + 150 mV, to a minimum at + 350 mV after which it rapidly increases. The slight inflection at + 150 mV corresponds with the pitting potential in the anodic polarisation characteristics.

(b) 3% (0.2M) Sodium Sulphate

Figure 4.18 shows the form of the fluctuating current signal using the same format as for Figure 4.16. The signal is approximately sinusoidal with a frequency of 24 Hz for potentials in both the passive and transpassive region. In the passive region the maximum corrosion current corresponds with the maximum tensile stress, but in the transpassive region the maximum corresponds with the maximum rate of tensile strain. Figure 4.19 shows the variation in amplitude of the fluctuating current with applied potential, together with the relevant anodic polarisation curve for

comparison. The following important features are apparent:

(i) The magnitude of the fluctuating current decreases on application of an anodic polarising potential from the rest potential to + 900 mV,

(ii) above + 900 mV the fluctuating current quite rapidly increases.

(c) 3% (0.1M) Potassium Dichromate

Figure 4.20 shows the form of the fluctuating current signal using the same format as for Figures 4.16 and 4.18. The signal is again approximately sinusoidal with a 24 Hz frequency for potentials in both the passive and transpassive range. The results are similar to those for sodium sulphate, in that the maximum corrosion current in the passive range corresponds with the maximum tensile stress, whereas the maximum corrosion current in the transpassive range, corresponds with the maximum tensile strain rate.

Figure 4.21 shows the variation in amplitude of the fluctuating current with applied potential together with the relevant anodic polarisation curve characteristics. Two sets of results are given, determined after different elapsed cycles, i.e. $\sim 10^3$ and $\sim 2 \times 10^6$. The following important features are evident:

(i) On anodic polarisation the magnitude of the fluctuating current decreases, slowly at first and then more rapidly as the applied potential approaches + 900 mV. The decrease is more

marked for the curve determined after the larger number of elapsed cycles.

(ii) Above + 900 mV the amplitude of the fluctuating current increases very rapidly for the smaller and rather less rapidly for the larger number of elapsed cycles.

4.6.3. Variation of Fluctuating Current Amplitude with Elapsed Cycles

These results were obtained using the circuitry in its final form:

(a) 3% (0.5M) Sodium Chloride

Figure 4.22 shows the variation of the fluctuating current together with the total net current as functions of elapsed cycles with a constant applied potential of - 240 mV. This potential is significantly less noble than the rest potentials for either static or dynamic conditions so that the test-piece was cathodically protected. The magnitude of the fluctuating current decreased continuously throughout the fatigue life and the total net current increased from 1.7 to 9.2 μA in the first 20,000 stress cycles with subsequent variation by about $\pm$ 5 μA but with little general change. This test was terminated after 5×10^7 elapsed cycles, because failure did not occur.

Figure 4.23 gives corresponding results but with an applied potential of 0mV, holding the test-piece in the passive range. The corrosion current decreased rapidly between 0 and 3,000 elapsed cycles and then remained at a constant low value until 260,000 cycles had elapsed after which it increased, at first slowly and then very rapidly until failure.

The fluctuating current decreased slightly until 260,000 cycles had elapsed, whereupon it increased at first slowly and then rapidly until failure.

Figure 4.24 gives the result of a replicate test showing that the same general form is preserved despite considerable variation in the absolute values from test to test.

Figure 4.25 gives results for an applied potential of + 200 mV, holding the test-piece in the pitting range. The corrosion current decreased slightly between 0 and 100,000 elapsed cycles and then increased, at first slowly and then rapidly just before failure. The fluctuating current decreased rapidly at first and then more gradually to a minimum at 80,000 cycles, it then increased more and more rapidly until failure.

(b) 3% (0.2M) Sodium Sulphate

Figure 4.26 shows the variation in amplitude of the fluctuating current and total current as functions of elapsed cycles with an applied potential in the passive range i.e. 0mV. The fluctuating current decreased throughout the fatigue test, rapidly at first and then more gradually. The corrosion current decreased to a minimum after 10^6 elapsed cycles, then increased to a constant value after 1.6×10^6 elapsed cycles. The test was terminated after 5×10^7 cycles because failure had not occurred

Figure 4.27 gives corresponding results but with an applied potential of + 1400 mV, holding the test-piece in the transpassive range. The corrosion current decreased slightly between 0 and 15,000 elapsed

cycles and then steadily increased up to about 375,000 elapsed cycles above which it increased rapidly until final failure. The fluctuating current decreased initially to a minimum after 4000 elapsed cycles, then increased to a maximum after 80,000 elapsed cycles, decreased again to a second minimum after 3×10^5 elapsed cycles and finally increased rapidly until failure.

(c) Figure 4.28 shows the variation in amplitude of the fluctuating corrosion current and total current as functions of elapsed cycles with an applied potential in the passive range, i.e. OmV. The fluctuating current decreased throughout the test. The corrosion current decreased rapidly until 10,000 cycles had elapsed and then very gradually thoughout the test. The test was terminated after 5×10^7 cycles because failure had not occurred.

(d) Fatigue lives of Samples subjected to Electrochemical Tests

The Electrochemical experiments under constant applied potentials incidentally yield values for the fatigue lives and these are summarised in Table 4.2.

(e) Phase Shift of Fluctuating Current Associated with Failure

In all of the dozen or so tests at controlled potential in sodium chloride, there was a quarter wave phase shift in the fluctuating potential signal at the onset of the rapid increase in amplitude immediately preceding failure. This is a most important observation because it has the following significance. The maximum in the fluctuating current wave form co-incides with the tensile maximum in the cyclic stress for most of the fatigue life but with the maximum tensile strain rate immediately prior to failure.

Table 4.2

The fatigue lives of test-pieces held at set potential.

Stress	Environment	Applied Potential	Fatigue Life
MN m^{-2}		mV	Cycles x 10^5
±320	Air	–	500+
	3% NaCl (0.5M)	None	10.2
	3% Na Cl (0.5M)	0	3.04
	3% Na_2 SO_4 (0.2M)	0	500+
	3% K_2 Cr_2 O_4 (0.1M)	0	500+
	3% Na Cl (0.5M)	+ 200	2.84
	3% Na_2 SO_4 (0.2M)	+ 1400	3.84
± 320	3% Na Cl (0.5M)	- 240	500+

A + sign next to the fatigue life indicates that the test-piece did not fail. The air fatigue result is included for comparison.

4.6.4. Measurement of the corrosion current flowing at the static rest potential

In this experiment the static rest potential was measured for a period of two hours and was found to be -155 mV. A fatigue run was then started with a control potential of -155 mV and the corrosion current measured. Figure 4.29 shows the variation of corrosion current for the first two hours. The corrosion current initially increased to 15 μA but rapidly settled down to a value of about 1 μA at which it remained for 40 minutes ($\simeq$ 58,000 elapsed cycles). From this point it increased reaching a steady value of 57 μA after 100 minutes (144,000 elapsed cycles).

Figure 4.30 shows, on a coarser scale, the subsequent changes in current in the same test over an extended period of about 50 hours (4.32×10^6 elapsed cycles). This exhibited a general trend towards a lower corrosion current between 2 and 50 hours ($\simeq$ 173,000 elapsed cycles) although there were considerable random superimposed variations.

4.7 Fractography

4.7.1. Rotating Bend Fatigue Tests in Air

The pits produced by pre-corrosion were 20-200 μm in diameter and distributed as illustrated in Figure 4.31. Cursory examination in the SEM gave a misleading impression that the pits were irregular (Figure 4.32 to 4.34) but the true shape was hemispherical as revealed after removing an overlying thin residue derived from the original surface covering the pits (Figure 4.35).

Pre-pitted test-pieces exhibited irregular fractures produced by multiple crack initiation at the bases of pits (Figure 4.36) and at higher resolution cracks were visible radiating from the pits (Figure 4.35). In contrast, unpitted test-pieces exhibited relatively flat fractures characterised by single initiation points.

At high resolution in the SEM,"ductile" striations were observed on the fracture faces, concentric with the initiation points and normal to the crack propagation direction (Figures 4.37 to 4.39). Some fracture surfaces exhibited small isolated flat areas on which pits and linear markings could be resolved at high magnification (Figures 4.40 to 4.42).

4.7.2. Reverse-Bend Fatigue Tests

4.7.2.1. Macrofractography

Figure 4.43 gives a typical general view of a fatigue fracture in an aqueous environment. Most of the fracture surface was generated by fatigue crack propagation, final fracture contributing only a small area. Adherent films of corrosion product are visible close to the initiation point in Figure 4.43. The fractures also bore "river markings" radiating from the initiations points, typical of fatigue fractures (Figure 4.44 and 4.45).

4.7.2.2. Microfractography

(a) Fractures from Fatigue Test in Air

The principal crack leading to fracture was often accompanied by some secondary cracking particularly for the higher stresses (Figure 4.46). The final fracture was "dimpled", characteristic of the ductile fracture expected for the material (Figure 4.47).

Ductile striations (as defined earlier) were aligned approximately normal to the crack propagation direction (Figure 4.48).

(b) Fractures from Fatigue tests in Aqueous Environments

The fractures produced in aqueous environments were rougher than those produced in air (Figure 4.49) and often characterised by multiple initiation.

Striations were invariably observed on fractures examined in the SEM. Unlike those on air fatigue fractures, they were not necessarily aligned normal to the crack propagation directions and occurred only in isolated areas. On unprepared fracture surfaces, the striations were partly obscured by adherent films of corrosion product (Figure 4.50), but they were easily discernible after applying the film stripping procedure described earlier, although this introduced minor pitting as an artefact (Figures 4.51 and 4.52). The striated fracture faces were often decorated with particles of non-metallic compounds around which the fatigue cracks propagated (Figures 4.53 to 4.55). Striation spacings cannot be measured using scanning electron fractographs unless the orientation of the area in view to the electron collector is known. This information can be obtained by recording the angle of the collector to the specimen for each micrograph of a stereo-pair (Figure 4.56).

Many test-pieces exhibited small 'flats' more numerous than those observed for fractures from rotating -bend tests but with the same general features, i.e. linear markings and pits, although some of the pitting may be attributable to the film stripping procedure (Figures 4.57 - 4.60).

Fractures produced in 3% (0.5M) sodium chloride solution exhibited not only the expected appearance of fatigue failure but also occasional features more characteristic of stress-corrosion cracking, e.g. a "fir tree" effect (Figures 4.61 and 4.62).

Certain special effects were associated with crack initiation points. There was evidence of step-face attack on the fracture surface (Figures 4.63 and 4.64) and also selective attack in the adjacent area (Figures 4.65 and 4.66). The initiation point was usually, but not invariably associated with a pit even in the non-chloride environments (Figures 4.67 to 4.69). Conversely even in chloride media cracks could be found which were not associated with pits (Figure 4.70). An additional point of interest in Figure 4.69 is some attack near the initiation point suggestive of associated stress-corrosion cracking.

Other points of resemblance to fractures produced in air were secondary cracking visible on the sides of fractured test-pieces (Figure 4.71) and the ductile "dimpled" appearance of the final fracture (Figure 4.72).

5. DISCUSSION

5.1 Critical Assessment of Techniques and Results

5.1.1. Pre-pitting Experiments

(a) Pre-corrosion Treatment

The pre-corrosion treatment used did not give the control of pit size, density and morphology expected. In the event, all of the test-pieces exhibited randomly distributed pits in the size range 20-200 μm, diameter. The reason for this lack of control is the inherent variability in the pitting process.

The main variability in the pitting process occurs in the initiation stage, and it is at this stage that there is uncertainty in the mechanism. This has been discussed in detail in the literature survey but it is worth reiterating here some of the more important factors contributing to pit initiation. One of the most important pre requisites for pitting and one common to nearly all the mechanisms proposed for pit initiation is the adsorption of the aggressive ion by the passive layer. This is a time-dependent phenomena and the time required for sufficient adsorption varies between samples with a consequent inherent variability in pitting behaviour of samples. This variability will be aggravated by the heterogeniety of the metal surface which is a very important factor in the pit initiation process, e.g. the presence of non-metallic inclusions is a prime factor in pit initiation. The model proposed by Wranglen [117] discussed earlier is probably the most likely, although little direct evidence of such a mechanism has been found from the present work. More definitive experiments are required to establish the operative mechanism.

Although in the scanning electron micrographs treatment (Figures 4.32 to 4.34) the pits appear to be irregularly shaped, closer examination revealed that there is a thin film covering the pit obscuring the fact that it is hemispherically shaped as expected from the proposed pit growth mechanism.

A more controllable method of pre-corrosion pitting would be to apply a high potential (+ 600 mV) for a short time to induce multiple pit initiation and then to reduce the potential to a lower constant value (+300 mV) allowing pit growth. This treatment should produce less variability in pit size, although some variability is probably unavoidable.

(b) Rotating-Bending Fatigue Tests

The results of these fatigue tests were found in general to be reasonably reproducible bearing in mind that fatigue failure is a stochastic process for which some scatter of results is inevitable as will be discussed later. The variations occurring in the pitting produced by pre-corrosion treatment was an additional factor exacerbating the scatter of fatigue results.

Although it is desirable to quantify errors in experimental results it was not possible for this work because of the inherent scatter discussed above.

5.1.2. Reverse-Bend Fatigue Tests

During the course of this work the following deficiencies in the test-rig became apparent:-

(a) The setting-up of test-pieces was found to be a lengthy procedure. This could be reduced considerably by ensuring that all test-pieces were perfectly flat and

of the same thickness before testing, hence eliminating the need to equalise the deflection before each test.

(b) The stress experienced by the test-piece varied along its length. This made it necessary to measure the position of the final fracture from the point of application of the load to find the actual stress at the point of failure. The equation used was that derived in Appendix A:-

$$\sigma = \frac{6Wgh}{bw^2}$$

A new test-piece design could be made to solve this problem by producing a uniform stress over the gauge length. Another advantage of a uniform stress would be to define more clearly the relationships between stress levels and electrochemical measurements.

(c) The operation mode of the test-rig is constant strain, which means that as the effective cross-sectional area of the test-piece decreases during crack propagation, the actual stress at the crack tip increases. This makes any relationships in the crack propagation range difficult to define.

(d) No provisions were made for the deaeration of test solutions which would have facilitated the interpretation of certain electrochemical information. This improvement was not possible in the time available for this project because extensive modifications to the physical arrangement of the test rig would have been required.

(e) During long term tests loss of the test solution by evaporation was a problem. It was greatly reduced by enclosing the test cell in polythene and placing

croffles on the solution but the provision of a reservoir to maintain the solution level would be of value and allow tests of greater duration.

The scatter of results was found to be larger for tests in aqueous environments than in air. The reasons for this will be discussed in detail in a later section, suffice it here to say that much of this increased variation is due to the complex environmental interactions.

5.1.3. Electrochemical Experiments

The significance and reliability of the various electrochemical equipment and experiments will be discussed later.

It is worth noting here that the reproducibility of the results from electrochemical experiments on the test-pieces was very good, although there were inherent differences between test-pieces with regard to the magnitude of the fluctuating corrosion characteristic signals, due perhaps to slight differences in surface condition, environment etc.

In determining the anodic polarisation characteristics for dynamic conditions, the currents recorded contained a small A C potential manifest as a slight vibration on the trace from the pen recorder. The values given in the results represent the envelope of the lower limit of the vibrating signal so that only increases in the general corrosion characteristics are considered. The vibration is most probably due to the contribution from the fluctuating current attenuated by the slow response of the pen recorder which cannot follow a 24 Hz variation. This means that the total corrosion current measured under fatigue is the instantaneous current time-averaged over the whole stress cycle. The amplitude of the vibrations on the pen recorder was found to be of the order of only 1 to 2μA.

The oscilloscopic techniques allowed the measurement of the abovementioned instantaneous corrosion characteristics which were inaccessible using the normal potentiostatic test. Before accepting the fluctuating corrosion characteristic as a valid phenomenon it was of course necessary to discount any experimental side effects. Several possible spurious effects were considered which might invalidate the results. The most plausible of these was that the movement of the test-piece varied the test-piece to counter electrode distance and hence the IR drop yielding a varying signal. This was considered improbable because all of the test solutions used had a high conductivity and such a variation in the IR drop would have been very small. To prove whether or not this was true a proving trial was carried out in which a fatigue test-piece was set up in the normal manner with the exception that rubber grommets were placed on both sides of the securing bolts to the bottom mount. In this way the test-piece was free to move in the solution such that there was no constraint against which stress was developed during the test. No fluctuating corrosion characteristics were observable in this experiment. When the rubber grommets were removed and the bottom bolts fully tightened, however, allowing stress to be developed in the test-piece, a fluctuating corrosion signal of the normal form was observed. The anodic polarisation characteristics were also determined for the same unstressed condition, i.e. with the test-piece just oscillating in the solution. There was no significant difference between this curve and curves obtained for static test-pieces. This proving trial also discounted other possible spurious explanations for the signal such as vibration of the test solution induced by the motor, electrical interference etc.

5.1.4. Fractography

Most of the fractography was carried out using the scanning electron microscope (SEM). This method has overwhelming advantages

over other high resolution techniques such as transmission electron microscopy (TEM) in that very little specimen preparation is necessary and the whole fracture can be examined. The resolution of this technique is not so good as that of the TEM, being about 0.1 μm for SEM and 0.01μm for TEM but it is sufficient for most purposes. A restriction in the use of the SEM is that it does not allow magnifications of less than X20. This limitation was overcome by the use of an optical stereo-microscope which has a very good depth of focus and allows magnifications in the range X1 to X80 .

5.2 Interpretation of Results from Cycles-to-Failure Fatigue Tests

5.2.1. S/N Curves from Rotating-Bending Fatigue Tests

The S/N curve for unpitted test-pieces exhibits a definite fatigue limit, at $\pm$ 300 MN m^{-2}, as is normal for steels. The existence of an air-fatigue limit for steels is an important observation requiring explanation, because other metals, notably aluminium exhibit no such fatigue limit in air. The fatigue limit is most probably a feature of the crack initiation processes. As discussed earlier in Section 2.7, the most important factor in the crack initiation process is the formation of persistent slip bands and their subsequent development into cracks. Brown (140) proposed that the fatigue limit is determined by the critical strain amplitude required to form persistent slip bands. This model implies that all materials should exhibit a fatigue limit and this may well be true in a perfect vacuum. Whether a fatigue limit exists or not for a particular material in any other environment depends on the possible environmental interactions.

Scatter in fatigue-test results is normally ascribed to variation in propagation rate between test-pieces. This does not seem adequate to explain the extent of observed scatter, especially as in rotating bend fatigue tests, the time to failure is dominated by the initiation processes. A more plausible explanation is

provided by "blocking of reverse slip" model [220] for crack initiation because this process is, by its very nature, stochastic.

The S/N curve for pre-pitted test-pieces shows a marked decrease in fatigue life compared with that for un-pitted test-pieces (Figure 4.1). This is expected because the pits act as stress-concentrators, effectively reducing the nominal applied stress for crack initiation. This may not be the only role of such pits, however, because if this were true the S/N curve for pre-pitted test-pieces would also exhibit an air fatigue limit albeit at a greatly reduced stress level. This reduced nominal stress cannot be calculated accurately because of variations in pit size and distribution but for a limiting case in which it is assumed that the pits are of the largest size observed and form a circumferential groove at the section of highest stress, a calculation can be made, as in Appendix C. yielding a value of 215 MN m^{-2}. Failure actually occurred at stresses far below this value, indicating that some other process is also operating. One possible explanation is that the cleaning treatment of the test-pieces was insufficient to remove all of the salt from the pits. The residual salt could thus form occluded cells in which corrosion processes persist stimulating an unsuspected corrosion fatigue mechanism, as described later.

The increased scatter in these tests can be ascribed to two causes. Firstly the variability in the pre-corrosion treatment can influence pit size and distribution, exacerbating scatter. Secondly the uncertain influence of occluded cells may still further exacerbate scatter.

5.2.2. S/N Curves from reverse-bend Fatigue Tests

(a) Air

The S/N curve for fatigue tests in air exhibits the normal behaviour observed for steels, i.e. there is a fatigue limit, at $\pm$ 340 MN m^{-2}. The significance of a fatigue

limit and the reasons for the observed scatter have already been discussed in Section 5.2.1.

A significant feature of these results, evident in Figure 4.2, is that the scatter increases as the stress is reduced so that it is at its greatest near the fatigue limit. This observation supports the argument that the scatter occurs predominantly in the initiation stage because the stage becomes more dominant at lower stresses.

(b) 3% (0.5M) Sodium Chloride

The S/N curve for 3% (0.5M) aqueous sodium chloride, given in Figure 4.2, differed from that for air in that no fatigue limit was observed. The expected deterioration in fatigue properties in the chloride environment was considerable. Except for the results at high stresses, the reduction in fatigue life is probably too great to be accommodated within the crack propagation period, so that it is reasonable to assume that the primary effect occurs in the initiation stage.

The forms of the S/N curves given in Figure 4.2 suggest three distinct modes of corrosion fatigue as follows:-

(1) Where the stress is above the true fatigue limit failure is certain to occur, regardless of environment so that the role of the environment is to accelerate the process. Its influence is therefore of greater significance on crack propagation than on crack initiation. This may appropriately be described as 'corrosion-enhanced fatigue'.

It should be emphasised that only in vacuum can the fatigue process be regarded as a purely mechanical phenomenon for which the true fatigue limit is determined.

(2) At low stresses and for long times of exposure to the environment, the stress for fracture is so much lower than that for fracture in air (and vacuum) that environmental assistance for crack initiation must be assumed. The most logical explanation is that the exposure time is so long, that the stress-raising effect of corrosion damage is sufficient to initiate failure. This is best described as 'Corrosion-initiated fatigue'.

(3) For intermediate stresses and times of exposure where the stress is insufficiently high for fatigue failure to occur by purely mechanical means but the time of exposure is insufficient to produce appreciable corrosion damage, the interaction between dynamic-fatigue stress and environment is synergistic. Thus this form of corrosion fatigue failure can be best described as "synergistic corrosion-fatigue".

It is the synergistic mode of corrosion-fatigue failure about which least is known and which is thus the most unpredictable. The electrochemical studies in the present work were devised to investigate this phenomenon. For this reason the S/N curves in Figure 4.2 were essential in selecting the appropriate stress levels.

As briefly discussed earlier (Section 2.8) there is considerable controversy over whether the effect of environment is more significant in the initiation or propagation stages of fatigue.

From the preceding conception of three modes of corrosion fatigue it is apparent that there is no single answer to this question, but that the particular test conditions are of prime importance. In tests of the forms usually used to measure crack propagation rates the stress levels are sufficiently high for 'corrosion-assisted fatigue' to occur and so the results obtained highlight changes in crack propagation rate. In the special test devised for the present work, however, the stress level and test-piece configuration define a condition where corrosion-fatigue crack initiation is the primary factor.

When applying time-to-failure (S/N) results to the resolutions of problems in components, it is essential to identify the precise conditions the component will experience so that the relative importance of the initiation and propagation stages can be assessed.

5.2.3. Summary

As already discussed in detail (Section 2.9) many possible mechanisms have been proposed to explain the reduction in fatigue properties experienced in aqueous environments. Although information from usual fatigue tests, e.g. those yielding S/N curves is of some limited value in assessing mechanisms of 'corrosion-assisted fatigue' and 'corrosion-initiated' fatigue, it is of little or no value when applied to 'synergistic corrosion fatigue'.

The acquisition of information appropriate to 'synergistic corrosion fatigue' requires the development of new tests based on totally different concepts such as that used in the present work. In the following section the development of the test is discussed and the information obtained is assessed.

5.3. Interpretation of results from Electrochemical Tests

5.3.1. Rest Potential Measurements

The results of these tests can be summarised as follows:

(i) In 3% (0.5M) sodium chloride solution the rest potential moved to more negative values on the application of cyclic stress.

(ii) In 3% (0.2M) sodium sulphate solution and 3% (0.1M) potassium dichromate solution the rest potential again moved but this time to more positive values, the shift being greater for 3% (0.1M) potassium dichromate solution.

(iii) The rest potential under fatigue conditions reach a constant value within 30,000 cycles of applied stress.

Other investigators have also observed that the rest potential is different when the metal is stressed. Notably Karlashov and Batov [276] and Paul and Velland [277] observed a shift of rest potentials to more negative values. Hoar and his co-workers [278,279] have suggested that such shifts occur because yielding directly assists in the removal of cations from the metal lattice, greatly reducing the activation polarisation for anodic dissolution. Additionally there is little doubt that yielding metal should exhibit more negative rest potentials as a consequence of the rupture of the protective oxide films, exposing bare metal anodic to the rest of the surface. From the present work, however, this is not always found to be true and it is apparent that the situation is more complex. The rest potential as usually defined is the potential at which there is a balance between anodic and cathodic reactions such that no net current flows. So as well as changes in the anodic reactions already discussed, changes in the cathodic reactions also affect the rest potential. It is well known that cathodic reactions are sensitive

to surface condition. Thus the characteristics of cathodic reactions on yielding metal may well be different from those on static metal, leading to a situation such as that envisaged in Figure (5.1). A further factor is that under fatigue conditions the solution is constantly stirred by the movement of the test-piece. The effects of stirring on the rest potential have not been fully investigated. Stirring must certainly reduce concentration polarisation with a corresponding change in the rest potential. In the present work in which the solutions were dilute only a small effect on the rest potential would be expected, as was found in the proving trials discussed in section 5.1.2.

It is experimentally difficult to separate the effects of fatigue stressing on the anodic and cathodic reactions because the two reactions cannot be easily isolated. A further complicating factor in the present work is the fact that there are two possible cathodic reactions, i.e. the reduction of hydrogen ions:

$$2H^+ + 2e \rightleftharpoons H_2 (g) \quad \text{.....(35)}$$

and the reduction of oxygen:

$$O_2 + 2H_2O + 4e \rightleftharpoons 4OH^- \quad \text{.....(36)}$$

In neutral solutions such as those used in this work, reaction (36) predominates under static conditions for stainless steels but the relevant importance of the two cathodic reactions may well be altered as a consequence of fatigue causing changes in the rest potential.

5.3.2. Anodic Polarisation Curves

(a) Polarisation curves for Static Test-pieces

The anodic polarisation curves for static test-pieces in the

three environments as given in Figures 4.3 to 4.9, show the expected characteristics which can be summarised as follows:

(i) In sulphate and dichromate media the steel exhibited passivity over a wide range of potentials, the passive current being slightly higher in the sulphate medium.

(ii) For sulphate and dichromate media the passive range was terminated by the onset of transpassivity, this change being more gradual in the case of sulphate media.

(iii) In chloride media the steel exhibited passivity over a smaller range of potentials terminated by the onset of pitting.

(b) Polarisation Curves during Fatigue

When the test-pieces were subject to fatigue the anodic polarisation characteristics were modified as shown in figures 4.3 to 4.9, summarised as follows:

(i) In the normal passive range, as defined from the anodic polarisation curves for static test-pieces, the corrosion current was increased by the application of fatigue to such an extent that the condition of the metal surface could no longer be considered truly passive.

(ii) The potential at which the onset of transpassivity or pitting occurred was markedly reduced.

(iii) The transition from passivity to transpassivity or pitting occurred over a wider potential range.

It must be remembered that these anodic polarisation curves determined for test-pieces under fatigue, represent instantaneous characteristics time-averaged over the whole stress cycle, so that they must be interpreted with great care. They yield qualitative information on the effect of fatigue on the corrosion characteristics

of the metal, even if the quantitative significance is uncertain. It is apparent from these curves that an important effect of cyclic stressing is to degenerate the passive state. This effect can once again be related to modification under fatigue of one or both of the complementary anodic and cathodic reactions. Such modifications could arise as follows:

(a) Anodic Reactions

The essential considerations in the modification of anodic reaction by fatigue are the processes occurring at the metal surface and the general surface condition. Two important surface conditions must be considered, firstly the situation where the metal surface is bare and unfilmed and secondly where it is protected by a passive layer.

For the case of bare, unfilmed metal surface it is the formation of slip steps which is the determining factor. The ingression of new material into the metal surface caused by slip step formation causes an increase in the corrosion rate, associated with an increase in the anodic reaction. Preferential attack occurs at the emergent slip steps because they are anodic to the matrix; these ideas were discussed in more detail in section 2.6. Other factors can enhance these increases in the anodic current. Lihl [168] for example suggested that low over-voltage impurities can precipitate at the emerging slip bands increasing the reactivity at these areas, Simnad [167] has also suggested that anodic polarisation is reduced during cyclic stressing.

For metals protected by a passive layer the situation is more complex because the layer influences both the production of slip steps and the corrosion characteristics of the metal surface. In fatigue mechanical breakdown of the passive film probably occurs through perforation by emerging slip steps. The number of perforations and the area of active metal at the slip steps piercing

the passive layer depends on many factors e.g. the thickness of the passive layer and the form of the slip steps. These factors were considered in detail in Section 2.6. Once the passive layer is mechanically broken by such mechanisms, the new bare surface is exposed to the aqueous environment. This newly formed surface repassivates and in the process metal is consumed from the surface of the slip step, constituting an effective increase in the overall anodic reaction. The repassivation process and hence the effect on the anodic reaction depends on the chemistry of both the metal alloy and the environment, in accordance with the earlier discussion in Section 2.6.

(b) Cathodic Reactions

Unfortunately little or no information is available on the effects of stressing upon the cathodic reactions. The possible effects can therefore be only a matter of speculation. As already mentioned, it is well known that cathodic reactions are very sensitive to surface condition. These cathodic reaction on cyclically stressed surfaces may well differ from the same reactions occurring on static surfaces. Indeed cathodic reactions might be expected to fluctuate during the course of stress cycles in synchronism with the applied stress. It is worth noting that Despic et al. (126) found that elastic straining can cause an increase in the reactivity of the metal due mainly to a change in the rate of hydrogen evolution.

Figures 4.4, 4.5 and 4.9 show the effect of the elapsed cycles prior to the determination of anodic polarisation characteristics under fatigue. Although it is apparent that there is a significant effect, results do not lend themselves to easy interpretation and it is evident that a different approach is required to investigate this phenomena. It was for this reason that experiments were carried out in which the corrosion current was measured during the course of fatigue experiments with a fixed, constant applied potential. These experiments are discussed in detail in section 5.3.4.

Another obviously important factor affecting the polarisation curves under fatigue is the magnitude of the applied stress. Unfortunately insufficient time was available to examine this variable and although anodic polarisation curves for two stress levels are presented, these were determined using different potentiostats employing different recording systems, as described in Appendix A, and are thus not amenable to direct comparison. This particular difficulty was an inevitable consequence of successive improvements in technique. This said, however, it is interesting to note that for the chloride media, at the lower stress level of $\pm$ 250 MN m^{-2} the pitting potential increased and the passive current decreased during the fatigue life. At $\pm$ 320 MN m^{-2}, the pitting potential decreased and the passive current increased during the fatigue life.

This difference in behaviour can be taken as reflecting different mechanisms of failure for the two stress levels on the principles developed earlier from a consideration of S-N curves. The lower stress level is well below the fatigue limit for air (340 MN m^{-2}) and a long fatigue life would be predicted, so that the most likely mechanism operating is 'corrosion-initiated fatigue' The higher stress level is not much below the air fatigue limit and a relatively short fatigue life is predicted from the S-N curve so that it is reasonable to suppose that 'synergistic corrosion fatigue' will predominate.

5.3.3. Fluctuating Potential Measurements

These experiments constituted the early work on the measurement of the fluctuating corrosion characteristics occurring in fatigue.

The features of this fluctuating potential signal can be summarised as follows:

(i) It is a fluctuating A.C. potential difference between the working and counter electrodes.

(ii) The signal has the same frequency as the stressing frequency applied to the test-piece (24 Hz) and is synchronised with it.

(iii) The signal is evident from the start of stressing and needs no significant incubation period.

The significance of this signal is that it is a measure of the changing corrosion characteristics of the metal during cyclic stressing. This quantity is observed across the test cell between the working electrode (test-piece) and the counter electrode. The magnitude of the signal thus depends upon the resistance of the test-cell and this makes the comparison of different aqueous environments impossible unless their resistances are known. Another danger in interpreting such results is that the cell resistance may not remain constant during the course of experiments, invalidating the results. A series of proving trials, discussed in detail earlier (section 5.1.3), eliminates this possibility so that any variations in cell resistance can be safely ignored for the sake of the following discussion.

Some possible explanations for a fluctuating signal worth considering are:

(a) The change in surface area of the test-piece during cyclic stressing due to the opening and closing of cracks.

(b) Breakdown in the protective film on the metal surface induced by cyclic stressing.

(c) Intermittent dissolution at the fatigue crack tip.

(d) Increases in surface attack due to emerging slip steps.

(e) Changes in cell resistance during cyclic stressing due to the changing Working/Counter electrode distance. This possibility has already been discounted by the proving tests described in section 5.1.3.

Possibilities (a) and (c) can be discounted because the fluctuating potential is detected from the start of cyclic stressing before cracks have been initiated. This leaves explanations (b) and

(d) which are both worthy of further serious consideration, but explanation (b) is, of course, only applicable to test-pieces held in the passive range. The significance of these two theories can be ascertained by considering the magnitude of the fluctuating potential as a function of the applied potential as shown in Figures 4.10 to 4.13. The essential characteristics of this relationship can be summarised as follows:

In sulphate and dichromate media, on the initial application of an anodic polarising potential, the magnitude of the fluctuating potential falls rapidly and then assumes an approximately constant value until the applied potential reaches about +800 mV SCE, where it starts to decrease again ultimately reaching a lower constant value for applied potentials above about +1000 mV.

In chloride media the fluctuating potential falls progressively on anodic polarisation, at first rapidly, then more gradually until the applied potential reaches + 100 mV. It then falls abruptly to a constant value for applied potentials above about +300 mV.

These results can be interpreted in terms of the two possible explanations for the fluctuating potential signal introduced earlier. For all three environments in the "passive" range of the anodic polarisation curve determined for test-pieces subject to fatigue, the value of the fluctuating potential is relatively high and this can be interpreted in terms of the influence of persistent slip bands on the surface condition, as described in section 5.3.2. When the persistent slip bands pierce the passive layer during fatigue, these local active regions form in a surface generally protected by a passivating film. The local reactivity in these regions is therefore much higher than that of the surface generally, generating higher values of the corrosion current which are detected as higher values of the fluctuating potential. The dissolution of these local active regions is further exacerbated by the stimulus of the active/passive cells produced and this will further

increase the fluctuating potential.

This is the only real information which can be gained from a study of the fluctuating potential. As already discussed this particular version of the technique is sensitive to the cell resistance and no comparison of the effect of the three environments on the fluctuating corrosion characteristics can be made. From the consideration of the effects of applied potential, it is evident that the thickness of the passive layer increases as the applied potential is made more positive. This obviously changes the cell resistance with corresponding changes in the fluctuating potential. A more significant change in resistance occurs at the breakdown potential of the passive film when the cell resistance is reduced. These considerations introduce serious uncertainties into quantitative use of the results.

It is apparent from the above arguments that there was a great need to refine the technique so that it could record the fluctuating corrosion current, and hence the fluctuating corrosion characteristics directly, to overcome these problems. This stimulated the development of the system for measuring fluctuating corrosion currents yielding the more fruitful results discussed in the following sections.

5.3.4. Fluctuating Corrosion Current Measurements during Anodic Polarisation runs

The first task using this improved technique was to compare it with the earlier technique of measuring fluctuating potentials. The results of this comparison are given in figures 4.14 and 4.15. These curves show that there is a good general correlation between the two methods when used to assess fluctuating corrosion characteristic as a function of applied potential, but there are two significant points of difference. Firstly in the "passive" range revealed by the anodic polarisation curve for test-pieces under fatigue

fluctuating current does not rapidly decrease in magnitude on initial polarisation of the test-piece and as the overpotential is further increased in the passive range, the fluctuating current decreases more rapidly than the fluctuating potential. Secondly, as evident in Figure 4.17, the magnitude of the fluctuating current measurement begins to increase again after the breakdown of passivity. The cause of these differences was probably the variation in cell resistance due to the formation and dissolution of the passive film, confirming the reservations discussed in the previous section.

This preliminary work using the fluctuating current technique revealed certain deficiencies. Although these deficiencies did not detract from the significance of the results already obtained using the method, modifications were required to exploit the full potential of the method.

These deficiencies were as follows:

(i) There was not enough 'offset' of the signal entering the opto-isolator to allow measurement of the fluctuating current in cases where a large corrosion current was present, because the signal was out of the range of the opto-isolator.

(ii) It was difficult to ensure that the instrument was working within the linear range of the opto-isolator, which is the only range in which accurate quantitative measurements could be made.

(iii) More amplification of the fluctuating signal was needed for accurate quantitative measurements.

(iv) A permanent record of the exact shape of the fluctuating signal, needed for detailed examination, could not be made.

(v) No facility was available for automatically sampling the signal, which meant that the apparatus could be used only

when an operator was present. This limited the application of the technique to short-term tests.

Modifications were made to eliminate these deficiencies as described in detail in the Experimental Procedures section. Briefly, deficiencies (i) to (iii) were eliminated by modifications to the opto-isolator circuit; deficiency (iv) was eliminated by the purchase and use of a storage oscilloscope with a print-out facility, deficiency (v) was eliminated by the design and construction of an automatic sampling facility.

Once these modifications were completed the measurements of the fluctuating corrosion characteristics as functions of applied potential were repeated.

Since the waveform of the fluctuating signal has a prominent role in the discussion of these results, it is convenient first to examine its characteristics both in the "passive" range and at potentials above that for breakdown of passivity.

Figure 4.16, 4.18 and 4.20 show the waveform of the fluctuating current signal in both these ranges. The essential features of the fluctuating current signal can be summarised as follows:

(i) The signal is in all cases approximately sinusoidal with the same frequency as the stressing cycle (24 Hz) and synchronised with it.

(ii) The signal is evident from the start of stressing, i.e. there is no incubation period.

(iii) For all three environments in the "passive" range and also for chloride in the pitting range, the maximum of the corrosion current cycle corresponds with the maximum tensile stress.

(iv) For sulphate and dichromate media in the transpassive range the maximum of the corrosion current cycle

corresponds with the maximum rate of tensile strain.

(v) In all cases a small signal of higher frequency ($\simeq$ 50 Hz) is superimposed on the 24 Hz signal and not synchronised with the loading cycle.

Feature (v) is not a measure of the cyclic change in corrosion characteristics of the test-piece with fatigue and is most probably due to residual mains hum, of insufficient amplitude to affect the significance of the fluctuating current measurements.

The same arguments for the existence of a fluctuating potential signal can be advanced to explain a fluctuating current signal; they are, in fact, essentially measurements of the same parameter. Detailed examination of the print-outs of the fluctuating current signal provides further opportunity to characterise and account for it.

Feature (iii) of the signal applies when the surface is either completely passivated or the passivity is only locally destroyed. This suggests that for these cases it is the breakdown of the protective layer by cyclic stressing which is important. Such a mechanism would depend not so much upon the rate at which slip steps are produced at the metal surface, but rather on the height of the slip steps formed, because it is this factor which determines how many slip steps pierce the protective passive layer and by how much. Figure 5.2 shows the effect that the slip step height can have on the rupture of a protective film.

When the passive layer is pierced by a slip step in such a manner, the repassivation process occurs by a transient dissolution event which continues until the film heals again. Figure 5.3 shows the kind of attack which can occur in this way. The attack will be very localised because these active areas occur in an otherwise passive surface. Payer and Staehle [188] have reported local corrosion currents at breaks in a passive film as high as 1 to 10 A cm^{-2} for

a short time where the general corrosion current before rupture was only 10^{-9} to 10^{-5} A cm $^{-2}$. It is thus quite conceivable that fluctuations of corrosion current of the amplitude measured in the present work can be produced by such a mechanism.

Feature (iv) applies in transpassive ranges where the metal is bare and unfilmed. This suggests that the important factor in this case is the emergence of slip steps from the metal surface and their inherently greater reactivity. Because the surface is film-free, the increased corrosion current cannot be attributed to the breakdown of a protective layer. Many investigators (167,170,277) have suggested that the atoms at newly formed slip steps can have a lower activation energy for dissolution which stimulates preferential dissolution at these sites. Such an effect, although possible in principle when the metal is in the passive state, is submerged by the mechanism already discussed. When the metal surface is in the transpassive state, however, such a mechanism could be very significant; it is thus necessary to discuss the reasons for such an effect in detail. Figure 5.4 shows a schematic model of an edge dislocation approaching a metal surface with the subsequent formation of a slip step. It is apparent from this figure that the Gibbs free energy for Atom A in position (ii), i.e. at the saddle point, is higher than when it is in position (i) or (iii), the reason for this difference is that at the saddle point atom A is less fully co-ordinated with the surrounding atoms.

The free energy change required for solvation of atom A in positions (i) and (iii) can be expressed by:

$$\Delta G_{(solv)} = \Delta G^{*} - \Delta G \qquad \text{.....(79)}$$

In position (ii) the free energy change necessary for solution of atom A becomes:

$$\Delta G_{(solv.)ii} = \Delta G^{*} - \Delta G\,ii \qquad \text{.....(80)}$$

It is apparent from the figure that:

$$\Delta G_{(solv.)\ ii} < \Delta G_{(solv.)}$$

hence in this situation less energy is required for atom A to be solvated. Substitution of the appropriate values for activation energy for A atoms in the Tafel constants shows that the polarisation is less for atoms at the saddle point. It follows from this argument that dissolution rates are higher for metals in which slip steps are being formed because more atoms will attain the energy required for solution. This model can be extended to explain why the maximum corrosion current should coincide with the maximum tensile strain rate. At the maximum tensile strain rate slip steps are emerging from the metal surface at the maximum rate so that the enhancement of dissolution rate and hence the corrosion current, will be at a maximum.

The above discussion obviously applies to an idealised situation and in a real situation many other mechanisms also contribute to the overall process. Pyle et al [172,186] have shown experimentally that edge sites atoms such as those present in outcropping slip steps, require lower activation energies for dissolution than plane site atoms. This observation supports the theory advanced above but Pyle advances an alternative explanation as follows:-

The binding energy of the metal ion to the metallic lattice depends on the frequency of vibration of the ions in the surface. For atoms in a plane surface the only vibrations which can be utilised are those normal to the surface being solvated. For atoms at edge sites, however, vibrations in the plane of the surface can also be utilised thus permitting dissolution of edge site ions at lower activation energies.

Figures 4.17, 4.19 and 4.21 show the effect of applied potential on the magnitude of the fluctuating corrosion current for the three environments. The important features of these curves can be summarised as follows:-

(i) For all three environments, on anodic polarisation the magnitude of the fluctuating current decreases throughout the "passive" region.

(ii) For chloride media, on the onset of pitting there is a further and more rapid decrease in the magnitude of the fluctuating current until the applied potential reaches + 350 mV above which it rapidly increases.

(iii) For sulphate and dichromate media, on the onset of transpassivity the magnitude of the fluctuating current begins to increase rapidly.

(iv) In the "passive" range the magnitude of the fluctuating corrosion current was generally greatest for the chloride media, least for the dichromate media and of an intermediate value for sulphate media.

Feature (i) of these curves can be explained using the model already discussed in explaining the wave form of the fluctuating corrosion current in the passive region. As has already been mentioned briefly in the discussion the thickness of the passive layer increases during anodic polarisation until the breakdown potential is reached, Figure 5.5, shows the variation of film thickness with applied potential for iron base alloys exposed to sodium sulphate solution at pH 4 (188). These increases in passive film thickness influence both the number of slip steps which pierce the passive layer and the area of fresh metal so exposed. The thicker the passive layer, the less the number of slip steps which are able to pierce it, this effect is shown schematically in Figure 5.6. Further to this, the area of unfilmed metal exposed to the solution is inversely related to the passive film thickness for the same slip step height, an effect shown schematically in Figure 5.7. The decrease in the magnitude of

the fluctuating current signal with increasing applied potential in the passive range is thus quite consistent with the film rupture model because the amount of unfilmed material exposed and so the number of transient dissolution events occurring which comprise the fluctuations in corrosion current, is reduced as the applied potential is increased.

Feature (iii) of these curves can be explained by applying the model described for film free metal surfaces as exist in the transpassive region. Once passivity has been terminated and the metal is in the transpassive condition, further increases in the applied potential markedly increase the magnitude of the fluctuating current showing that the different polarisation characteristics for yielding metal are maintained as the overpotential is increased.

Feature (ii) of these curves for chloride media needs careful interpretation because the prevalent situation is quite complex. There is an interaction between the mechanical breakdown of the passive film which still exists in the pitting region and the pitting process itself. It is possible that the decrease in the magnitude of the fluctuating current at the onset of pitting is due to a dominant effect of the pitting process at points where the passive layer is perforated, preventing the repassivation on which the magnitude of the fluctuating current parameter depends. The increase in the magnitude of the fluctuating current for higher potentials in the pitting range is more difficult to explain and further work is needed to clarify this aspect of the investigation before mechanisms to explain this behaviour can be proposed with any confidence. Information is required on the effect of cyclic stressing on the pitting process; such an effect might be quite significant; the condition of the passive layer at high pitting potentials will also be an important factor. Another important factor is the change in the

composition of the solution in pits compared with the bulk solution.

Feature (iv) of these curves concerns the relative magnitude of fluctuating currents in the passive range for the three environments. This depends on the relative thicknesses of the passive films present and the nature of the anion in solution. The thickness of the passive film determines the amount of unfilmed metal surface exposed to the solution as already discussed. The nature of the anion in the solution determines the peak current density and the rate of repassivation. Both factors combine to determine the amount of dissolution which occurs and hence the magnitude of the fluctuating current signal. Figure 5.8 shows the effect of the rate of repassivation on the amount of transient dissolution. It is apparent from this figure that if the rate of repassivation is rapid, the amount of transient dissolution is small, whereas if the repassivation rate is slow, the amount of transient dissolution is large. Higher peak current densities also increase the amount of transient dissolution.

For the three environments used in the present work no quantitative information is available on the relative thicknesses of the passive films. However dichromate media are known to have a very good inhibiting effect on the corrosion of stainless steels, an effect usually ascribed to thicker passive films so produced.

This explains to some extent the lower magnitude of fluctuating current in dichromate media but it is not the only possible mechanism.

Another very important factor is the nature of the anion in the environment. From their known effects it is logical to assume that the repassivating rate for dichromate media is much higher than for chloride media and that the rate for sulphate media is intermediate,

these rates determine inter-alia the magnitude of the fluctuating current signal in the passive region and thus explain the differences between the three environments. A further factor for discussion is the relative magnitudes of the peak current density. Unfortunately no such information is available for the three environments.

It is apparent from the foregoing discussion that the principle obstacle in providing complete explanations for the differences in fluctuating current magnitude in the passive region between the three environments is lack of suitable information. There is considerable scope for further experimental work.

5.3.5. Fluctuating Corrosion Current Measurements during fixed potential runs

Figures 4.22 to 4.28 show the variation in both the total corrosion current and the magnitude of the fluctuating corrosion current as a function of elapsed cycles. The important features of these curves can be summarised as follows:

(i) In the passive range, for both sulphate and dichromate media, premature failure was not experienced, i.e. the fatigue life exceeded 5×10^7 cycles. The magnitude of both the total corrosion current and fluctuating corrosion current either decreased or remained constant throughout the test period.

(ii) For sulphate media in the transpassive range premature failure occurred well below the air fatigue life. The total corrosion current increased throughout the fatigue life, escalating rapidly just before failure. The magnitude of the fluctuating current, after increasing slightly early in the fatigue life, decreased to a minimum and then increased rapidly until failure.

(iii) For chloride media in both the passive and pitting ranges all of the samples failed prematurely. The total

corrosion current increased throughout the fatigue life, escalating rapidly just before failure. The magnitude of the fluctuating corrosion current decreased slightly early in the fatigue life to a minimum and then increased rapidly until failure.

(iv) For chloride media premature failure was suppressed by the application of small cathodic polarising potentials. The total current remained approximately constant throughout the test period and the magnitude of the fluctuating current decreased continuously.

(v) In all the controlled potential experiments there was a short initial period corresponding to a few hundred cycles in which conditions stabilised. This is normal in electrochemical tests and is of no particular significance in the present work.

It is apparent from these features that for all tests in which premature failure was not observed the magnitude of the fluctuating current fell throughout the course of the test. Applying the film breakdown model developed for the passive range, the decrease in the magnitude of the fluctuating current for the sulphate and dichromate media indicates that the rate of repassivation is rapid enough to suppress appreciable attack at the points of film rupture so that the cumulative damage is insufficient to initiate cracks. It is probable that during the fatigue life, the number of outcropping slip bands decreases because the slip processes are effectively 'locked' by the repassivation events producing oxide barriers. This could explain why the magnitude of the fluctuating current signal decreases. The small corrosion current remains constant or decreases during the fatigue life, confirming that the damage is not cumulative.

The effect of small cathodic polarisations is to protect metal exposed at slip steps and thus, corrosion does not contribute to the accumulation of damage with the result that premature damage does not occur.

For tests in which premature failure is observed the general relationship between the fluctuating current magnitude and the number of elapsed cycles is as described by features (ii) and (iii). For chloride media in the passive region, the film breakdown model can be used to explain the sequence of events during the fatigue life as follows:

In the early stages of fatigue, before any appreciable 'damage' had accumulated, the repair mechanism described for sulphate and dichromate media dominates, causing the slight decreases in the magnitude of the fluctuating current. It is not clear why a transition should occur and the fluctuating current should start to increase again, but a possible explanation is that the repair mechanism reduces the number of active sites, concentrating the corrosion on fewer sites and thereby intensifying the damage to the point where repair is inadequate, so that the magnitude of the fluctuating current increases. There are two ways in which this could occur, firstly the reduction in the number of active sites could produce more effective active/passive cells, intensifying the attack at the anodic regions. Secondly the 'locking' of some slip bands by the repair mechanism could concentrate the stress at the remaining slip bands intensifying the slip and thus both creating larger anodic regions at which attack can occur, and aiding crack initiation at these sites.

The rapid increase in fluctuating corrosion current towards the end of the fatigue life was associated with a phase shift in the fluctuating current signal relative to the phase of the stress cycle. For most of the test, the maximum of the signal coincided with the maximum tensile stress at the surface of the test-piece but as the

signal increased towards the end of the test, the maximum of the signal coincided with the maximum tensile strain rate. This probably marks the transition in the fatigue crack development from initiation to propagation. At this transition both the stress and corrosion attack are concentrated at the point of crack initiation. The association of maximum corrosion rate with maximum strain rate implicit in the phase change in the signal, indicates that the crack tip region is anodic to the rest of the test-piece and film free, a situation analogous to that for the transpassive range. The rapid increase in the magnitude of the signal just prior to failure can be associated with the rapidly increasing rate of crack propagation and the consequent increasing size of the anodic region at the crack tip. Another important aspect of this rapid increase is the actual stress experienced at the crack tip. As has already been discussed, the reverse-bend fatigue test employs a constant amplitude mode of stressing and so the actual stress at the crack tip increases during crack propagation, thereby possibly increasing the amplitude of the fluctuating corrosion current signal.

The variation of the total corrosion current during the test period can also be explained by the film breakdown mechanism, because the model predicts that corrosion current increases in proportion to the increasing surface area activated by slip processes. The large increase just prior to failure can again be associated with the transition from crack initiation to crack propagation.

In the pitting range the general characteristics of the curve are the same as for the passive region so that similar explanations can be applied in principle because a passive layer is still present, but the situation is obviously more complex because of the intervention of the pitting process.

The interplay between mechanical mechanisms of film

breakdown and depassivation implicit in the pitting process makes the interpretation of the results very difficult. The intractable problems in this task have been referred to earlier.

For sulphate media in the transpassive range, the film breakdown mechanism cannot apply because the metal is film free so that a different concept is needed. Such a concept has already been examined using the model in which the enhanced corrosion currents are associated with active out-cropping slip bands. The variation in the magnitude of the fluctuating current during the test period can be explained on the basis of such a model. The sequence of events is as follows:

At the onset of fatigue, slip bands are formed easily because their formation is not impeded by the presence of any oxide films. There will then be two competitive processes. One is the 'locking' of slip processes by work hardening and the other is the effective unlocking of these slip processes by the preferential dissolution events at the outcropping slip steps as shown in Figure 2.42. Which of these dominates will be determined by the prevalent conditions. Early in the fatigue life the dissolution mechanism probably dominates in view of the slight increase in the fluctuating current magnitude. As the dislocations accumulate, the locking mechanism probably dominates and the stress, and hence the slip and preferential dissolution, is concentrated at the remaining slip bands reducing the fluctuating current amplitude. A point will be reached where the conditions promote crack initiation with subsequent crack propagation markedly increasing the fluctuating current magnitude.

The variation in the total corrosion current during the fatigue life once again supports the proposed mechanism for the same reasons as were given in the discussion of chloride media.

5.3.6. Summary

It is now possible to use the evidence from the present work to assess the various mechanisms of corrosion fatigue which have been proposed. Before doing this, however, it is important to note that the discussion applies only to the system considered in this work and in other systems and for other conditions, other mechanisms may dominate.

The mechanisms advanced can be summarised as follows:

(i) Stress intensification at local corrosion damage.

(ii) Reduction of surface energy by the adsorption of species from the environment (Rebinder Mechanism).

(iii) Localised dissolution due to plastic deformation.

(iv) Rupture of protective surface films during fatigue.

(v) Hydrogen-assisted cracking.

(vi) Wedging action by corrosion products.

(vii) The prevention of crack rewelding by environmental interactions.

The present work has been concerned principally with the initiation of fatigue cracks and so mechanisms (vi) and (vii) are irrelevant to this discussion.

From the pre-pitting work it is apparent that, although stress intensification at local corrosion damage is obviously an important factor in solutions in which localised corrosion can occur, other mechanisms can significantly effect the corrosion-fatigue behaviour. One such mechanism is the operation of pits as occluded cells. A similar kind of mechanism may be envisaged for fatigue tests at potentials in the pitting range.

For solutions and conditions in which appreciable local corrosion damage does not normally occur, other mechanisms for premature fatigue failure must be sought. In the present work two

basic situations have been investigated, (1) crack initiation in passive metal and (2) crack initiation in unfilmed metal.

(1) For conditions in which a metal surface is passive, the most important factor appears to be the mechanical rupture of the passive film during fatigue and subsequent repassivation events. Both of these factors depend on the nature of the aqueous environment and of the passive film. Figure 5.9 shows schematically how transient dissolution can propagate deep into the metal. The stress concentrating factor of such a dissolution trench together with other factors, such as possible variations in the composition of the solution in the dissolution trenches compared with the bulk solution, can be used to explain premature crack initiation. It is important to note, however, that other mechanisms can act as aggravating factors still further reducing the fatigue life. For example, the ingress of hydrogen into the metal at slip bands, where it is associated with moving dislocations, can further reduce the crack initiation time. The enhanced activity of the moving slip steps and the increase in the amount of plastic strain due to preferential dissolution, also accelerates crack initiation as can the operation of a "Rebinder" mechanism as described in section 2.9.

(2) For an unfilmed metal surface the rupture of surface films mechanism is obviously irrelevant. The most important factor is the emergence of slip steps and their inherently greater reactivity, i.e. the preferential dissolution model together with the enhancement of plastic strain as described in section 2.9. Once again it is possible for other mechanisms to act as aggravating factors. For example the adsorption of surface active agents at the emerging slip steps by lowering the surface energy (Rebinder mechanism), can accelerate crack initiation. At the high positive potentials required for transpassivity it is hard to imagine how a hydrogen-assisted cracking mode can operate, because the generation of hydrogen by corrosion processes is highly improbable.

5.4. Fractography

Several interesting features were observed in the fractographic examination of the failed test-pieces, the more important being:-

(i) The nature and appearance of striations.

(ii) The nature and appearance of the point of initiation.

(iii) The occurrence of "flats" in the fracture face.

5.4.1. Nature and Appearance of Striations

For all the fractures examined the striations were ductile in appearance, as expected for stainless steel (227). No direct evidence has been obtained from the present work, but it is probable that the surface matching of the fracture is of the peak-to-peak and valley-to-valley type. A mechanism of the production of ductile striations such as that proposed by Laird and Smith (220) is favoured.

For air-fatigue tests using plain, polished test-pieces the pattern of striations was typical, radiating from the point of initiation in the direction of crack propagation to the final fracture region. The behaviour was similar for pre-pitted test-pieces except cracks initiated from many points, the advancing cracks coalescing and causing final fracture. These observations showed that the crack propagation was structure insensitive and was essentially a macroscopic phenomenon. It must be noted, however, that there are certain microscopic features which can modify the rate and direction of the fatigue crack propagation. The production of 'flats' on the fracture surface is one example of this phenomena. Generally, however, the striations lie in a direction parallel to the macroscopic crack growth direction. The evidence from the pre-pitted test - pieces suggests that any corrosion-fatigue mechanisms which occur, influence the crack initiation stage rather than the propagation stage.

For fatigue tests in aqueous environments the pattern of striations was much more erratic. The striations changed direction frequently and occurred only in isolated areas. This indicates that the direction of crack propagation also changes frequently because it is structure sensitive. This is only conjecture, but it seems to suggest that the presence of an aqueous environment induces structure sensitivity during crack propagation, perhaps because of the influence of the microstructure on the corrosion component.

A variation in the striation spacing was associated with the changes in direction of the propagating fatigue crack. This is expected because the acting stress intensity varies with the direction of crack propagation, varying the propagation rate and hence the striation spacing. As already observed, large areas of the fracture face were free of striations. Plumbridge and Ryder [204], have suggested four reasons for the "invisibility" of striations on fatigue fracture faces as follows:-

(i) the spacing may be too small for resolution by the observational technique used,

(ii) there may be insufficient ductility at the crack tip for a recognisable plastic deformation to be observed,

(iii) a fatigue-fracture mode may be in operation which does not produce striations.

(iv) Striations may be obliterated by damage subsequent to fracture.

Reason (i) can probably be discounted because the resolution of the SEM (0.1 μM) used to observe striations is better than the smallest striation spacing expected, reason (ii) can be discounted because the material tested is characterised by good ductility. Thus reasons (iii) and (iv) are the most likely. One possible explanation is that the crack can spread lateraly over considerable distances

during a single cycle if a salient of the crack front in one region is far advanced into the bulk of the material, because the resulting lateral stresses are then very great. This would result in the large striation-free areas with small isolated pockets of recognisable striations as observed. Assuming that each striation is produced during one stress cycle, it is apparent that the crack propagation stage occupies only a relatively small period of the total fatigue life, much the greater part of the life being spent on crack initiation (and/or stage I fatigue fracture). Thus very little information can be gained from a detailed study of fracture surfaces produced by the tests used in the present work.

It is also apparent from the observations of striations that accurate calculation of propagation rates from the striation spacings are impossible in such tests. Specially designed tests would be needed for the purpose.

5.4.2. Nature and Appearance of the Initiation Point

(1) For pre-pitted test-pieces the cracks normally initiated at the base of corrosion pits. This can be ascribed to the stress concentrating effect of such pits and their possible operation as occluded cells.

(2) For tests in aqueous environments, pits were frequently found associated with the crack initiation point. If produced prior to crack initiation they would, of course, have the same stress-raising and occluded cell effects as the pits in the pre-pitted test-pieces. Alternatively it is possible that the pits are produced after crack initiation, i.e. as a result rather than a cause of crack initiation.

Observation of the fracture surface surrounding the initiation point reveals that some sort of selective corrosion attack occurs in aqueous environments, especially sodium chloride, indicating perhaps a preferential dissolution mechanism or incipient stress

corrosion failure. The evidence does not warrant more than conjecture although it is probable that an element of stress-corrosion failure is associated with corrosion fatigue, especially in chloride media.

5.4.3. Occurrence of 'Flats' in the Fracture Surface

The occurrence of flat i.e. featureless facets in fatigue fracture faces have been observed by other investigators. In AISI 316 stainless steel Priddle and Walker (280) have suggested that they may be 'quasi-cleavage' facets, the cleavage being an integral part of the fatigue process and not an isolated area of fast fracture. This idea is consistent with the observations in the present work, the cleavage possibly occurring along twin boundaries. The observation that the facets are more profuse in aqueous media suggests that the process is aided by corrosion processes such as preferential attack at the twin boundaries. The presence of linear markings on the facets is more difficult to explain. One possible explanation is that they are outcropping slip steps, produced during fracture.

6. CONCLUSIONS

6.1 A fluctuating corrosion current signal was observed for AISI 316 stainless steel samples under potentiostatic control in aqueous environments on the application of a sinusoidal cyclic stress.

6.2 This fluctuating corrosion current signal was approximately sinusoidal, with the same frequency as the stressing cycle (24 Hz) and synchronised with it.

6.3 Although corrosion pits can undoubtedly act as stress raisers, other mechanisms can occur which significantly affect the fatigue behaviour of pre-pitted fatigue test-pieces tested in air, e.g. the operation of such pits as occluded corrosion cells.

6.4 For conditions in which the metal surface was passive a mechanism is proposed which involves the mechanical rupture of the passive film during fatigue leading to premature crack initiation.

6.5 For conditions in which the metal surface was transpassive (active) a mechanism is proposed which involves the preferential dissolution at emergent slip steps with resultant enhancement of plastic strain and premature crack initiation.

7. SUGGESTIONS FOR FURTHER WORK

7.1 Modification to the present equipment:-

(i) The introduction of a facility into the instrument measuring the fluctuating current for the automatic adjustment of the opto-isolator bias voltage to the required value.

(ii) The use of a variable speed motor on the reverse-bend fatigue rig to investigate the effect of varying frequency on corrosion-fatigue and on the fluctuating current parameter.

(iii) The addition of a facility for deaerating test solutions in the reverse-bend fatigue rig to aid the interpretation of electrochemical results.

(iv) The introduction of a 'reservoir' system for the test solutions to alleviate problems of evaporation.

7.2 An investigation of the repassivation rate, peak current density and passive film thickness in test solutions at different applied potentials and the effect of these parameters on the corrosion fatigue characteristics and fluctuating current measurements.

7.3 A detailed investigation of the effect of stress level on the fluctuating current parameter and other corrosion characteristics.

7.4 Measurement of the fluctuating current parameter during corrosion-fatigue crack propagation by modifying conventional crack propagation experiments.

7.5 An investigation of the effect of material variables, e.g. microstructure, heat treatment, surface condition, on the corrosion fatigue properties and the fluctuating current parameter.

7.6 A detailed investigation of the effect of fatigue on cathodic reactions.

7.7 Investigation of the effect of pit parameters on fatigue properties using better pre-corrosion treatments and of artificially produced

pits, in which no corrodents are trapped.

7.8 A comparison of pit parameters on static test-pieces and test-pieces under fatigue and a detailed investigation into the effect of pitting on the fluctuating current parameter.

7.9 An investigation of the initial effect of fatigue on the corrosion characteristics.

7.10 A detailed investigation of the occurrence of 'flats' on fatigue fracture faces and the mechanisms by which they are produced.

7.11 The application of the fluctuating current measurement technique to a 'push-pull' fatigue test in which problems such as stress gradients in the fatigue test-piece and the need for complicated 'masking' techniques can be alleviated.

APPENDIX A

The Potentiostat-Principle and Application to Corrosion Studies

The metal/solution interface at which a natural aqueous corrosion process is proceeding adopts a rest potential, $E_{R\,1}$ of such a value that the vector sum of the currents flowing from all of the contributing electrochemical reactions is zero. If the potential is artificially displaced from E_R , the magnitude of the net current flowing at the interface yields information on the corrosion characteristics of the system. The function of a potentiostat is to impose a controlled potential of the required constant value, or to follow any pre-determined potential programme scan and to record the resultant external current. This is accomplished as follows:

A sample of the metal (the working electrode) is exposed to the selected environment in a suitable cell, its potential relative to the solution is measured by a capillary probe (luggin probe) close to it and connected via a salt bridge to a vessel containing a reference electrode (e.g. a saturated calomel electrode). The potentiostat compares the actual potential with a pre-set control potential of opposite sign and applies the difference (the error signal) to the input of a DC power amplifier which supplies a correcting current between the working electrode and a third electrode in the cell (a counter electrode) of such a direction and magnitude as to eliminate the error signal. The current supplied is the required external current and is recorded by a chart recorder.

The applied potential can be programmed by superimposing the output of a motor driven potentiometer on the constant control of the potentiostat. If the potentiometer potential is scanned continuously with time the technique is termed "potentiodynamic"

and if varied in regular discreet steps it is termed "potentiostatic".

The features of a good potentiostat instrument which determine its performance are:

(i) rapid response

(ii) electrical stability, especially during periods when the external circuit exhibits the unstable electrical characteristic of decreasing current with increasing potential.

(iii) sufficient output power

(iv) high impedance at the reference electrode input.

The potentiostat used for the earlier experiments in the present work was a Wenking Type 70 TS1 having the following characteristics:

Response Time	$< 10\ \mu s$
Output Power	25W, $\pm$ 25V at $\pm$ 1A
Input Impedance	> 10 w
Output current characteristics	0-200 μA linear
	200 μA - 1mA transition range
	$>$ 1mA logarithmic

The main disadvantage of this potentiostat was the semi-logarithmic output current characteristics which make the interpretation of the polarisation curves difficult.

The instrument was replaced by a Wenking Type LB75L potentiostat when it became available. The new instrument had the following characteristics:-

Response time	$< 1\ \mu$ sec
Output power	25W, $\pm$ 25V at $\pm$ 1A
Input Impedance	$>$ 10w

Output current characteristics multiple ranges 10μA upto 1A correspond to 3V output voltage and full scale deflection on meter, linear output characteristics

A further great advantage of the Wenking Type LB75L potentiostat is the very low current output noise and ripple ($< 0.1 \mu A$) over the full bandwidth.

Test Procedure

The procedure was based on ASTM recommendation (281) outlined in the following summary:-

(i) all equipment was thoroughly washed in distilled water

(ii) the required electrolyte was prepared from 'Analar' grade reagents and distilled water.

(iii) if required, the electrolyte was purged with oxygen-free nitrogen, to deaerate the solution, for at least 30 minutes before immersing the specimen and then throughout the test.

(iv) the specimen was prepared for testing, and degreased just prior to immersion.

(v) the salt bridge probe was positioned adjacent to the immersed specimen.

(vi) the rest potential of the specimen, E_R , was recorded 60 minutes after immersion.

(vii) to determine anodic polarisation characteristics the specimen potential, Ec, was then increased anodically from E_R in 10mV steps at a rate of one step per minute and the resultant current was recorded by a pen recorder.

Alternatively, for a fixed potential run, the required potential was pre-set and the current variation with time recorded by a pen recorder.

APPENDIX B

A calibration curve was required for use in adjusting the throw of the reverse bend machine to apply any prescribed amplitude of cyclic stress.

The curve was drawn through co-ordinates relating measured values of the deflection of a test-piece to corresponding values of the maximum stress, calculated from known loads applied normal to the axis of a test-piece using a pulley system. Separate calibration was carried out for test-pieces of different thicknesses.

The stress, σ , was calculated from the applied load as follows:-

The maximum stress in a beam section is given by:

$$\sigma = \frac{My_{max}}{I} \qquad \text{.....(B1)}$$

Where M is the bending moment

I is the second moment of area

y_{max} is the section thickness

Modulus of section = $Z = \frac{I}{y_{max}}$ .....(B2)

therefore $\sigma = \frac{M}{Z}$ .....(B3)

For a rectangular section breadth b and width w

$$Z = \frac{bw^2}{6} \qquad \text{.....(B4)}$$

Hence $\sigma = \frac{6M}{bw^2}$ .....(B5)

But $M = L\,h$ .....(B6)

Where L is the force

h is the distance from point of application of force to the axis of rotation

and $L = W\,g$ .....(B7)

where W is the load applied

g is the acceleration due to gravity

Thus $\sigma = \frac{6 W g h}{b w^2}$

For these test-pieces used in this work:

W - load in k g

w - thickness in m

g - 9.81 m s^{-2}

h - 0.124 m

b - 0.0254 m

Thus $\sigma = 287 \times \frac{W}{w^2}$

Using these results the calibration curve given in Figure A1 of deflection d, against stress, σ, was constructed. It is evident from this figure that small differences in sample thickness did not significantly alter the calibration curve.

APPENDIX C

Calculation of the reduction in fatigue limit due to a semi-circular groove (282) :

$$K_f = \frac{\text{Fatigue strength of un-notched test-piece}}{\text{Fatigue strength of notched test-piece}} \quad \ldots\ldots(C1)$$

$$q = \frac{K_f - 1}{K_t - 1} \quad \ldots\ldots\ldots\ldots\ldots(C2)$$

Where q is the Notch sensitivity factor of the material

K_t is the theoretical stress concentration factor

and $$K_t = \frac{\sigma m}{\sigma n} \quad \ldots\ldots\ldots\ldots\ldots(C3)$$

Where σm is the maximum stress

σn is the nominal stress

K_t is an idealised factor, applying only when the stress is normal. In real situations the stress is biaxial at a notch and is taken into account by introducing a factor K_t' , known as the combined factor, where:

$$K_t' = m K_t \quad \ldots\ldots\ldots\ldots\ldots(C4)$$

and where m is a factor taking account of the Mises criterion. Thus equation (C2) becomes

$$q = \frac{K_f - 1}{K_t' - 1} \quad \ldots\ldots\ldots\ldots\ldots(C5)$$

Using this equation the value of q is required to evaluate K_f An average value of q is normally used in this evaluation and equation (C5) becomes:

$$K_{t'f} = q (K_t' - 1) + 1 \quad \ldots\ldots\ldots(C6)$$

Where $K_{t'f}$ is the estimated combined fatigue notch factor calculated using the average value of q.

For a semi-circular groove, (see Figure C1)

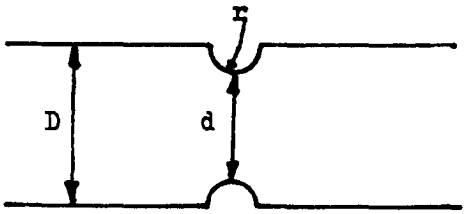

Figure C.1 Parameters of semi-circular groove

Using the appropriate values of D,d and r for the pre-pitted test-pieces i.e.

$D = 3.81$ mm

$d = 3.61$ mm

$r = 0.1$ mm (radius of larger pits)

then $K_t' = 2.325$ (from tables in reference 282)

Substituting for K_t' in equation (C6)

$$K_{t'f} = 1 + q\ (2.325 - 1)$$

It is usually assumed that a reasonable value for q in these calculations is 0.3.

Hence

$$K_{t'f} = 1.3975$$

But

$$K_{t'f} = \frac{\sigma_{f\ max}}{\sigma_{t'f}} \qquad \text{.....(C7)}$$

where $\sigma_{f\ max}$ is the fatigue limit for un-notched test-pieces and $\sigma_{t'f}$ is the expected fatigue strength of a test-piece with a circumferential semi-circular notch.

From figure 4.1 $\sigma_{f\ max} = 300\ MN\ m^{-2}$

Therefore $\sigma_{t'f} = \frac{300}{1.3975}\ MN\ m^{-2}$

$= 215\ MN\ m^{-2}$

REFERENCES

(1) Haigh, B.P., J. Inst. Metals, 18, 1917, p. 55

(2) McAdam, D.J., Proc. ASTM., 26, II, 1926, p. 224

(3) Journeaux, G.E., Ph. D., Thesis, Brunel University, 1976

(4) Wohler, A., Engineering, 11, 1871, p.199

(5) Forrest, P.J., "Fatigue of Metals", Pergamon Press, 1962

(6) Weibull, W. (Ed.), "Fatigue Testing and Analysis of Results" Pergamon Press, 1961

(7) A.S.T.M., "Manual of Fatigue Testing", A.S.T.M., S.T.P.91, 1949

(8) Barsom, J.M., Devereux, O.F., et. al. (Eds.) "Corrosion Fatigue : Chemistry, Mechanics and Microstructure", University of Connecticut, Storrs, Connecticut, 1971, p.424

(9) Atkinson, J.D., and Linley T.C., "The Influence of Environment on Fatigue", I.Mech.E., Conference publications 1977-4, 1977, p. 65

(10) Stephenson N., National Gas Turbine Establishment Memo M320, 1958

(11) Endo, K., and Miyao, Y., Bulletin of Jap. I.S.M.E. 1 , 1958 p.374

(12) Atkinson, M., J.Iron and Steel Inst., 195, 1960, p.64

(13) Epremian, E., and Mehl, R.F., A.S.T.M., S.T.P., 137, 1953

(14) Spahn, H., and Fabler, K., Materialprufungsbericht BASF., 1975

(15) Spahn, H., Metalloberflache, 16 , 1962, p.370

(16) Gould, A.J., Engineering, 141, 1936, p.495

(17) Cornet, I., and Golan, S., Corrosion, 15, 1959, p.292

(18) Inglis, C.E., Trans. Int. Nav. Arch., 55, 1911, p.2919

(19) Griffith, A.A., Phil. Trans. Roy. Soc., A221, 1920, p.163

(20) Griffith, A.A., Proc. Int. Congr. App. Mech., Delft, 1924, p.55

(21) Irwin, G.R., 9th Int. Congr. App. Mech., VIII, Paper 101 (II), University of Brussels, 1957, p.245

(22) Paris, P.C., and SIH G.C.M., A.S.T.M., S.T.P., 381, 1965, p.30

(23) Dugdale, D.S., J.Mech. Phys. Solids, 8 , 1960, p.100

(24) B.S. 5447, "Fracture Toughness Testing"

(25) A.S.T.M., "Fracture Toughness Testing" A.S.T.M. S.T.P. 381, 1964

(26) A.S.T.M., "Materials Research and Standards", 4 , (3), 1964, p.107

(27) Cottrell,A.H., Iron and Steel Inst. Spe. Rep. 69, 1961, p.281

(28) Wells, A.A., "Crack Propagation Symposium Proceedings", Cranfield College of Aeronautics, 1 , 1961, p.210

(29) Knott, J.F., "Fundamentals of Fracture Mechanics", Butterworths, London, 1973, p.153

(30) Rice, J.R., "Fracture - An Advanced Treatise", Ed. H. Leibowitz, Academic Press, New York, 1968, p.191

(31) Rice, J.R., J, Appl. Mech. (Trans. A.S.M.E.), 1968, p.379

(32) Bucci, R.J., et. al., A.S.T.M. S.T.P. 514, 1972, p.40

(33) Boyd, G.M., Eng. Fract. Mech., 4 , 1972, p.459

(34) Johnson, H.H. and Paris, P.C., Eng. Fract. Mech., 1 , 1968, p.3

(35) Paris P. and Erdogan, F., Trans. A.S.M.E., J. Basic Eng., 85 1963, p.528

(36) Ritchie, R.O., Fatigue 77,Preprints Cambridge, 1977, p.61

(37) Laird, C. and Smith, G.C., Phil. Mag. 7, 1962, p.847

(38) Pelloux, R.M.N., Eng. Fract. Mech. 1, 1970, p.697

(39) Tomkins, B. "The Mechanics and Physics of Fracture", Metal Society, London, 1975, p.226

(40) Ritchie, R.O. and Knott, J.F., Mater. Sci. Eng., 14, 1974, p.7

(41) Austen, I.M. and Walker, E.F., "The Influence of Environment on Fatigue", I. Mech. E., Conference publications, 1977-4, 1977, p.1

(42) Gallagher, J.P., and WEI R.P. As reference 8, p. 409

(43) McEvily, A.J. and WEI R.P. As reference 8, p.381

(44) Pickering, F.B., International Metals Reviews, Review 211, 1976, p. 227

(45) Keating, F.H., "Chromium-Nickel Austenitic Steels", Butterworths, London, 1956

(46) Schneider, H., Foundry Trade J., 108, 1960, p.562

(47) Pickering, F.B., "Heat-treatment aspects of metal-joining processes", The Iron and Steel Institute, London, 1972, p.84

(48) Irvine, K.J. et. al., J. Iron Steel Inst. 207, 1969, p.1017

(49) Irvine, K.J. et. al., Ibid, 199, 1961, p.153

(50) Pickering, F.B., "Towards improved ductility and toughness", Climax Molybdenum Company Synposium, Kyoto, 1971, p.9

(51) Shreir, L.L. (Ed.) "Corrosion" George Newnes Ltd., 1965

(52) Evans, U.R. "The Corrosion and Oxidation of Metals" Arnold, 1960

(53) Bockris, J. O'M and Reddy, A.K.N., "Modern Electrochemistry" Macdonald and Co. Ltd., 1970

(54) West, J.M., "Electrodeposition and Corrosion Processes", D. Van Nostrand Co. Ltd., 1965

(55) Pourbaix, M. Corrosion, 25, 1969, p.269

(56) Schwerdtfeger, W.J. and McDorman O.N., J. Electrochem. Soc. 99 1952, p.407

(57) Pearson, J.M., Trans. Electrochem. Soc. 81 1942, p.485

(58) Stearn, M. and Geary, A.L. J. Electrochem. Soc. 104, 1957, p.56

(59) Stearn, M. and Weisart, E.D. Proc. ASTM., 59 , 1959, p.1280

(60) Cihal, V. and Prazak, M. J.I.S.I. 193 1959, p.362

(61) Florianovitch, G.M., Kolotyrkin, Y.M., and Smirnova, N.K. Dok 1, Akad, Nauk USSR., 61 p. 664

(62) Morioka, S. and Sakivama K., J. Japan Inst. Met., 19, 1955, p.438

(63) Rochel, M.B., Corrosion, 29, 1973, p.393

(64) Olivier, R. Proc. 6th meeting CITCE., Butterworths Scientific Pubs., London, 1954, p.314

(65) King, P.F., and Uhlig, H.H., J. Phys. Chem. 63, 1959, p.2026

(66) Kolotyrkin, Y.M. Z Elektochem. 62, 1958, p.664

(67) Aronowitz, G. and Hackerman, N. J.Electrochem Soc. 110, 1963, p. 633

(68) Frankenthal, R.P., J.Electrochem. Soc., 116, 1969, p.1646

(69) Okamoto, G., Corrosion Science, 13, 1973, p.471

(70) McBee, C.L., and Kruger, J., Electrochem. Acta, 17, 1972, p.1337

(71) Holliday, J.E. and Frankenthal, R.P. J. Electrochem. Soc., 119 1972, p.1190

(72) Okada, H., Ogawa, H., Itoh, I. and Omata, H. "Passivity and its breakdown on Iron and Iron Alloys" Eds. Staehle, R.W., and Okada, H., U.S., and Japan Seminar, N.A.C.E., Hawaii, 1975 p.82

(73) Yahlon, J. and Ives, L.K., as ref. 72, p.69

(74) Lumsden, J.B., and Staehle, R.W., as ref. 72, p.75

(75) Shimodaira, S., as ref. 72, p.194

(76) Nagayama, N. and Foley, R.T., as ref. 72, p.85

(77) La Que, F.L., and Cox, G.L., Proc. ASTM., 4, 1940, p.670

(78) Jesper, H. and Grutzner G., "Corrosion effects on rust-resisting and acid-resisting steels" Fortuna Technical Report, April 1965

(79) Kinzel A.B., Trans. Amer. Inst. Min. Metallurg. Eng. 194 1952 p.469

(80) Stickler, R. and Vinckier, A., Trans. Amer. Soc. Metals, 54 1952, p.362

(81) Pomey, G., Trans. Amer. Inst. Min. Metallurg. Eng. 218 1960, p.310

(82) Baumet, A. et. al. Corrosion Sci. 4 1964, p.89

(83) Brennert, S., J.I.S.I., 135 , 1937, p.101

(84) Hoar, T.P. and Jacob, W.R., Nature 216 1967, p.1299

(85) Broli, Aa, Holtan H., and Midjo M., Br. Corros. J. 8 1973, p.173

(86) Stolica, N. Corros. Sci. 9 1969, p.455

(87) Broli, Aa, Holtan H. and Andreassen, T.B., Werkstoff und Korrosion 27 1976, p.497

(88) Schwenk, W. Corrosion 20 1964, p.129t

(89) Szklarska-Smialowska, Z., and Janik-Czachor, M., Corrosion Science, 11 1971, p.901

(90) Hisamatsu, Y. as ref. 72 p.99

(91) Schwenk, W. Corrosion Science 5 1965, p.245

(92) Kolotyrkin, Y.M. Corrosion, 19 1963, p.261t

(93) Szklarska-Smialowska, Z., and Mankowski, J., Corrosion Science 12 1972, p.925

(94) Leckie, H.P., and Uhlig H.H., J. Electrochem. Soc. 113 1966, p.1262

(95) Kruger, J. as ref. 72 p.91

(96) Kolotyrkin, Y.M., J. Electrochem. Soc. 108 1961, p.209

(97) Bohn, H. and Uhlig, H.H., J. Electrochem. Soc. 116 1969, p.906

(98) Uhlig, H.H., as ref. 72, p.110

(99) Rosenfeld, I.L., and Danilov, I.S., Corrosion Science 7 1967, p.129

(100) Wilde, B.E. as ref. 72, p.129

(101) Brauns, E. and Schwenk, W., Arch. Eisenhuttenwes 32 1961, p.387

(102) Uhlig, H.H. and Matthews, J.W., Corrosion 7 1951, p.419

(103) McBee, C.L., and Kruger J. "Localised Corrosion" Ed. Staehle, Brown, Kruger and Agrawal N.A.C.E., 1974, p.252

(104) Ambrose, J.R., and Kruger, J., Proc. 4th International Congress on Metallic Corrosion N.A.C.E., 1972, p.698

(105) Hoar, T.P., Mears, D.C. and Pryor, M.S. Corrosion Science 5 1965, p.279

(106) Evans, U.R., Bannister, L.C. and Britton S.C., Proc. Roy. Soc. A131 1931, p.367

(107) Richardson, J.A., and Wood, G.D., J. Electrochem. Soc. 120 1973, p.193

(108) Hoar, T.P., Corrosion Science 7 1967, p.341

(109) Sato, N., Electrochem. 19 1971, p.1683

(110) Videm, K., Kjeller Report KR-149 Institute for Atomenergi Kjeller, Norway, 1974

(111) Bond, A.P., and Lizlous, E.A., J. Electrochem. Soc. 115 1968, p.1130

(112) Herbsleb, G., and Schwenk, W., Corrosion Science 13 1973, p.739

(113) Kruger, J. and Ambrose, J.R., NBS Report, NB51R 74-583 September, 1974

(114) Szklarska-Smialowska, Z., and Janik-Czachor, M., Passivation and Anodic Protection ref. 6.4 p.651

(115) Szklarska-Smialowska, K., and Szummer A., and Janik-Czachor M., Br. Corrosion J. 5 1970, p.159

(116) Szummer, A., Szklarska-Smialowska, K., and Janik-Czachor, M., Corrosion Science 8 1968, p.827

(117) Wranglen, G., Corrosion Science 14 1974, p.331

(118) Ekland, G.S., J. Electrochem. Soc. 121 1974, p.469

(119) Overmann, F.F., Corrosion 22 1966, p.48

(120) Mankowski J., and Szklarska-Smialowska, Z., Corrosion Science 15 1975, p.493

(121) Staehle, R.W., as ref. 72 p.155

(122) Yamamoto "Theory of the straining electrode and effect of surface treatments on the straining electrode" Masters Thesis, Ohio State University, 1974

(123) Latanision, R.M. and Staehle R.W., Acta Metallurgica 17 1969, p.307

(124) Hoar, T.P. "Proceedings of Conference on Fundamental aspects of stress corrosion cracking" Ed. Staehle R.W., Forty, A.J., and Van Rooyan, D. N.A.C.E., Houston 1968, p.98

(125) Hoar, T.P., and Scully, J.C., 2nd International Congress on metallic corrosion, New York, 1963 N.A.C.E., Houston, 1966 p.184

(126) Despic A.R., Raicheff, R.G. and Bockris, J. O'M J. Chem. Phys. 29 1968 p.926

(127) Shibata, T. and Staehle, R.W., "Proceedings of 5th International Congress on Metallic Corrosion" N.A.C.E. 1974 p.487

(128) Pagetti, J., Lees D., Ford, P., and Hoar, T., C.R.Acad. Sc. Paris, Ser. C. 293 1971, p.1121

(129) Ambrose, J. and Kruger, J. Corrosion 28 1972 p.30

(130) Tomashov, N.D., and Vershina, L.P. Electrochem. Acta. 15 1970, p.501

(131) Beck, T.R. J. Electrochem. Soc. 15 1968, p. 890

(132) Okada, H., Abe S., and Murata, T., as ref. 72 p.147

(133) Galvele, J.R., de Wexler S.B., and Gardiazabac, I., Corrosion 31 1975, p.352

(134) Galvele, J.R., and Maier, I., as ref. 72 p.178

(135) Ohtami, N., and Hayashi, Y., as ref. 72 p.169

(136) Staehle, R.W., International Conference on SCC and hydrogen embrittlement of iron base alloys, Firminy, France, 1973

(137) Matsushima, I., as ref. 72 p.181

(138) Matsushima, I., unpublished work

(139) Forsyth, P.J.E., Proc. Crack Propagation Symposium, Cranfield 1961, 1962 p.76

(140) Brown, L.M., Fatigue '77 Preprints,Conference , Cambridge, 1977 paper No. 7

(141) Winter, A.T., Phil. Mag. 28 1973 p.57
30 1974 p.19

(142) Laird, C. and Finney, J.M., Phil. Mag. 31 1975 p.339

(143) Laird, C. Materials Science and Engineering 25 1976, p.187

(144) Lynch, S.P., Metal Science 9 1975, p.401

(145) Wood, W.A., "Fracture" John Wiley 1959, p.412

(146) Grosskreutz, J.C., Phys. Stat. Sol. b 47 1971, p.359

(147) Laird, C. "Fatigue Crack Propagation" S.T.P. No. 415 ASTM 1967, p.139

(148) Pelloux, R.M.N., "Fracture" Chapman & Hall, Brighton, 1969 p.731

(149) Schijve, J., as ref. 147 p.415

(150) Forsyth, P.J.E., and Ryder, D.A., Metallurgia 63 1961 p.117

(151) Laird, C., and Duquette, D.J., "Corrosion Fatigue : Chemistry Mechanics and Microstructure" N.A.C.E., Houston, 1972 p.88

(152) Thompson, N., Wadsworth, N.J., and Lovat, N., Phil. Mag. 1 1956, p.113

(153) Shen, H. Podlaseck, S.E., and Kramer, I.R., Acta. Met. 14 1966, p.341

(154) Kramer, I.R., and Demer, L.J. Prog. in Metal Physics p.133

(155) Bennett, J.A., J.Res. NBS 68C 1964, p.91

(156) Grosskreutz, J.C. and Bowles, C.Q., "Environment sensitive mechanical behaviour" Ed. Westwood and Stotoff; Gordon and Breach, 1967

(157) Grosskreutz, J.C., Surface Sci. 8 1967, p.173

(158) Wadsworth, N.J., and Hutchins, J., Phil. Mag. 3 1958, p.1154

(159) Laird, C. and Smith, G.C., Phil. Mag. 8 1963, p.145

(160) Achter, M., ASTM., STP., 415 1967 p.181

(161) Latanision, R.M., and Westwood, A.R.C., "Advances in corrosion Science and Technology" Plenum Pr. 1967, p.80

(162) McAdam, JR. D.J., and Geil, G.W., Proc. ASTM. 41 1928, p.696

(163) McAdam, JR. D.J., Proc. ASTM. 31 1931, p.259

(164) Laird, C. and Duquette, D.J., as reference 8 p.107

(165) Duquette, D.J., and Uhlig, H.H. Tran. ASM 62 1969 p.839

(166) Evans, U.R., and Simnad, M.T. Proc. Roy. Soc. A.188 1947, p.372

(167) Simnad, M.T., J. Electrochem. Soc. 97 1950, p.316

(168) Lihl, F. Metall. 4 1950 p.130

(169) Glikman L. and Suprun, L. Trudy Vsesoyuz Soveshshaniyx Po Bor'be Smorskol Korroziei Metal, Baku, 1956 p.102

(170) Spahn, H., Metalloberflache 16 1962, p.299

(171) Rollins, V, Arnold B and Lardner, E. Br. Corros. J. 5 1970, p.33

(172) Pyle, T., Rollins, V., and Howard, D., Corrosion Fatigue,1972 p.312

(173) Foroulis, Z. and Uhlig, H.H., J. Electrochem. Soc. 111 1964, p.522

(174) Greene, N.D., and Saltzmann, G.A., Corrosion 20 1964, p.293t

(175) Duquette, D.J. and Uhlig, H.H. Trans. ASM 61 1968, p.449

(176) Vedenkin, S. and Sinyavskii Bor'by S. Korrozei Azerb Inst. Neft I Khin 1962, p.30

(177) Lee, H.H., and Uhlig, H.H., Met. Trans. 3 1972 p.2949

(178) Revie, R.W., Ph.D., Thesis, MIT Cambridge Mass. 1972

(179) Asphahani, A.I., Ph.D. Thesis MIT Cambridge, Mass. 1975

(180) Simnad, M.T. and Evans, U.R. Proc. Roy. Soc. A188 1947, p.378

(181) Laute, K. Oberfalchentech 10 1933, p.281

(182) Spahn, H., as ref. 8, 1972, p.40

(183) Ryabchenkov, A.V., Z. fiz. khim. 26 1952 p.542

(184) Pyle, T., Rollins V., and Howard D., J.Electrochem. Soc. 122 1975, p.1445

(185) Patel, C., Pyle, T., and Rollins, V. Metal Science, 1977 p.185

(186) Patel, C., Pyle, T., and Rollins, V. Nature 266 1977, p.517

(187) Grosskreutz, J.C., as ref. 8 1972, p.201

(188) Payer, J.H., and Staehle, R.W., as ref. 8 1972, p.211

(189) Liktman, V., Shchukin, E., and Rebinder, P. "Physiochemical Mechanics of Metals" Academy of Sciences, U. S.S.R., Israel Programme for Scientific translations, Jerusalem, 1964, p.12

(190) Vensrem, K. and Rebinder, R.A. Z.Fiz. Khim 26 1952, p.12

(191) Kramer, I. and Demer, L. Prog. in materials science 9 , 1961 p.195

(192) Karpenko,G.Korroziya Metal. I Metody Bor'by S Neyu (Moscow: Gosudarst Izdatel Oboron Prom) Sbornik 1955, p.52

(193) Karpenko, G. Deyaki Pitannya fiz Khim. Mekum Metal Akad. Nauk. Ukr. RSR Inst. Machinoznushia Ta Automatiki, 1958 p.47

(194) Pelloux, R.M., Stoltz, R.E., and Moskouitz J.A. Materials Sci. Engineering 25 1976 p.193

(195) Howard, D. and Pyle, T. Br. Corros. J. 3 1968, p.302

(196) Spahn, H. and Wagner, G.H. Bruchuntersuchungen und Schadenklarung p.59

(197) Bradshaw & Wheeler App. Mat. Res. 5 1966, p.112

(198) Wei, R.R. Eng. Fract. Mech. 1 1970 p.633

(199) Ford, F.P. and Hoar, T.P. J.Electrochem. Soc. 1975 p.132

(200) Grosskreutz, J.C. J.Electrochem. Soc. 7 1970, p.940

(201) Gell, M. and Duquette, D.J. as ref. 8 p.366

(202) Grosskreutz, J.C., Physica Status Solidi 47 1971 p.11

(203) Tyson, W.R. & Alfred L.C.R. as ref. 8 p.281

(204) Plumbridge, W.J. and Ryder D.A., Metallurgical Reviews 136 1970 p.119

(205) McMillan, J.C. and Hertzberg, R.W. "Electron Fractography" ASTM., STP., 436 1968 p.89

(206) Broek, D. Int. Met. Review No. 185 1974 p.135

(207) McCall, J.L. "Electron Fractography" ASTM., STP., 436 1968 p.3

(208) Nageswararao, N. and Gerold, V. Metal Sci. 1977 p.31

(209) Gell, M. and Leverant, G.R. Acta Met. 16 1968 p.553

(210) Stubbington, C.A. and Forsyth, P.J.E. Metallurgica 74 1966 p.15

(211) Ham, R.K. and Wayman M.L. Trans Met. Soc. AIME 239 1967 p.721

(212) Berry, J.M. Trans. Am. Soc. Metals 51 1959 p.556

(213) Duquette, D.J. and Gell, M. Met. Trans. 2 1971 p.1325

(214) Zappfe, C.A. and Worden, C.D. Trans Amer. Soc. Metals 41 1949, p.396

(215) Forsyth, P.J.E., "A two-stage process of fatigue crack growth" Proceedings of the crack propagation symposium, College of Aeronautics, Cranfield, England 1 1961, p.76

(216) Forsyth, P.J.E. and Ryder, D.A. Aircraft Engineering 32 1960, p.96

(217) Stubbington, C.A. R.A.E. Report CPM 4 1963

(218) Stoltz, R.E. and Pelloux, R.M.N., Corrosion 29 1973 p.13

(219) Wanhill, R.J.H., Corrosion 31 1975 p.66

(220) Laird, C. and Smith G.C. Phil. Mag. 8 1945 1963

(221) Matting, A. and Jacoby, G. Aluminium 38 1962 p.654-667

(222) Meyn, D.A. Trans. ASM 61 1968 p.42

(223) Pelloux, R.M.N. Trans. ASM 62 1969 p.281

(224) Meyn, D.A. NLR Mem. Rep. No. 1707 1966

(225) Bates, R.C., Clark, W.G. and Moon D.M. ASTM., STP. 453 1969 p.192

(226) Barsom, J.M., Immof, E.J., and Rolfe, L.T., Eng. Fracture Mech. 2 1971 p.301

(227) Wareing, J. and Vaughan, H.G. Metal Sci. 1977 p.439

(228) Bathias, C. and Pelloux, R.M.N., Metall. Trans. 4 1973 p.1265

(229) Tomkins, B. J.Eng. Mater. Techn. 97 1975 p.289

(230) Hartman, A. et. al. Nat. Lucht. Ruimtevaartlab Tr-M-2182 1967

(231) Johnson, W.H. Iron 1 1873 p.291, p.452

(232) Broom, T. and Nicholson, A. J.Inst. Met. 89 1960 p.183

(233) Bernstein, I.M. and Thompson A.W. (Eds.) Hydrogen in Metals ASM U.S.A. 1973

(234) Taplin D.M.R. (Ed.) "Fracture 1977 - Advances in Research on the strength and fracture of materials" Pergamon Press N.Y. 1977

(235) Thompson, A.W. and Bernstein, I.M. "Effect of Hydrogen on behaviour of materials" Metallurgical Soc. of AIME, N.Y. 1976

(236) Troiano A.R. Hydrogen in metals ASM U.S.A. 1977 p.3

(237) Zapffe, C.A., Trans. ASM, 40 1948 p.315

(238) Williams, J.C. as ref. 235 p.367

(239) Bernstein, I.M., Garber, R. and Pressouyre, G.M., as ref. 235 1976, p.37

(240) Talbot, D.E.J. Int. Met. Reviews 20 Review 201 1975, p.166

(241) Foster, L.M. et. al. Nucleonics 21 1963 p.53

(242) Wriedt, H.A. and Darken, L.S., Trans. AIME, 233 1965 p.111,121

(243) Pfeil, L.B., Proc. Roy. Soc. A112 1926 p.182

(244) Troiano, A.R., Trans. ASM, 52 1960 p.54

(245) Oriani, R.A., Ber. Bunsenges, Phys. Chem., 76 1972 p.848

(246) Zappfe, C.A. and Sims, C.E., Trans. AIME, 145 1941 p.225

(247) Louthan JR. M.R. "Hydrogen in Metals" eds. I.M. Bernstein and A.W. Thompson, ASM., Ohio 1974 p.53

(248) Petch, N.O. and Stables, P. Nature 169 1952 p.842

(249) Williams, D.P. and Nelson, H.G., Met. Trans. 1 1970 p.63

(250) Van Leeuwen, H.P., Corrosion 31 1975 p.154

(251) Beachem, C.D., Met. Trans., 3 1972 p.437

(252) Westlake, D.G. Trans. ASM., 62 1969 p.1000

(253) Bastien, P. and Azou, P., C.R. Acad. Sci. 231 1951 p.69

(254) Louthan JR. M.R., Caskey JR. G.R., Donovan J.A. and Rawl Jr. D.E., Mater. Sci. Eng. 10 1972 p.357

(255) Fidelle, J.P., Broudeur, R., Roux, C. "Effect of Hydrogen on Behaviour of Materials", eds. A.W. Thompson and I.M. Bernstein, Met. Soc. AIME, Wyoming 1975 p.507

(256) Bernstein, I.M., and Thompson A.W., Int. Met. Reviews, Review 212 1976 p.269

(257) Oriani, R.A., Stress Corrosion Cracking and Hydrogen Embrittlement of Iron Base Alloys, R.D. McCright and R.W. Staehle eds. NACE., Houston 1976

(258) Rice, J.R. "Effect of Hydrogen on Behaviour of Materials" 1975 p.455

(259) Van Leeuwen, H.P. as ref. 258 1976 p.480

(260) Stollof, N.S. and Johnston, T.L., Acta Met. 11 1963 p.251

(261) Westwood, A.R.C. and Kamdar M.H., Phil. Mag. 8 1963 p.787

(262) Thompson, A.W. and Bernstein, I.M., "Fracture 1977" ed. D.M.R. Taplin, Vol. 2A, Pergamon Press, New York 1977, p.249

(263) Gerberich, W.W., Garry, J. and Lessar, J.F., as ref. 258 1976 p.70

(264) Cox, T.B., and Gudas, J.P. as ref. 258 1976 p.287

(265) Tetelman, A.S. as ref. 247 1974 p.17

(266) Johnson, H.H., as ref. 247 1974 p.35

(267) Louthan JR. M.R. and McNitt, R.P. as ref. 258 1976 p.496

(268) Scully, J.C. as ref. 258 1975 p.129

(269) Dutton, R. and Puls, M.P. as ref. 258 1976 p.516

(270) Magnani, N.J. as ref. 258 1976 p.189

(271) Odegard, B.C., Brooks, J.A. and West., A.J., as ref. 258 1976 p.116

(272) Frandsen, J.D. and Marcus, H.L. as ref. 258 1976 p.233

(273) Thompson, A.W., "Hydrogen in Metals" 1974 p.91

(274) Laurent, J.P. et. al. as ref. 233 p.559

(275) Thompson, A.W., as ref. 258 1976 p.506

(276) Karlashov, A.V. and Batov, A.P. Sov. Mater. Soi. 3 1967 p.211

(277) Paul, M. and Weiland, H. Sov. Mater. Sci. 5 1965 p.22-25

(278) Hoar, T.P. and Hines J.P. J.Iron and Steel Inst. 182 1956 p.124

(279) Hoar, T.P. and West, J.M. Nature 181 1958 p.835

(280) Priddle, E.K. and Walker, F.E. J.Mater. Sci. 11 1976 p.386

(281) A.S.T.M., Standard Reference Method for Making Polarisation measurements, A.S.T.M. GS-71 1971

(282) Petersen, R.E., "Stress Concentration Design Factors", John Wiley and Sons, New York, 1953

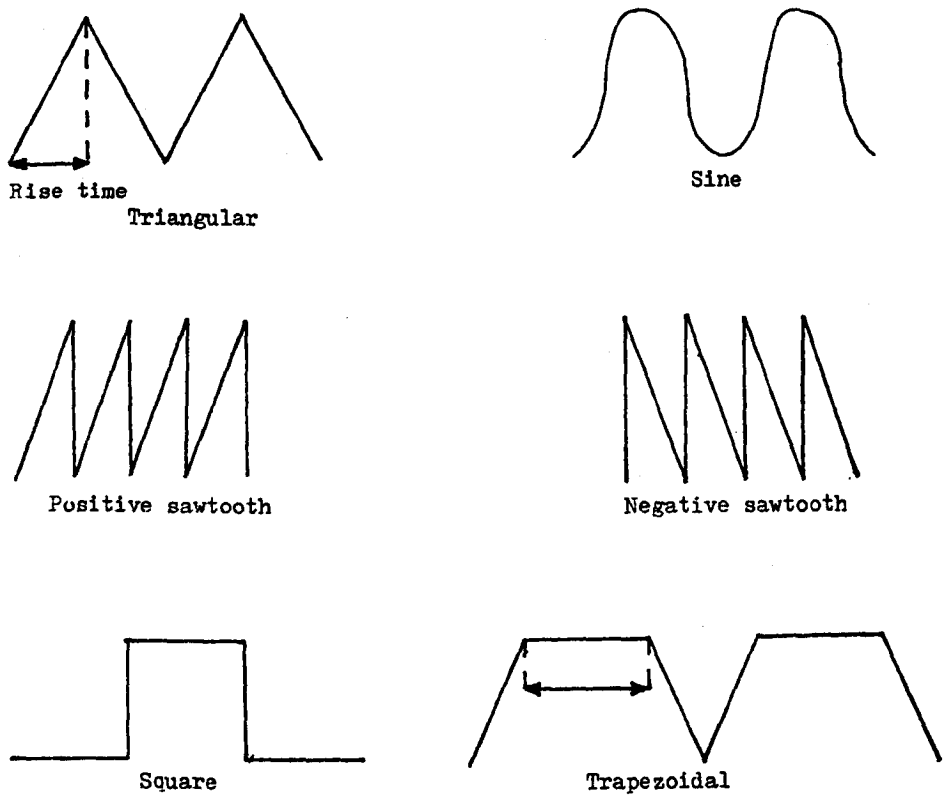

Fig. 2.1 Various types of waveform used in fatigue tests.

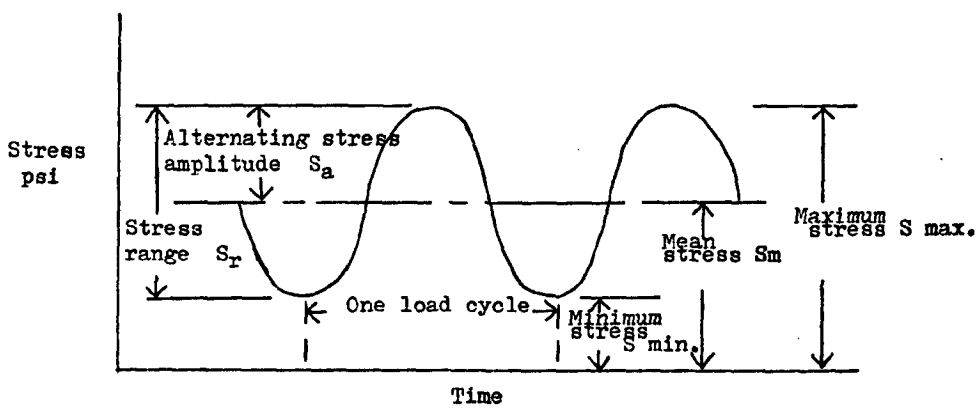

Note that $S_m = \frac{S_{max} + S_{min}}{2}$ $\quad S_r = S_{max} - S_{min}$

$S_a = \frac{S_r}{2} = \frac{S_{max} - S_{min}}{2}$

R or A = Stress ratio

$R = \frac{S_{min}}{S_{max}}$ $\quad A = \frac{S_a}{S_m}$

Figure 2.2 Nomenclature used in fatigue

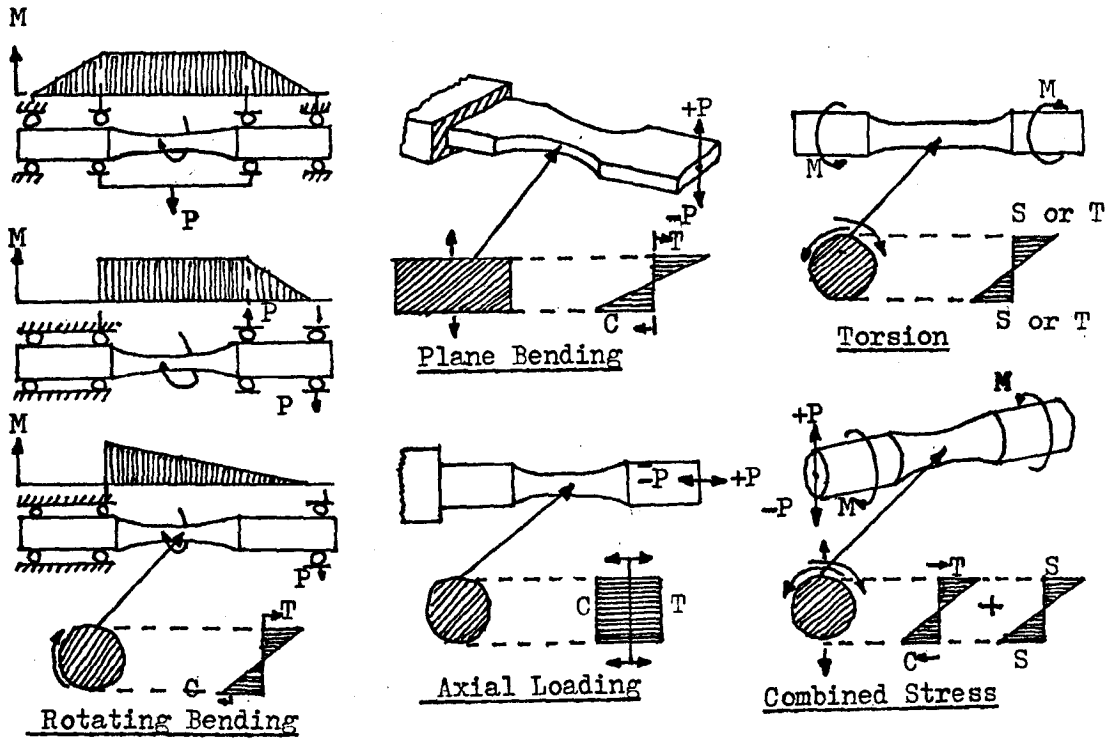

Fig. 2.3 Principles of main types of fatigue testing machines (T-Tension C-Compression S-Shear)

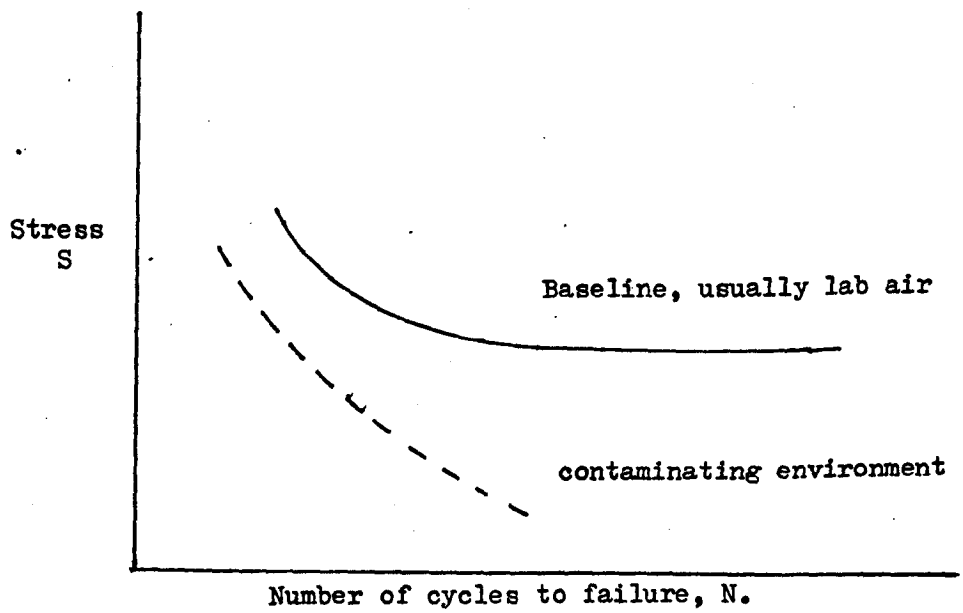

Fig. 2.4 The influence of environment on basic fatigue behaviour (S-N curve).

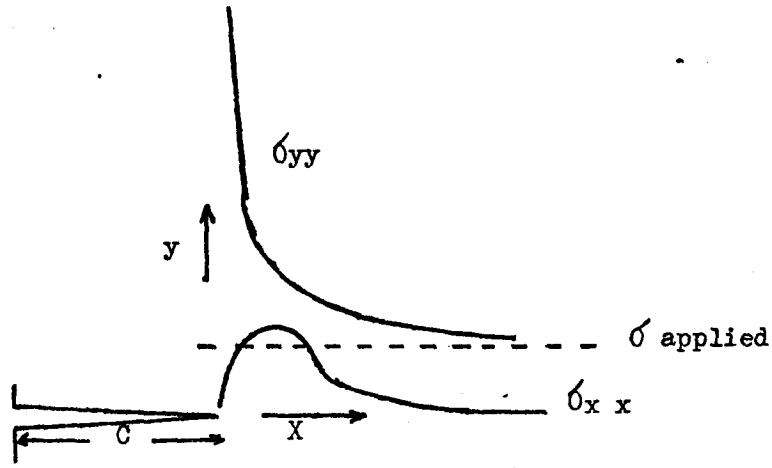

Fig. 2.5 Stress distribution for elliptical through - crack loaded in tension.

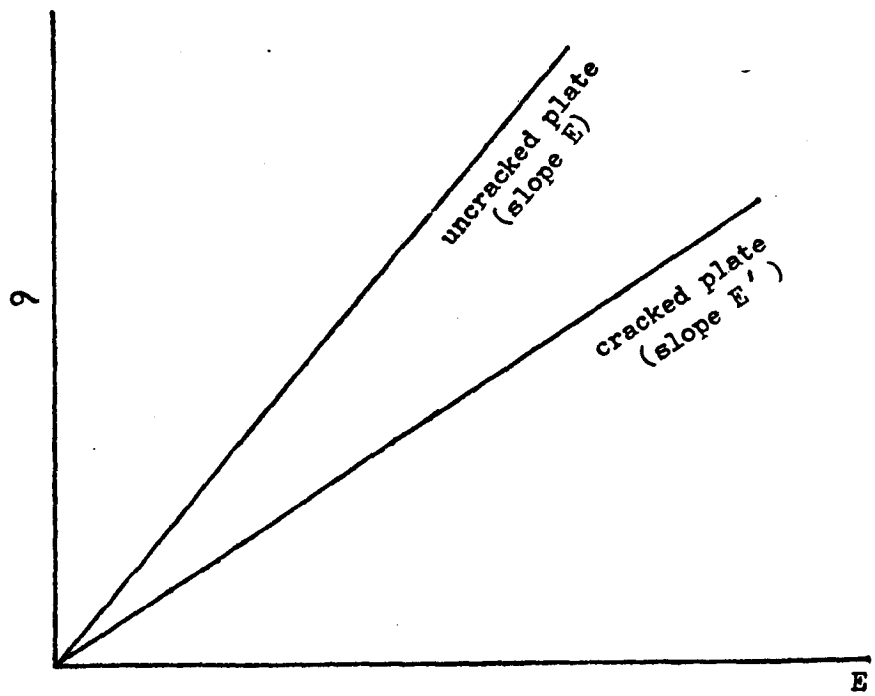

Fig. 2.6 Stress-strain curve under elastic loading showing the effect of pre-cracks on Young's modulus.

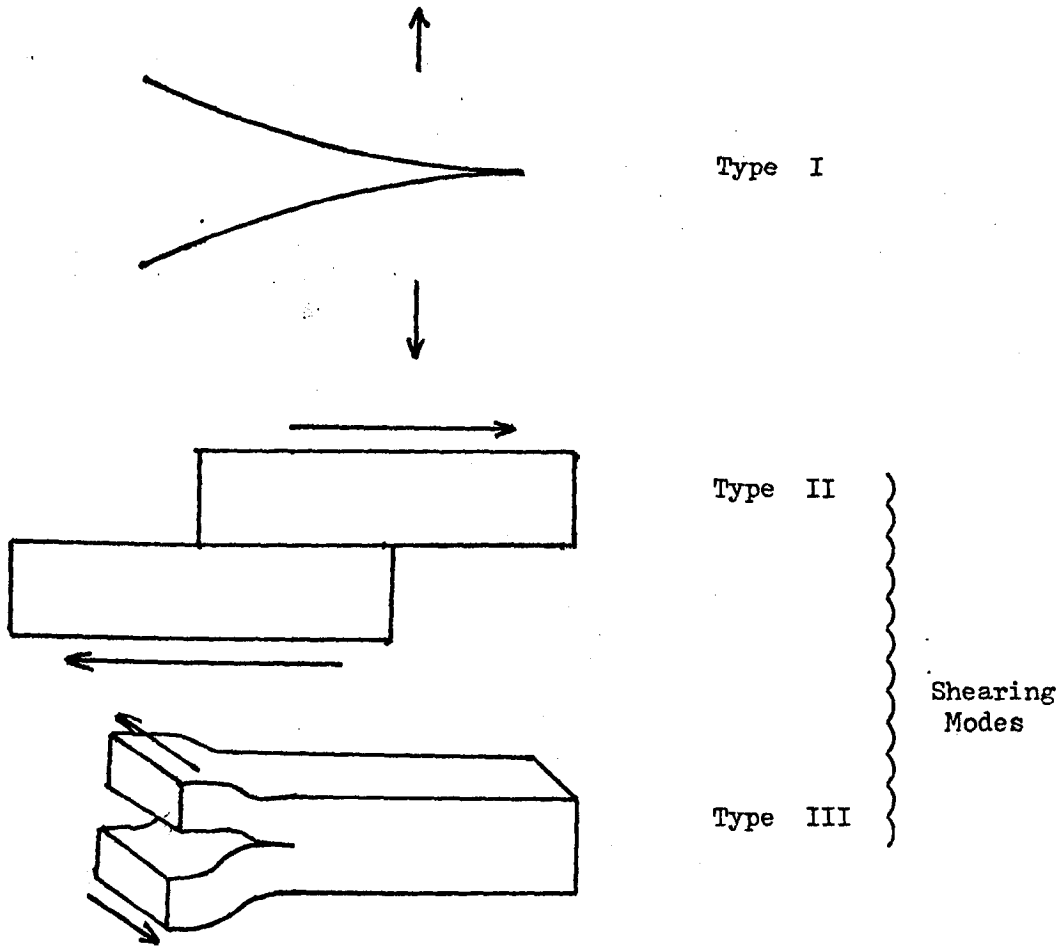

Fig. 2.7 Modes of crack propagation

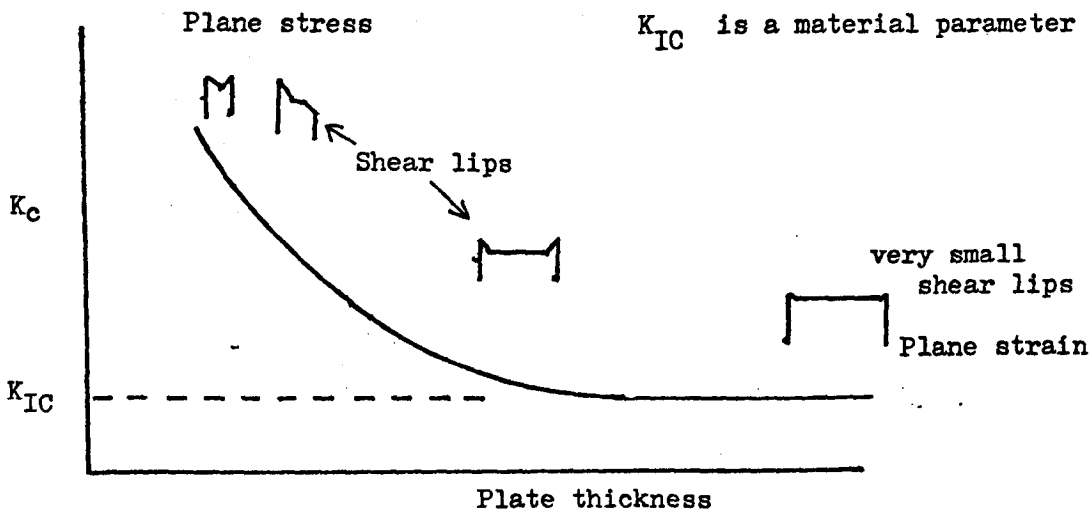

Fig. 2.8 Schematic illustration of change from plane stress to plane strain fracture.

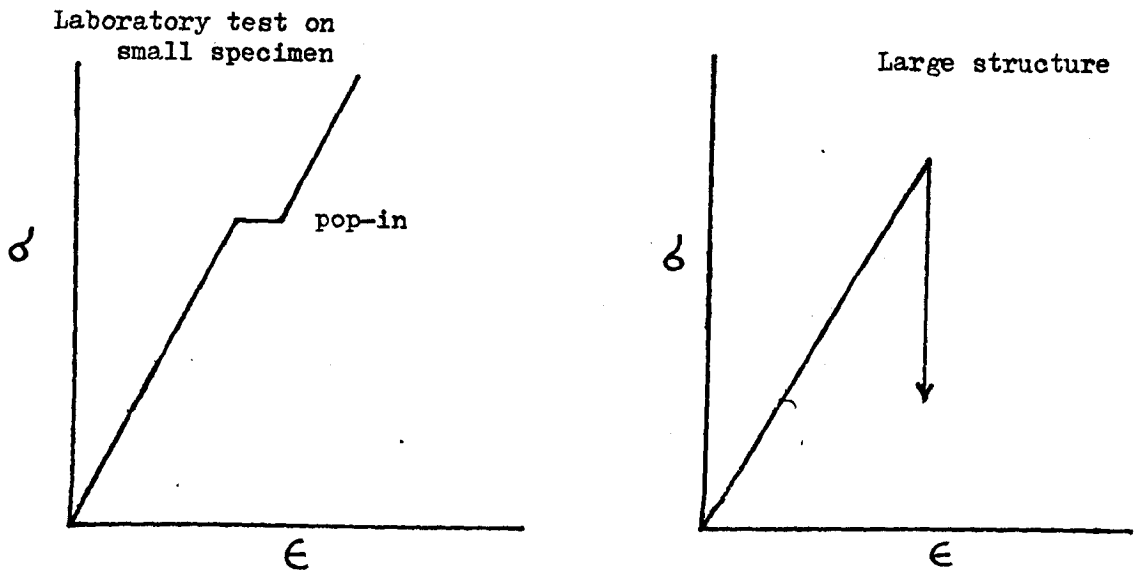

Fig. 2.9 Comparison of hypothetical stress-strain curves for laboratory specimen and "full-size" structure containing equivalent defects.

Fig. 2.10 Effect of plastic zone on shape of crack tip near conditions for instability.

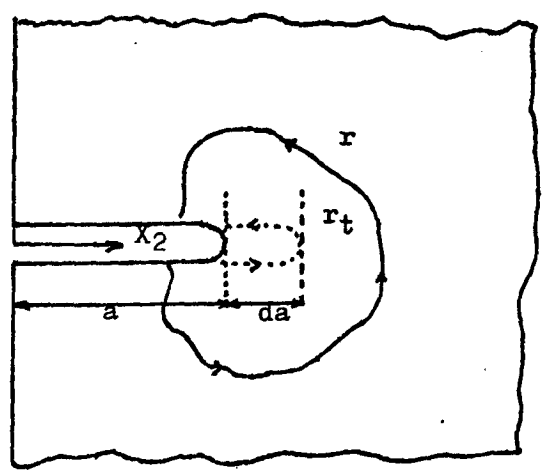

Fig. 2.11 Relationship between change in potential energy and line integral.

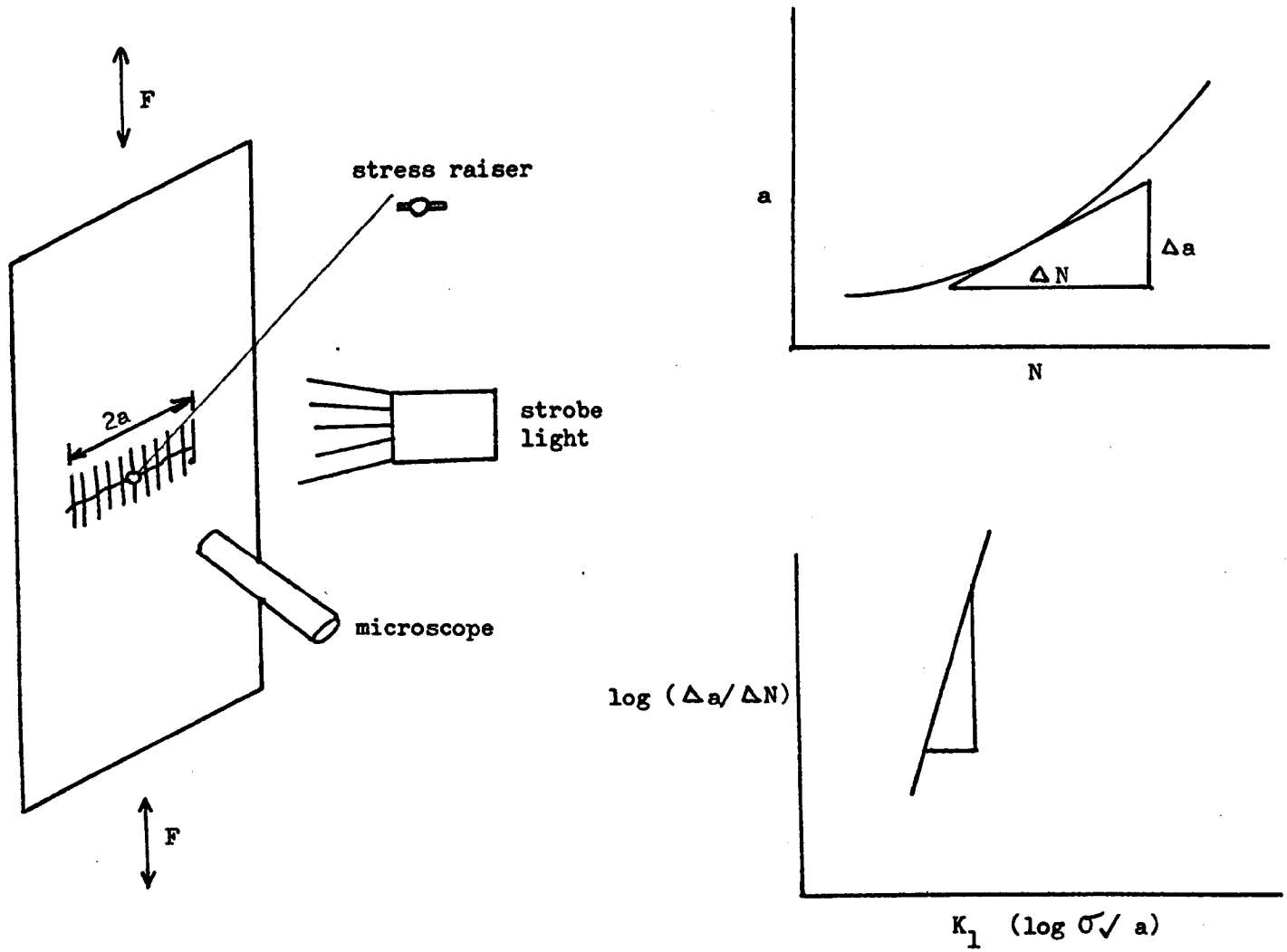

Fig. 2.12 Method of crack propagation rate determination

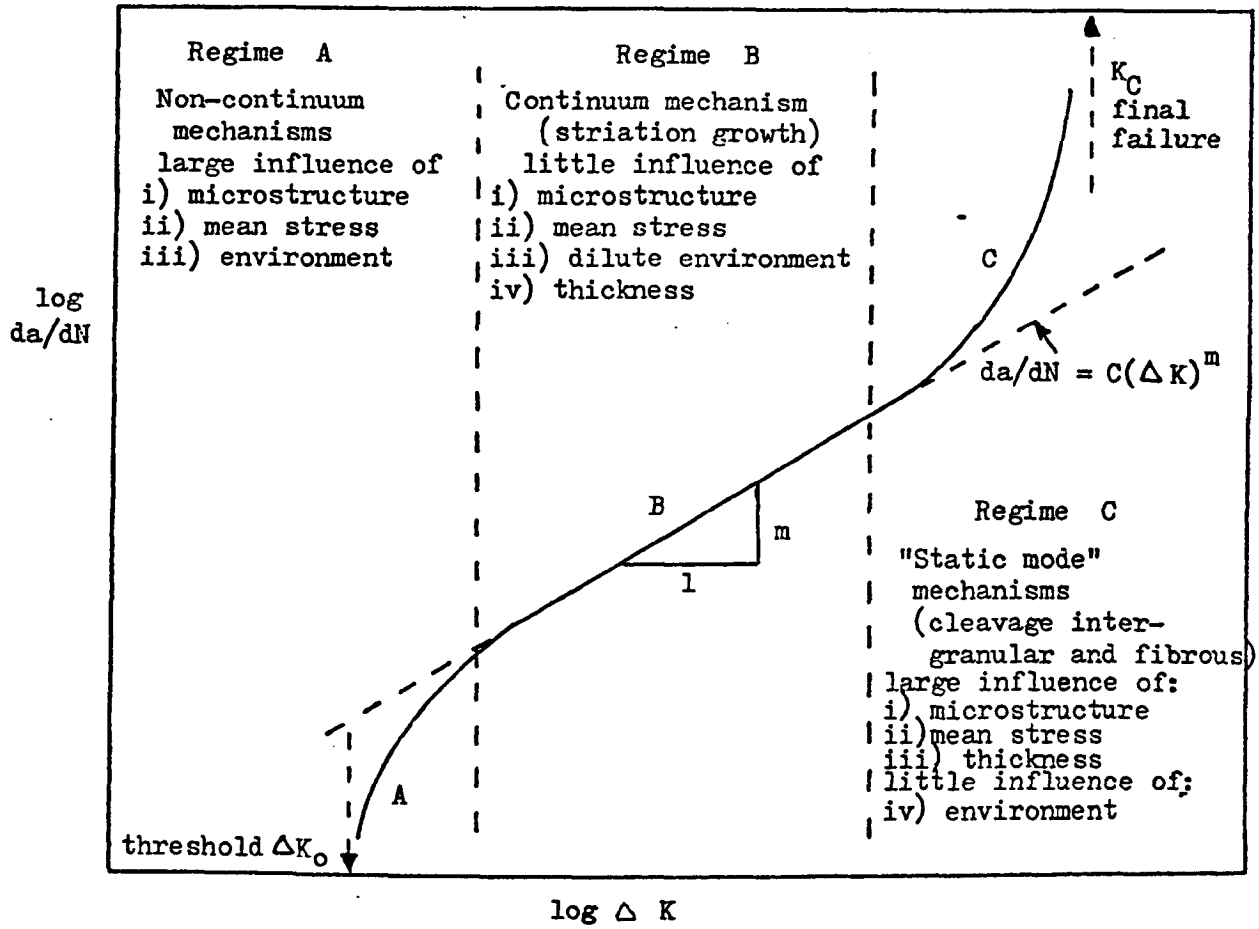

Fig. 2.13 Typical fatigue crack growth behaviour.

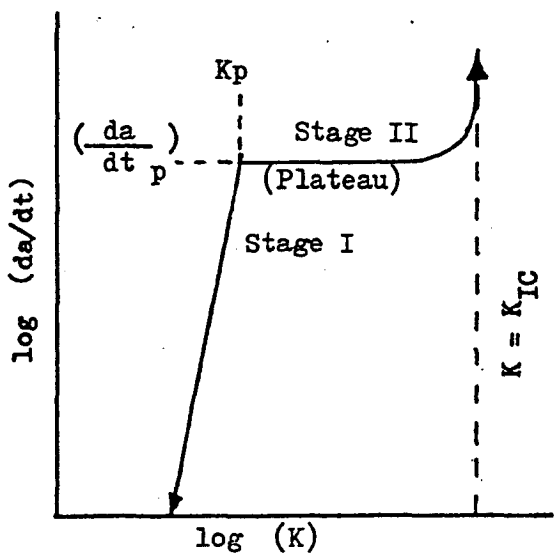

Figure 2.14 Typical stress corrosion crack growth behaviour.

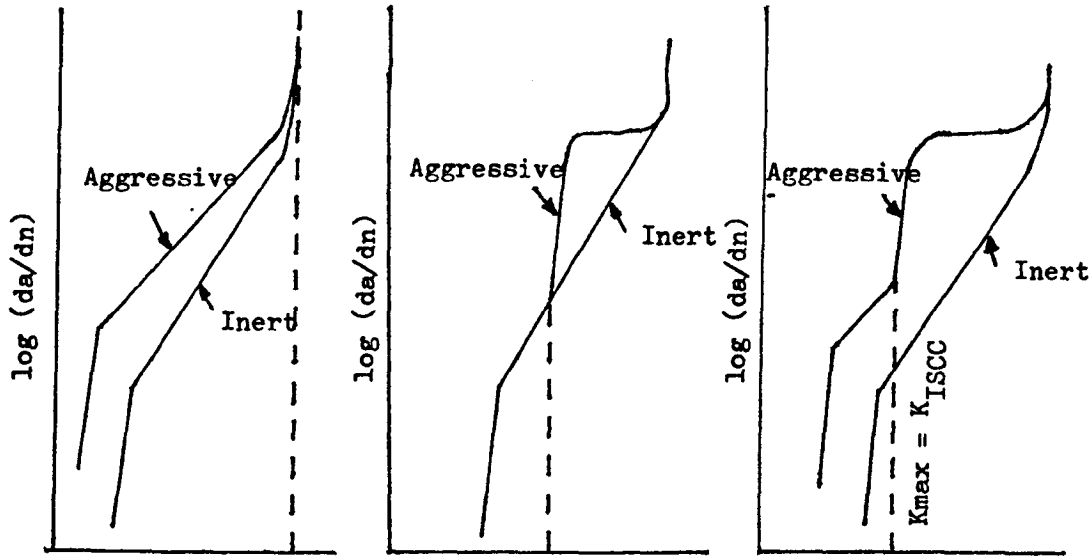

Fig. 2.15a Fig. 2.15b Fig. 2.15c

Fig. 2.15 Schematic illustrations of basic types of corrosion fatigue crack growth behaviour.

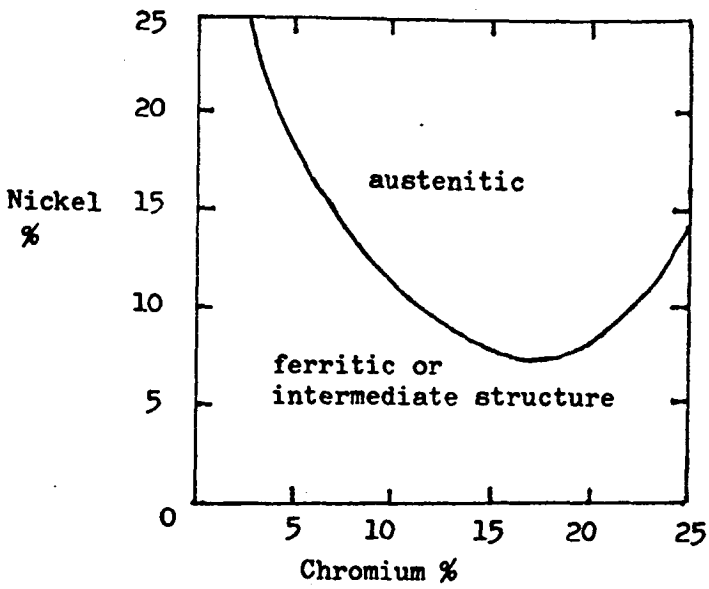

Fig. 2.16 Effect of nickel and chromium on constitution of 0.1%C steels. (ref. 45)

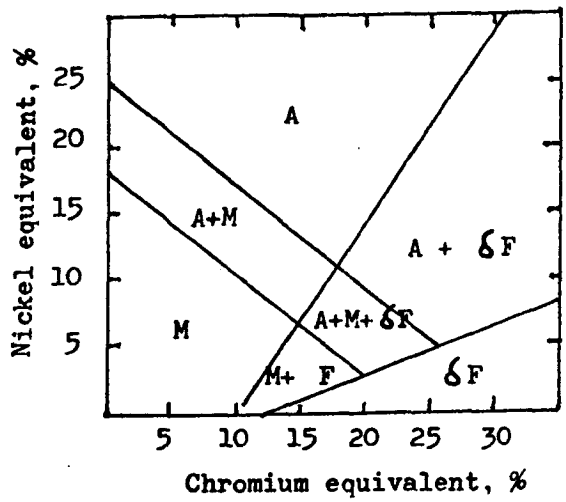

A = austenite M = martensite

δF = delta ferrite

Fig. 2.17 Effect of nickel and chromium equivalents on constitution of stainless steels. (ref. 46)

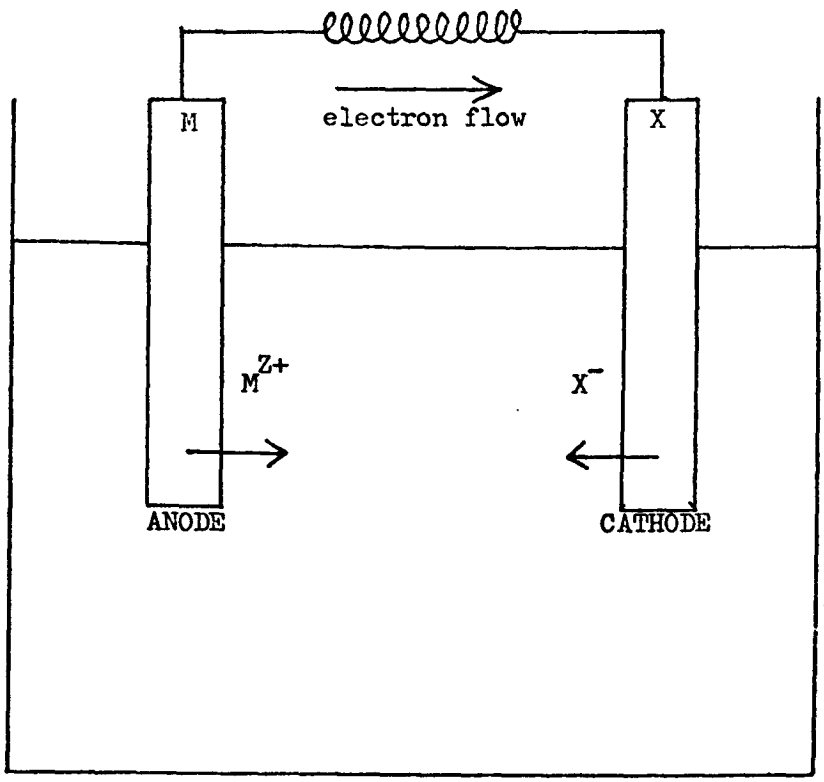

Fig. 2.18 Schematic layout of corrosion cell involving a metal M and a more noble electrode X/X^-

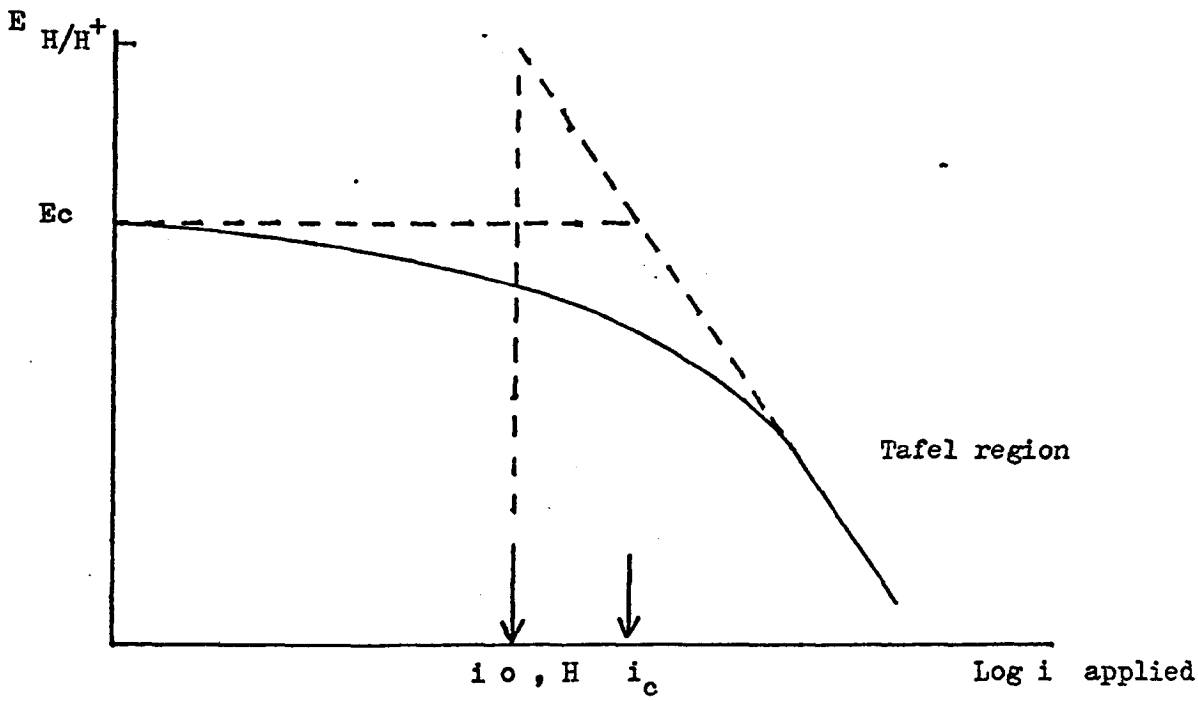

Fig. 2.19 Determination of the corrosion current (i_c) and the exchange current density for hydrogen ($io_{,H}$) by the cathodic polarisation method.

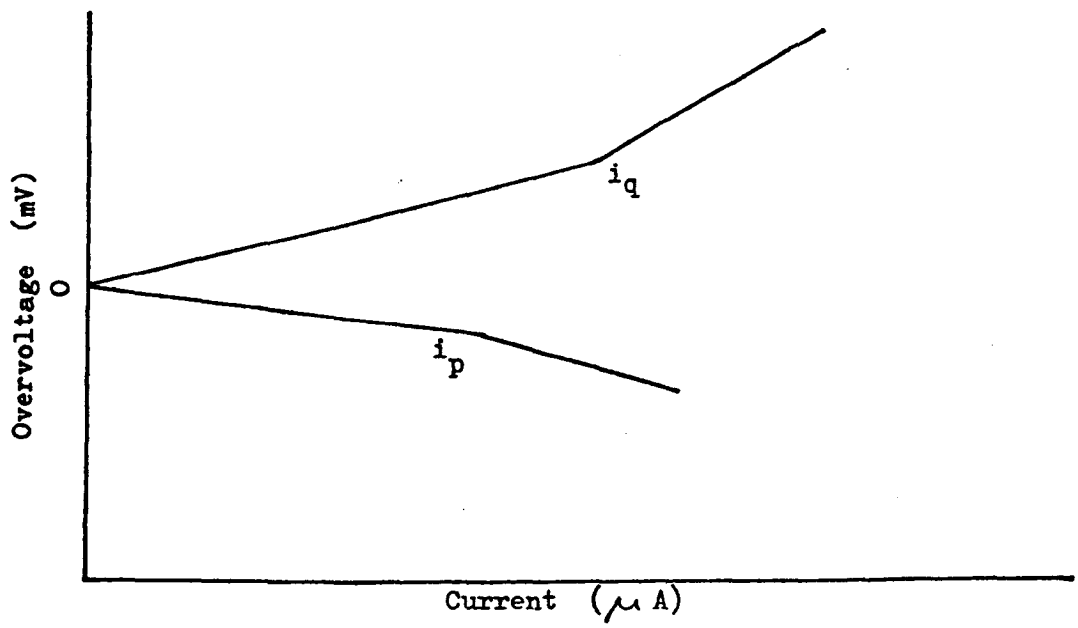

Fig. 2.20 Determination of i_c using the polarisation break method.

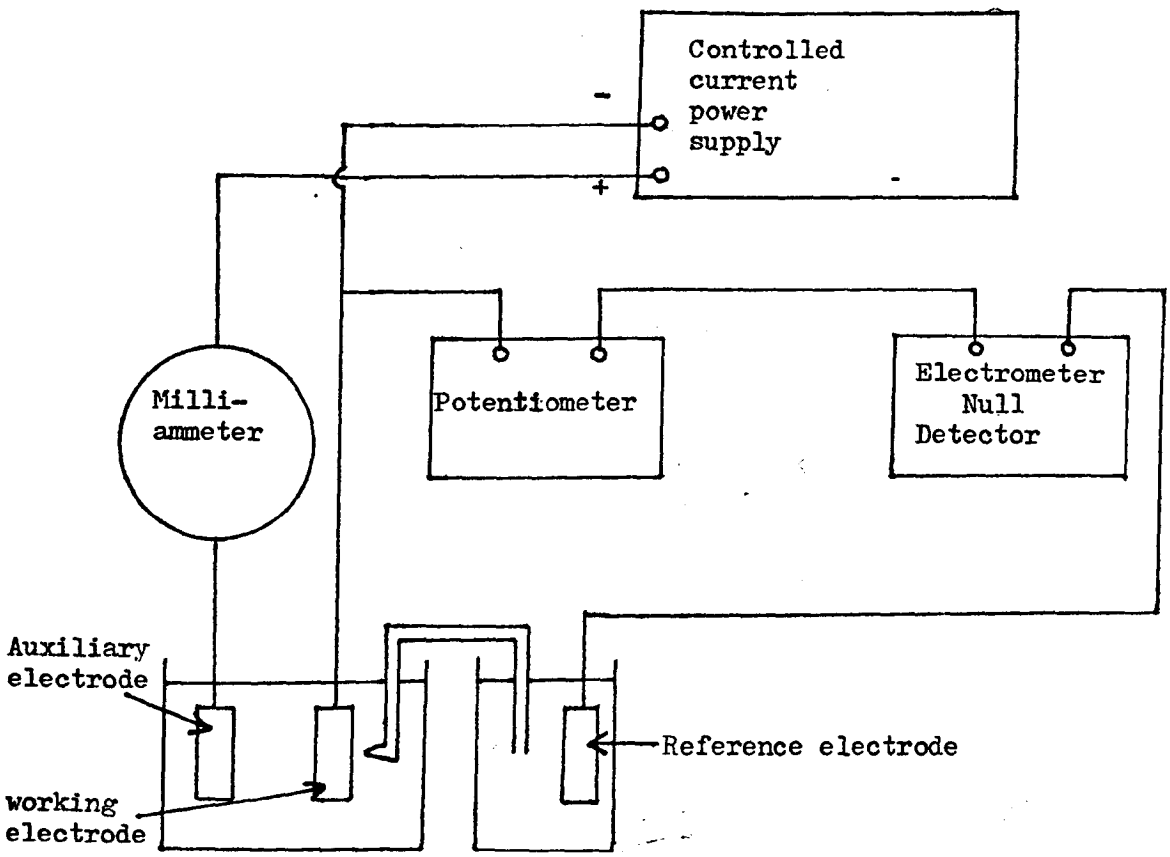

Fig. 2.21 Experimental set-up for Galvanostatic Tests.

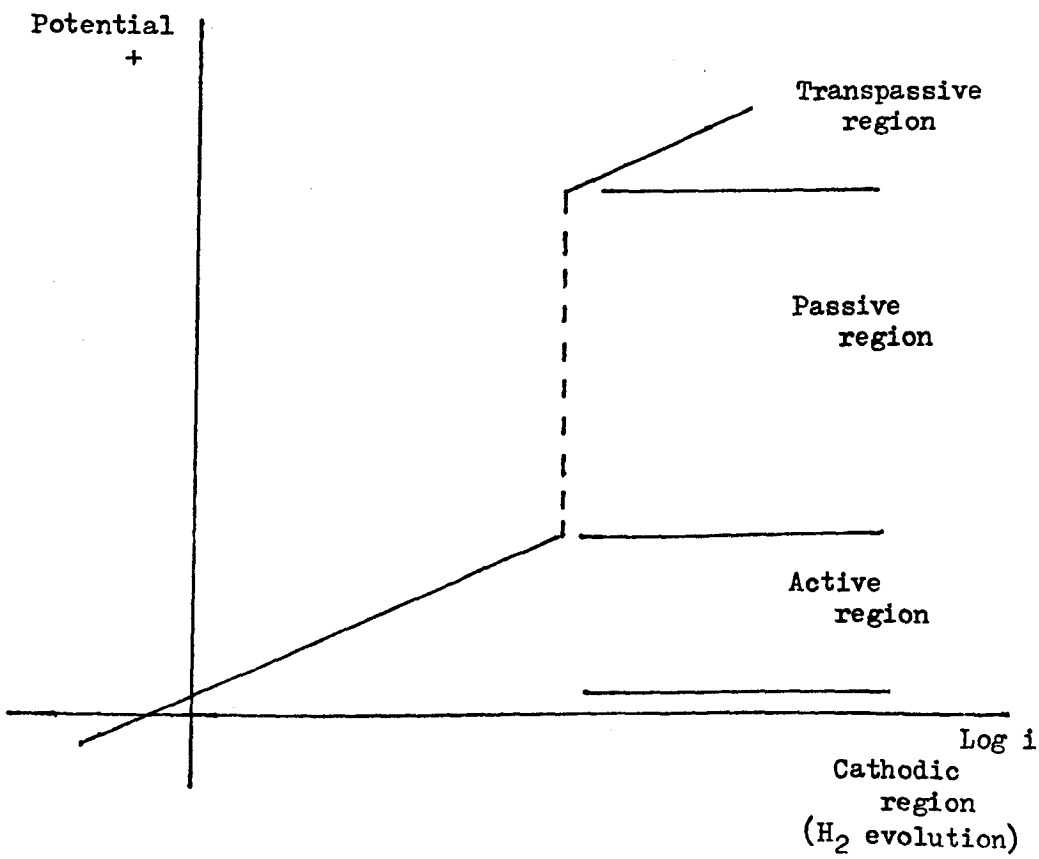

Fig. 2.22 Galvanostatic polarisation curve for a passivatable metal.

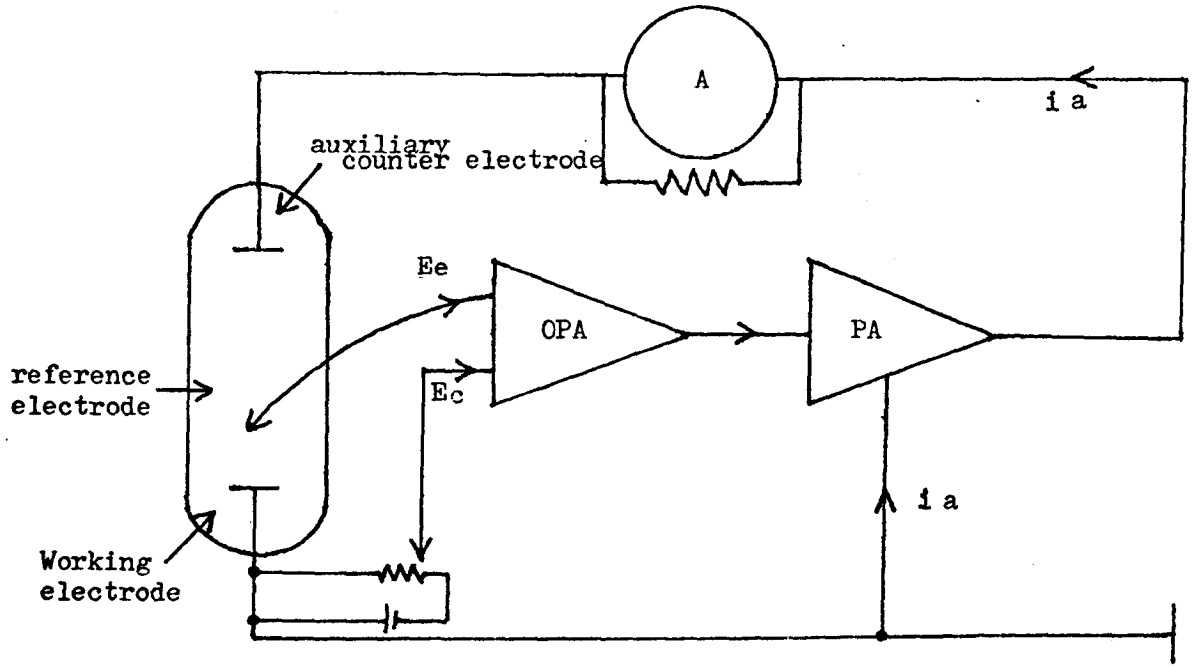

Fig. 2.23 Schematic diagram of the potentiostat with electrochemical cell.

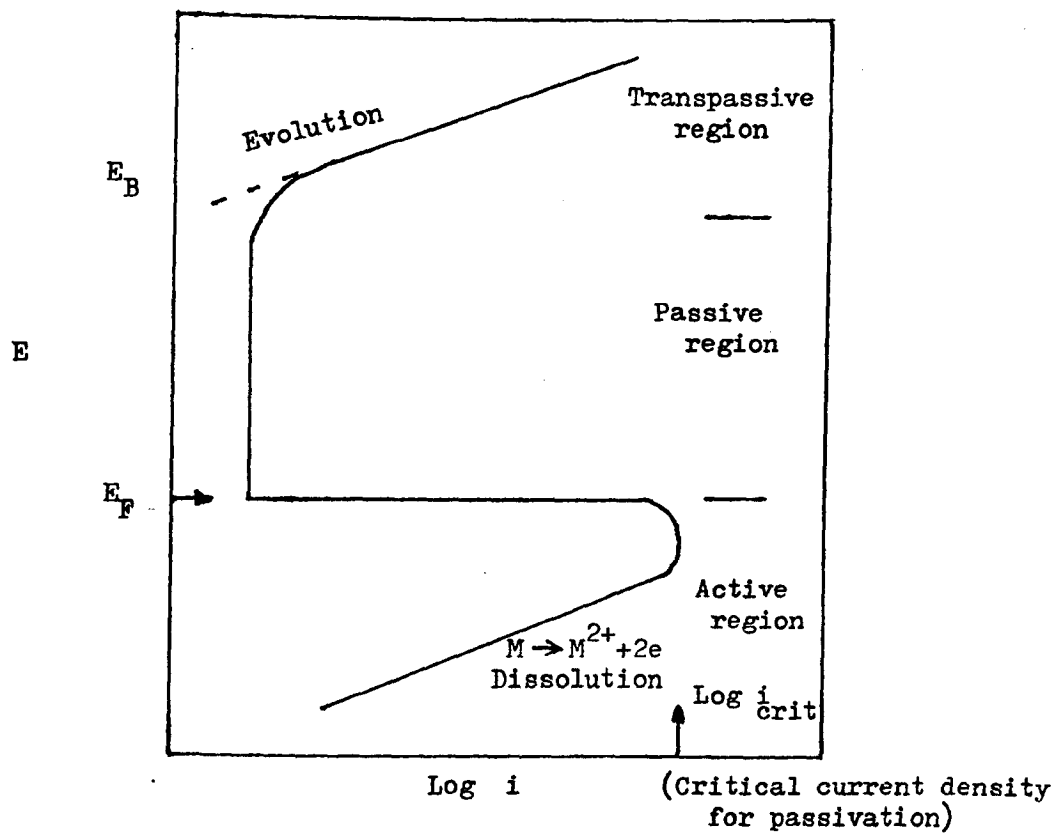

Fig. 2.24 Schematic anodic polarisation curve for metal M.

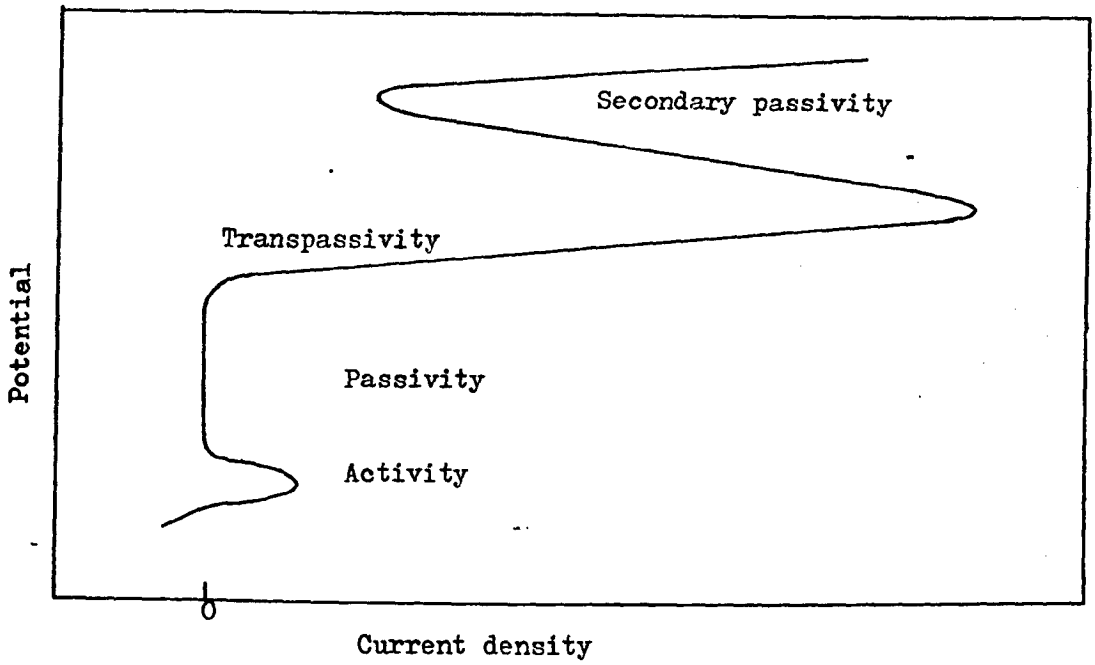

Fig. 2.25 Typical anodic polarisation curve for an 18% Cr 8% Ni stainless steel in 0.5M Sulphuric Acid.

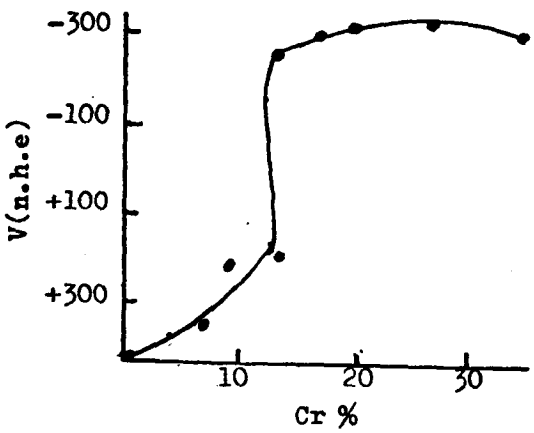

Fig. 2.26 Critical potential for passivity of Fe - Cr alloys as a function of Cr. (0.1N H_2SO_4)

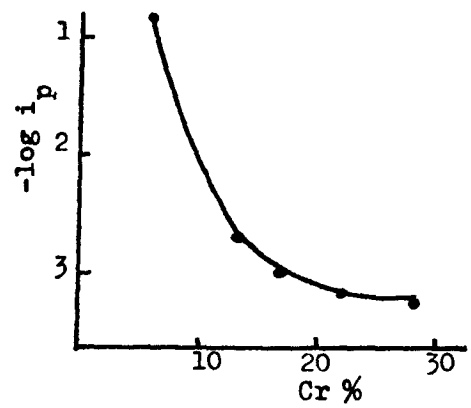

Fig. 2.27 Critical current density for passivity of Fe - Cr alloys as a function of Cr. (0.1N H_2SO_4)

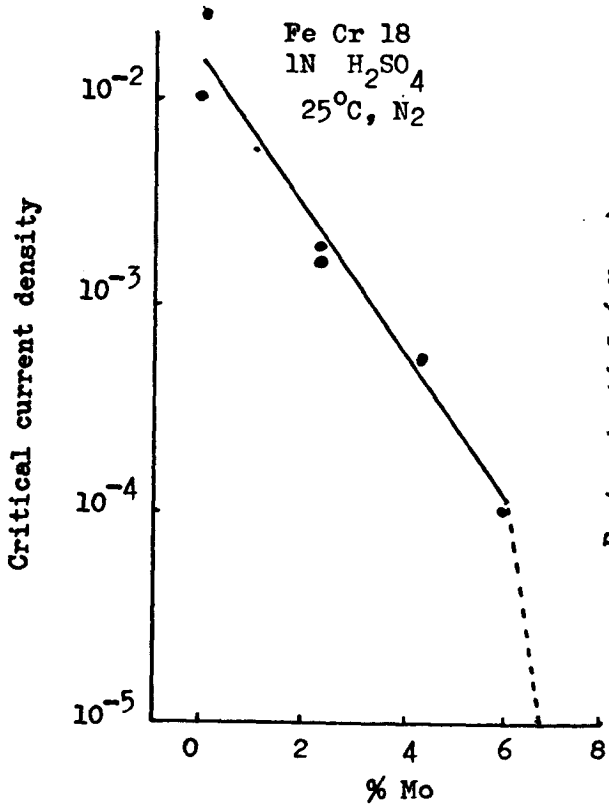

Fig. 2.28 Effect of Mo on the critical current density of Fe-18% Cr alloys in 1N H_2SO_4 at 25°C

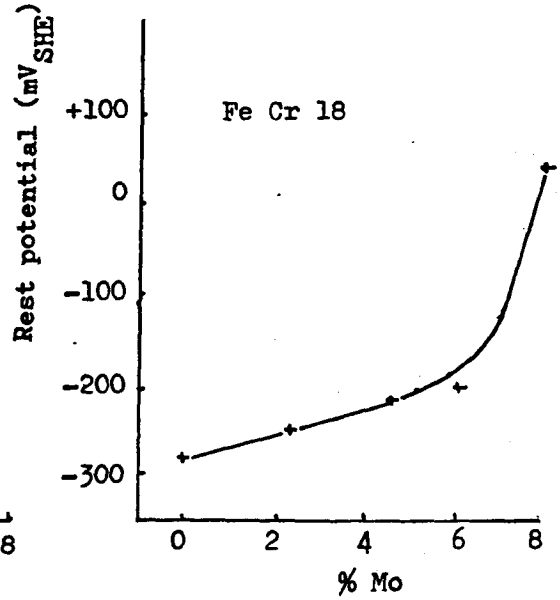

Fig. 2.29 Rest potential as a function of Mo for Fe-18% Cr alloys in 1N H_2SO_4 at 25°C

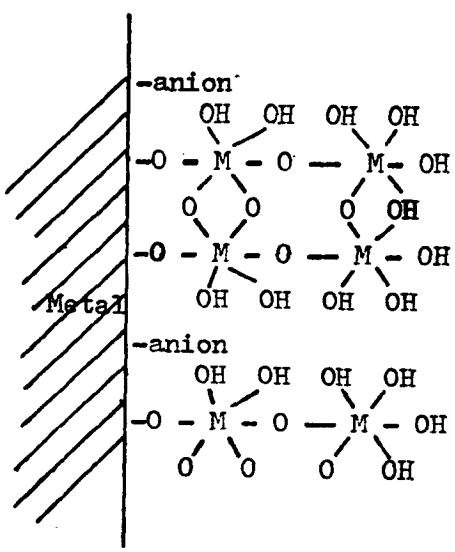

Fig. 2.30 Schematic model of passivated surface

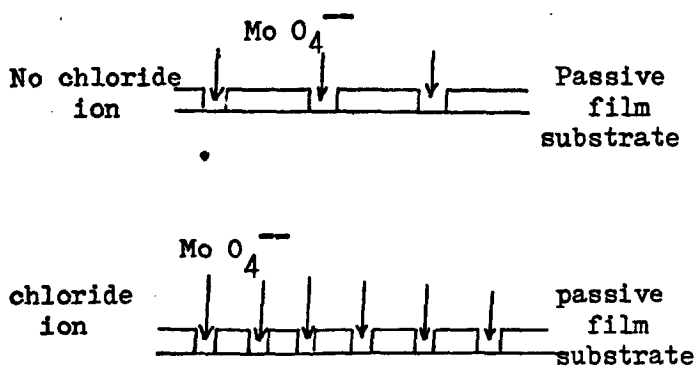

Fig. 2.31 Schematic illustration of the proposed model for the effect of molybdate and chloride ions on the breakdown of the passive film.

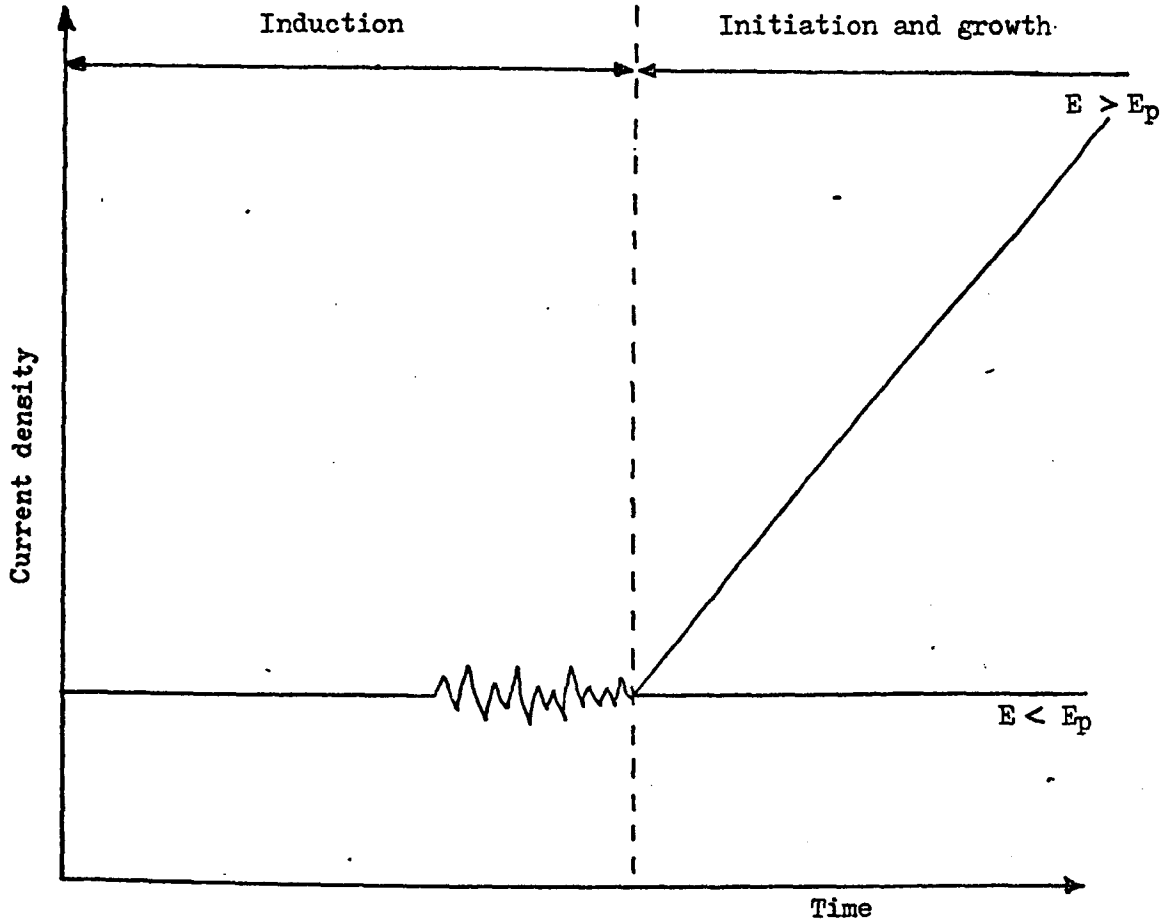

Fig. 2.32 Schematic plot of current density v. time for an electrode polarised to a fixed potential in a pitting medium.

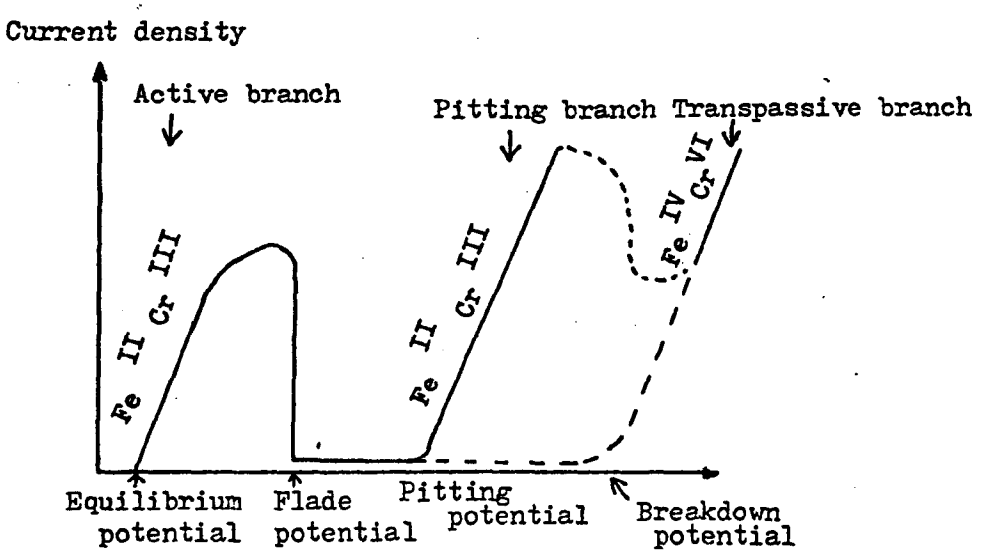

Fig. 2.33 Anodic current density/potential curve for a stainless steel subject to pitting.

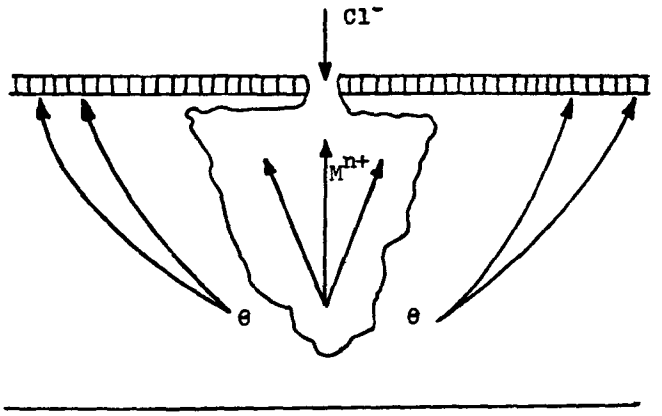

Fig. 2.34 Schematic representation of a closed pit

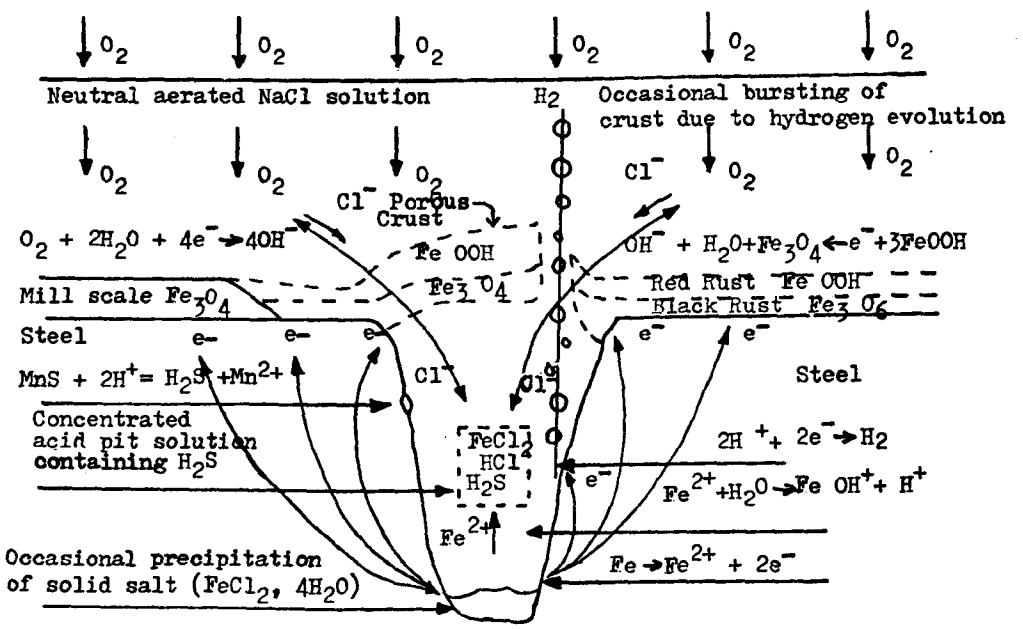

Fig. 2.35 Schematic illustration of the electrochemical mechanism for the propagation of a corrosion pit in steel in neutral chloride solution, showing the autocatalytic, self generating nature of pitting.

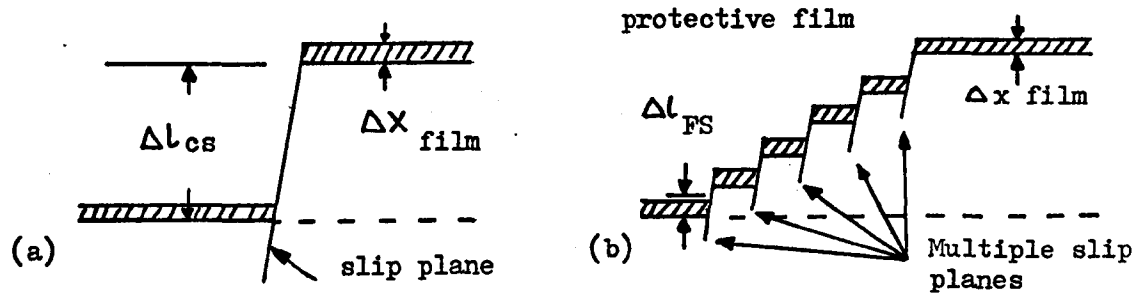

Fig. 2.36 Comparison of slip step heights with thickness of protective films (a) Coarse slip where slip step height $\Delta l_{cs} \gg \Delta x$ film (b) Fine slip where slip step height $\Delta l_{FS} \approx \Delta x$ film.

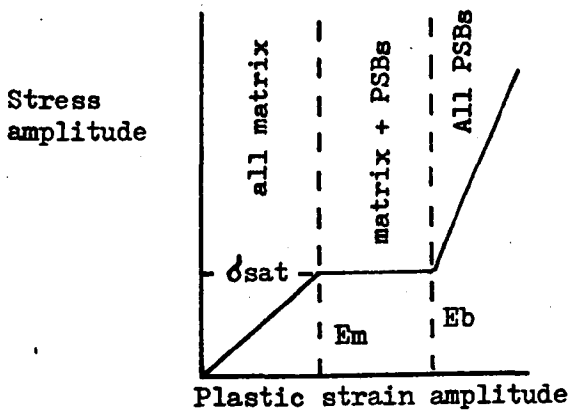

Fig. 2.37 Schematic relationship between stress amplitude and plastic strain amplitude.

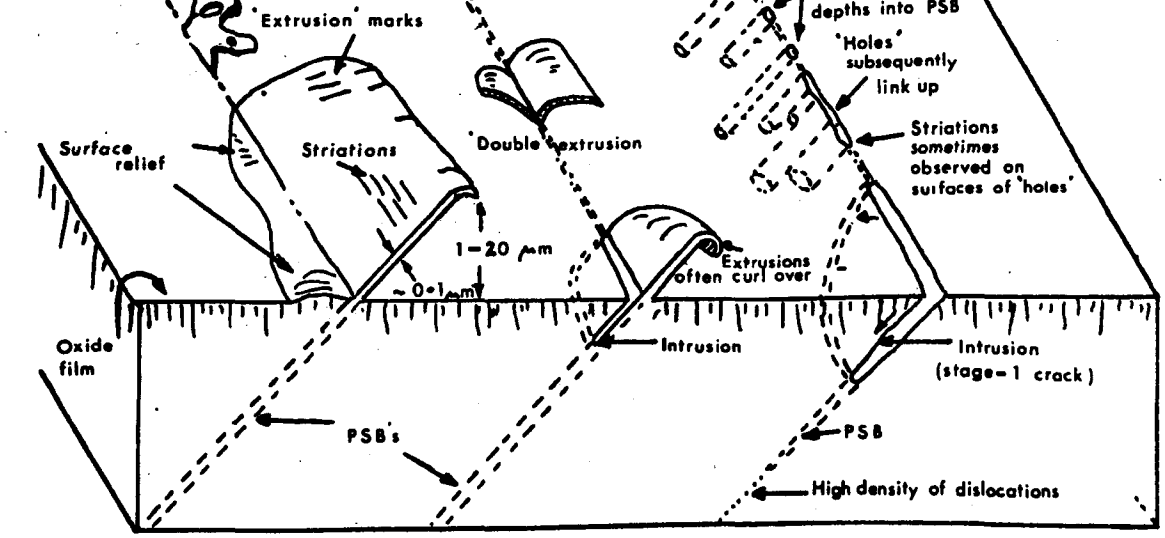

Fig. 2.38 Diagrammatic summary of important features of slip band extrusion and intrusion.

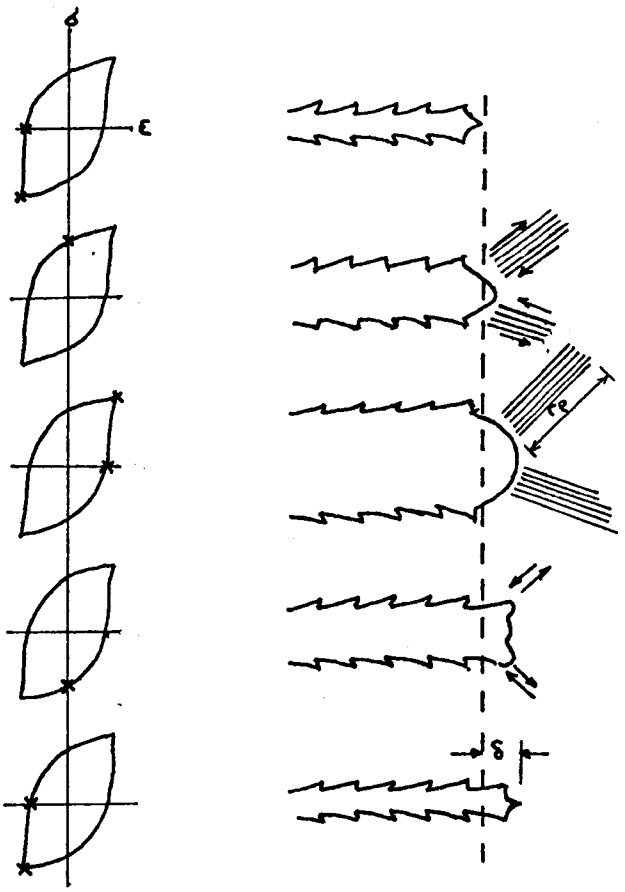

Fig. 2.39 Fatigue crack growth by plastic blunting mechanism. Drawings at left indicate points on the cyclic hysteresis loop for which the crack-tip geometry obtains.

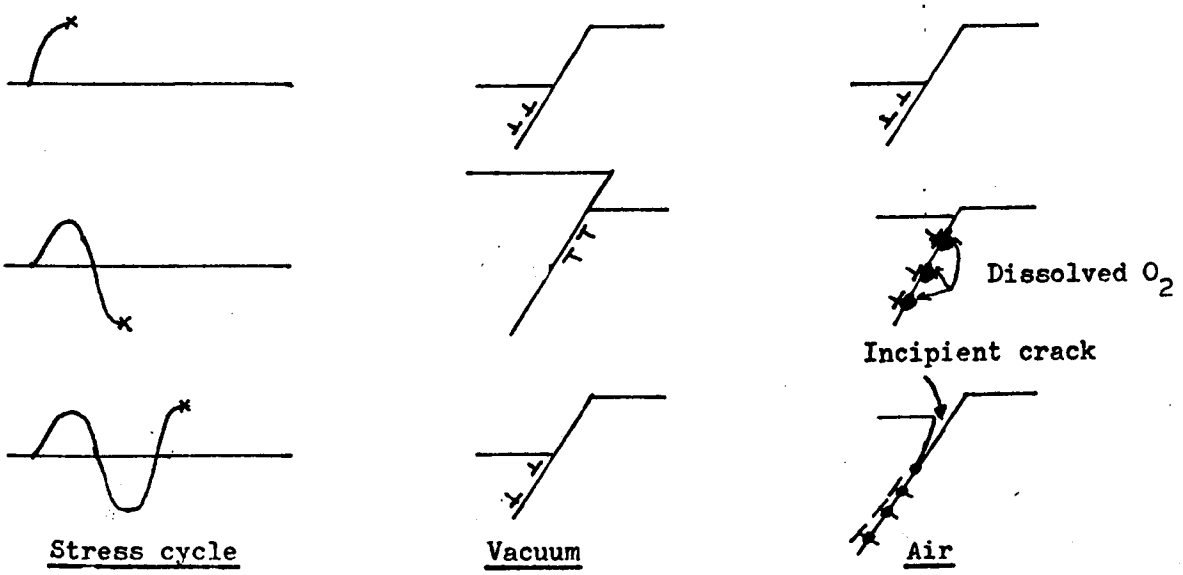

Fig. 2.40 Model for oxygen slip band interaction to affect fatigue crack nucleation.

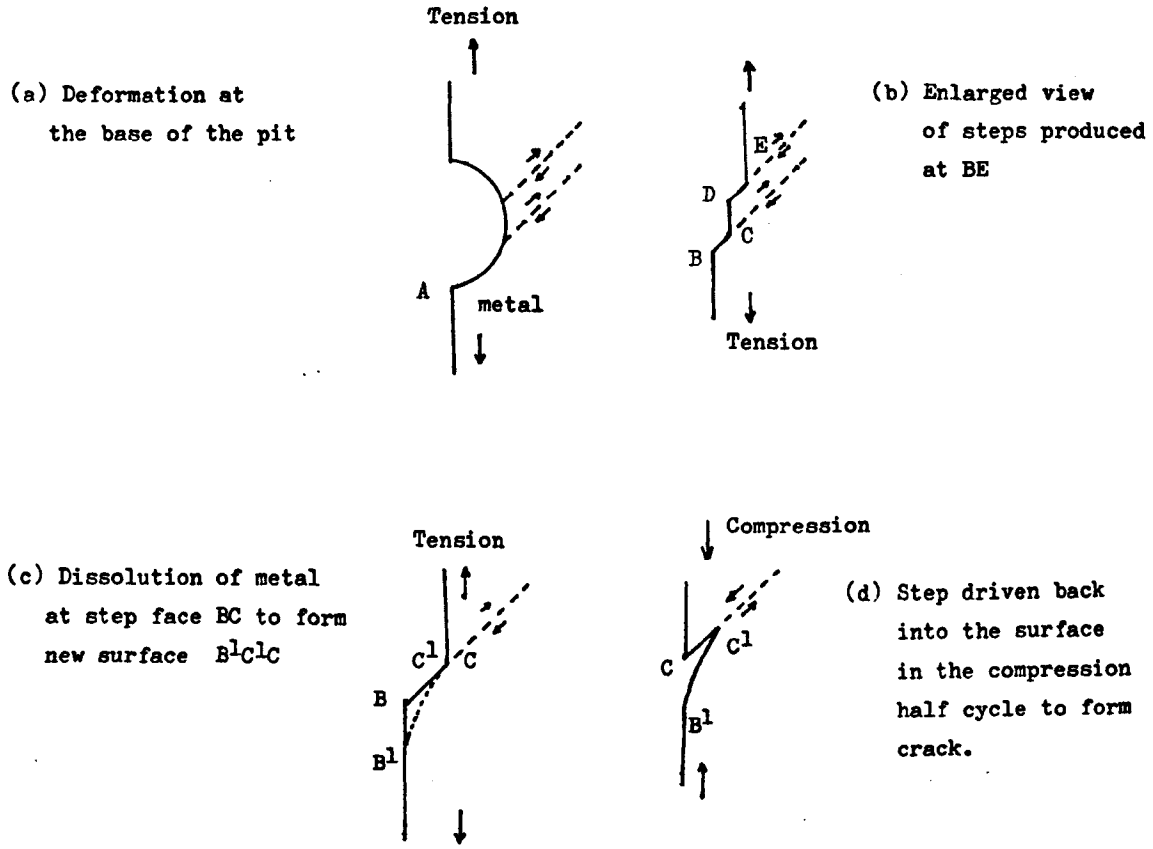

Fig. 2.41 Stages in the formation of a crack at the base of a pit.

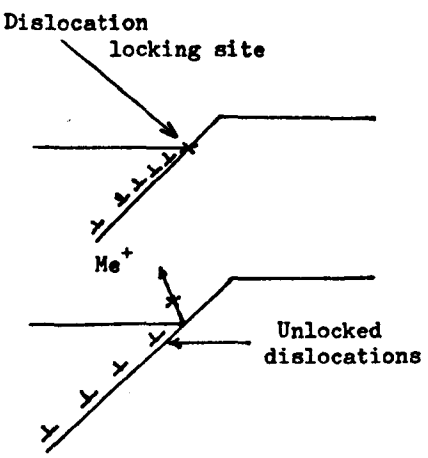

Fig. 2.42 Model to explain accelerated slip and subsequent early crack nucleation in corrosion fatigue.

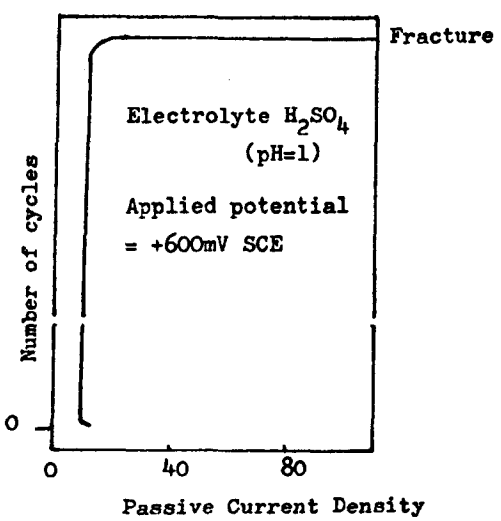

Fig. 2.43 Passive current density vs. number of cycles in rotating bending fatigue of a 17% Cr steel.

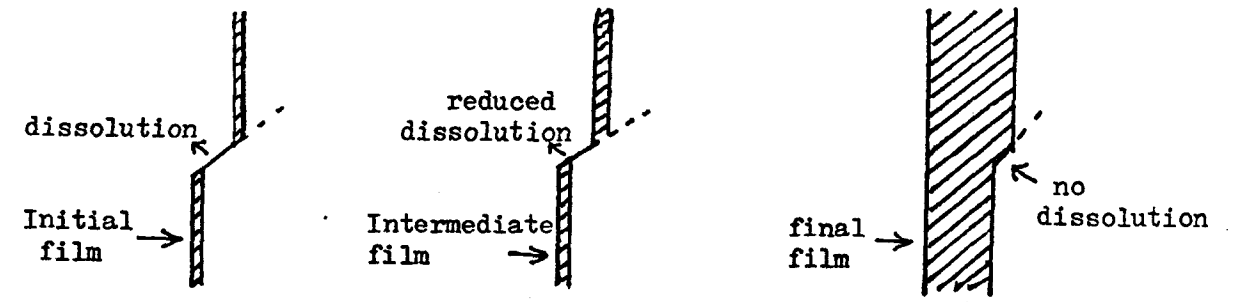

(a) Film thickening mechanism

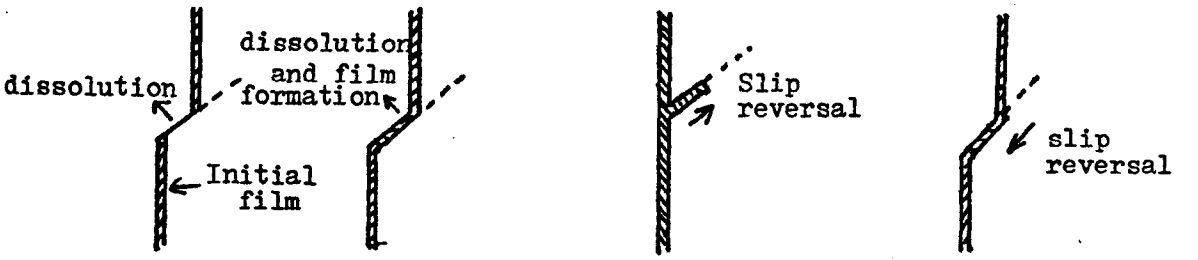

(b) Ingress of filmed step during reverse strain

Fig. 2.44 Models for the passivation of active slip steps

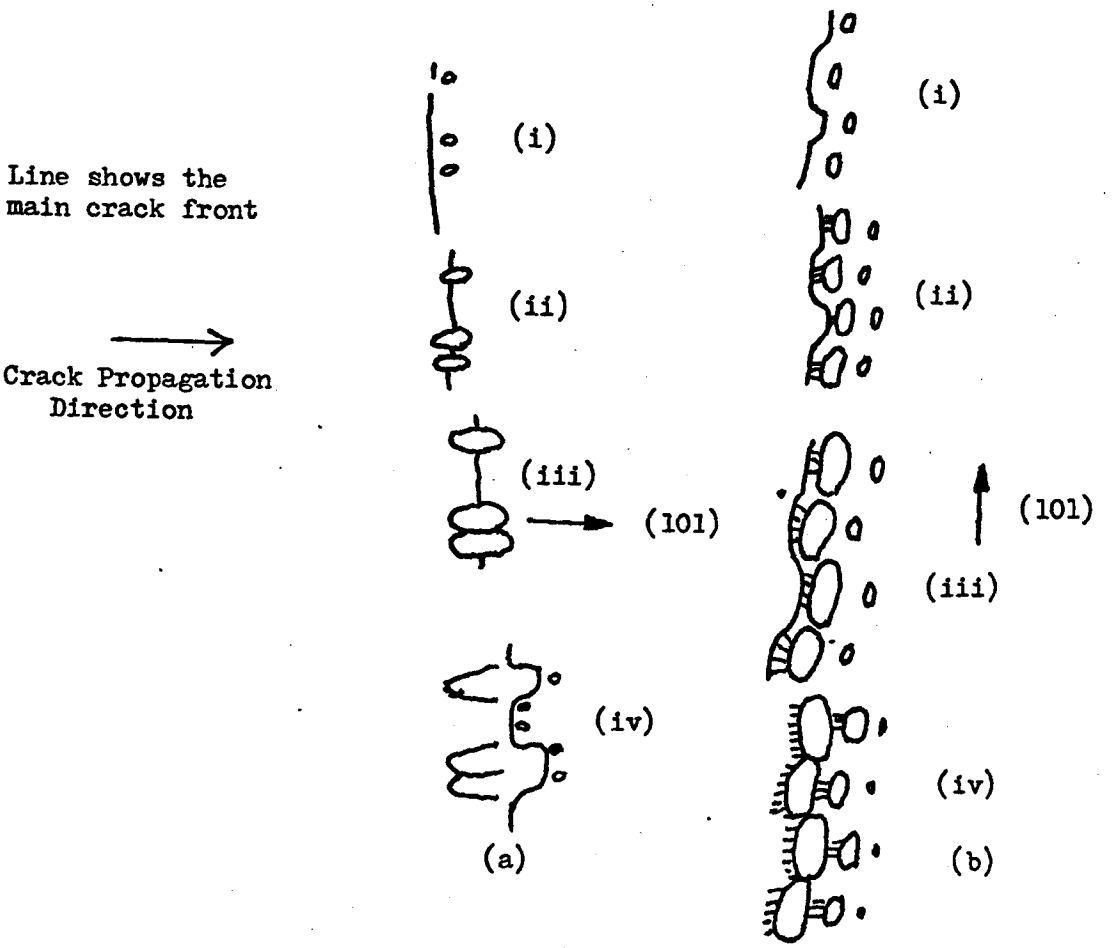

Fig. 2.45 Proposed sequence of events leading to linking of secondary cracks with main crack

Figure 2.46 A stage I fracture containing steps with slip traces in an almost horizontal direction. The direction is from upper left to lower right.

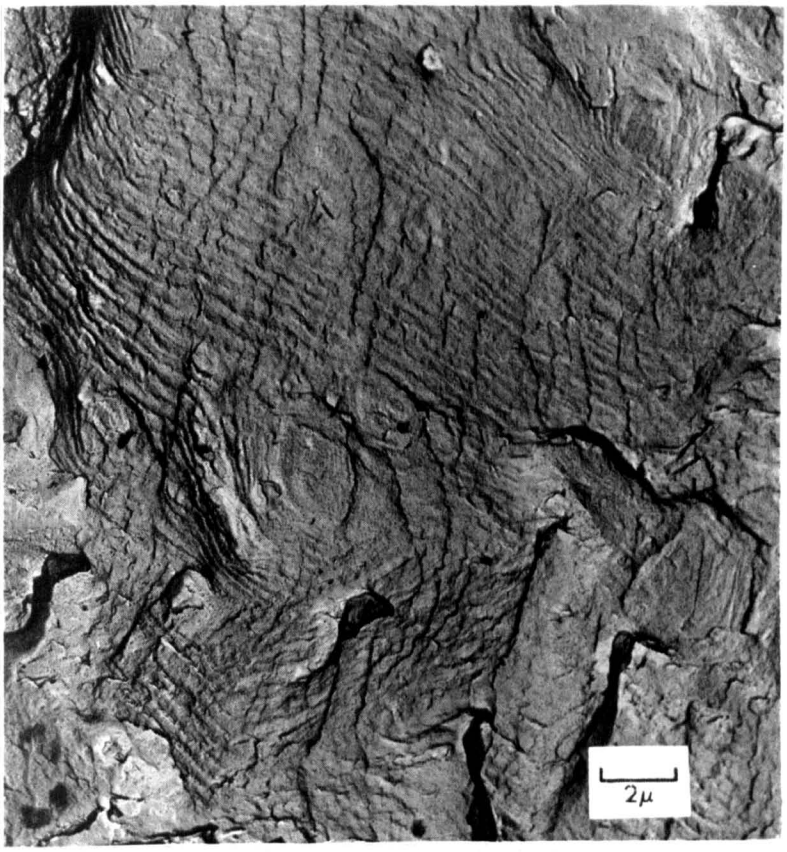

Figure 2.47 A portion of a stage I fracture containing striations. The direction of crack propagation is from upper right to lower left.

Figure 2.48 Fatigue striations in a programmed-loading test (7075-T6 aluminium) (as from Broek[206])

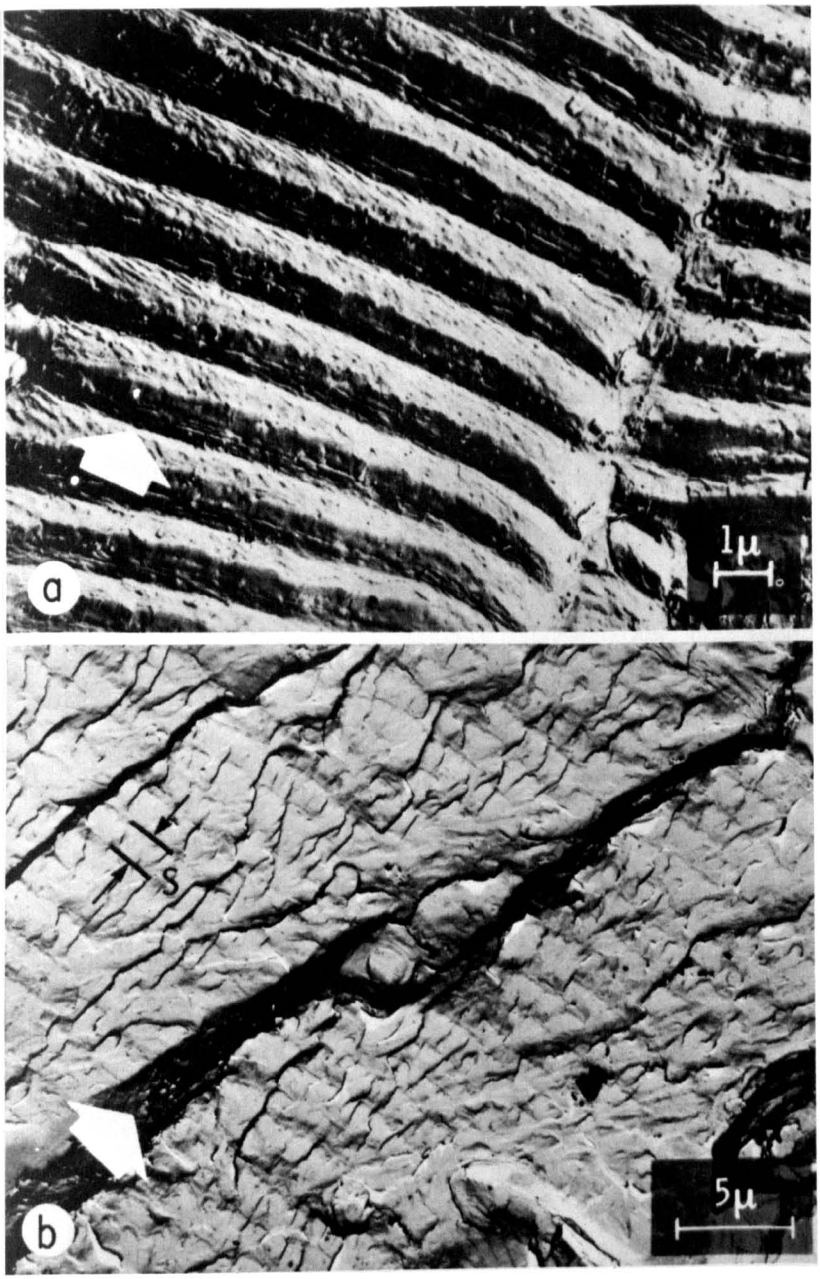

(a) Ductile fatigue striations

(b) Brittle fatigue striations

Figure 2.49 Electron fractographs of fatigue striations in an aluminium alloy.

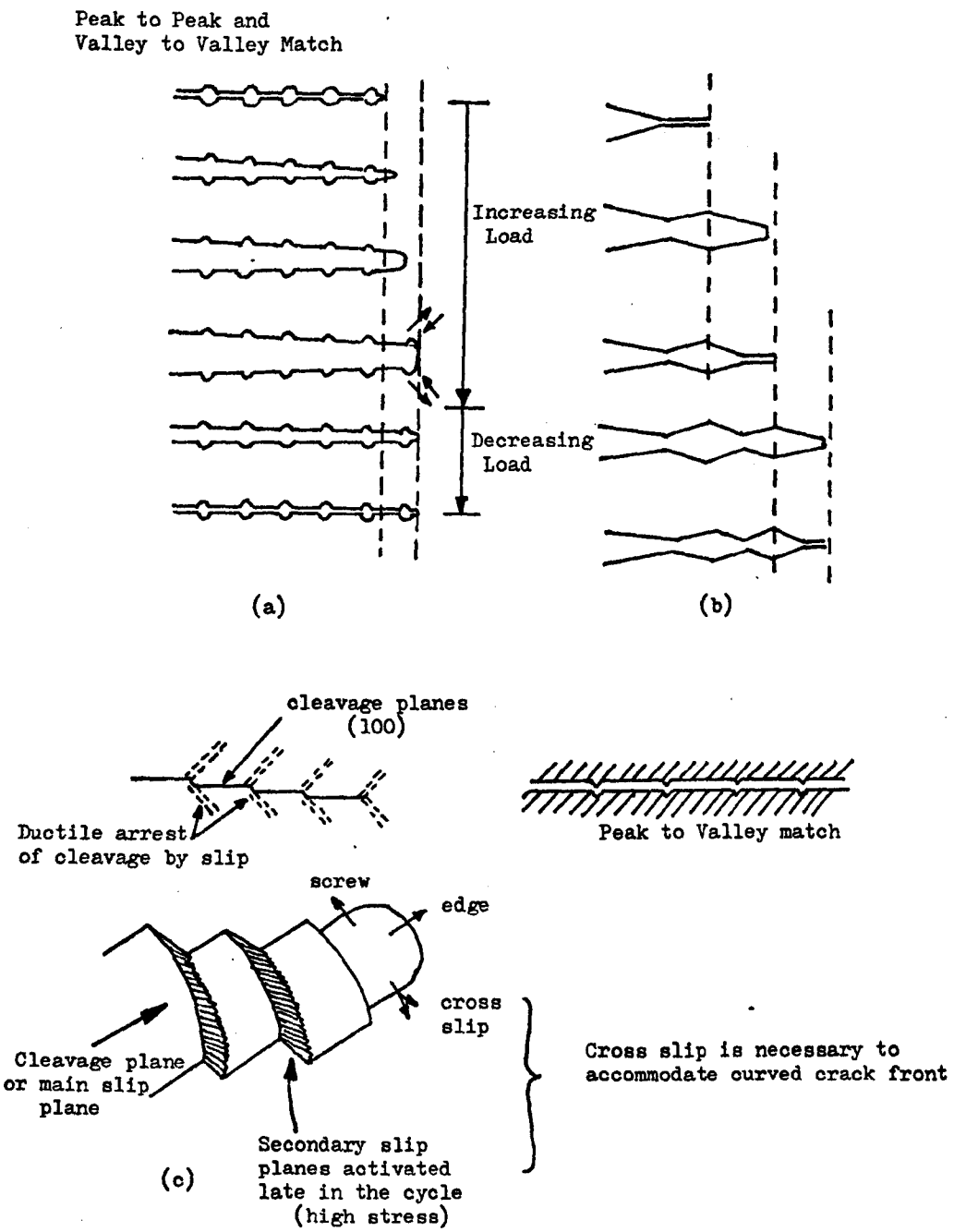

Fig. 2.50 Mechanisms of striation formation

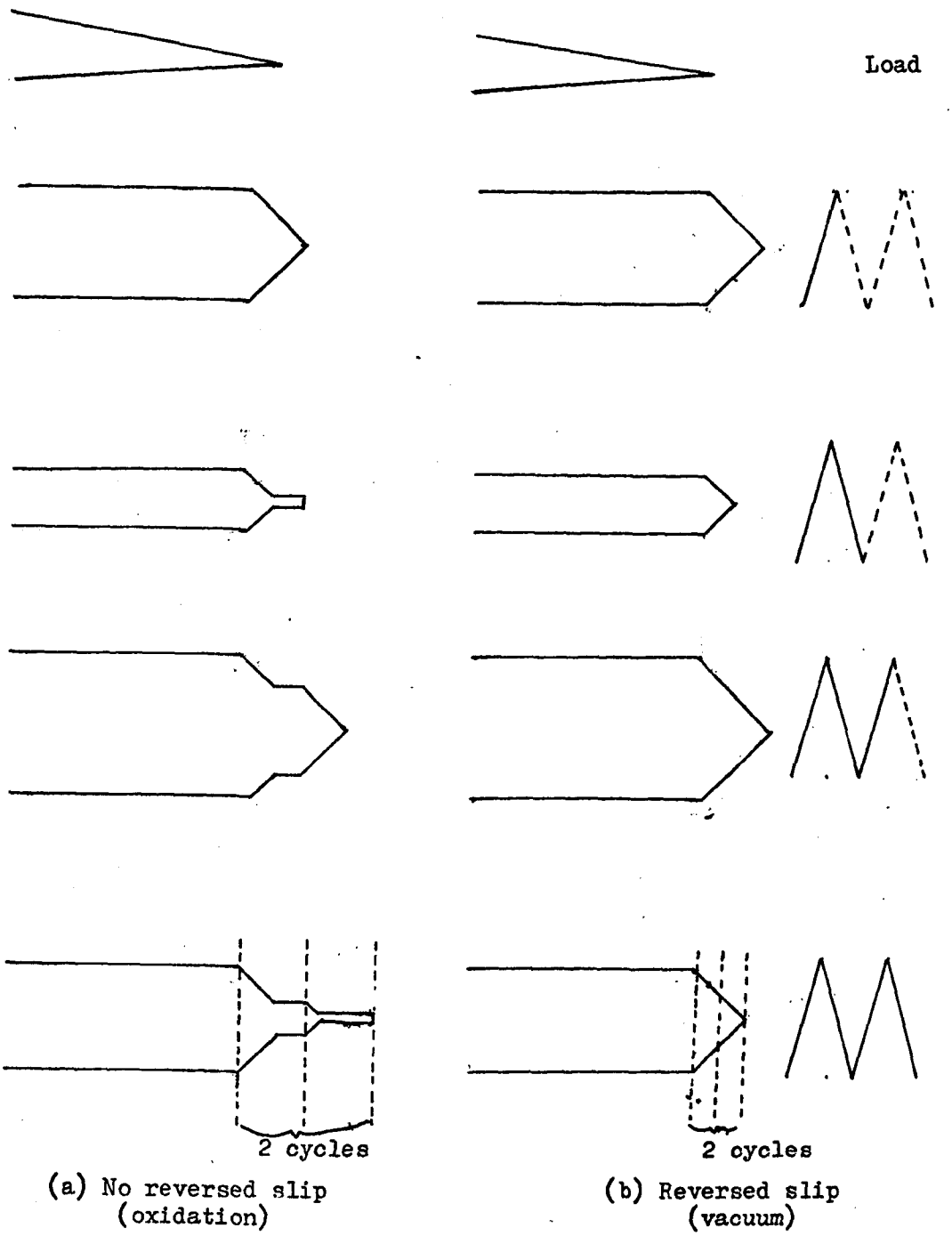

Fig. 2.51 Model comparing crack tip extension after two cycles in air and in vacuum

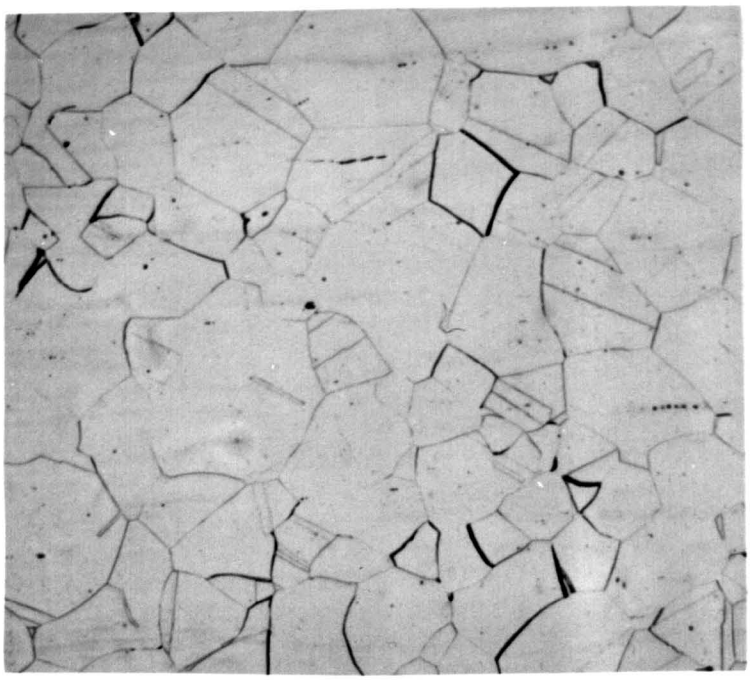

x500

Figure 3.1 Typical microstructure of the AISI 316 stainless steel, electrolytically etched in 10% hydrochloric acid.

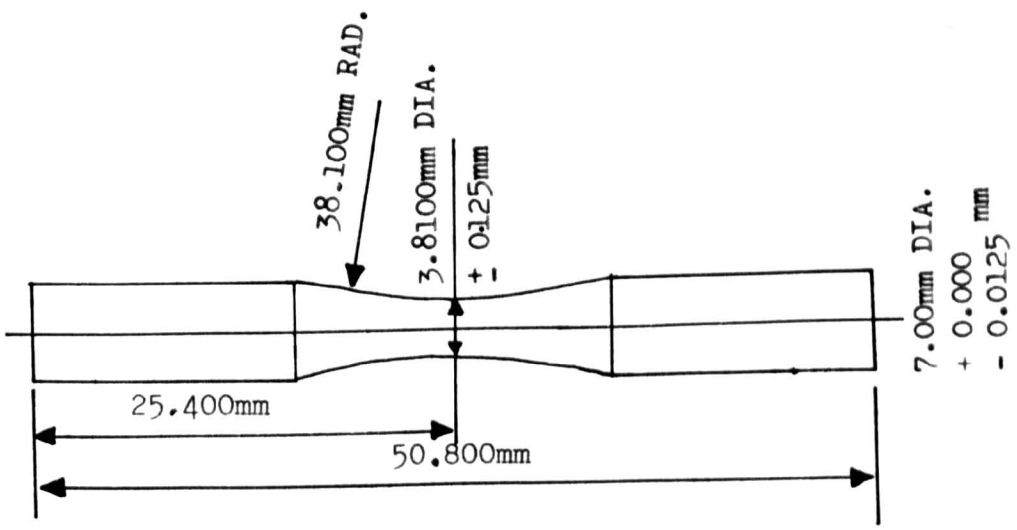

Figure 3.2 "K70B" rotating-bending fatigue test-piece

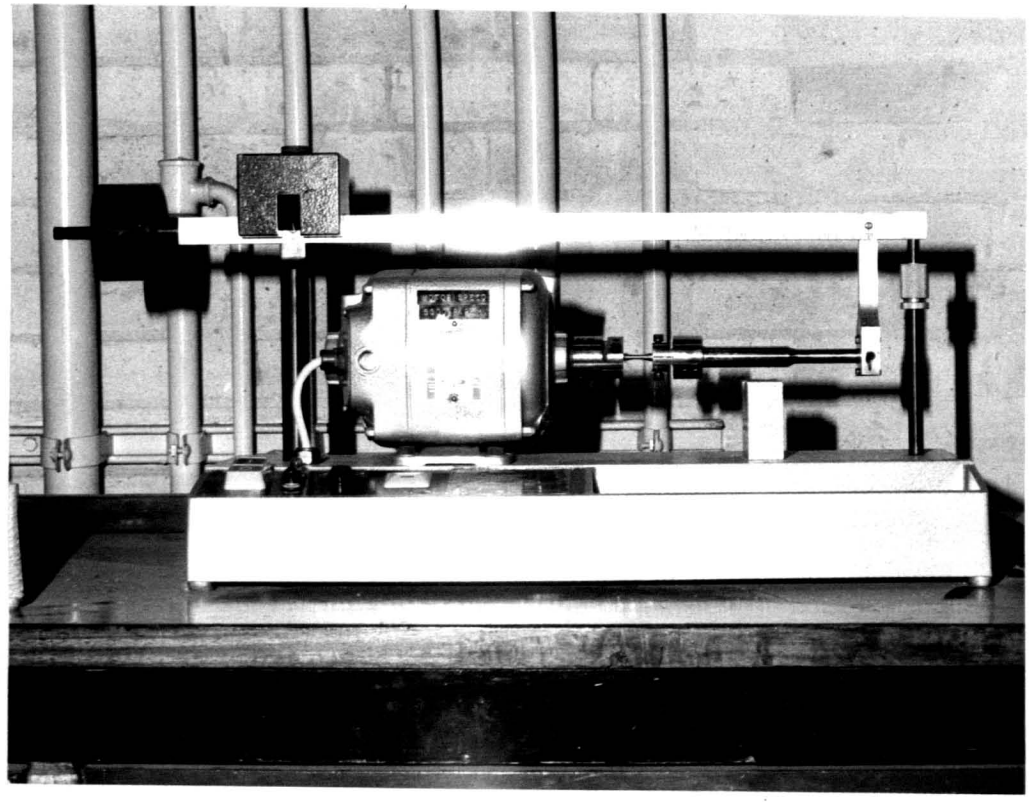

Figure 3.3 Rotating-Bending fatigue-testing machine set-up for an air fatigue test.

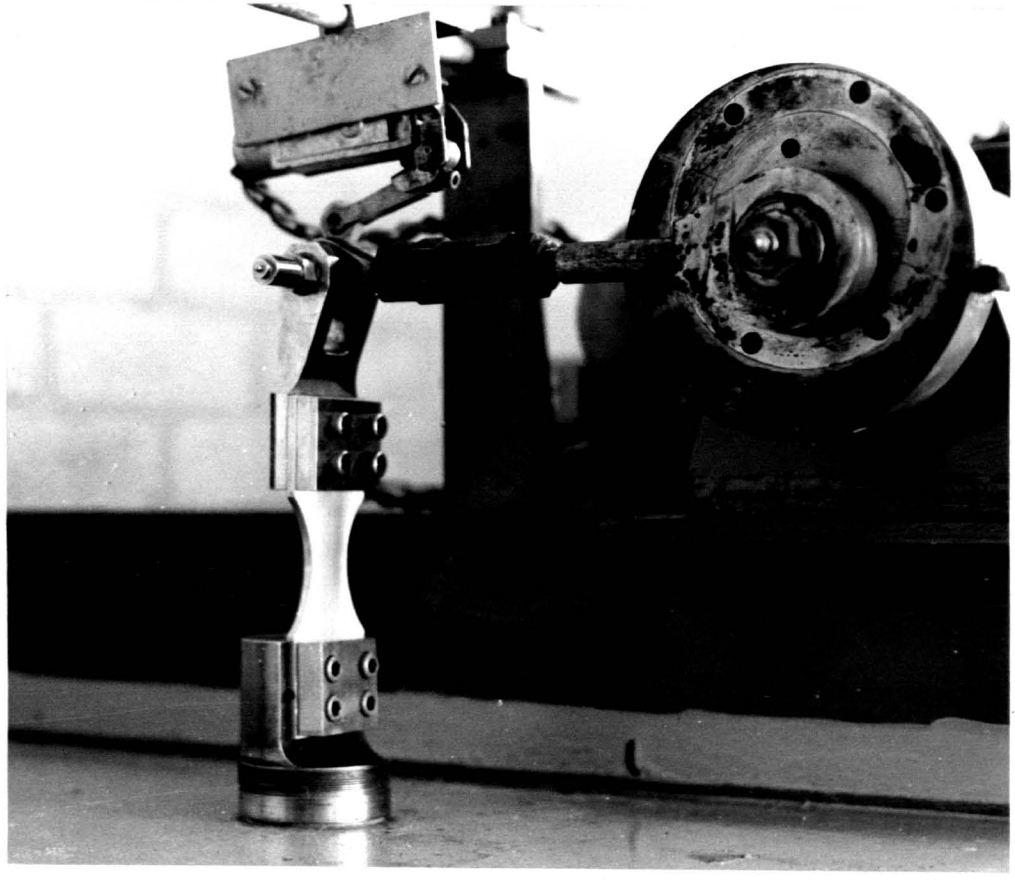

Figure 3.4 Reverse-bend fatigue-testing machine set up for an air fatigue test.

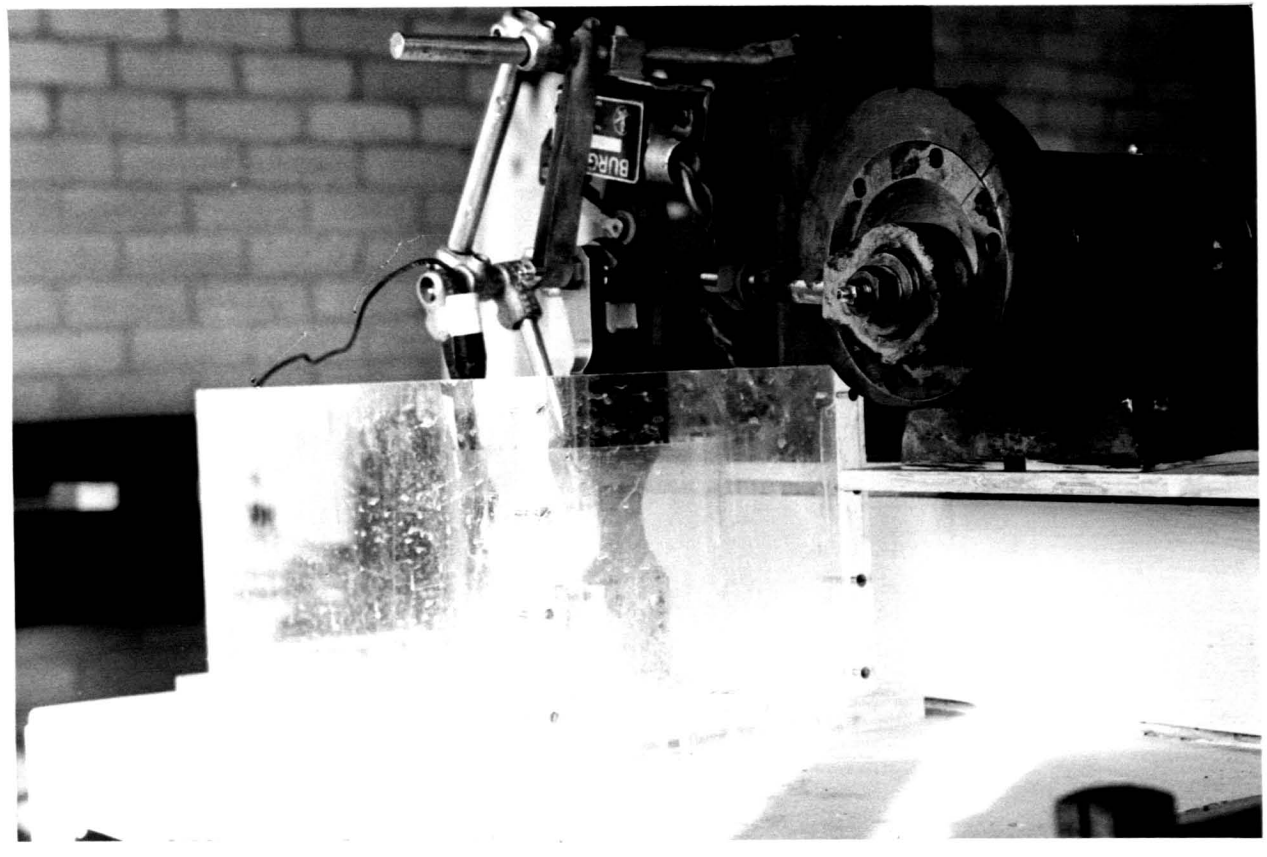

Figure 3.5 Reverse-bend fatigue-testing machine set-up for an aqueous corrosion-fatigue test; with the test cell in position.

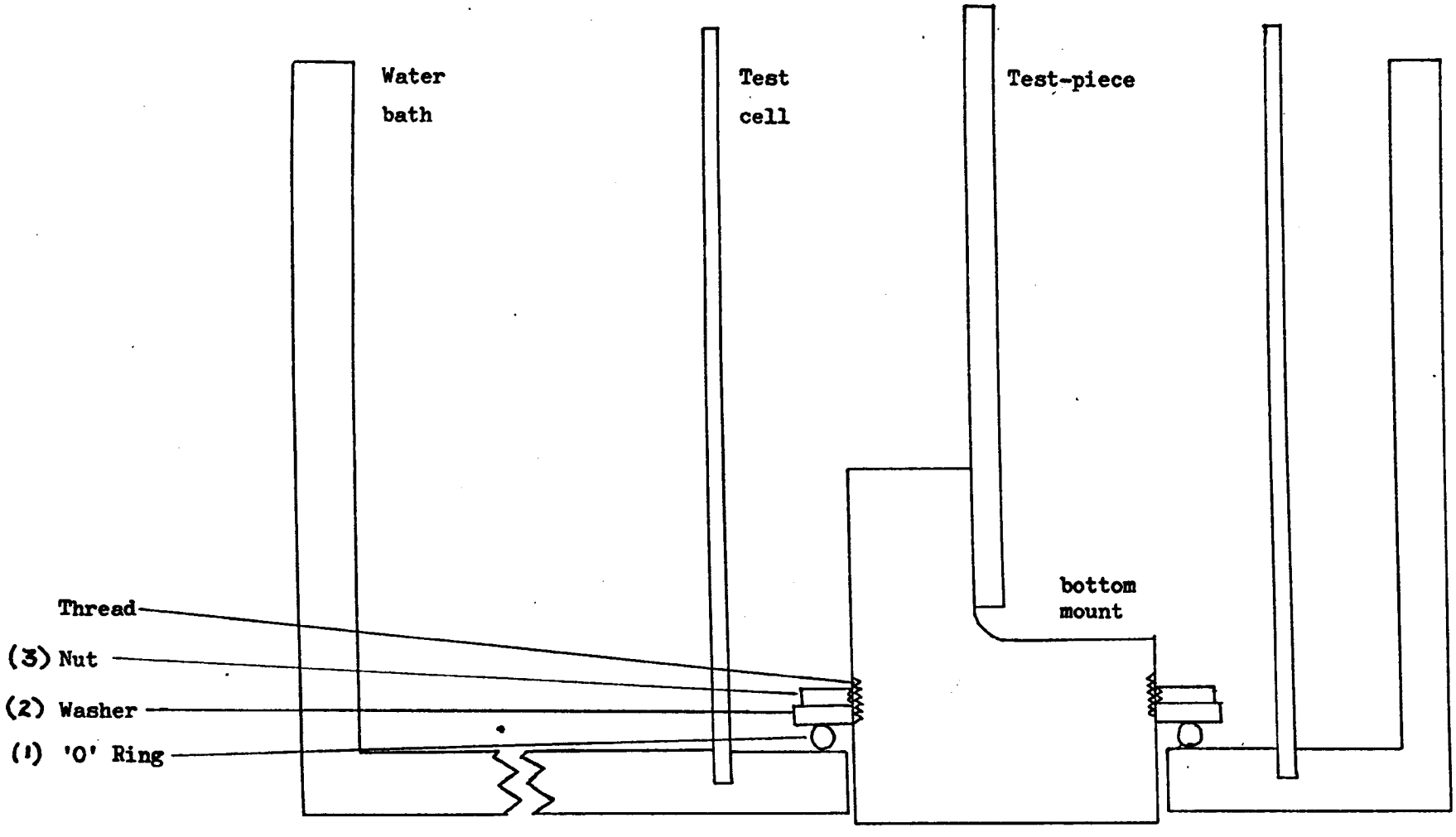

Figure 3.6 Test-cell design (not to scale)

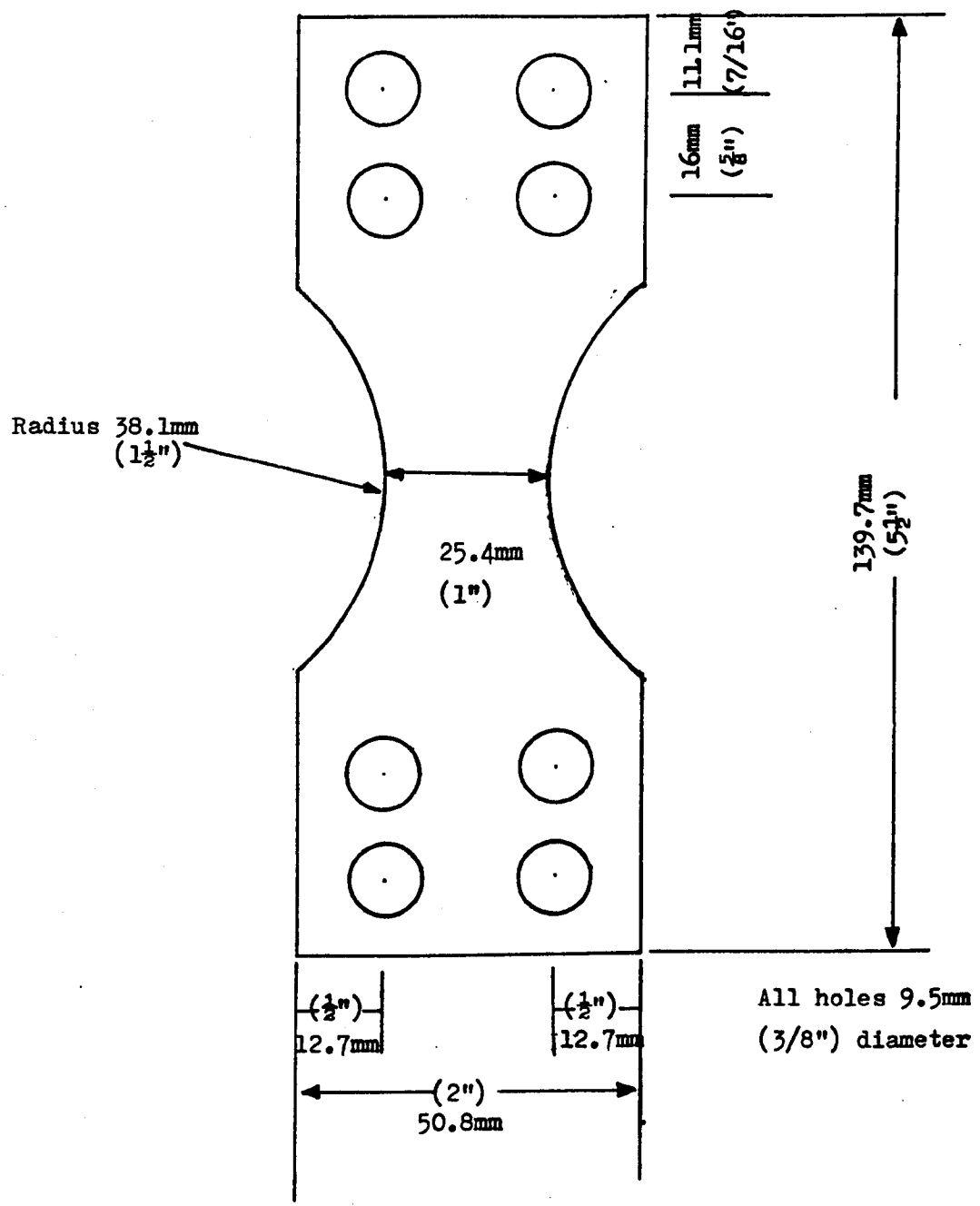

Figure 3.7 Reverse-bend fatigue test-piece

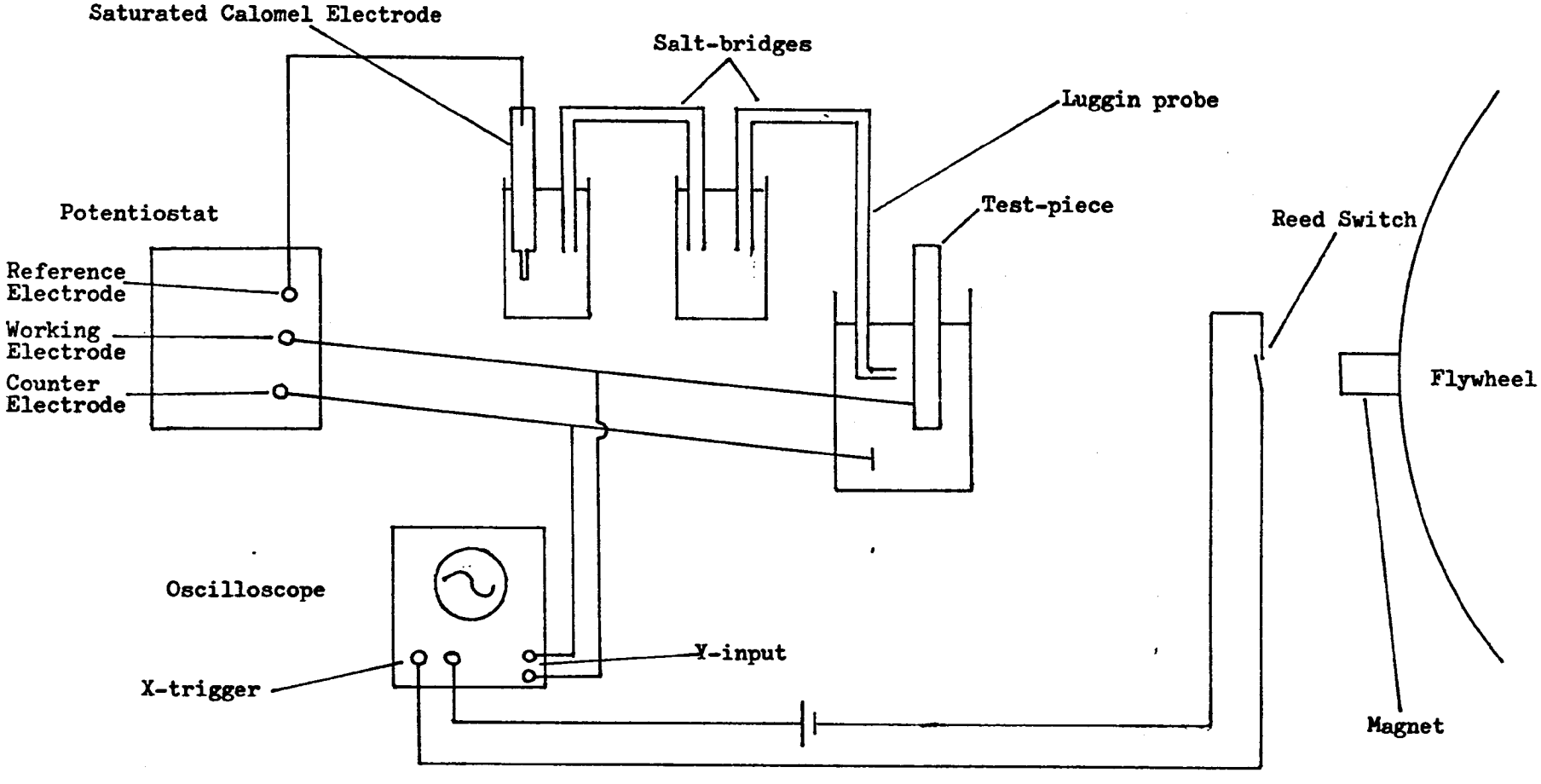

Figure 3.8 Schematic diagram of circuit used to measure potential fluctuations during fatigue

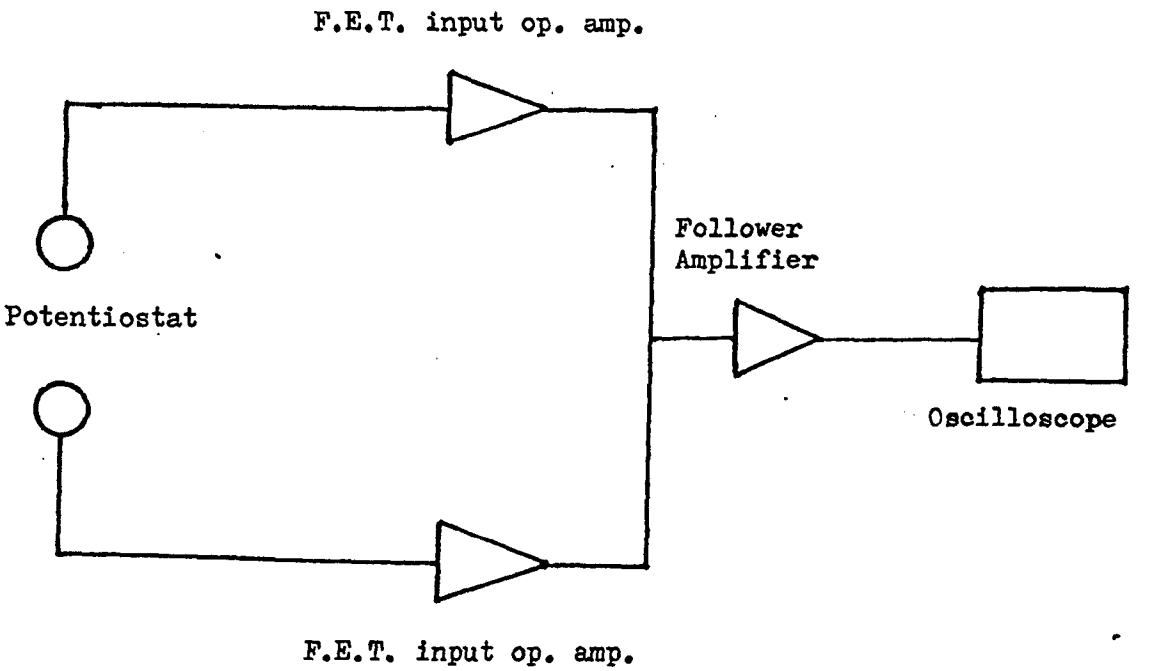

Figure 3.9 Schematic diagram of the original amplifier circuit.

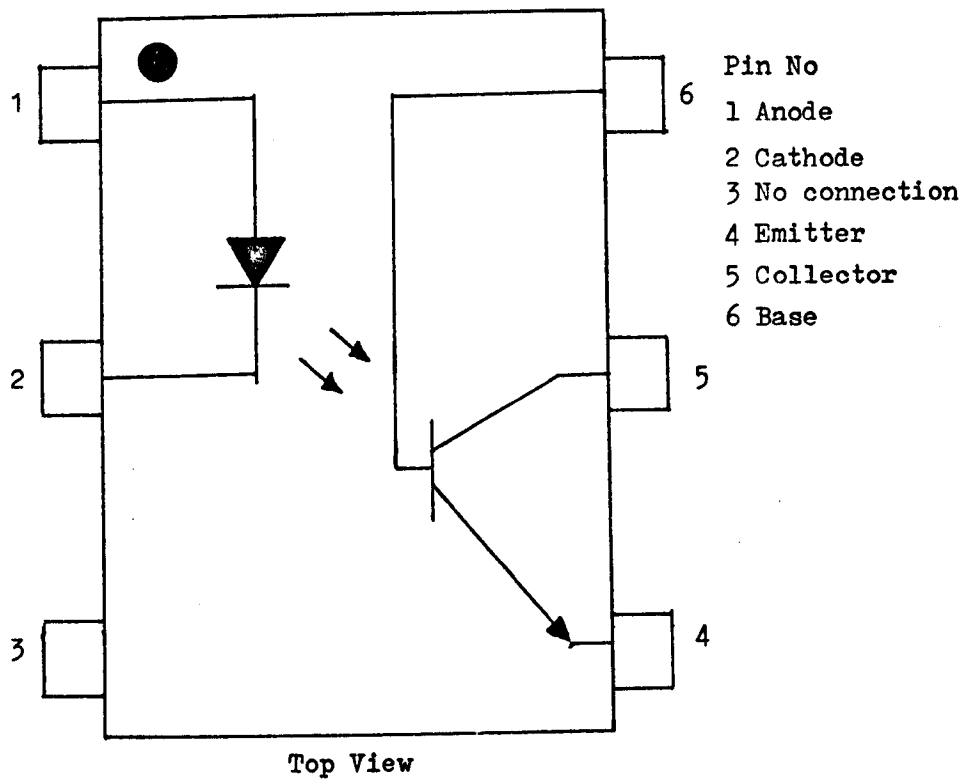

Figure 3.10a The opto-isolator, showing the pin configuration

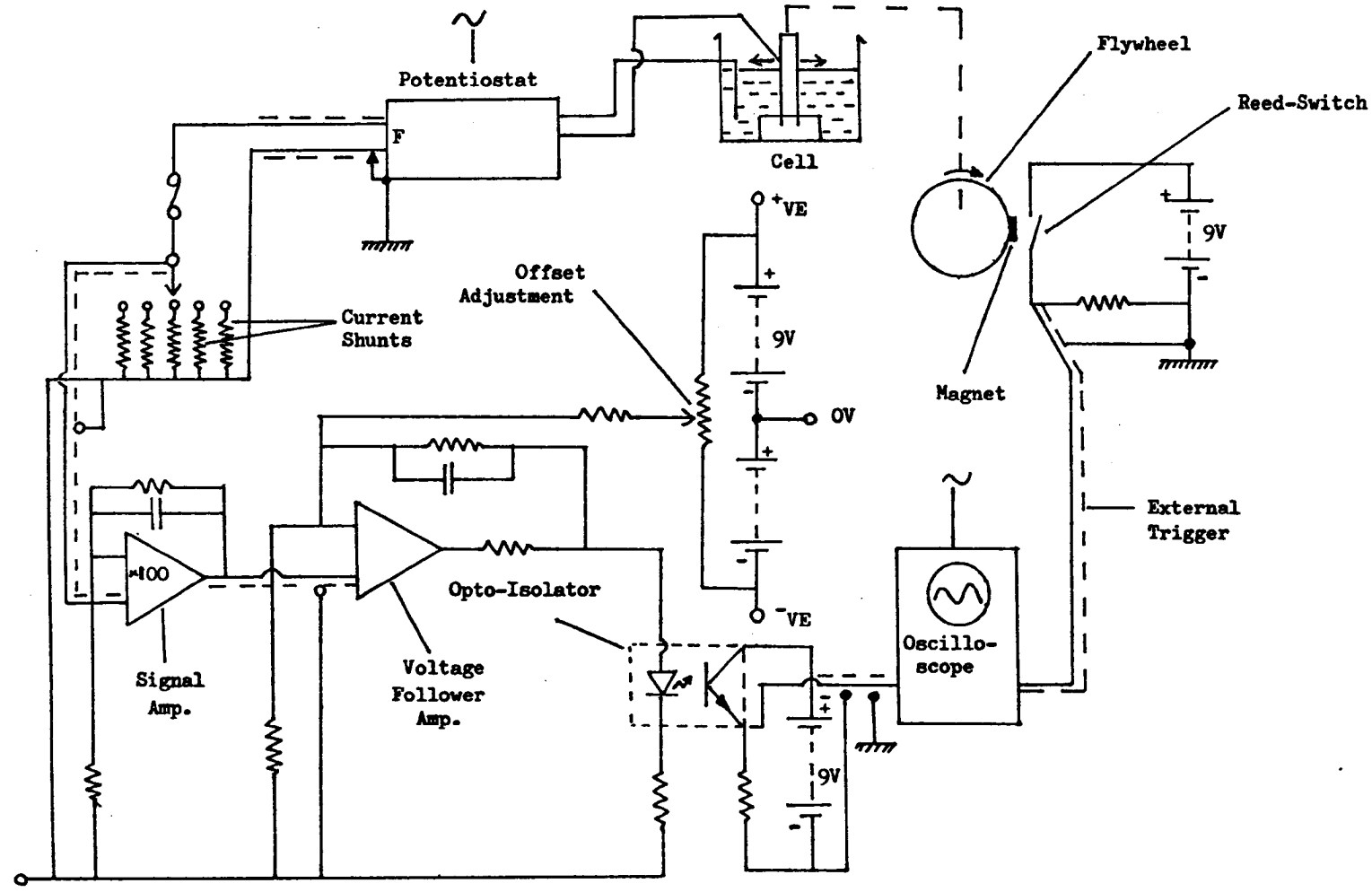

Figure 3.10b Schematic diagram of the original opto-isolator circuit used to measure fluctuations in the corrosion current during fatigue.

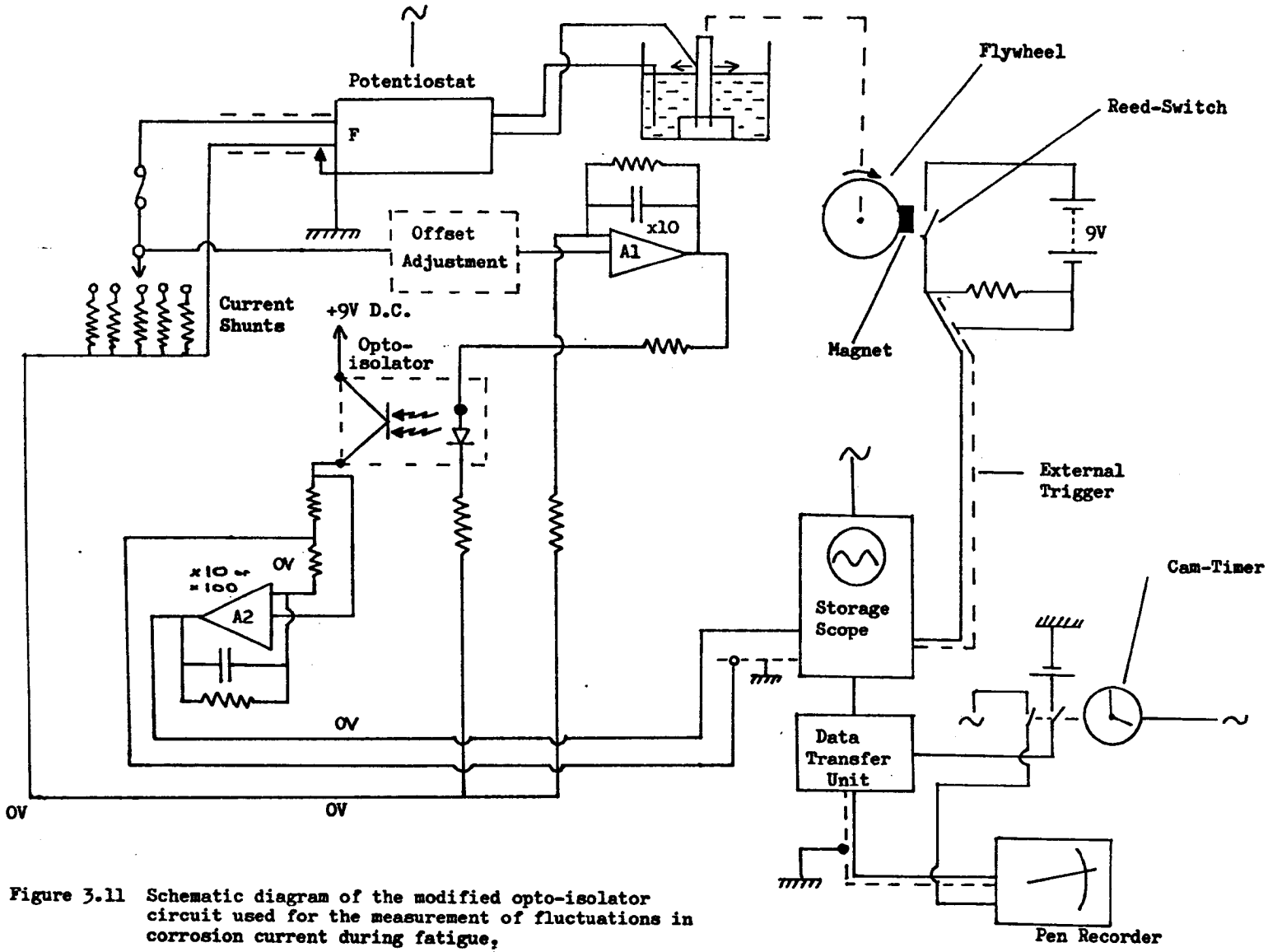

Figure 3.11 Schematic diagram of the modified opto-isolator circuit used for the measurement of fluctuations in corrosion current during fatigue.

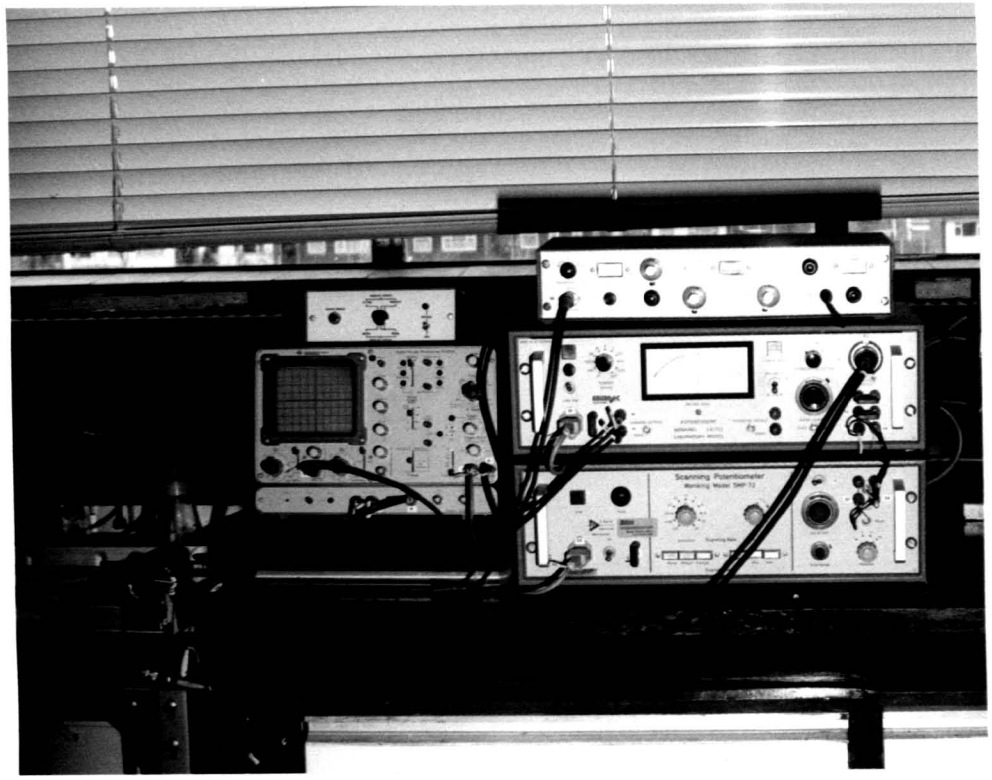

Figure 3.12 Final set-up of the equipment used in the measurement of fluctuations in corrosion current during fatigue.

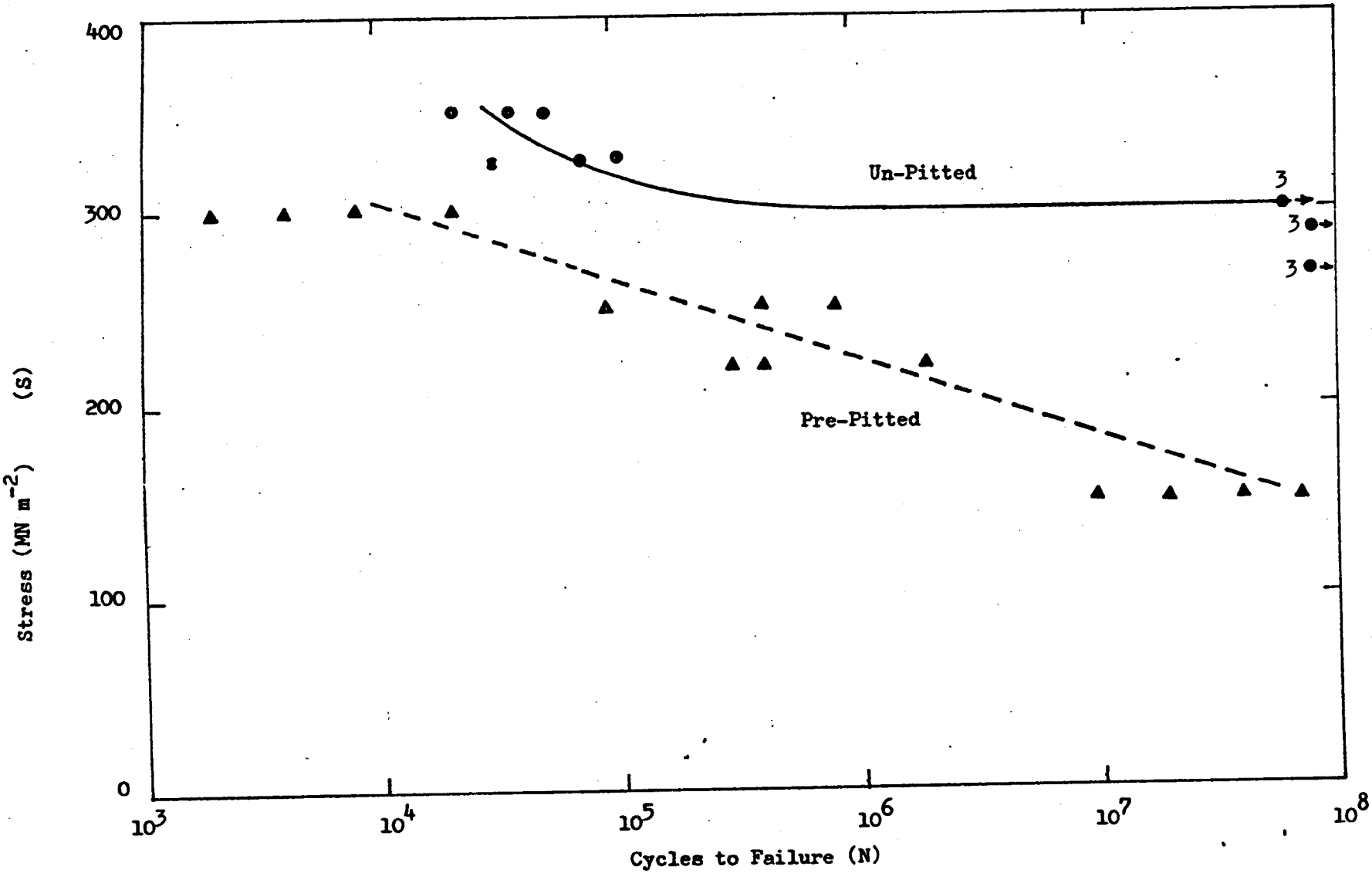

FIGURE 4.1 S/N Curves from rotating-bending fatigue tests in Air for pre-pitted and unpitted Test-pieces.

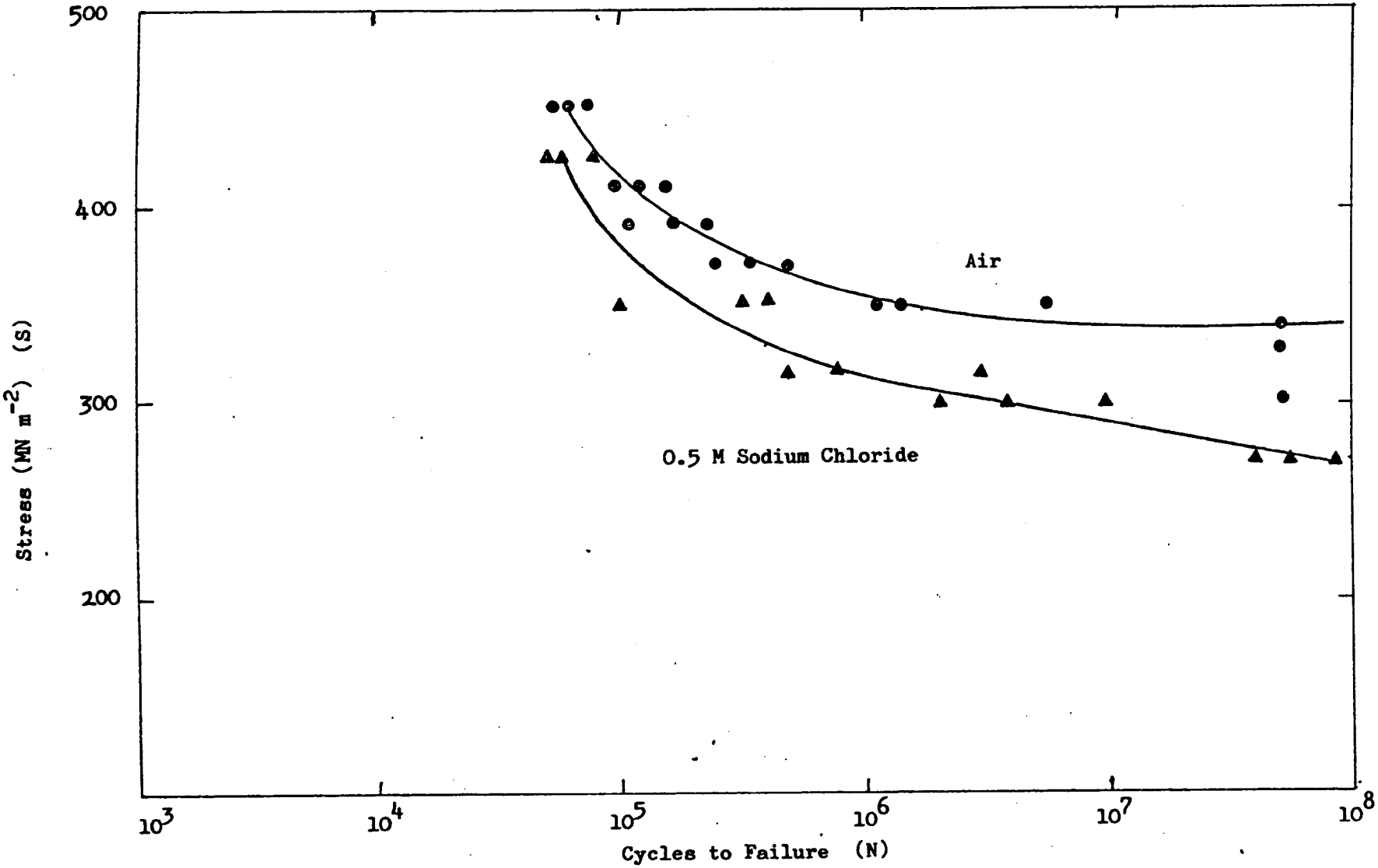

FIGURE 4.2 S/N Curves from reverse-bend fatigue tests for environments of Air and 0.5 M sodium chloride solution.

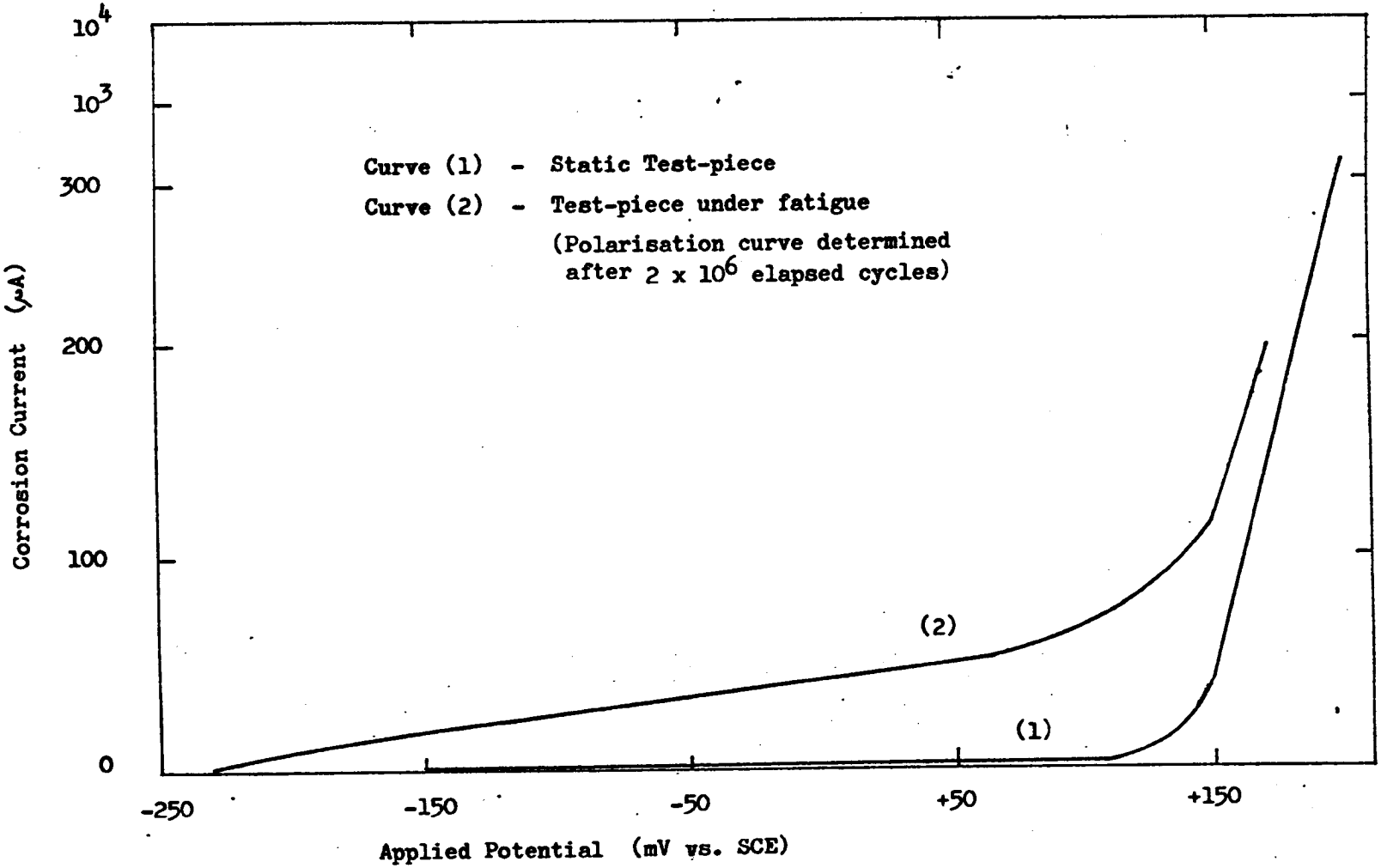

FIGURE 4.3 Anodic Polarisation Curves in 0.5 M sodium chloride solution for static test-pieces and test-pieces under fatigue (stress $\pm$ 250 MN m^{-2})

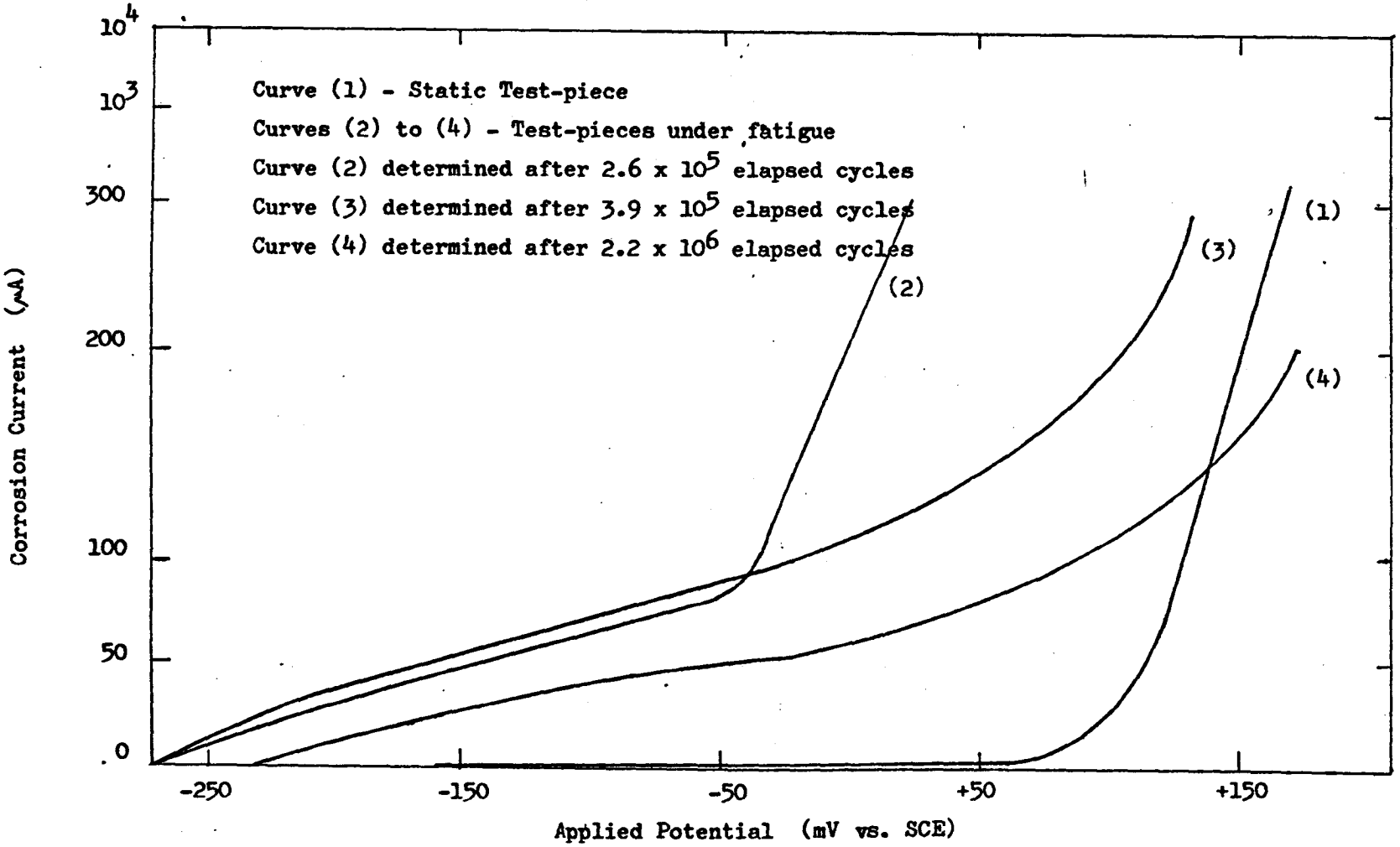

FIGURE 4.4 Anodic polarisation curves in 0.5 M sodium chloride solution for static test-pieces and test-pieces under fatigue (Stress $\pm$ 250 MN m^{-2})

FIGURE 4.5 Anodic Polarisation Curves in 0.5 M sodium chloride solution for static test-pieces and test-pieces under fatigue (Stress $\pm$ 320 MN m^{-2})

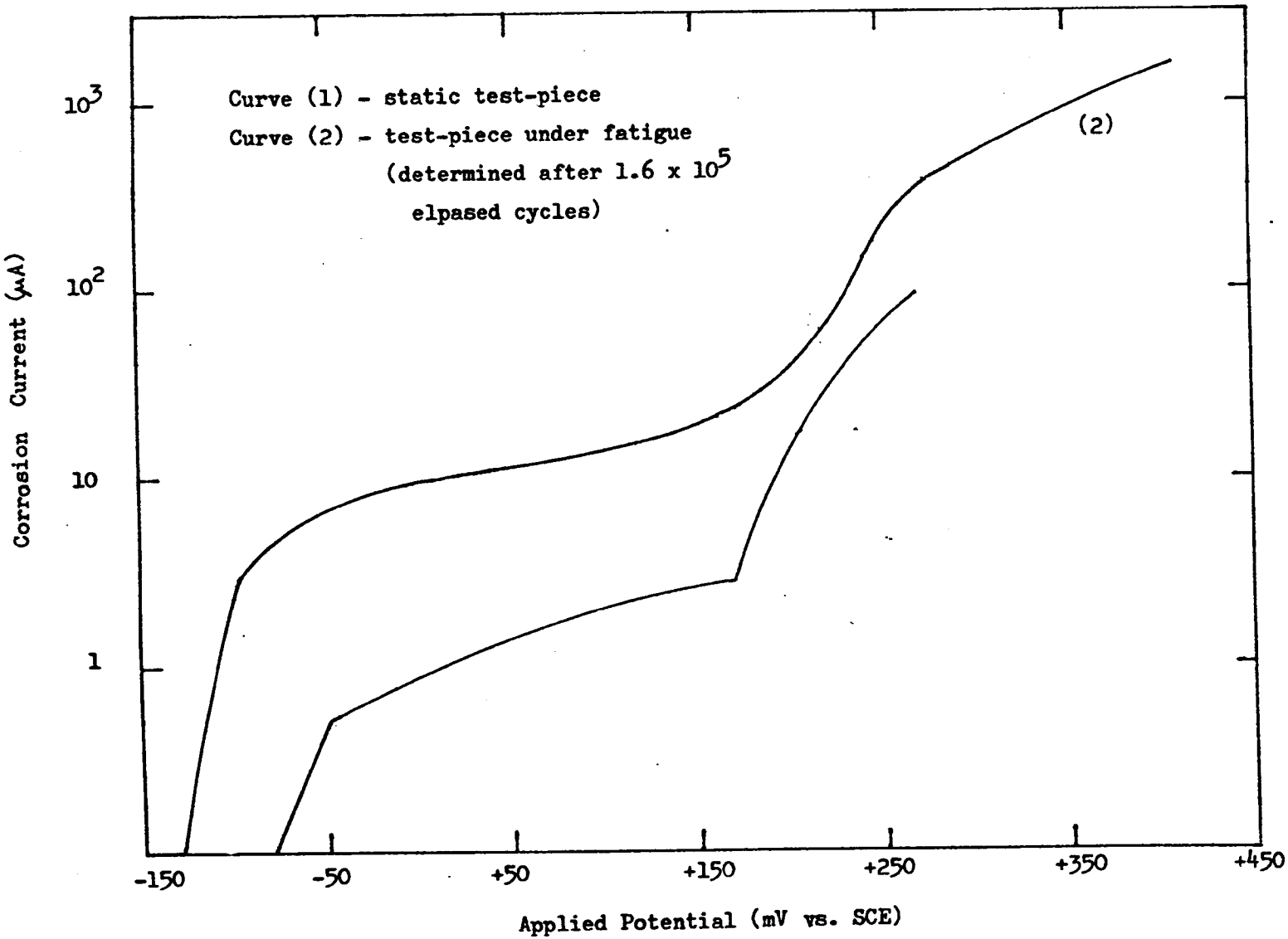

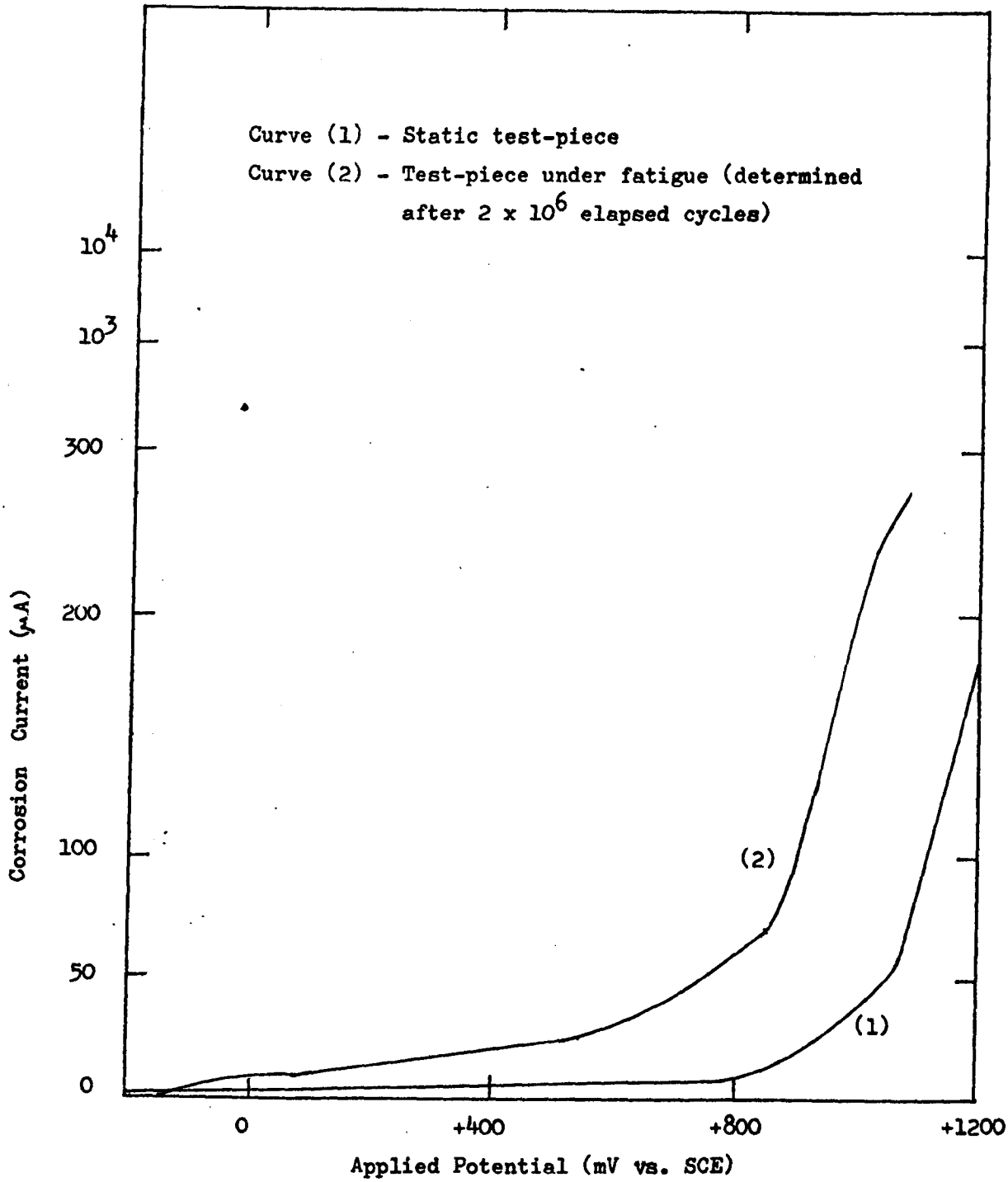

FIGURE 4.6 Anodic Polarisation curves in 0.2 M sodium sulphate solution for static test-pieces and test-pieces under fatigue. (Stress ± 250 MN m^{-2})

Figure 4.7 Anodic Polarisation Curves in 0.1M sodium sulphate solution for static test-pieces and test-pieces under fatigue (stress $\pm$ 320 MN m^{-2})

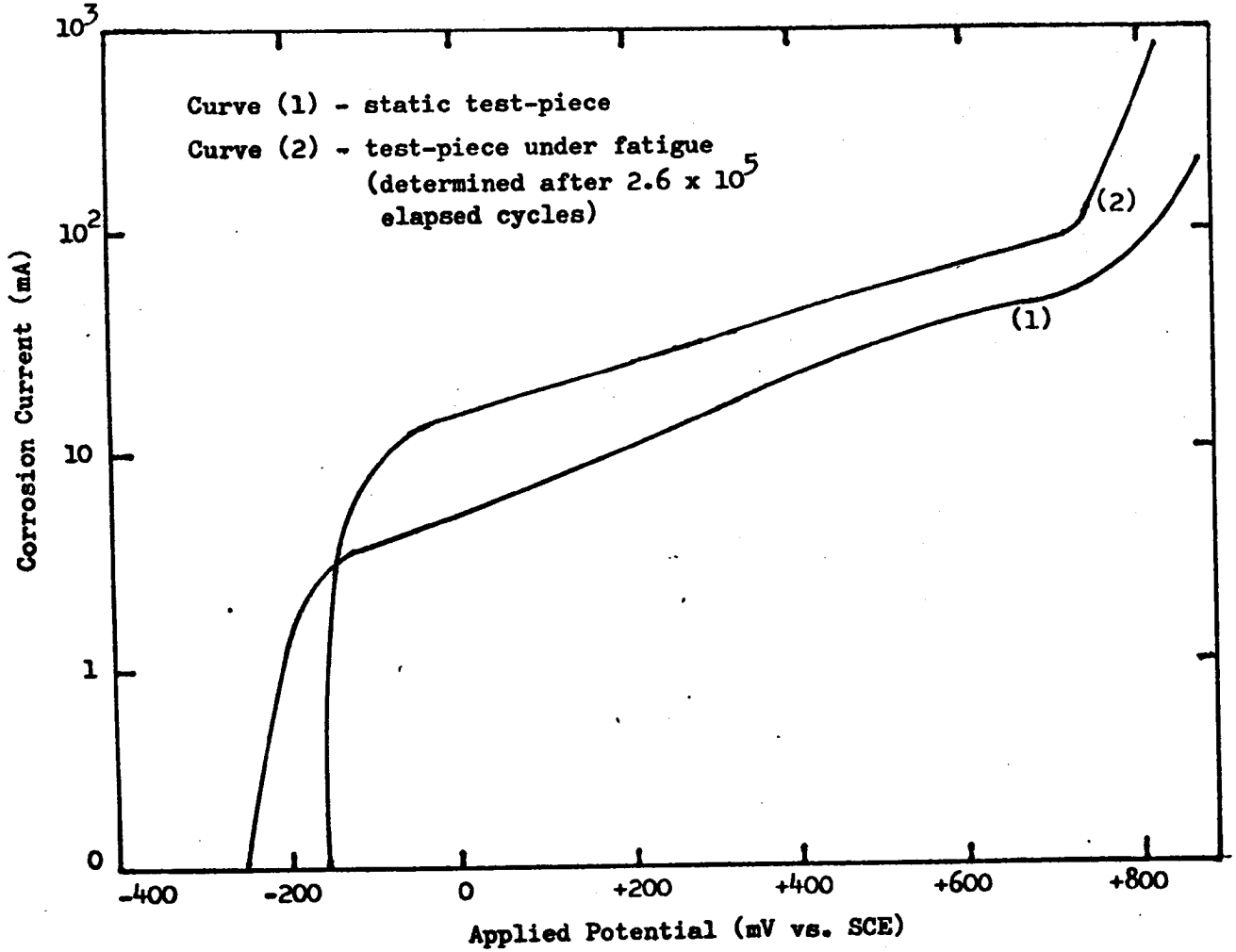

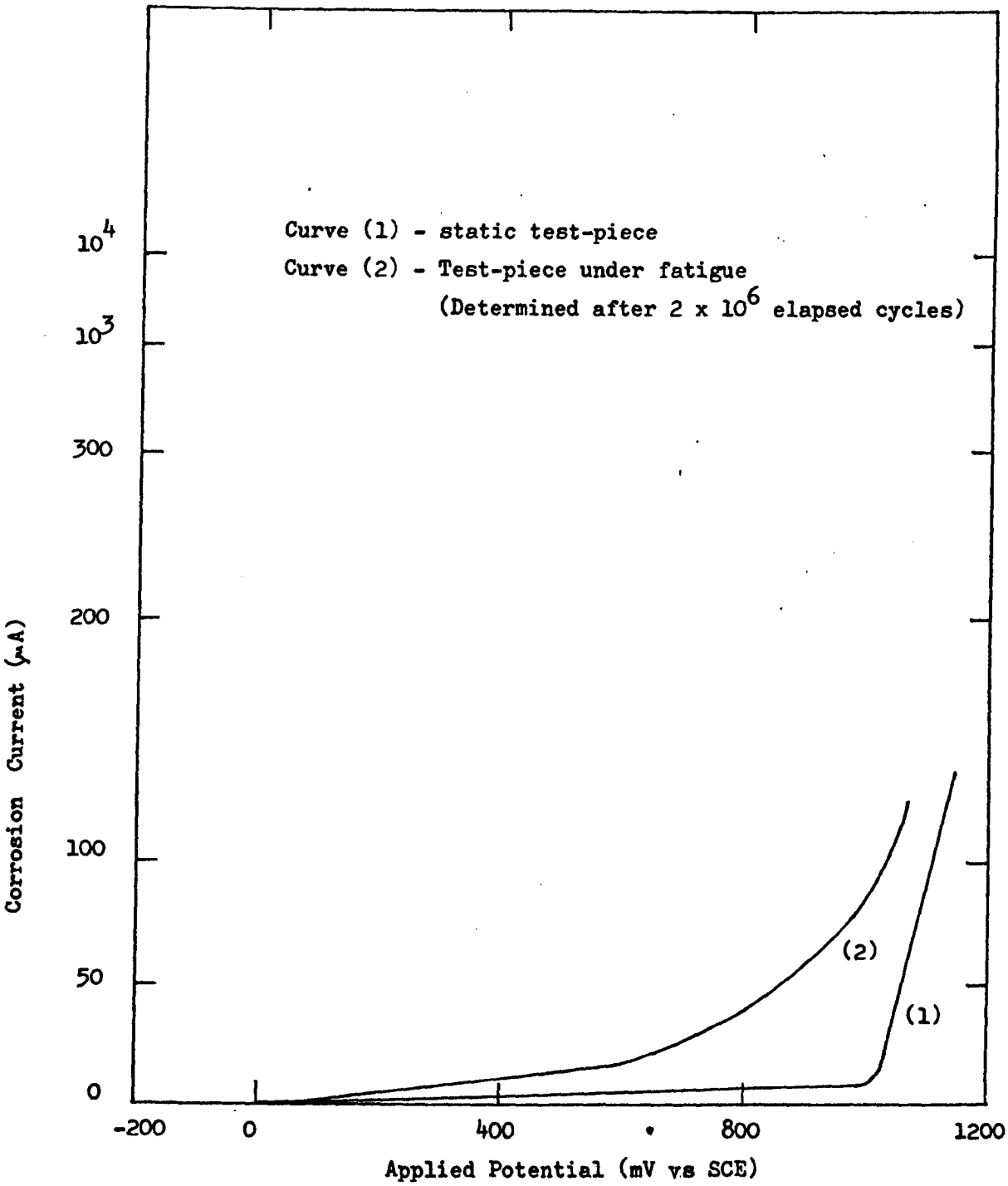

FIGURE 4.8 Anodic Polarisation curves in 0.1 M Potassium Dichromate solution for static test-pieces and test-pieces under fatigue.
(Stress ± 250 MN m^{-2})

FIGURE 4.9 Anodic Polarisation curves in 0.1 M Potassium Dichromate solution for static test-pieces and test-pieces under fatigue.
(Stress $\pm$ 320 MN m^{-2})

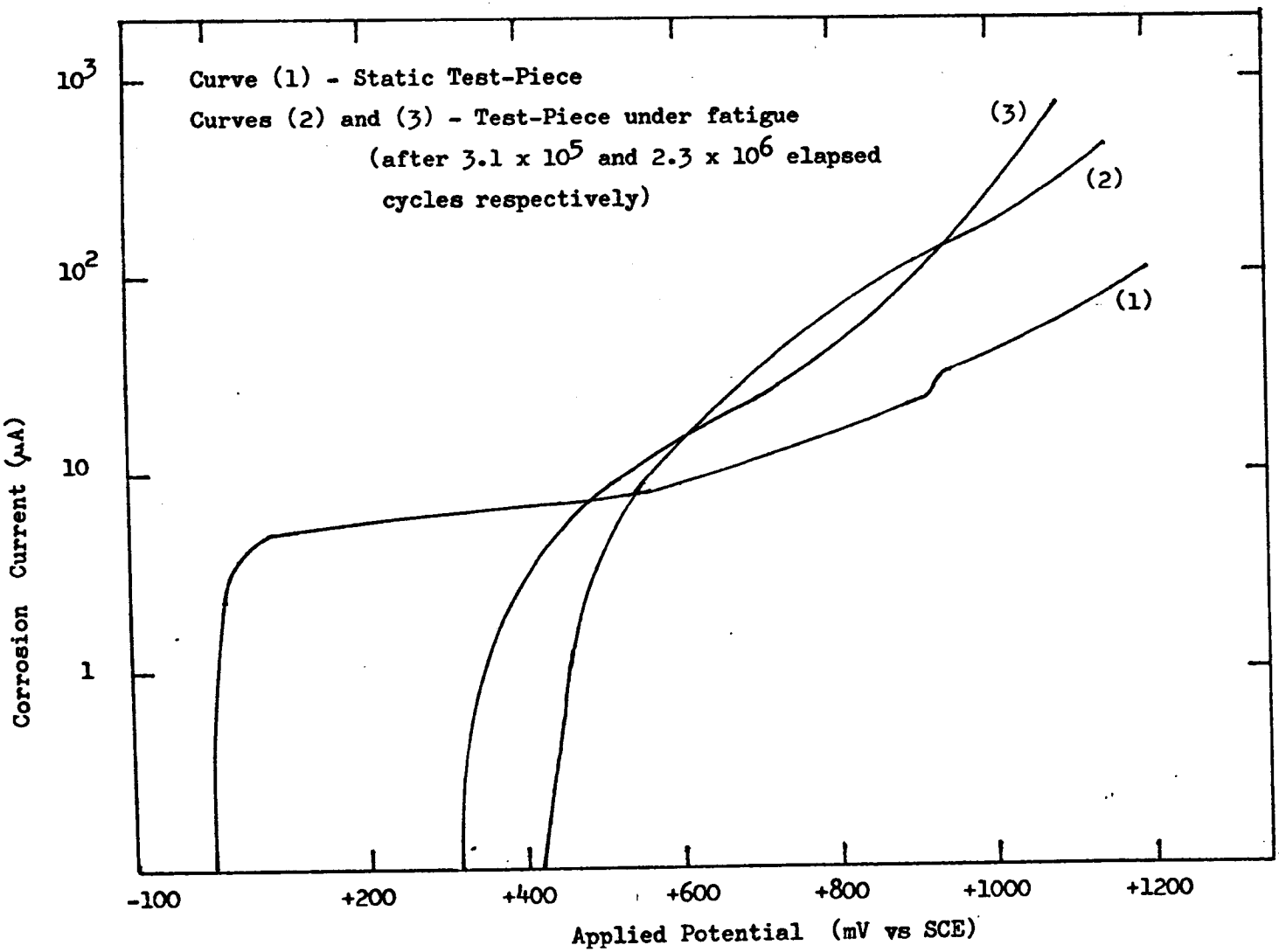

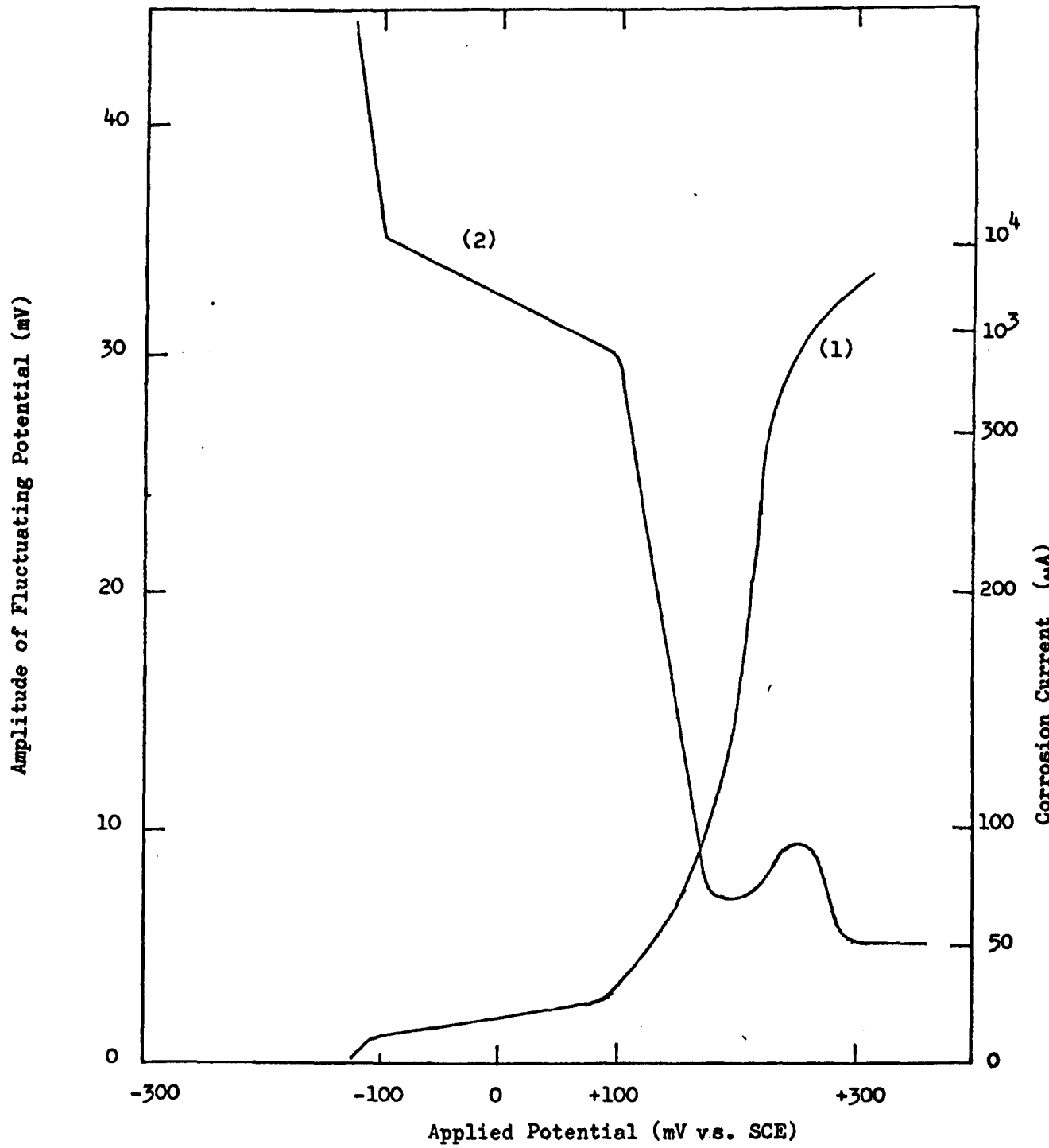

FIGURE 4.10 Variation of corrosion current (Curve (1)) and the amplitude of the fluctuating potential (Curve (2)) with applied potential in 0.5M sodium chloride solution during fatigue (stress ± 250 MN m^{-2}); determinations made after 1.8×10^5 elapsed cycles.

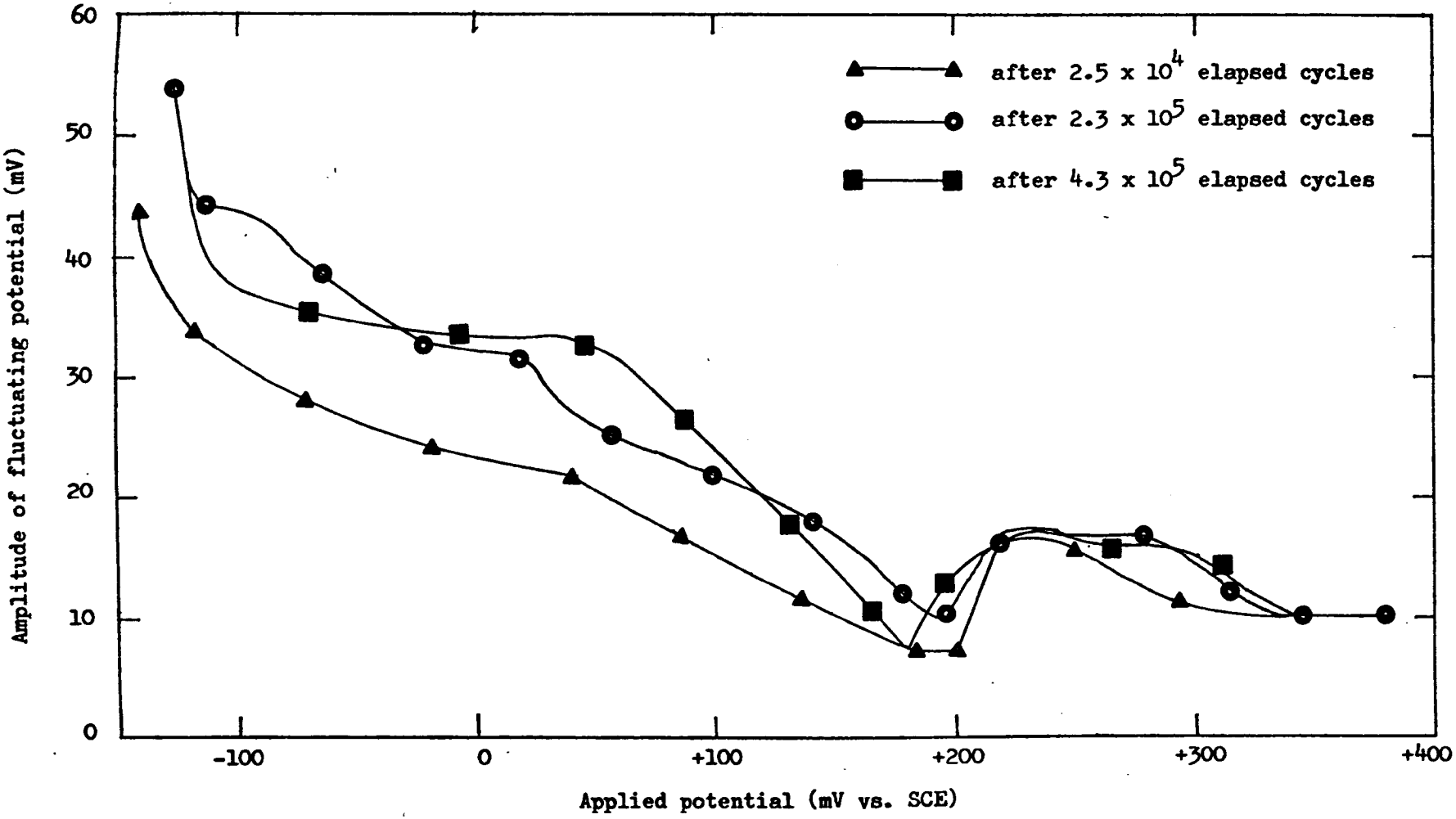

FIGURE 4.11 Variation of the amplitude of the fluctuating potential with applied potential in 0.5 M sodium chloride solution during fatigue. (Stress $\pm$ 250 MN m^{-2}); after different numbers of elapsed cycles.

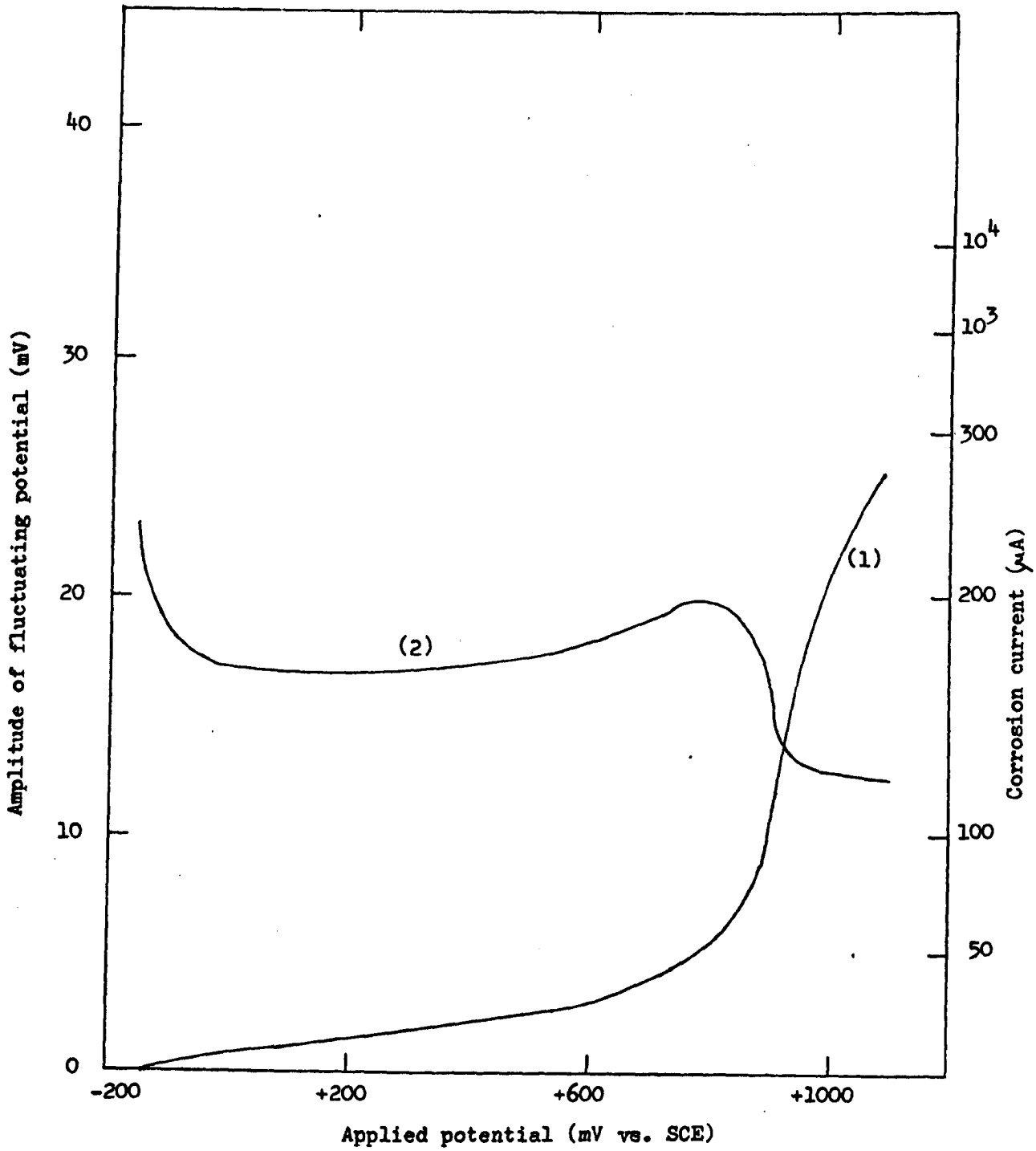

FIGURE 4.12 Variation of corrosion current (Curve (1)) and the amplitude of the fluctuating potential (Curve (2)) with applied potential in 0.2 M sodium sulphate solution during fatigue. (Stress $\pm$ 250 MN m^{-2}); determinations made after 2 x 10^6 elapsed cycles.

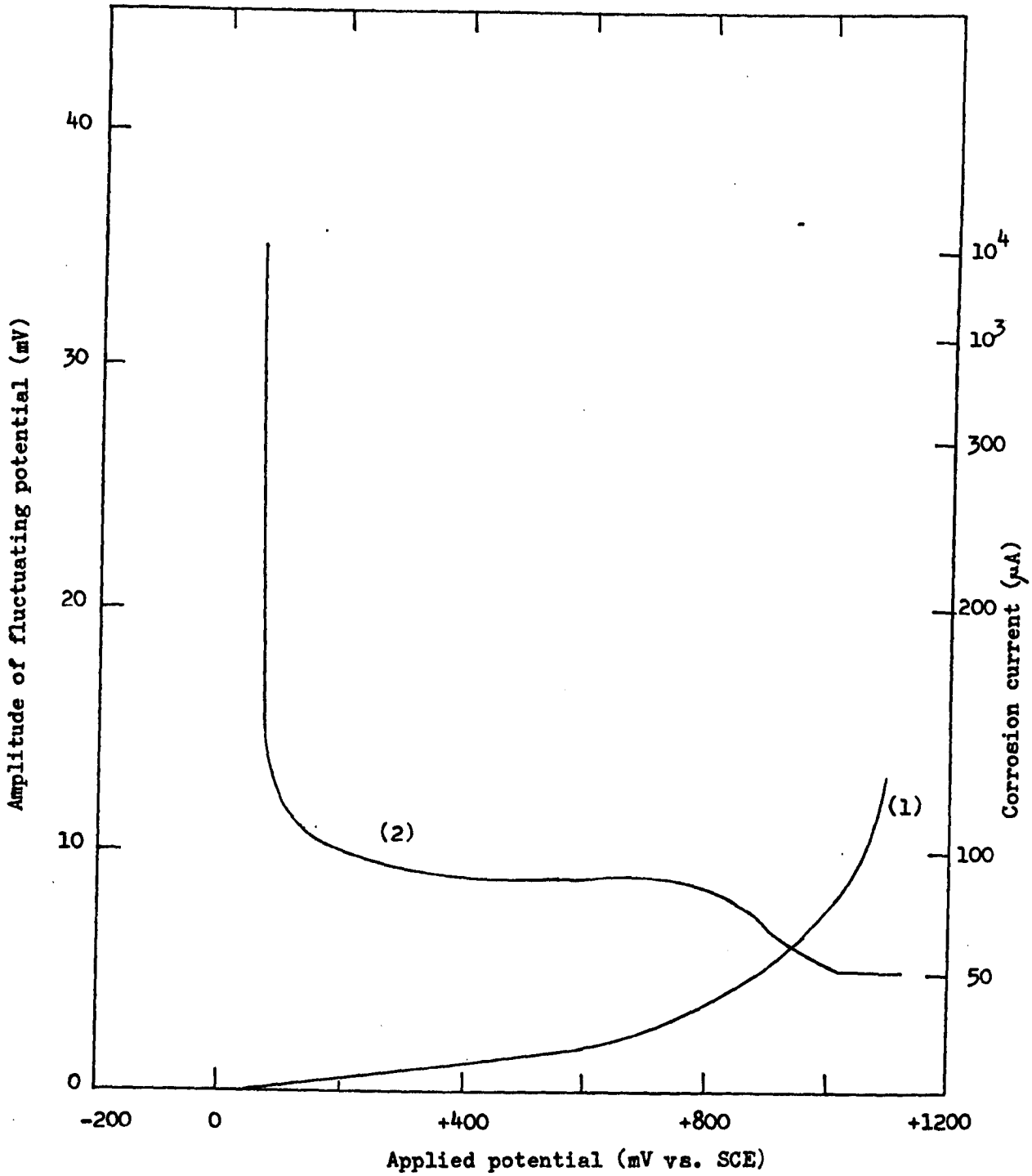

FIGURE 4.13 Variation of corrosion current (Curve (1)) and the amplitude of the fluctuating potential (Curve (2)) with applied potential in 0.1M Potassium Dichromate solution during fatigue. (Stress $\pm$ 250 MN m^{-2}); determinations made after 2 x 10^6 elapsed cycles.

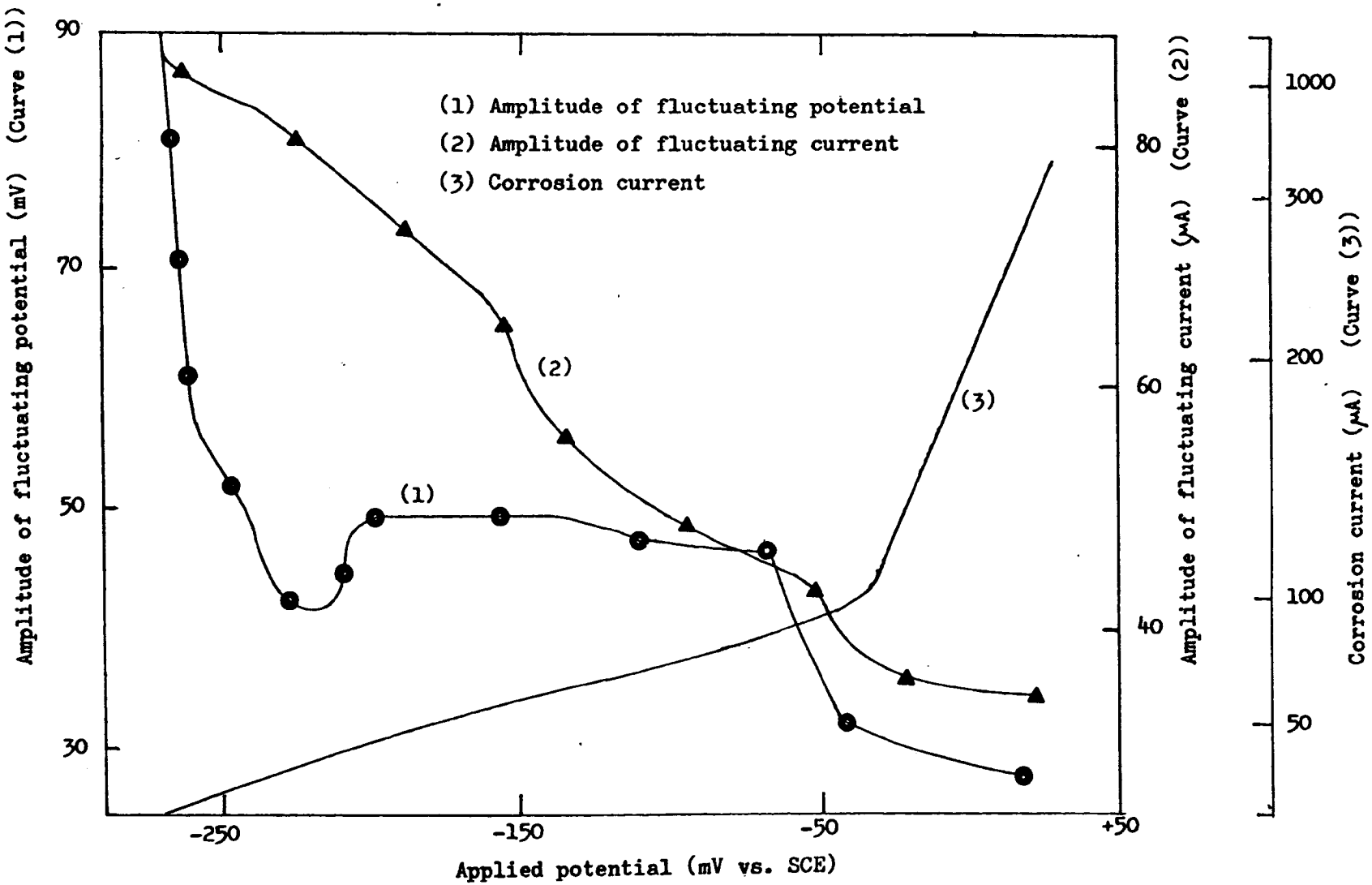

FIGURE 4.14 Comparison of the variation in the fluctuating current and potential measurements with applied potential in 0.5M sodium chloride solution during fatigue. (Stress ± 250 MN m^{-2}); determinations made after 2.6 x 10^5 elapsed cycles.

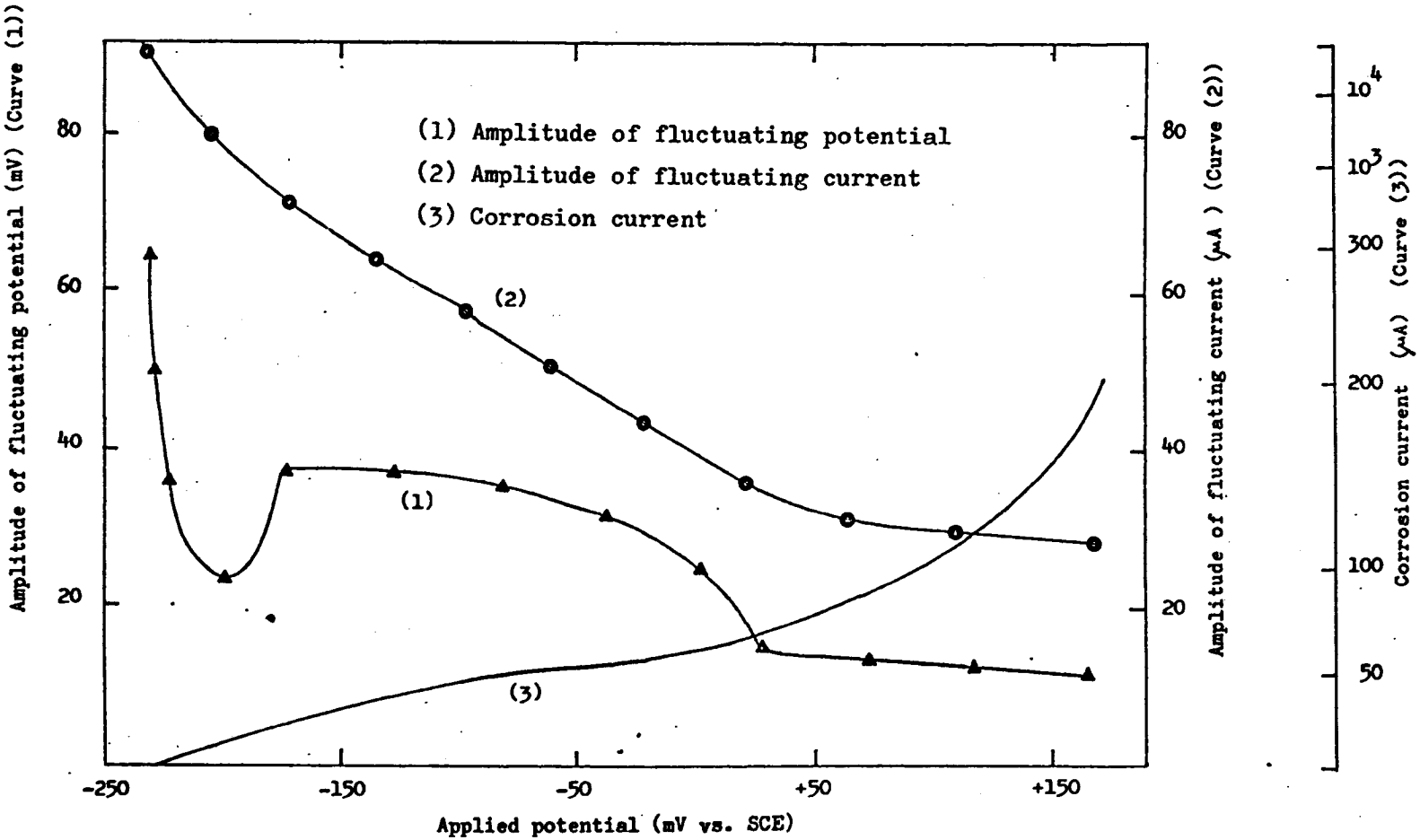

FIGURE 4.15 Comparison of the variation in the fluctuating current and potential measurements with applied potential in 0.5M sodium chloride solution during fatigue. (Stress ± 250 MN m^{-2}), determinations made after 2 x 10^6 elapsed cycles.

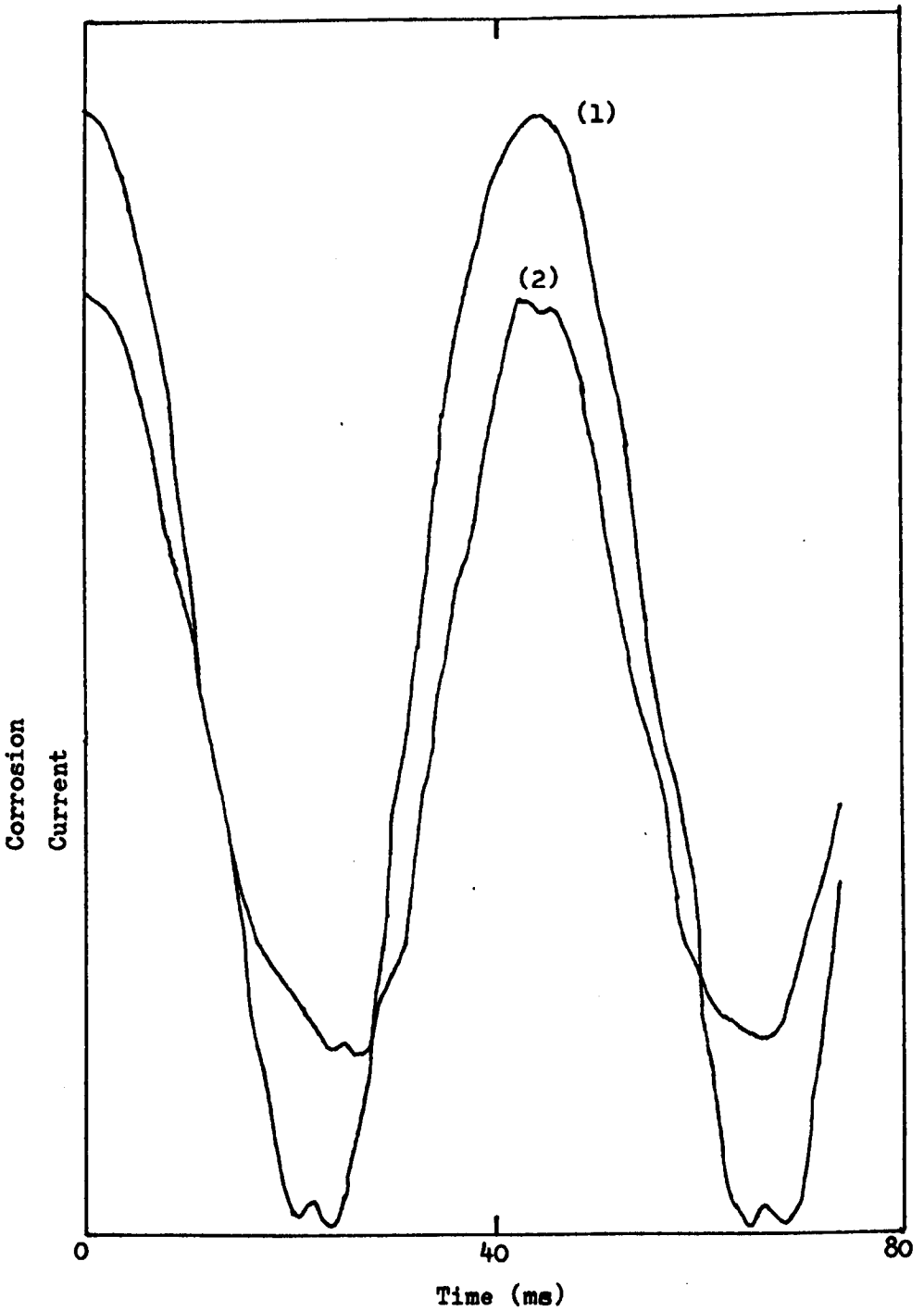

FIGURE 4.16 Form of the fluctuating current signal during fatigue in 0.5M sodium chloride solution at applied potentials of -260 mV vs SCE (Curve (1)) and +280 mV vs SCE (Curve (2)) after 2 x 10^6 elapsed cycles. (Stress ± 320 MN m^{-2}).

FIGURE 4.17 Variation of the amplitude of fluctuating current. (Curves (1) and (2)) and of corrosion current (Curves (3) and (4)) with applied potential in 0.5M sodium chloride solution during fatigue (Stress ± 320 MN m^{-2})

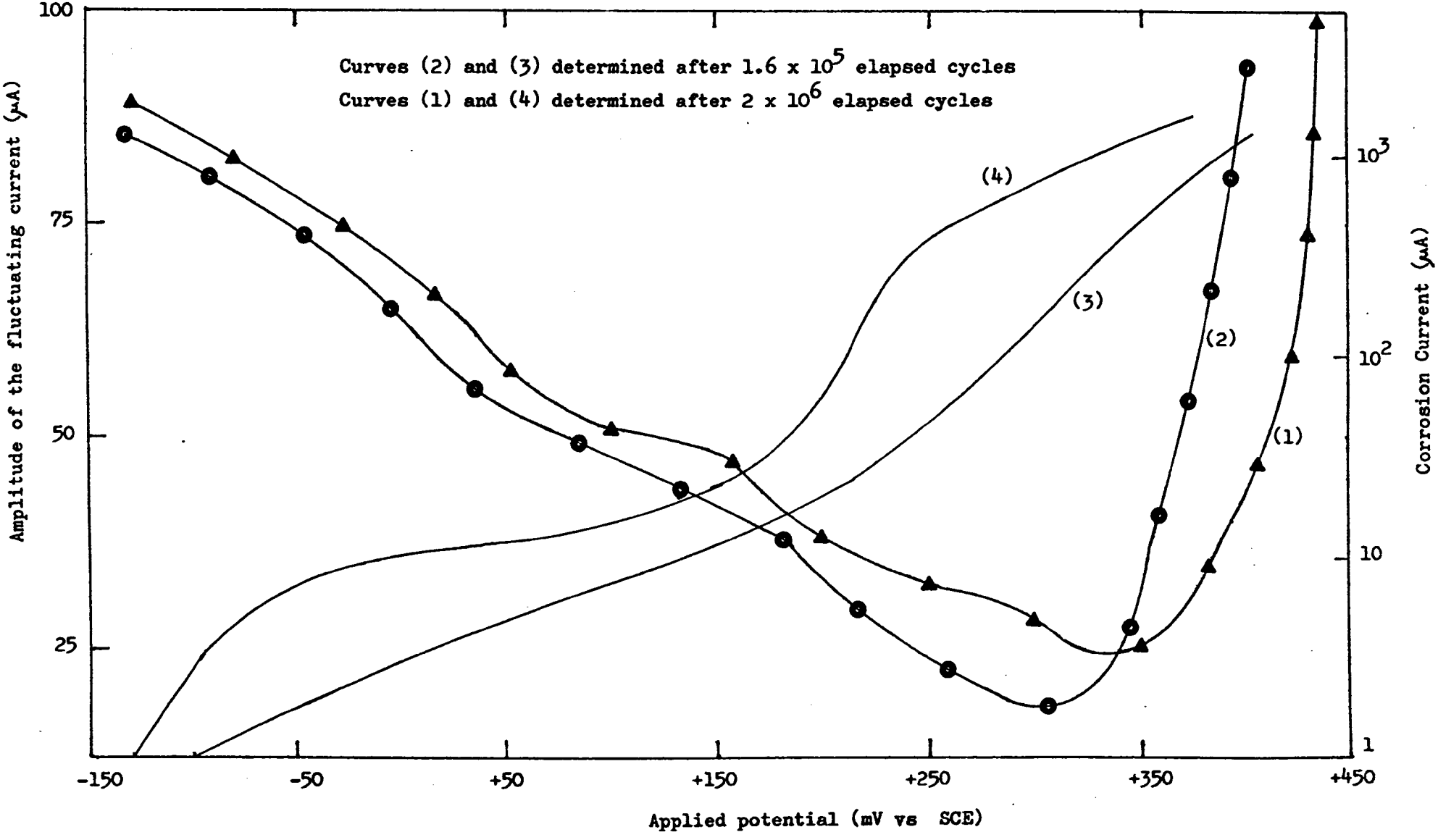

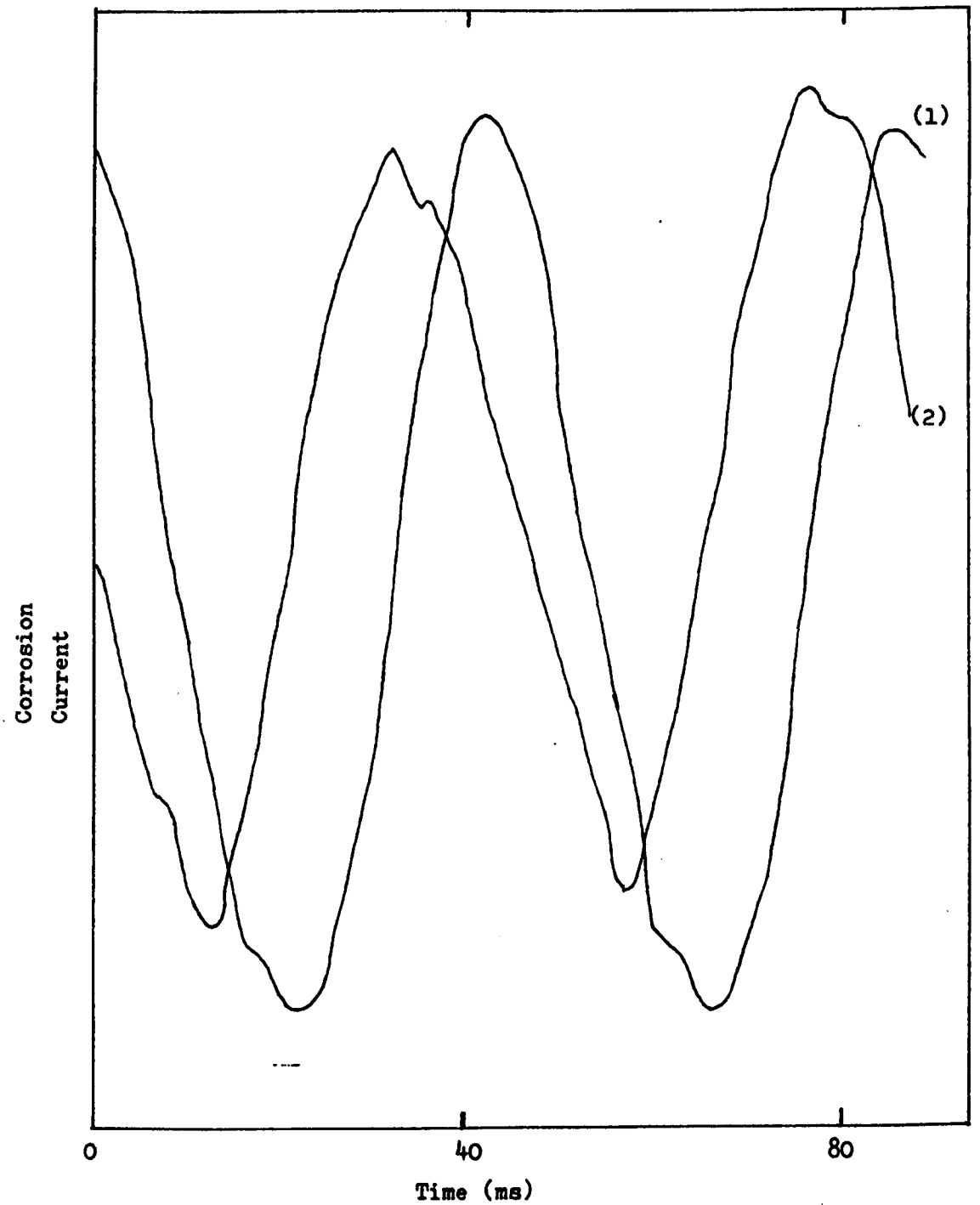

FIGURE 4.18 Form of the fluctuating current signal during fatigue in 0.2M sodium sulphate solution at applied potentials of -190 mV vs SCE (Curve (1)) and +1150 mV vs SCE (Curve (2)) after 2 x 10^6 elapsed cycles. (Stress $\pm$ 320 MN m^{-2})

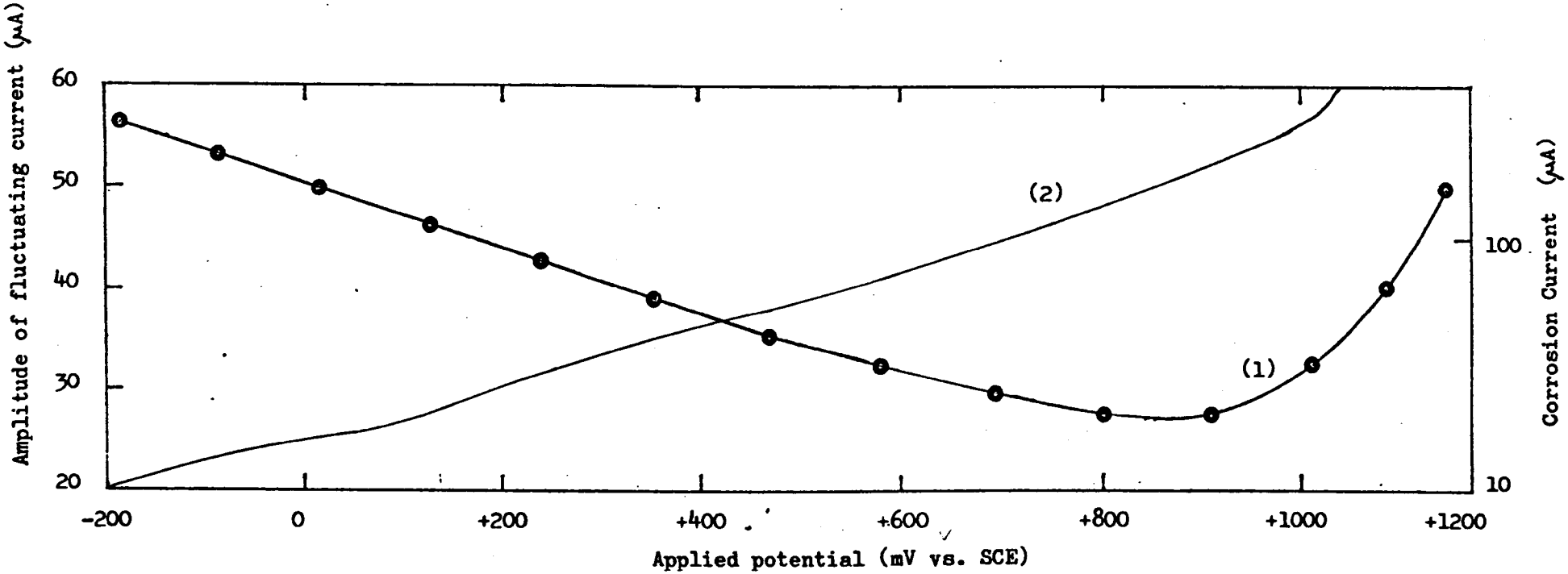

FIGURE 4.19 Variation of the amplitude of fluctuating current (Curve (1)) and corrosion current (Curve (2)) with applied potential in 0.2M Sodium Sulphate Solution during fatigue. (Stress $\pm$ 320 MN m^{-2}) ; determined after 2.6 x 10^5 elapsed cycles.

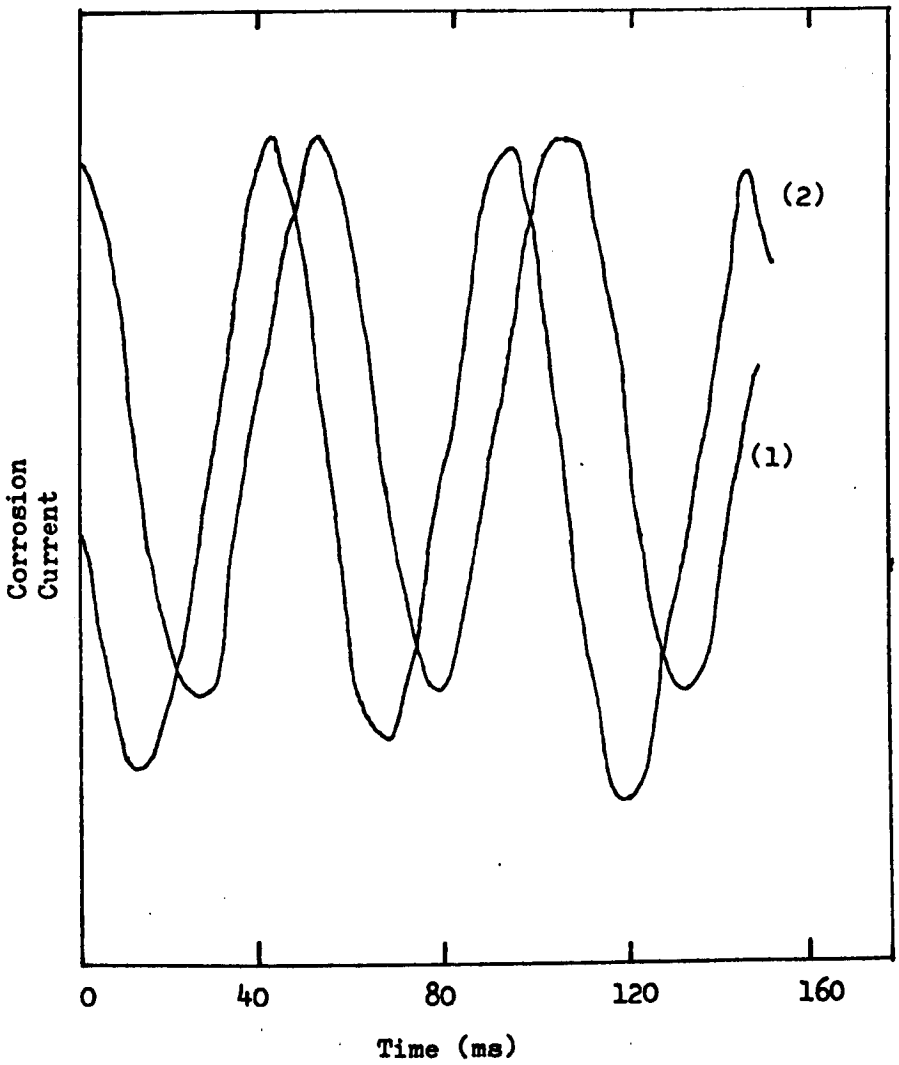

FIGURE 4.20 Form of the fluctuating current signal during fatigue in 0.1M Potassium Dichromate solution at applied potentials of +400 mV vs SCE (Curve (1)) and +1100 mV vs SCE (Curve (2)) after 2×10^6 elapsed cycles. (Stress $\pm$ 320 MN m^{-2}).

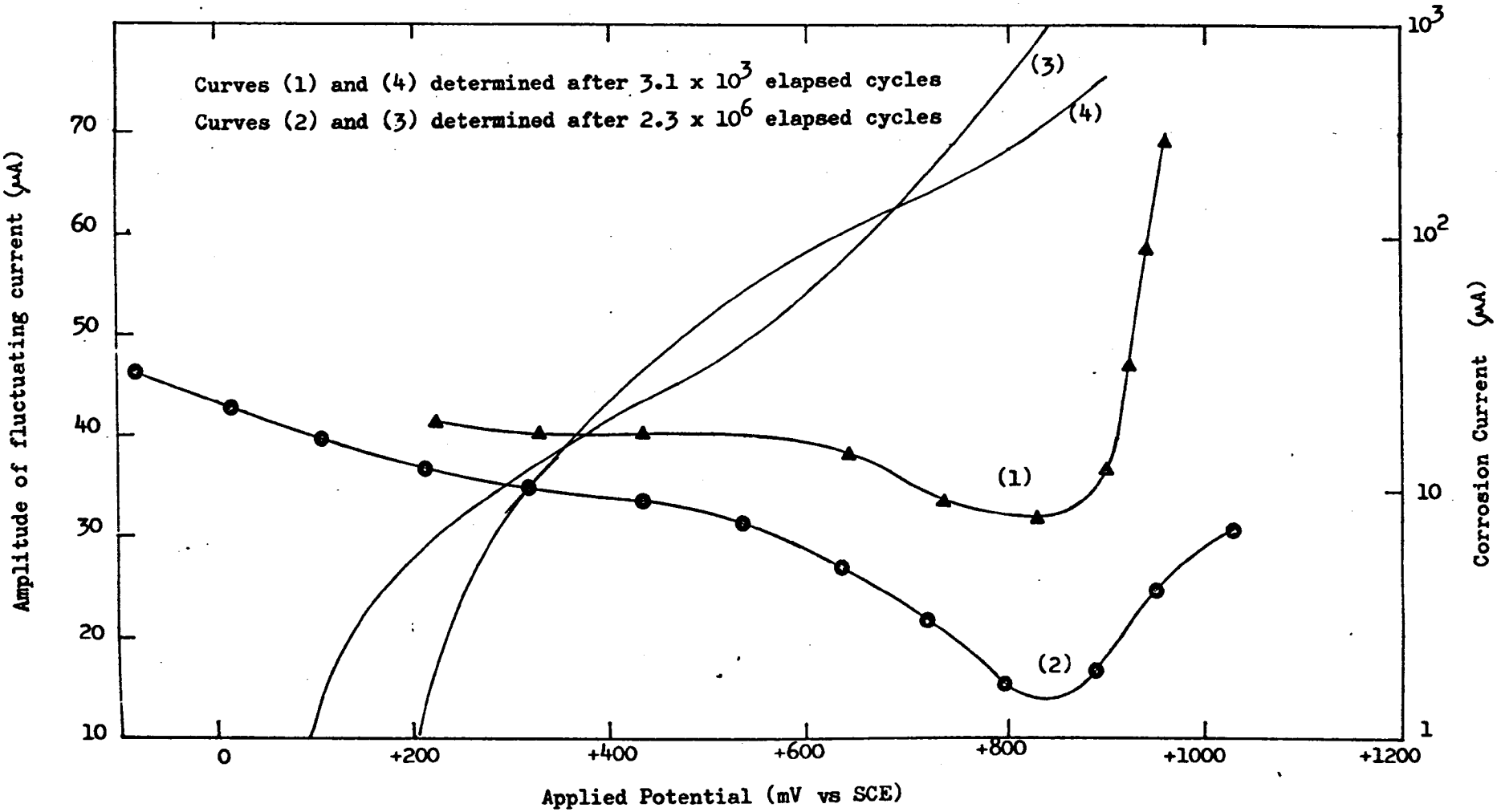

FIGURE 4.21 Variation of the amplitude of fluctuating current (Curves (1) and (2) and of corrosion current (Curves (3) and (4)) with applied potential in 0.1M Potassium Dichromate solution during fatigue. (Stress $\pm$ 320 MN m^{-2}).

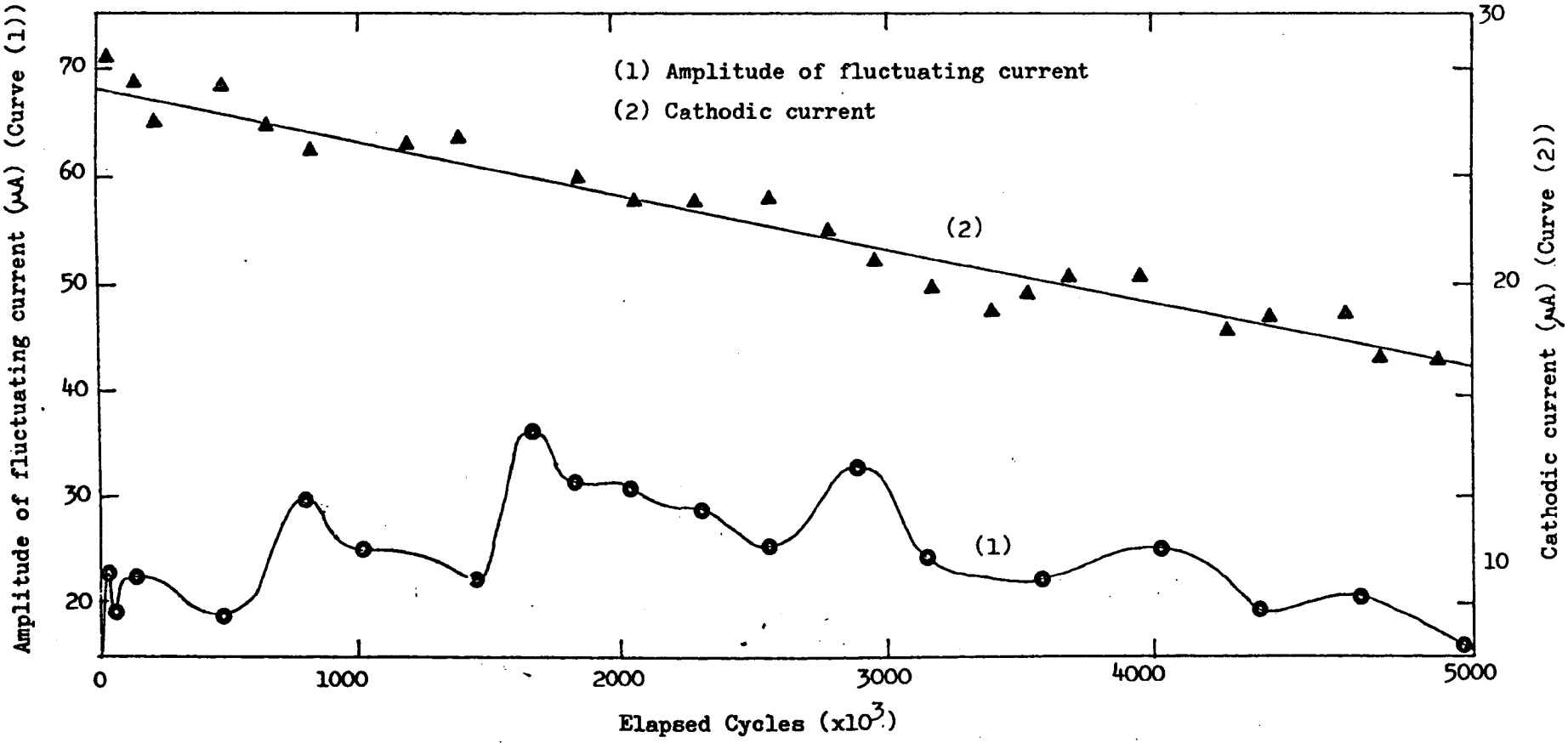

FIGURE 4.22 Variation of the amplitude of fluctuating current and corrosion current with elapsed cycles during a fatigue test. (Stress $\pm$ 320 MN m^{-2}) in 0.5M sodium chloride solution with a constant applied potential of -240 mV vs SCE.

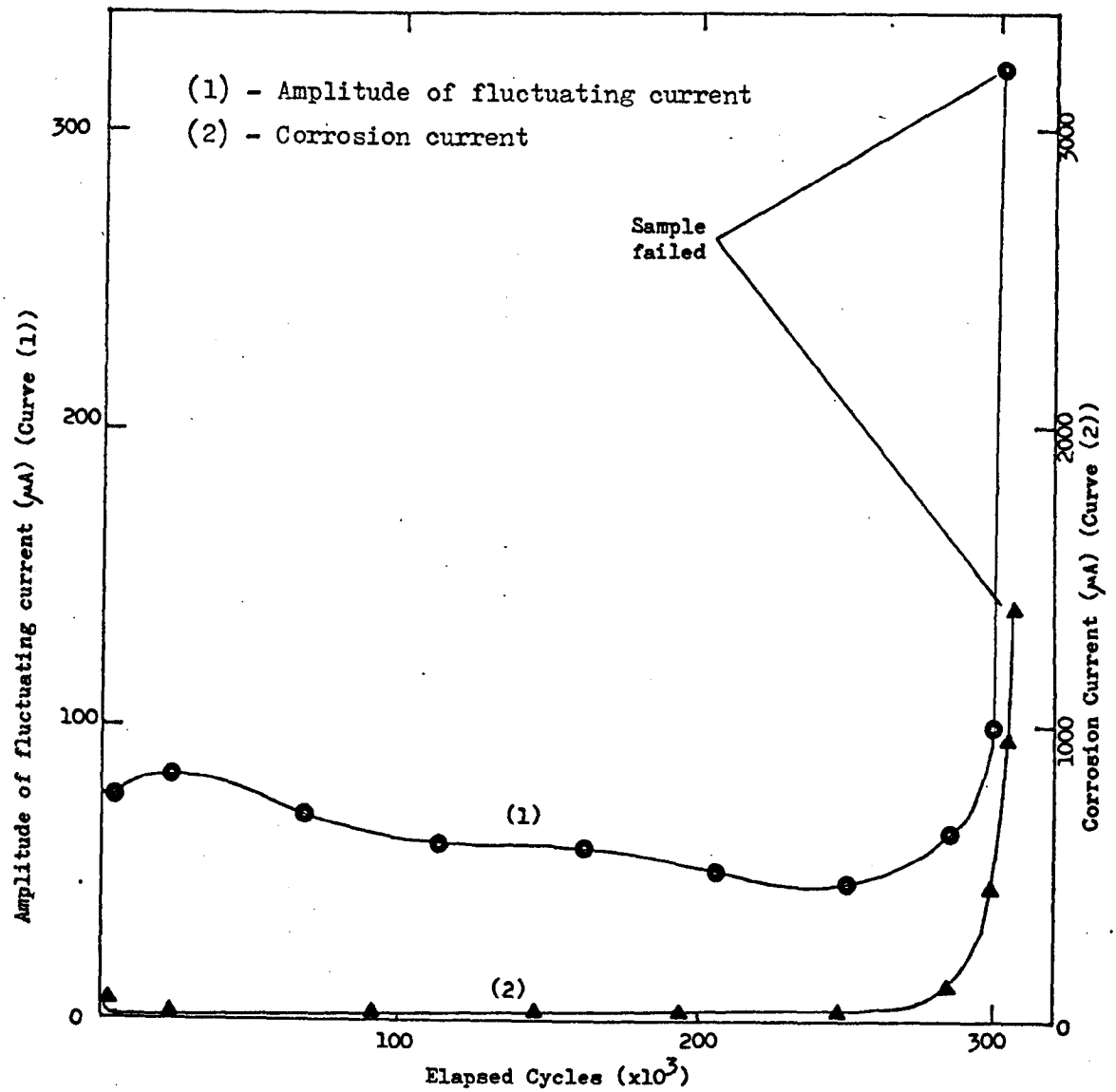

FIGURE 4.23 Variation of the amplitude of fluctuating current and corrosion current with elapsed cycles during a fatigue test. (Stress $\pm$ 320 MN m^{-2}) in 0.5M sodium chloride solution with a constant applied potential of 0 mV vs SCE.

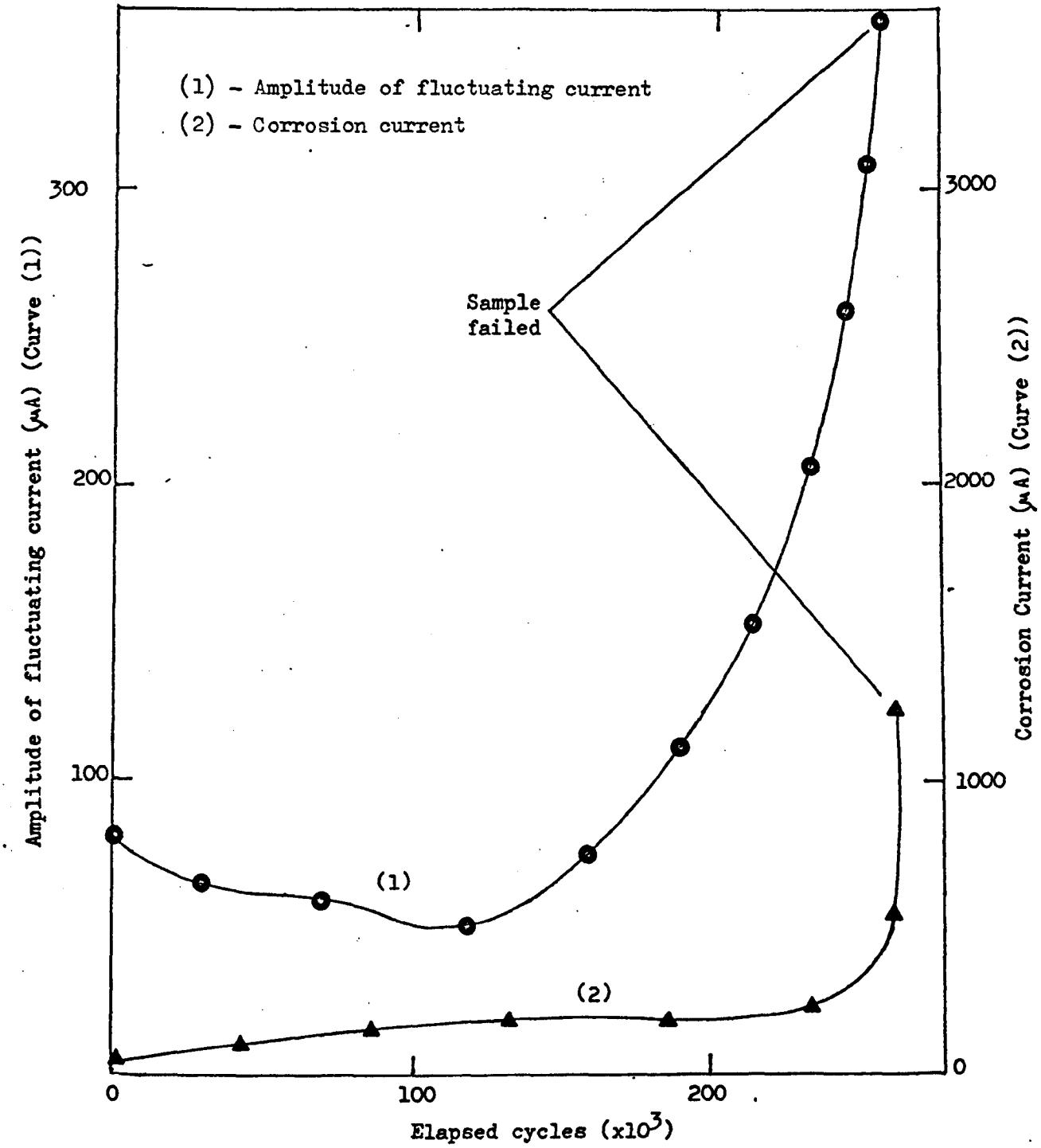

FIGURE 4.24 Variation of the amplitude of fluctuating current and corrosion current with elapsed cycles during a fatigue test. (Stress $\pm$ 320 MN m^{-2}) in 0.5M sodium chloride solution with a constant applied potential of 0 mV vs SCE.

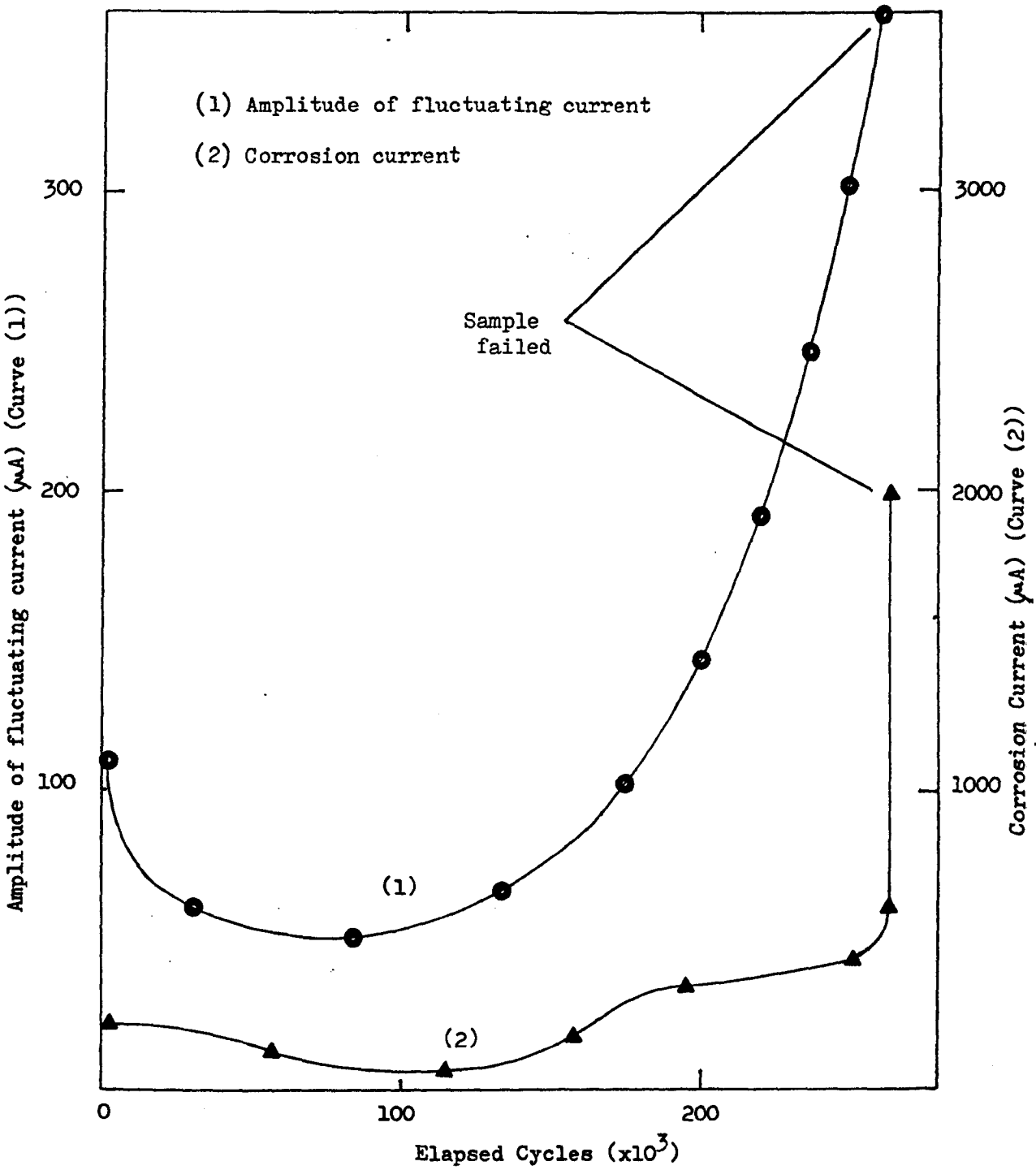

FIGURE 4.25 Variation of the amplitude of fluctuating current and corrosion current with elapsed cycles during a fatigue test. (Stress $\pm$ 320 MN m^{-2}) in 0.5M sodium chloride solution with a constant applied potential of + 200 mV vs SCE.

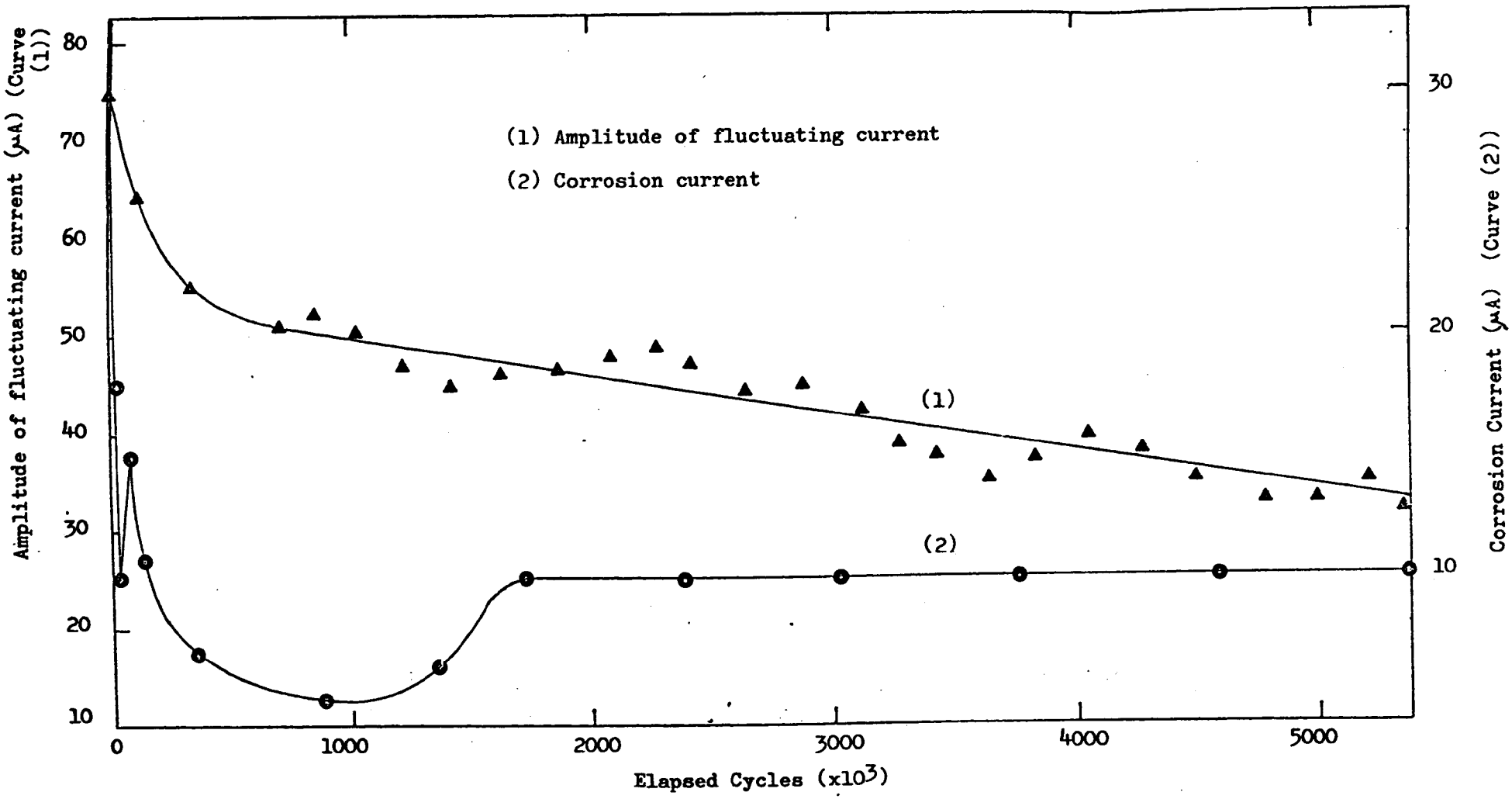

FIGURE 4.26 Variation of the amplitude of fluctuating current and corrosion current with elapsed cycles during a fatigue test. (Stress $\pm$ 320 MN m^{-2}) in 0.2M sodium sulphate solution with a constant applied potential of 0 mV vs SCE

FIGURE 4.27 Variation of the amplitude of fluctuating current and corrosion current with elapsed cycles during a fatigue test (Stress $\pm$ 320 MN m^{-2}) in 0.2M sodium sulphate solution with a constant applied potential of + 1400 mV vs SCE

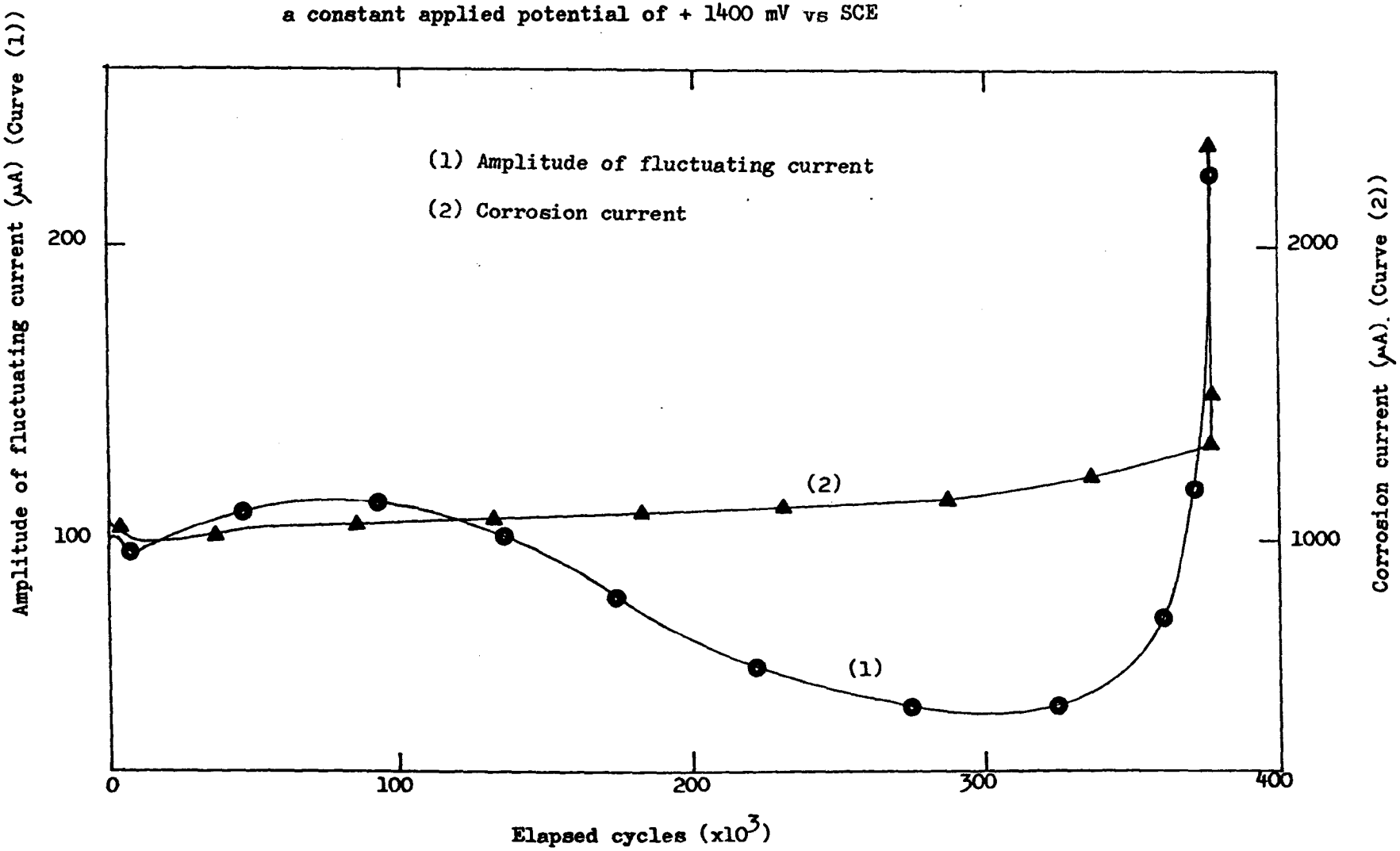

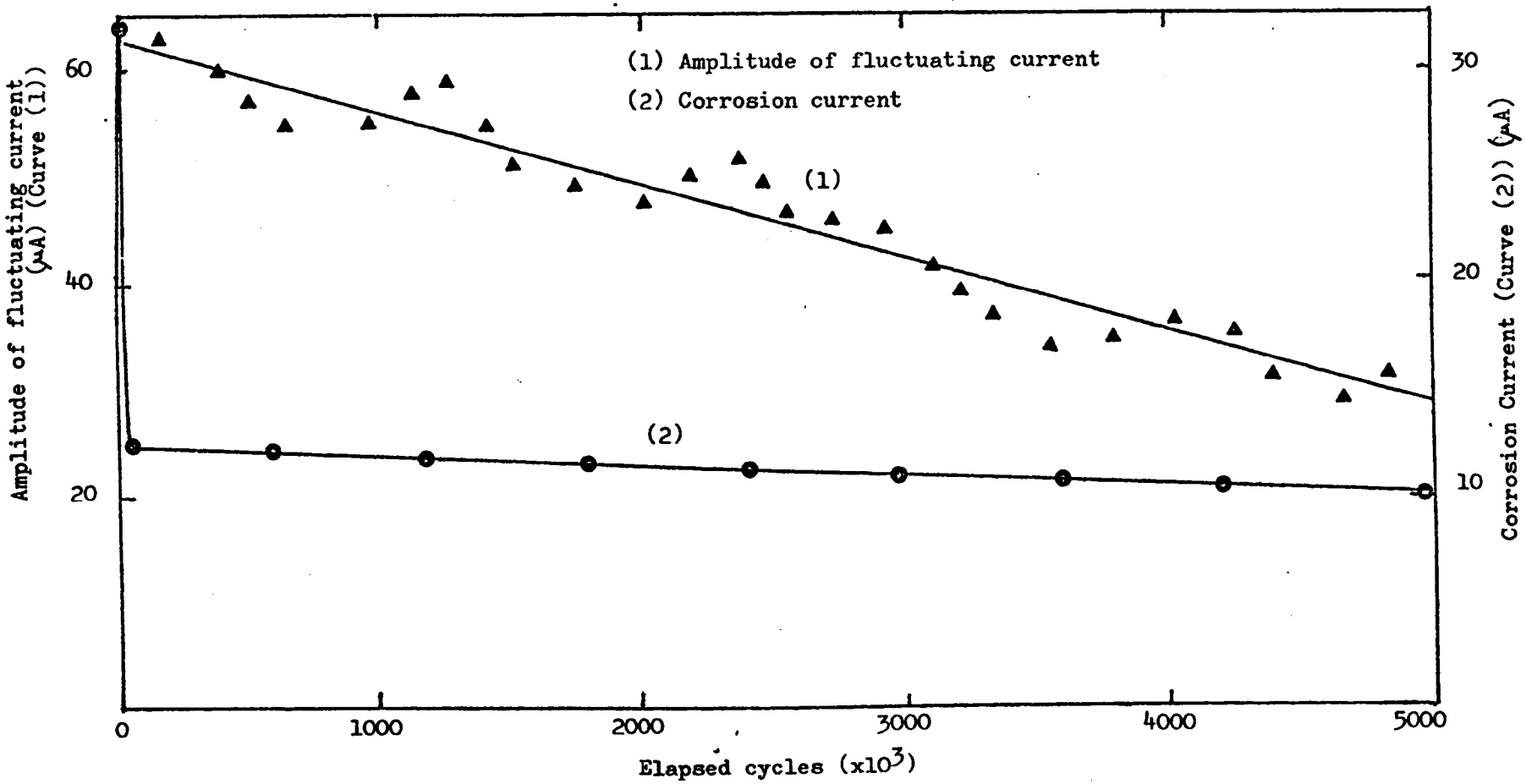

FIGURE 4.28 Variation of the amplitude of fluctuating current and corrosion current with elapsed cycles during a fatigue test. (Stress $\pm$ 320 MN m^{-2}) in 0.1M Potassium Dichromate solution with a constant applied potential of 0 mV vs SCE

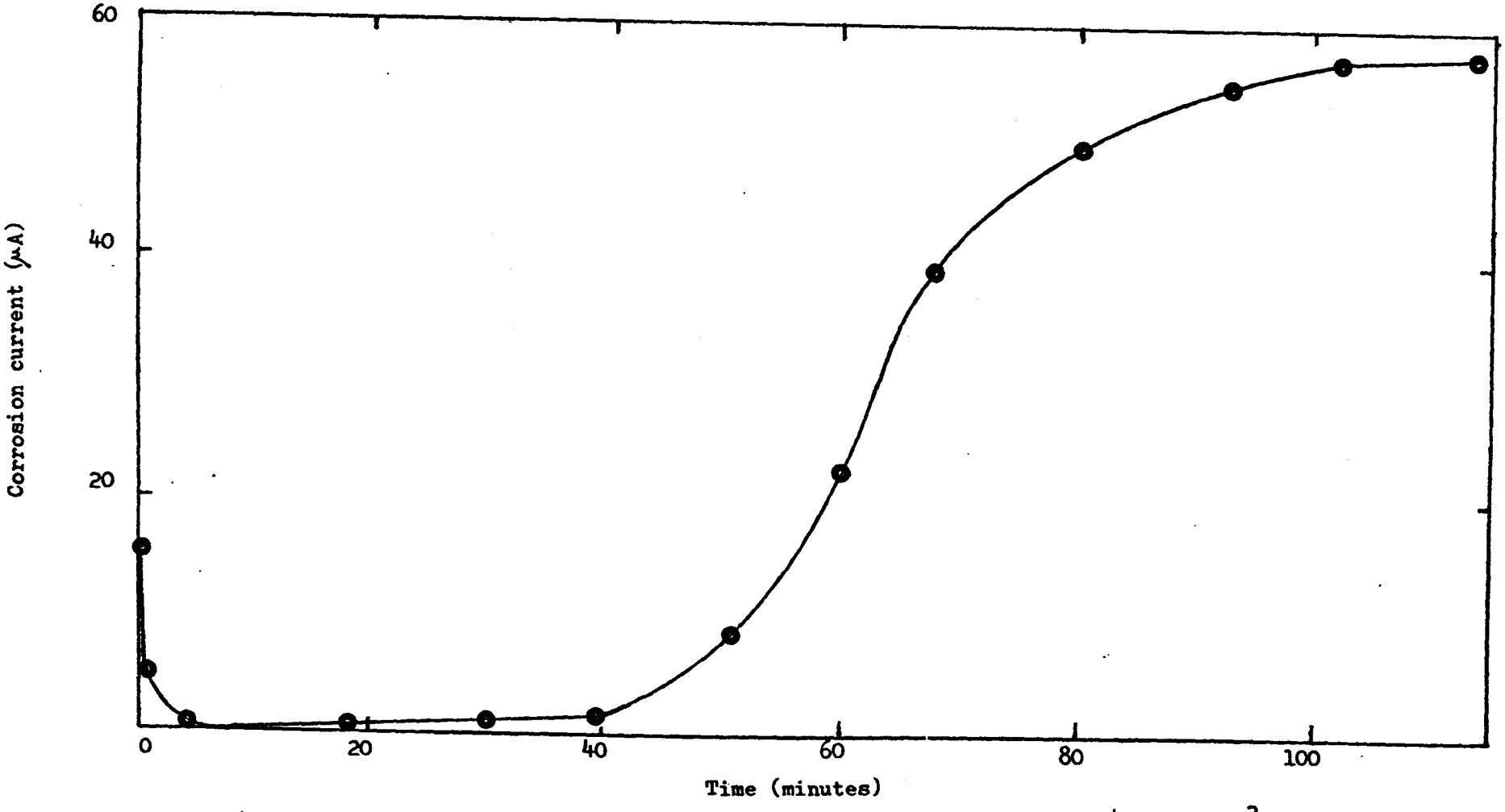

FIGURE 4.29 Variation of corrosion current with time during a fatigue test ($\pm$ 250 MN m^{-2}) in 0.5M sodium chloride solution with a constant applied potential equal to the rest potential of the static test-piece (-155 mV vs SCE)

FIGURE 4.30 Variation of corrosion current with time during a fatigue test ($\pm$ 250 MN m^{-2}) in 0.5M sodium chloride solution with a constant applied potential equal to the rest potential of the static test-piece (-155 mV vs SCE).

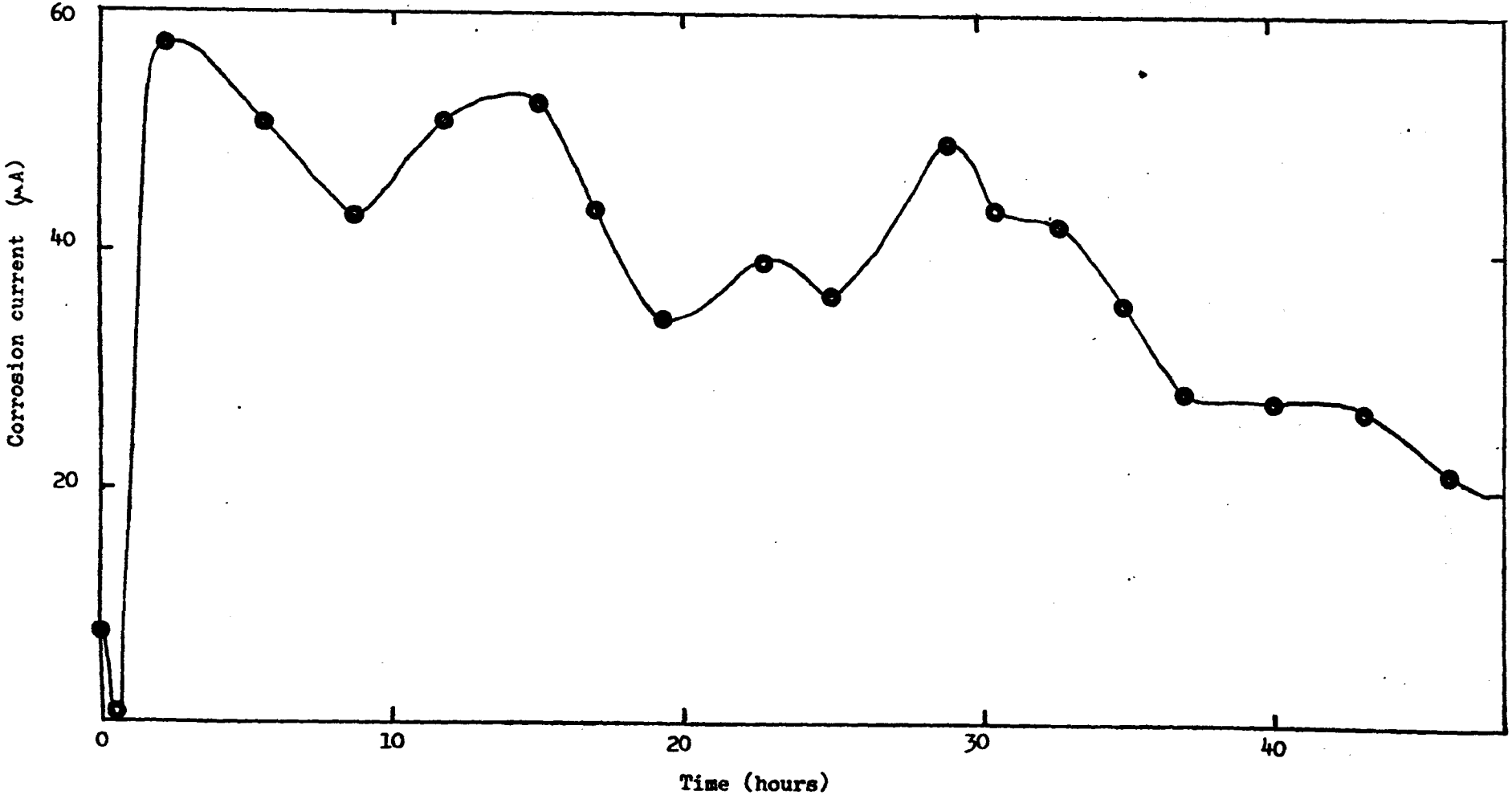

X20

Figure 4.31 Scanning Electron Fractograph of a pre-pitted rotating-bending fatigue test-piece showing the form of pitting attack produced by the pre-treatment.

X450

Figure 4.32 Scanning Electron Micrograph of a pit on the side of a pre-pitted rotating-bending fatigue test-piece.

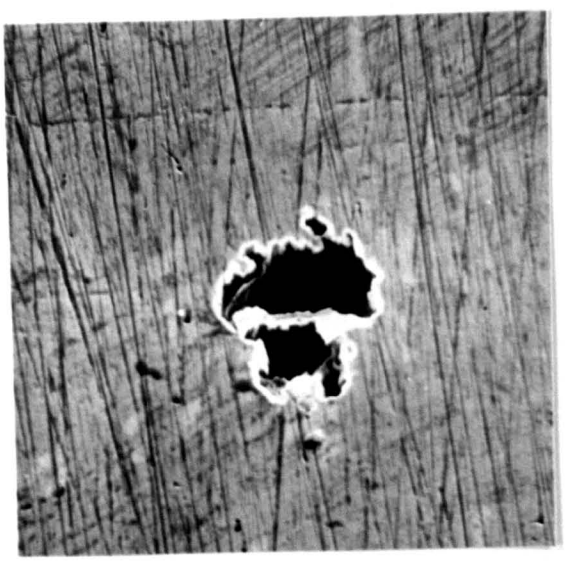

X160

Figure 4.33 Scanning Electron Micrograph of a pit on the side of a pre-pitted rotating-bending fatigue test-piece.

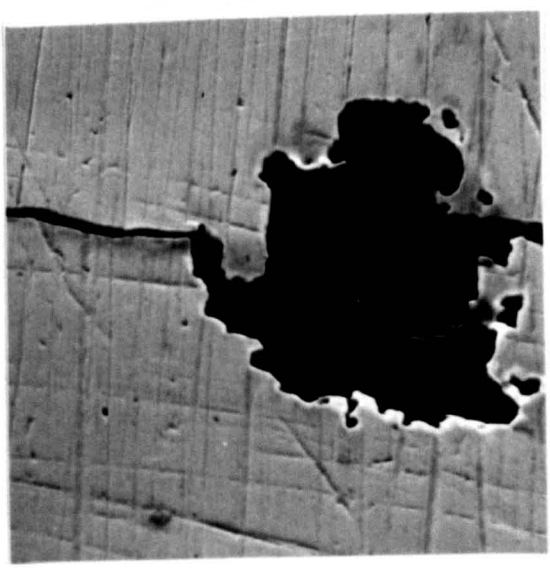

X200

Figure 4.34 Scanning Electron Micrograph of a pit on the side of a pre-pitted rotating-bending fatigue test-piece with a fatigue crack emanating from it (fatigue test at $\pm$ 300 MN m^{-2} in air, sample failed after 4,000 stress cycles).

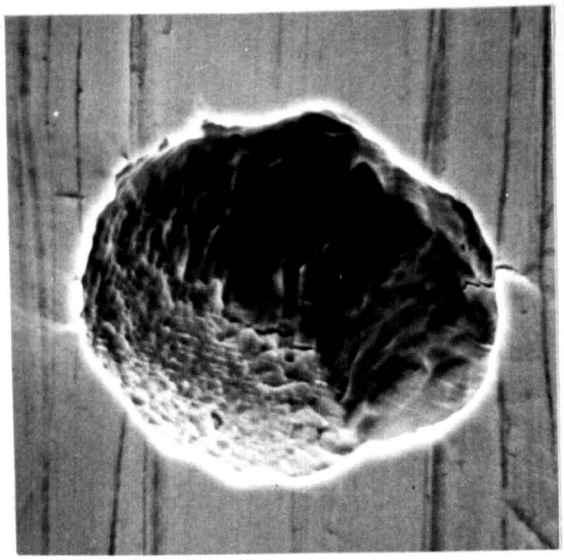

X200

Figure 4.35 Scanning Electron Micrograph of a pit on the side of a pre-pitted rotating-bending fatigue test-piece after the original surface covering has been removed.

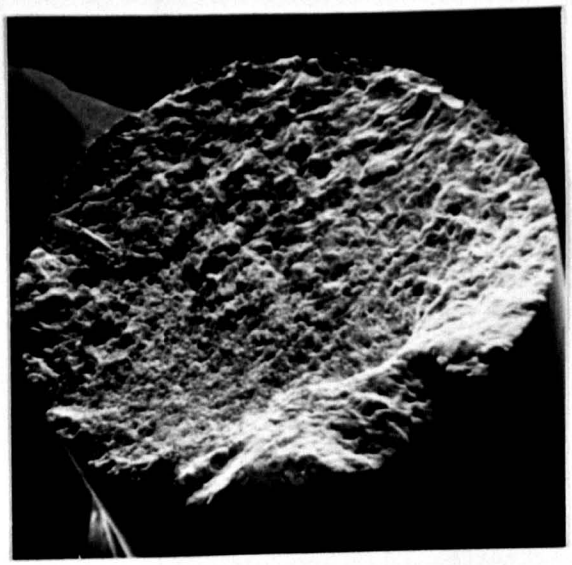

X20

Figure 4.36 Scanning Electron Fractograph of a pre-pitted rotating-bending fatigue test-piece showing the irregular nature of the fracture (fatigue test at $\pm$ 300 MN m^{-2} in air sample failed after 2000 stress cycles)

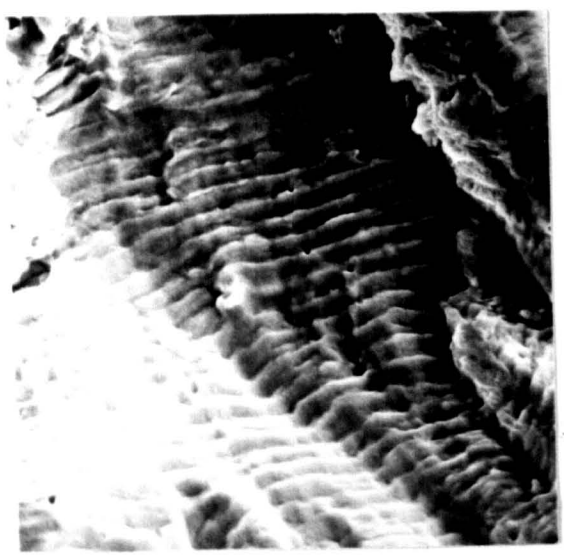

X6K

Figure 4.37 Scanning Electron Fractograph of a pre-pitted rotating-bending fatigue test-piece showing ductile fatigue striations (fatigue test at $\pm$ 300 MN m^{-2} in air. Sample failed after 4000 stress cycles).

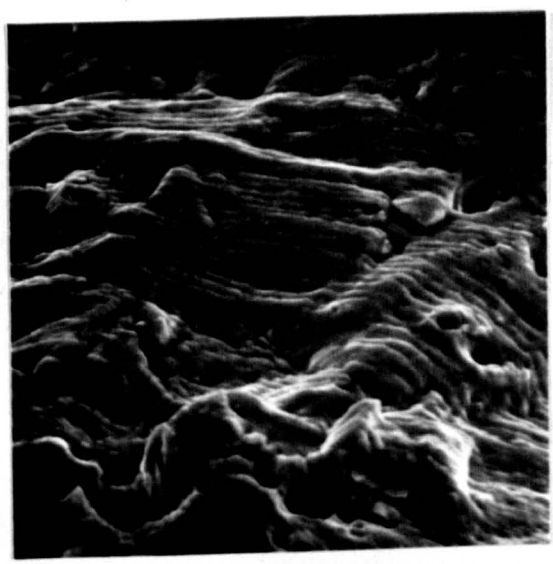

X2.2K

Figure 4.38 Scanning Electron Fractograph of a pre-pitted rotating-bending fatigue test-piece showing ductile fatigue striations (fatigue test at $\pm$ 300 MN m^{-2} in air. Sample failed after 2000 stress cycles).

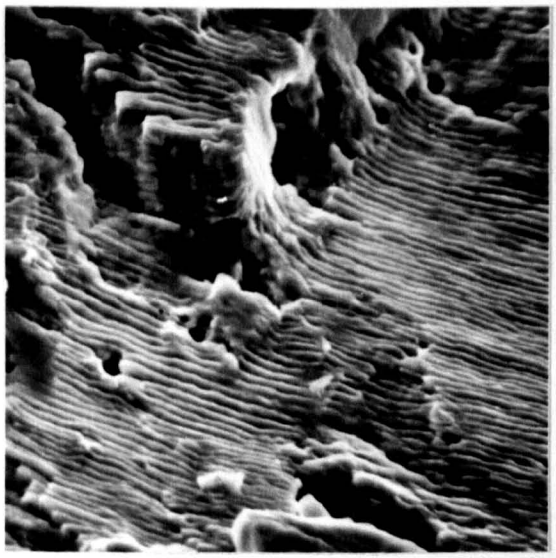

X2.4K

Figure 4.39 Scanning Electron Fractograph of a pre-pitted rotating-bending fatigue test-piece showing ductile fatigue striations (fatigue test at $\pm$ 300 MN m^{-2} in air. Sample failed after 8000 stress cycles).

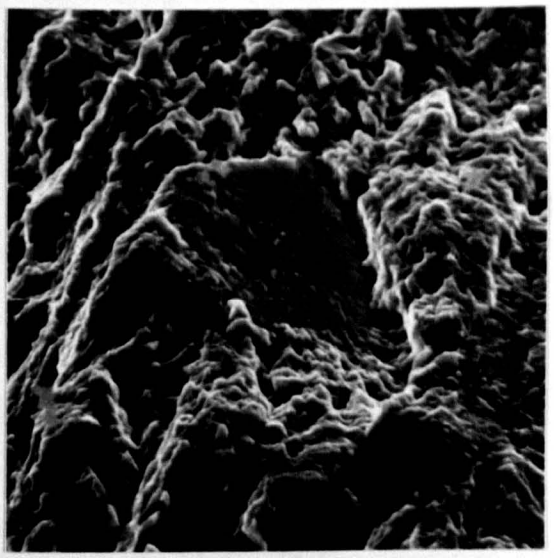

X2.3K

Figure 4.40 Scanning Electron Fractograph of a pre-pitted rotating-bending fatigue test-piece showing a flat on the fracture face. (Fatigue test at $\pm$ 300 MN m^{-2} in air. Sample failed after 4000 stress cycles).

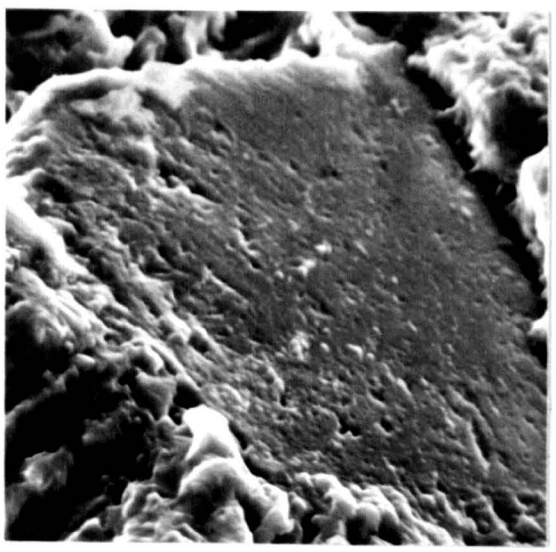

X5.7K

Figure 4.41

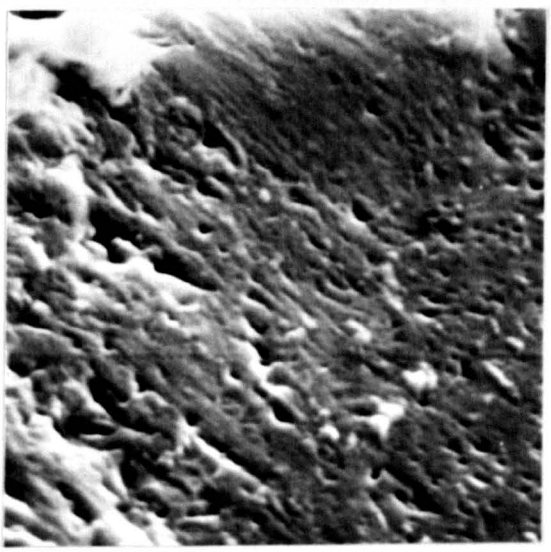

X11.5K

Figure 4.42

Scanning Electron Fractographs of a pre-pitted rotating-bending fatigue test-piece, showing a flat on the fracture face. (Fatigue test at $\pm$ 300 MN m^{-2} in air. Sample failed after 4000 stress cycles).

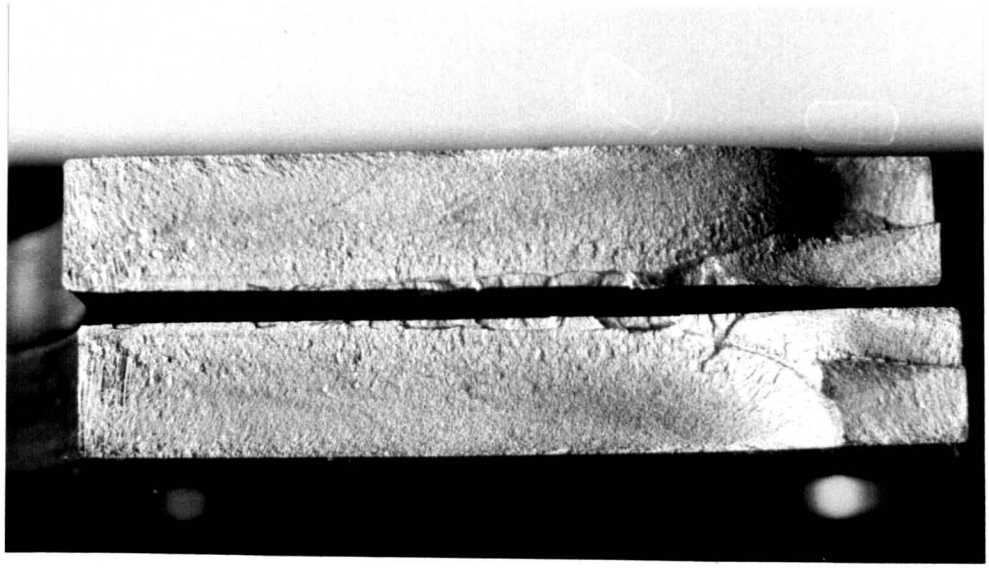

x ~4.5

Figure 4.43 Optical Fractograph of a reverse bend fatigue test-piece. (Fatigue test at $\pm$ 350 MN m^{-2} in 0.5M sodium chloride solution. Sample failed after 3 x 10^5 stress cycles).

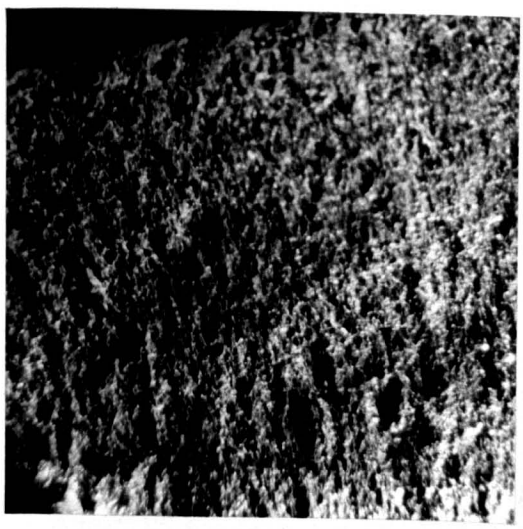

x ~20

x ~10

Figures 4.44 and 4.45 Optical Fractographs of a reverse bend fatigue test-piece showing "River Markings" radiating from the point of initiation. (Fatigue test at $\pm$ 350 MN m^{-2} in 0.5M sodium chloride solution. Sample failed after 3 x 10^5 stress cycles).

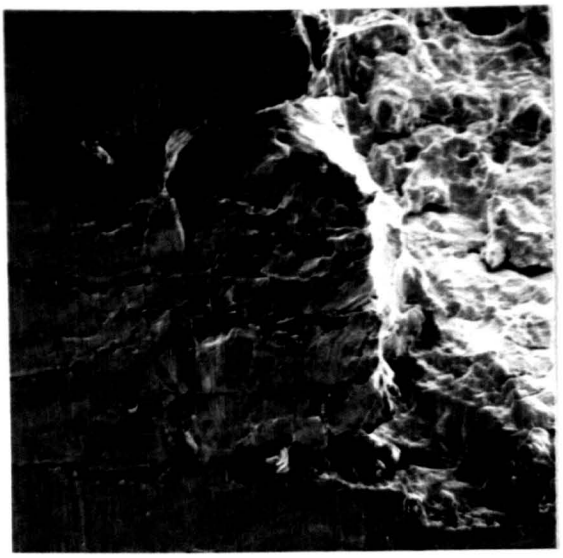

X220

Figure 4.46 Scanning Electron Fractograph of a reverse-bend fatigue test-piece showing secondary cracking on the side. (Fatigue test at $\pm$ 450 MN m^{-2} in air. Sample failed after 6 x 10^4 stress cycles).

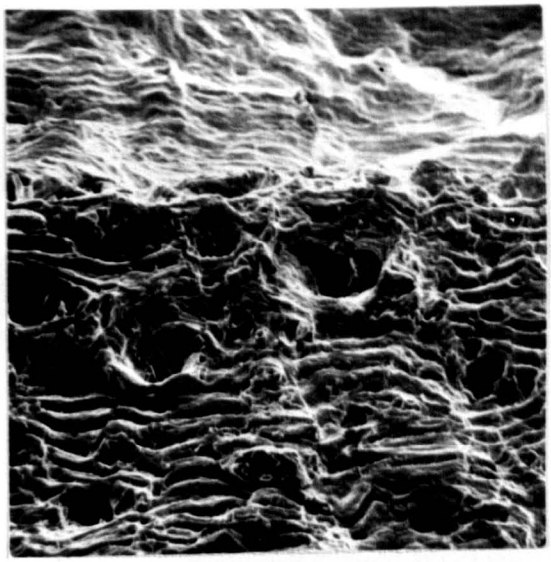

X550

Figure 4.47 Scanning Electron Fractograph of a reverse-bend fatigue test-piece showing the region of final fracture. (Fatigue test at $\pm$ 370 MN m^{-2} in air. Sample failed after 5 x 10^5 stress cycles).

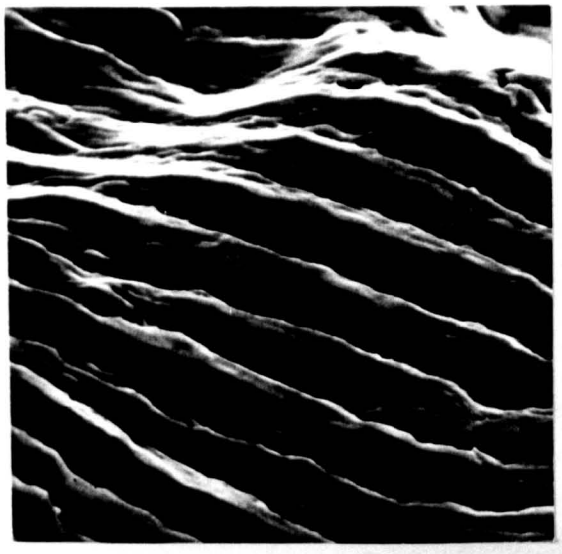

X5.5K

Figure 4.48 Scanning Electron Fractograph of a reverse-bend fatigue test-piece showing the ductile fatigue striations. (Fatigue test at $\pm$ 370 MN m^{-2} in air. Sample failed after 5 x 10^5 stress cycles).

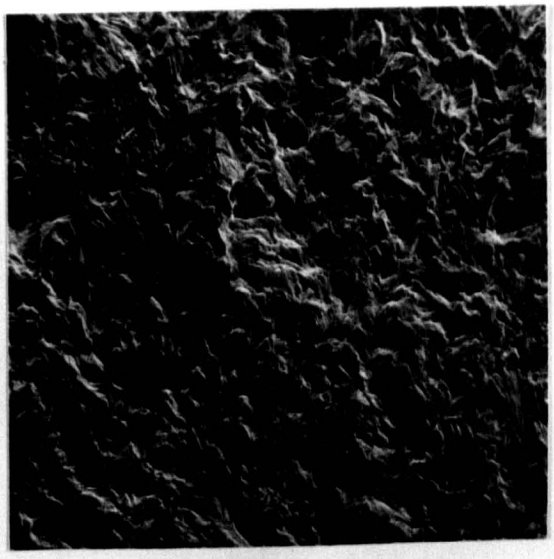

X100

Figure 4.49 Scanning Electron Fractograph of a reverse-bend fatigue test-piece showing the rough nature of the fracture. (Fatigue test at $\pm$ 175 MN m^{-2} in 0.5M sodium chloride solution. Sample failed after 3.4 x 10^6 stress cycles).

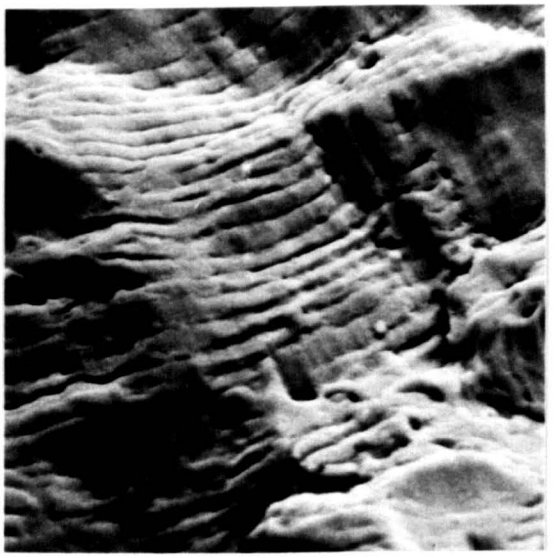

X7K

Figure 4.50 Scanning Electron Fractograph of a reverse-bend fatigue test-piece showing fatigue striations masked by an oxide film. (Fatigue test at $\pm$ 270 MN m^{-2} in 0.5M sodium chloride solution. Sample failed after 4 x 10^7 stress cycles).

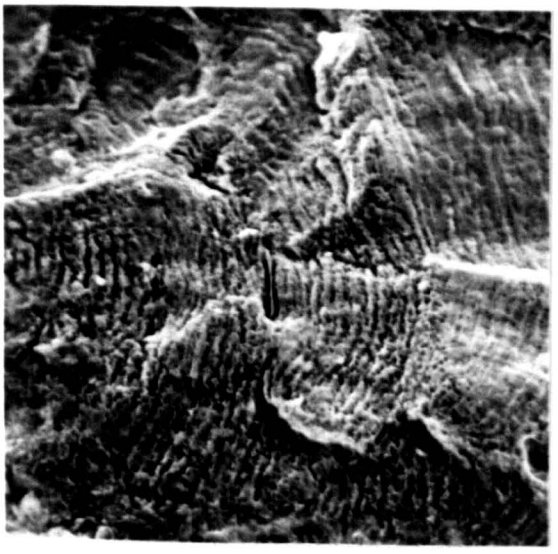

X3K

Figure 4.51

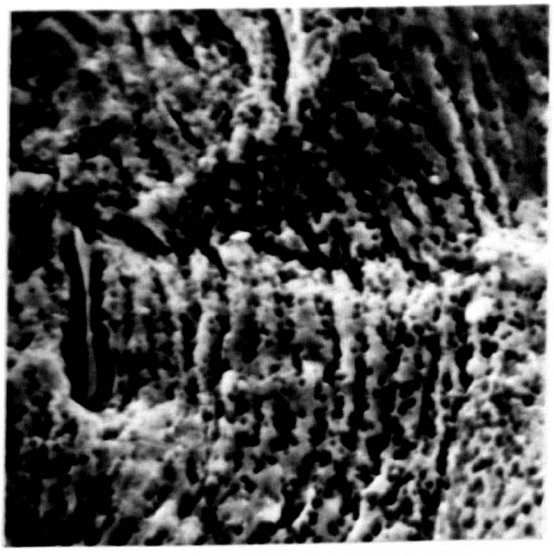

X7K

Figure 4.52

Scanning Electron Fractographs of a reverse-bend fatigue test-piece showing fatigue striations after the oxide film has been stripped off. (Fatigue test at $\pm$ 270 MN m^{-2} in 0.5M sodium chloride solution. Sample failed after 4 x 10^7 stress cycles).

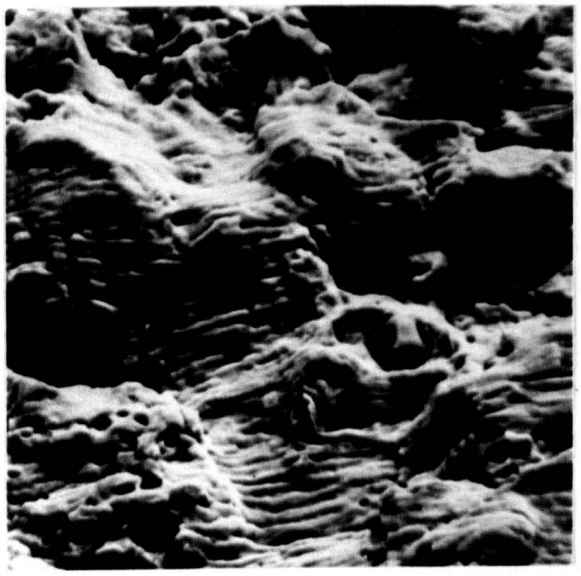

X1K

Figure 4.53 Scanning Electron Fractograph of a reverse-bend fatigue test-piece showing the presence of an angular non-metallic inclusion in the fracture piece.
(Fatigue test at $\pm$ 270 MN m^{-2} in 0.5M sodium chloride solution.
Sample failed after 5.4×10^7 stress cycles).

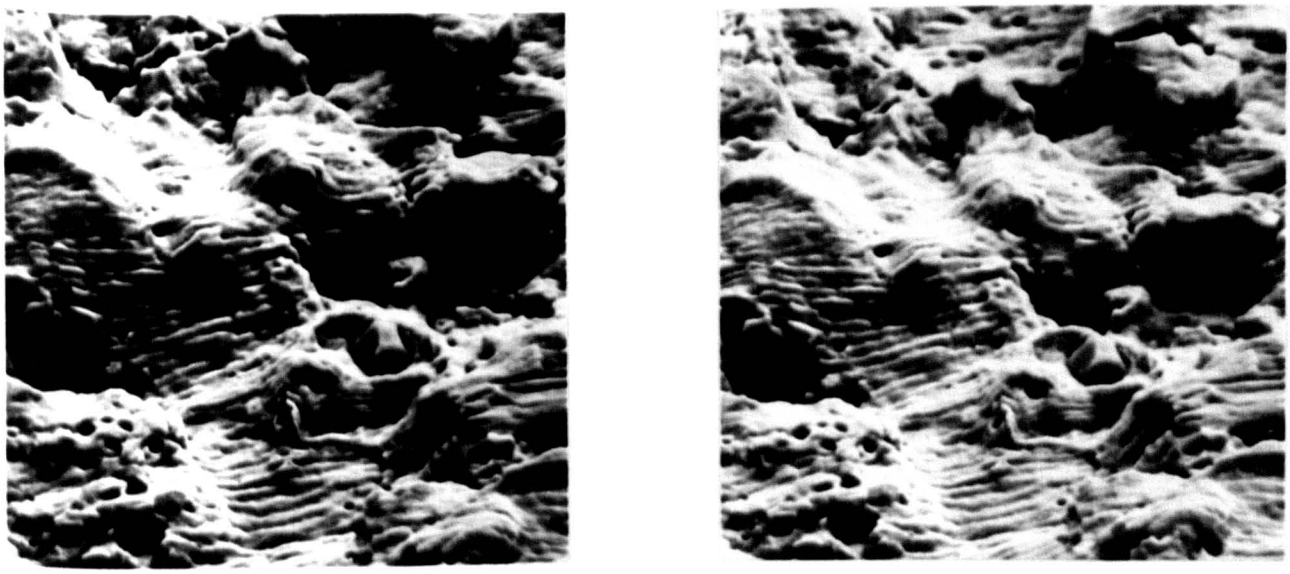

X1K

Figure 4.54 Stereo-pair of the same field of view as in figure 4.53.

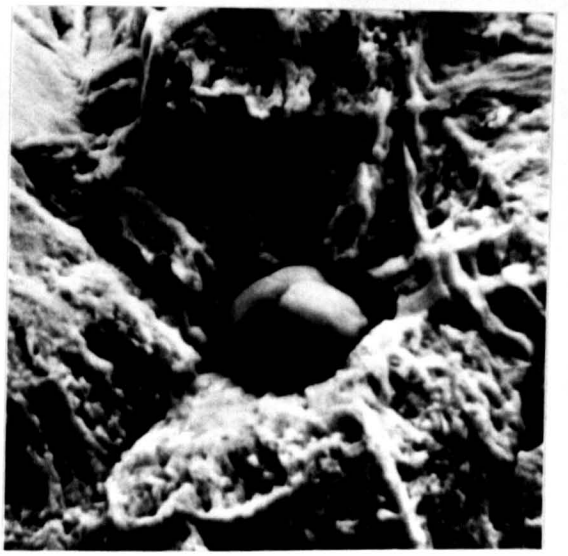

X2K

Figure 4.55 Scanning Electron Fractograph of a reverse-bend fatigue test-piece showing the presence of a spheroidal non-metallic inclusion in the fracture piece.
(Fatigue test at $\pm$ 300 MN m^{-2} in 0.5M sodium chloride solution. Sample failed after 1 x 10^7 stress cycles).

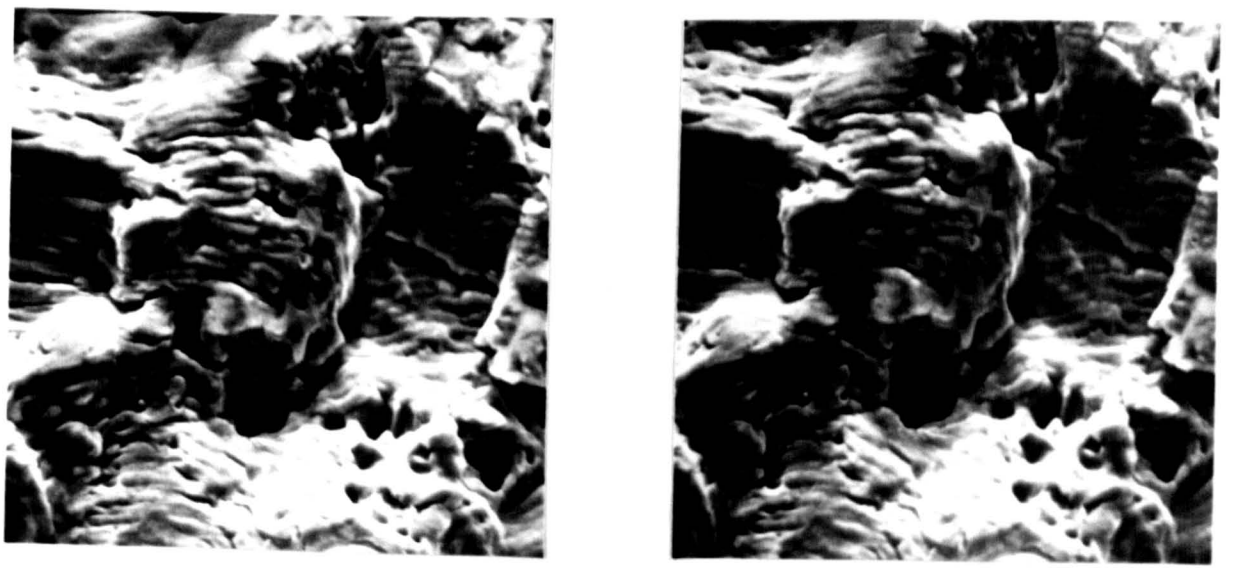

X1K

Figure 4.56 Scanning Electron stereo-pair of the fracture face of a reverse-bend fatigue test-piece exhibiting ductile striations.
(Fatigue test at $\pm$ 300 MN m^{-2} in 0.5M sodium chloride solution. Sample failed after 1 x 10^7 stress cycles).

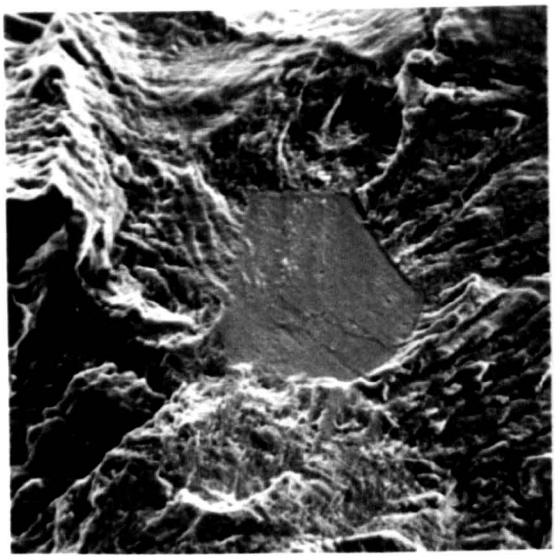

X2K

Figure 4.57

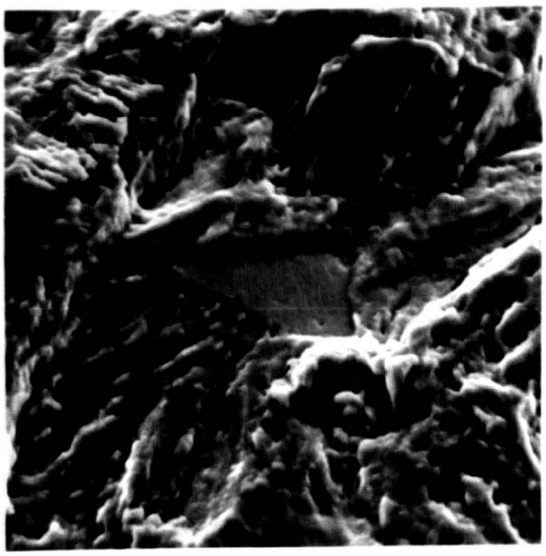

X2K

Figure 4.58

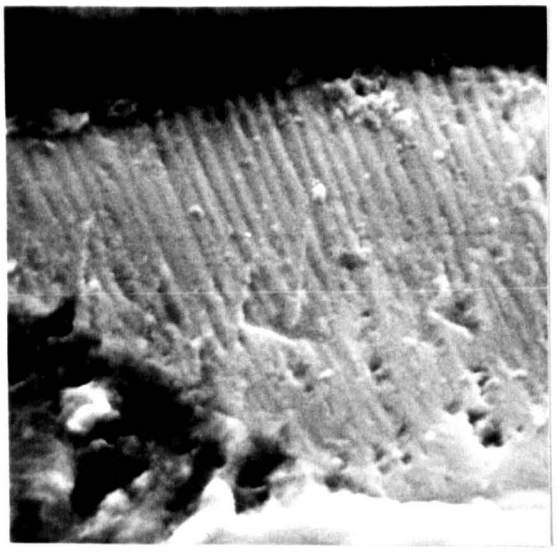

X5K

Figure 4.59

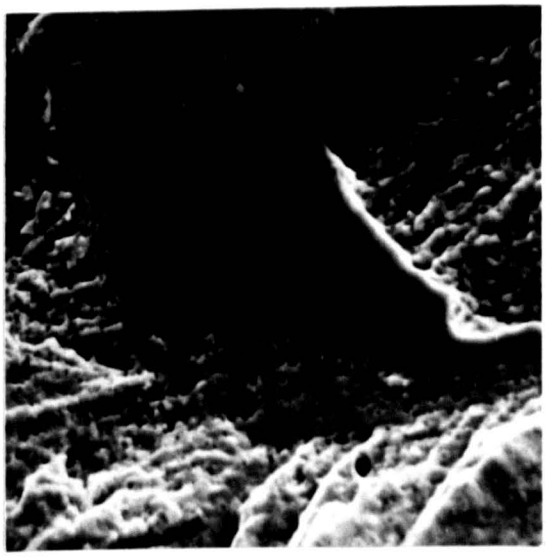

X2K

Figure 4.60

Figures 4.57, 4.58, 4.59, 4.60 Scanning Electron Fractograph of a reverse-bend fatigue test-piece showing the presence of "flats" on the fracture-face. Note the presence of linear markings on figure 4.59.
(Fatigue test at $\pm$ 270 MN m^{-2} in 0.5M sodium chloride solution. Sample failed after 4 x 10^7 stress cycles).

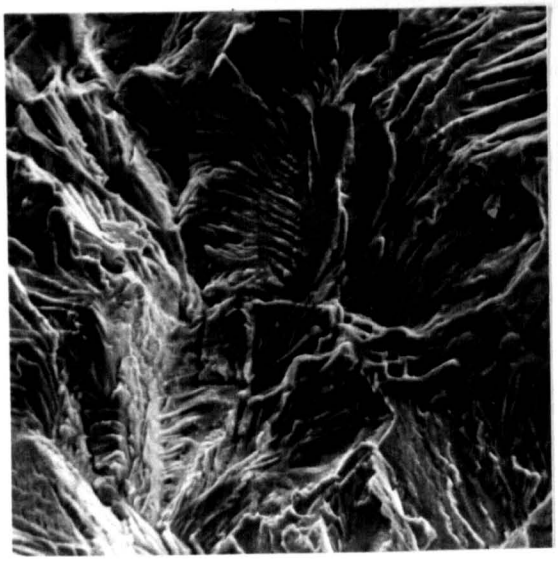

X2K

Figure 4.61 Scanning Electron Fractograph of a reverse-bend fatigue test-piece showing the presence of a "fir tree" effect characteristic of stress corrosion cracking. (fatigue test at ± 270 MN m^{-2} in 0.5M sodium chloride solution. Sample failed after 4 x 10^7 stress cycles).

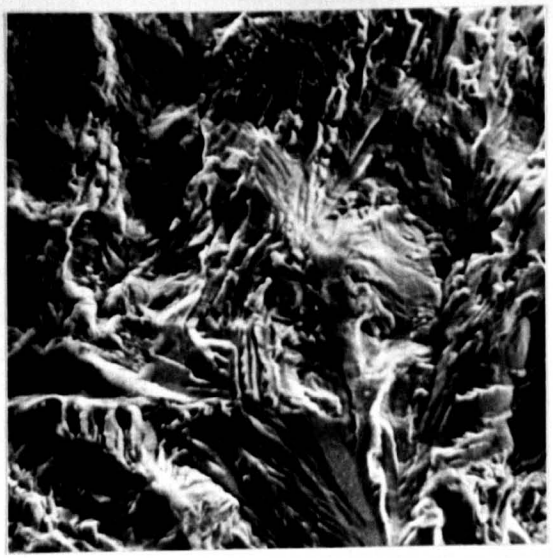

X2K

Figure 4.62 Scanning Electron Fractograph of a reverse-bend fatigue test-piece showing the presence of a "fir tree" effect characteristic of stress corrosion cracking. (fatigue test at ± 300 MN m^{-2} in 0.5M sodium chloride solution. Sample failed after 1 x 10^7 stress cycles).

5.5K

Figure 4.63 Scanning Electron Fractograph of a reverse-bend fatigue test-piece showing step-like features near the initiation point. (Fatigue test at ± 270 MN m^{-2} in 0.5M sodium chloride solution. Sample failed after 5.4 x 10^7 stress cycles).

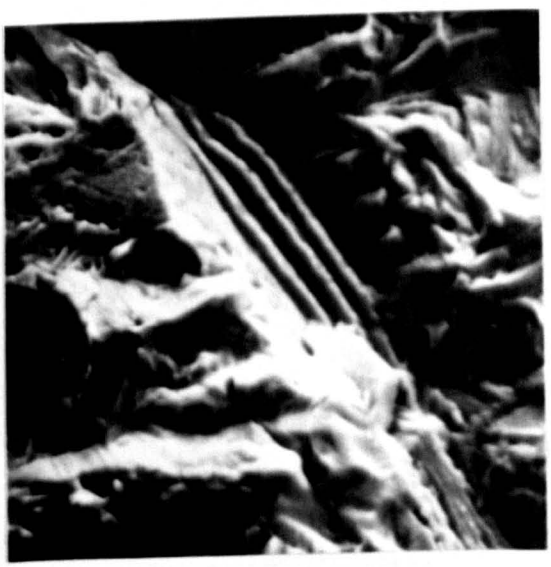

X2K

Figure 4.64 Scanning Electron Fractograph of a reverse-bend fatigue test-piece showing step-like features near the initiation point. (Fatigue test at ± 270 MN m^{-2} in 0.5M sodium chloride solution. Sample failed after 4 x 10^7 stress cycles).

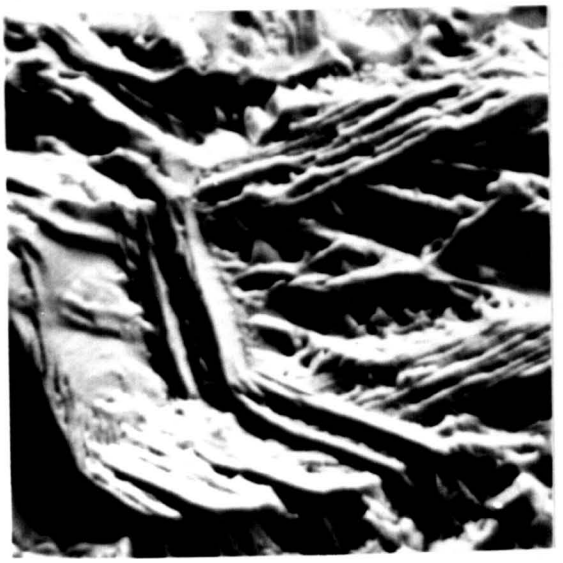

X2K

Figure 4.65 Scanning Electron Fractograph of a reverse-bend fatigue test-piece showing selective corrosion attack near the initiation point.
(Fatigue test at $\pm$ 300 MN m^{-2} Sodium Chloride. Sample failed after 2×10^6 stress cycles).

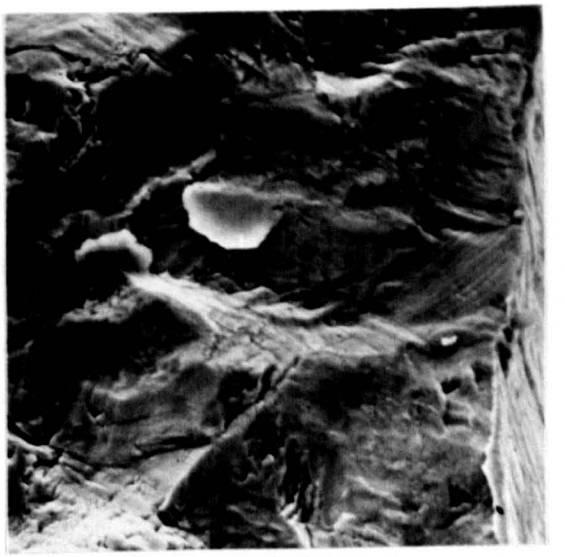

X1K

Figure 4.66 Scanning Electron Fractograph of a reverse-bend fatigue test-piece showing selective corrosion attack near the initiation point.
(Fatigue test at $\pm$ 300 MN m^{-2} Sodium Chloride. Sample failed after 4×10^6 stress cycles).

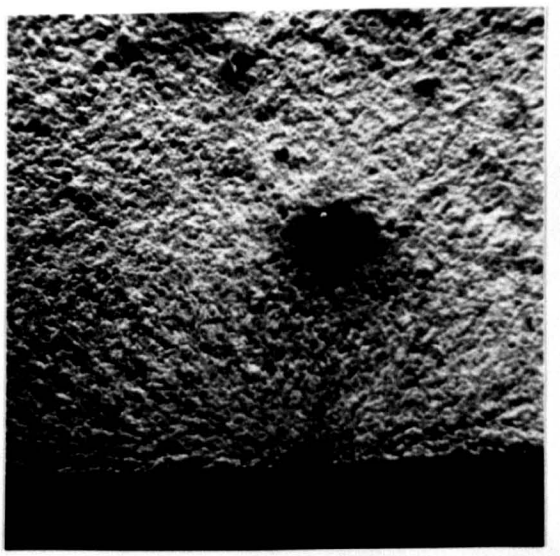

X20

Figure 4.67 Scanning Electron Fractograph of a reverse-bend fatigue test-piece showing the crack initiation point with an associated pit.
(Fatigue test at $\pm$ 350 MN m^{-2} in 0.2M Sodium Sulphate. Sample failed after 2.5×10^4 stress cycles).

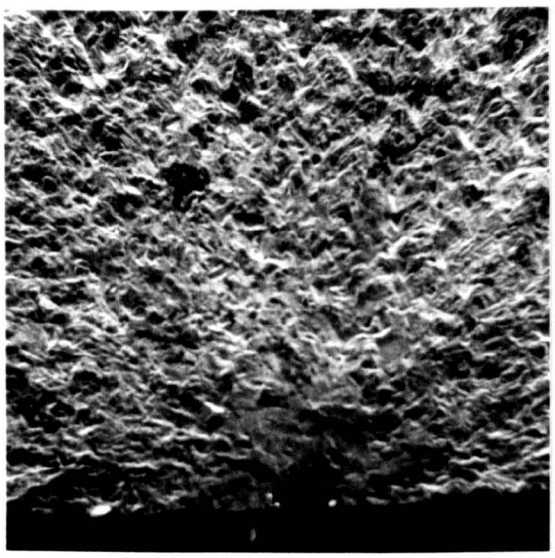

X100

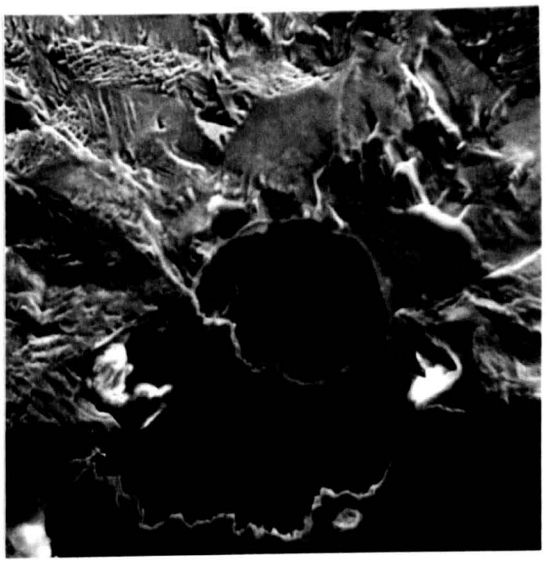

X500

Figures 4.68 and 4.69 Scanning Electron Fractographs of a reverse-bend fatigue test-piece showing the crack initiation point with an associated pit. (Fatigue test at $\pm$ 310 MN m^{-2} in 0.5M Sodium Chloride solution. Sample failed after 3 x 10^6 stress cycles).

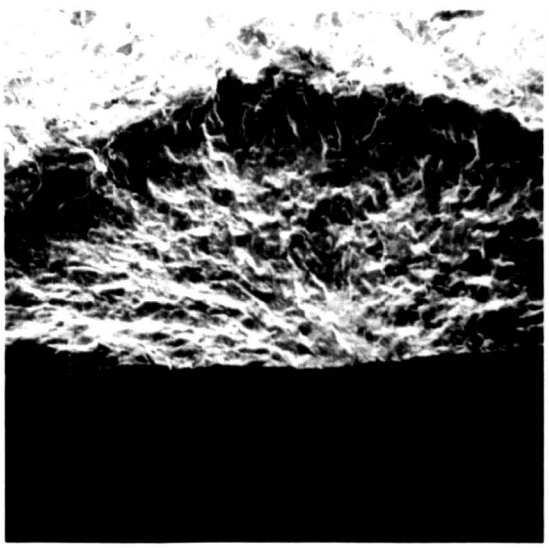

X20

Figure 4.70 Scanning Electron Fractograph of a reverse-bend fatigue test-piece showing the crack initiation point.
(Fatigue test at $\pm$310 MN m^{-2} in 0.5M Sodium Chloride solution. Sample failed after 8 x 10^5 stress cycles).

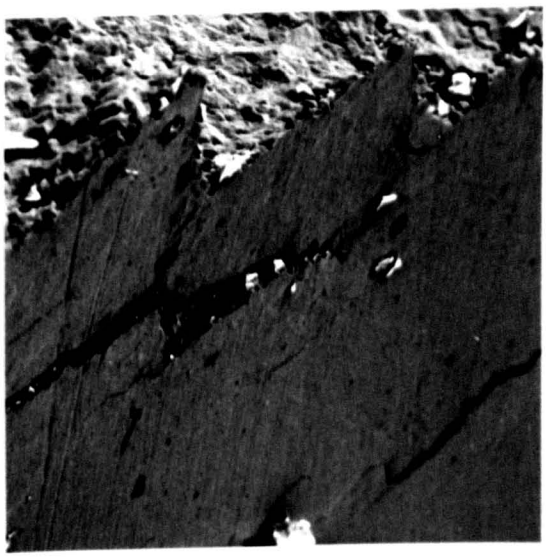

X140

Figure 4.71 Scanning Electron Fractograph of a reverse-bend fatigue test-piece showing secondary cracking on the side.
(Fatigue test at $\pm$ 300 MN m^{-2} in 0.5M Sodium Chloride solution. Sample failed after 1 x 10^7 stress cycles).

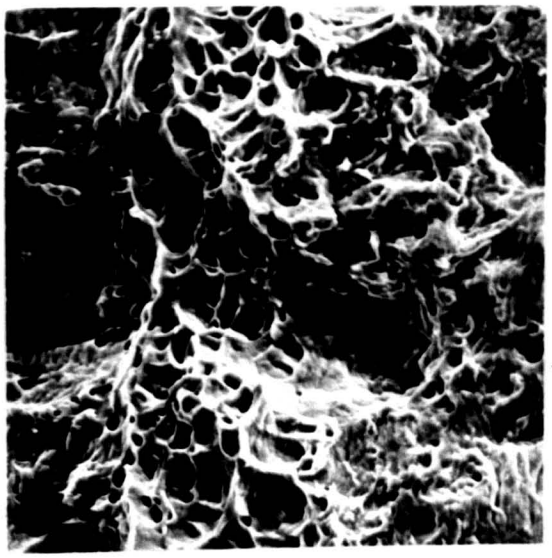

X1K

Figure 4.72 Scanning Electron Fractograph of a reverse-bend fatigue test-piece showing the region of final fracture.
(Fatigue test at $\pm$ 300 MN m^{-2} in 0.5M Sodium Chloride solution. Sample failed after 1 x 10^7 stress cycles).

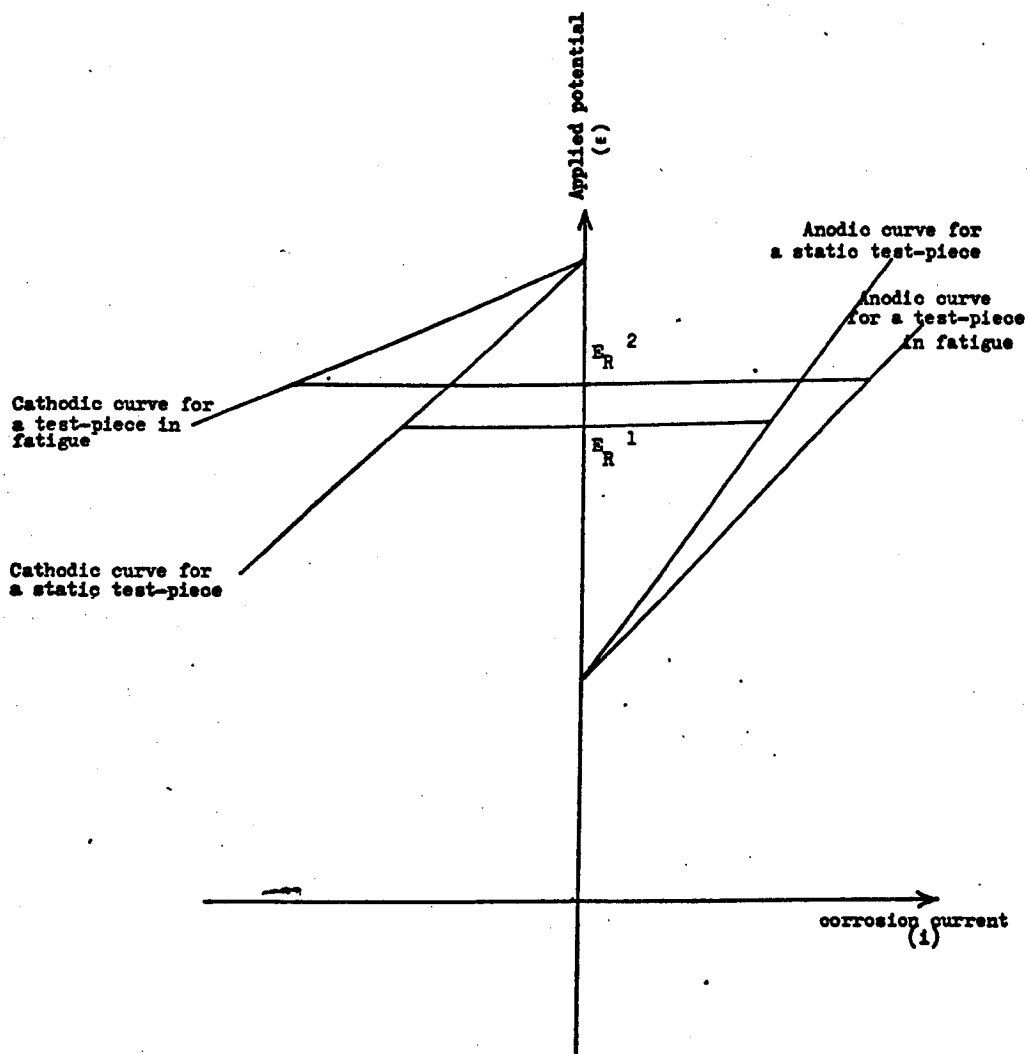

E_R 1 - rest potential for a static test-piece

E_R 2 - rest potential for a test-piece in fatigue

Figure 5.1 Effect of fatigue on the anodic and cathodic reactions and the resultant effect on the rest potential.

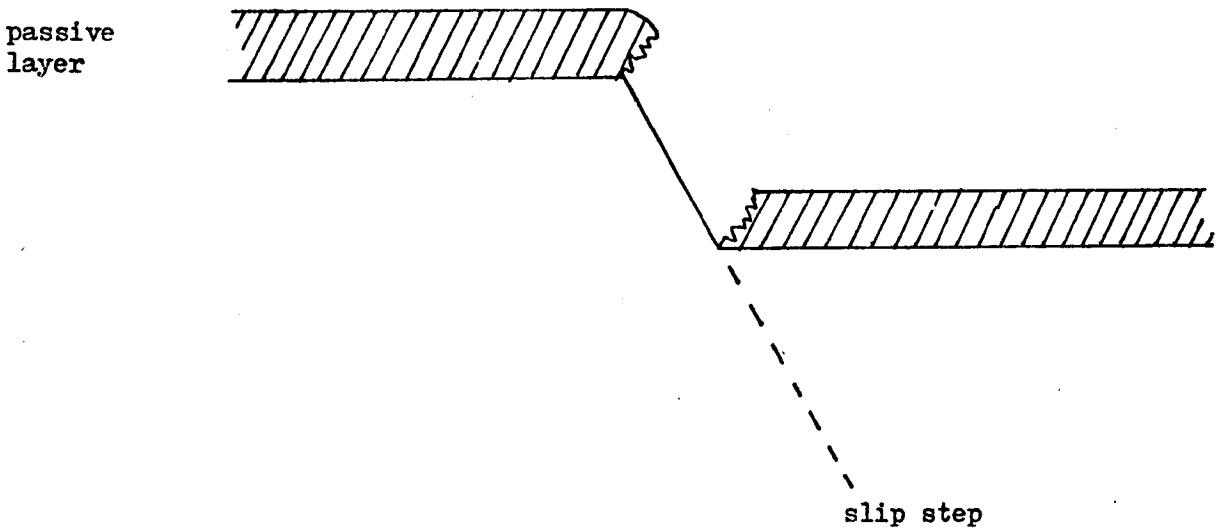

(a) large slip step piercing the passive layer

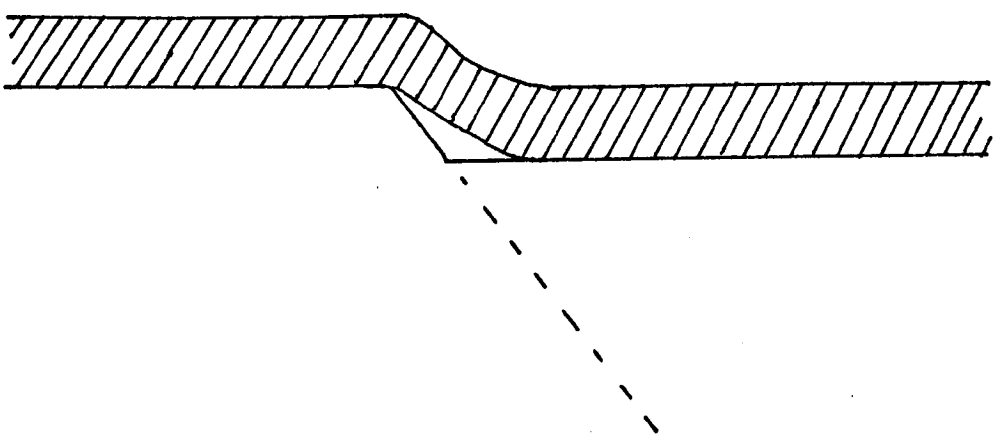

(b) small slip step insufficient to pierce the passive layer

Figure 5.2 Effect of slip step height on the rupture of the passive layer.

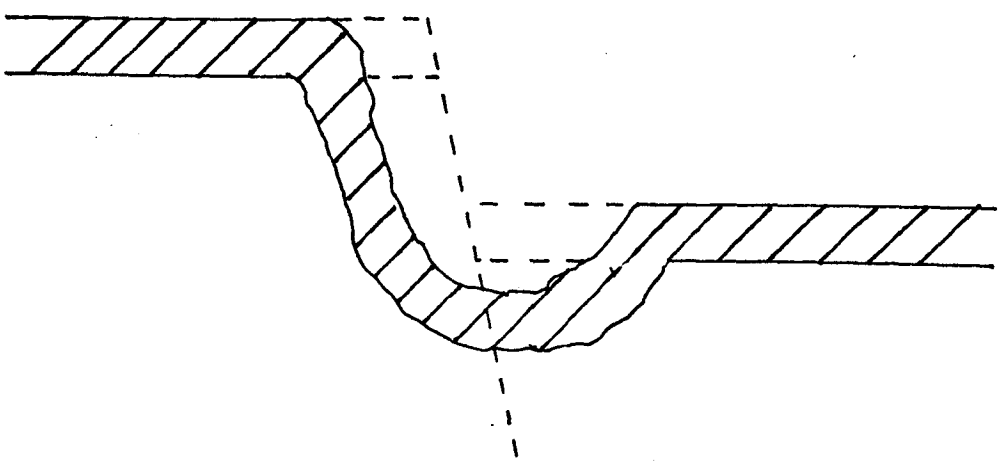

Figure 5.3 Form of the attack which can occur during the repassivation process after a slip step has pierced the passive layer.

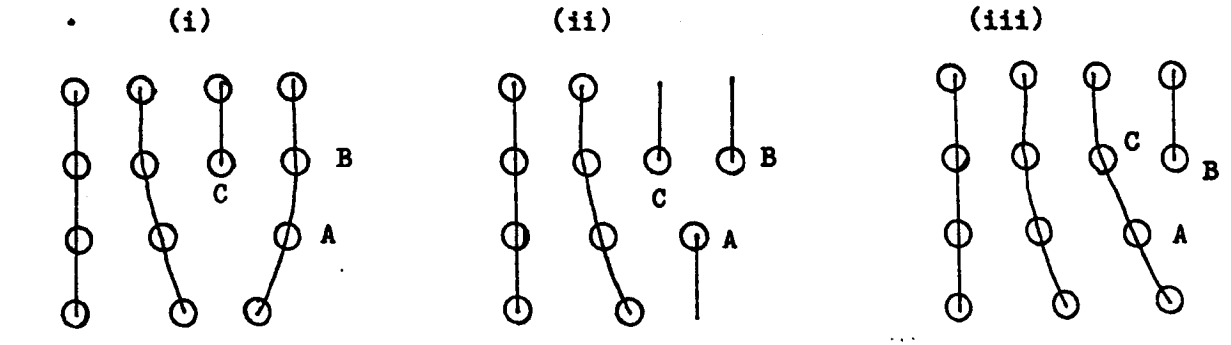

Atomistic model of an edge dislocation approaching the metal surface.

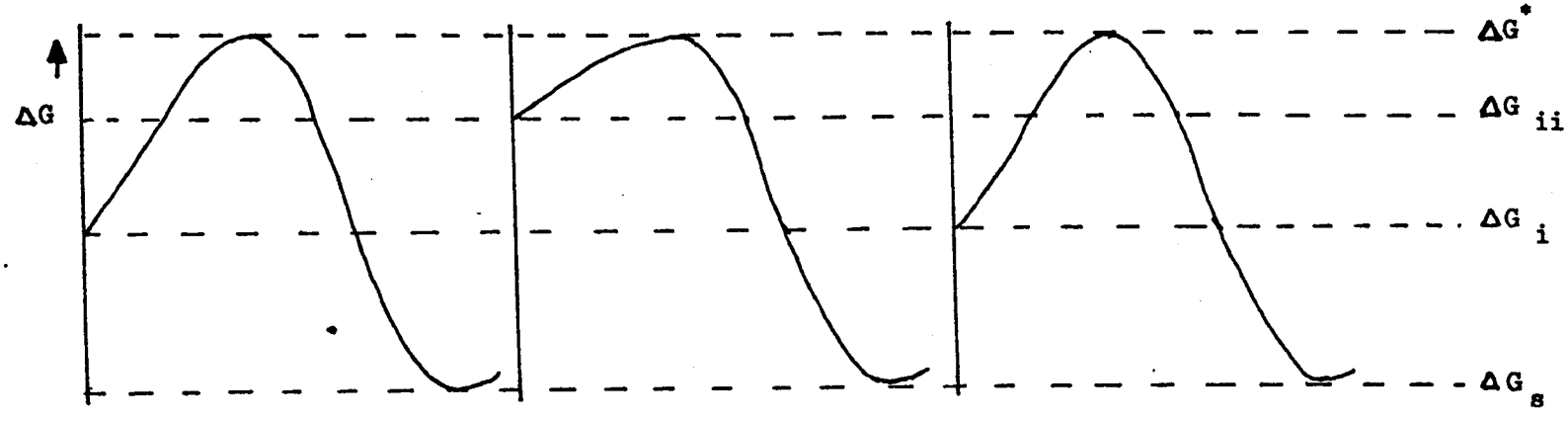

The chemical free energy profile for atom A passing directly into aqueous solution

ΔG_s is the free energy of a solvated metal ion

ΔG^* is the activation energy necessary for the chemical reaction to occur

ΔGi is the free energy of Atom A in position (i) or (iii)

ΔGii is the free energy of Atom A in position (ii)

Figure 5.4 Schematic model of an edge dislocation approaching a metal surface with the subsequent formation of a slip step.

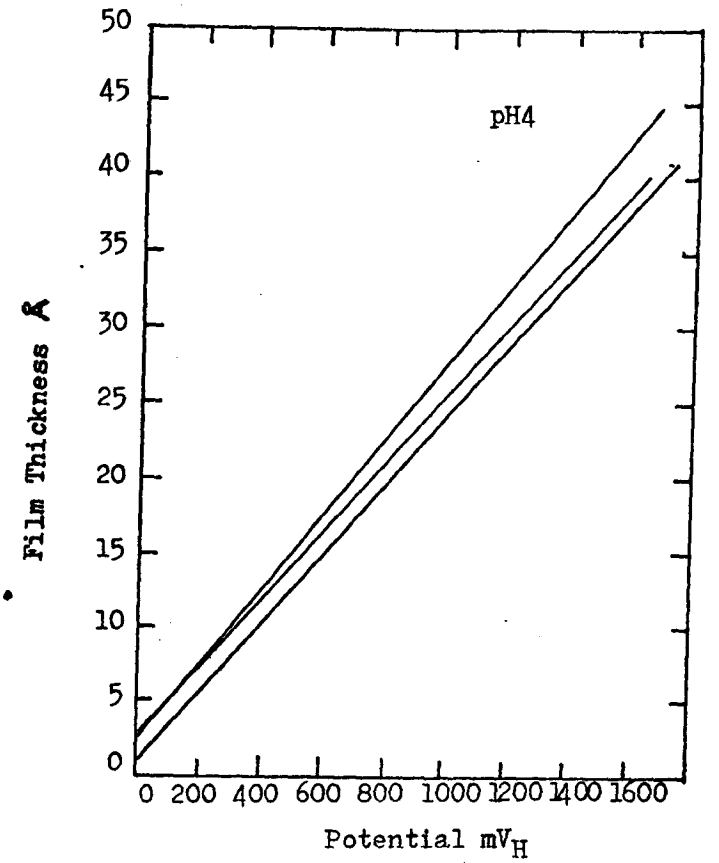

Figure 5.5 Film thickness vs. applied potential for iron base alloys exposed to a sodium sulphate solution at pH 4. Film thickness determined ellipsometrically after one hour exposure.

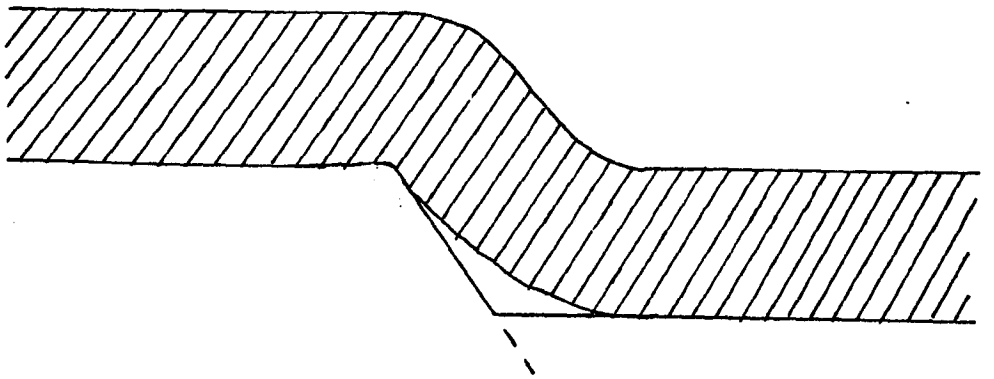

(a) thick passive layer

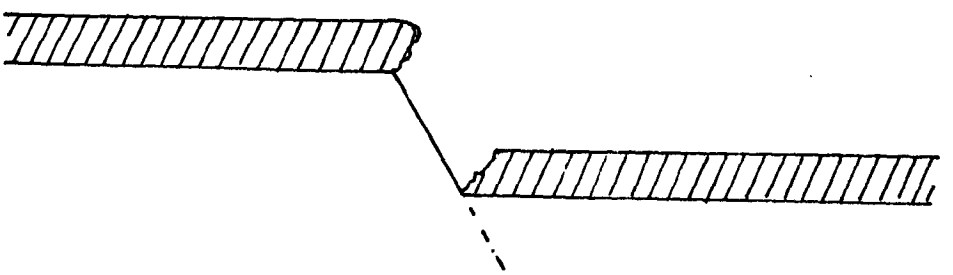

(b) thin passive layer

Figure 5.6 Effect of passive layer thickness on the ability of a slip step to pierce it.

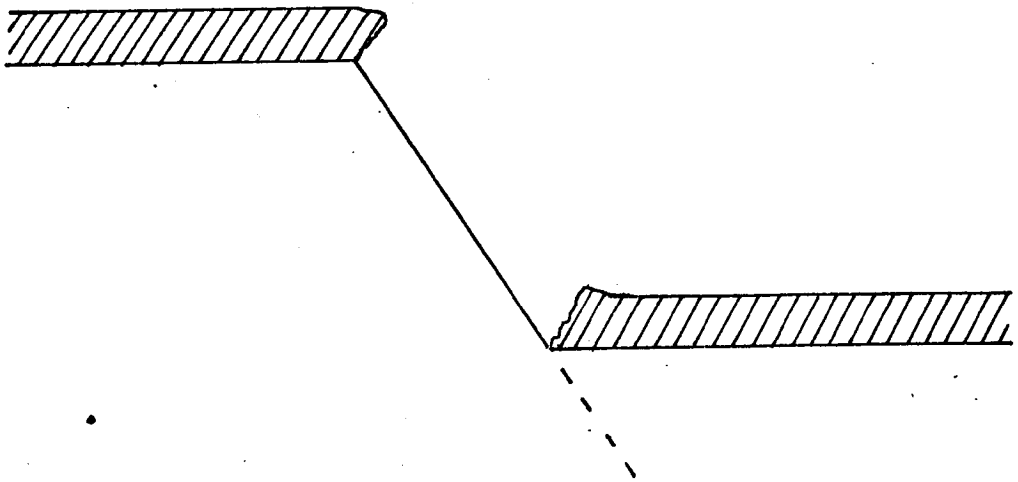

(a) thin passive layer

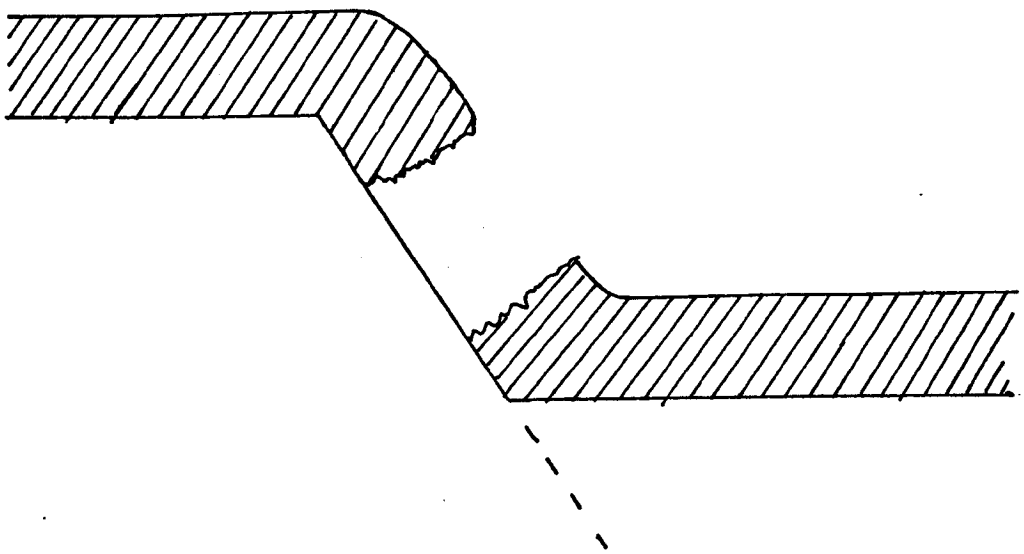

(b) thick passive layer

Figure 5.7 Effect of passive layer thickness on the amount of bare metal exposed by slip steps piercing it.

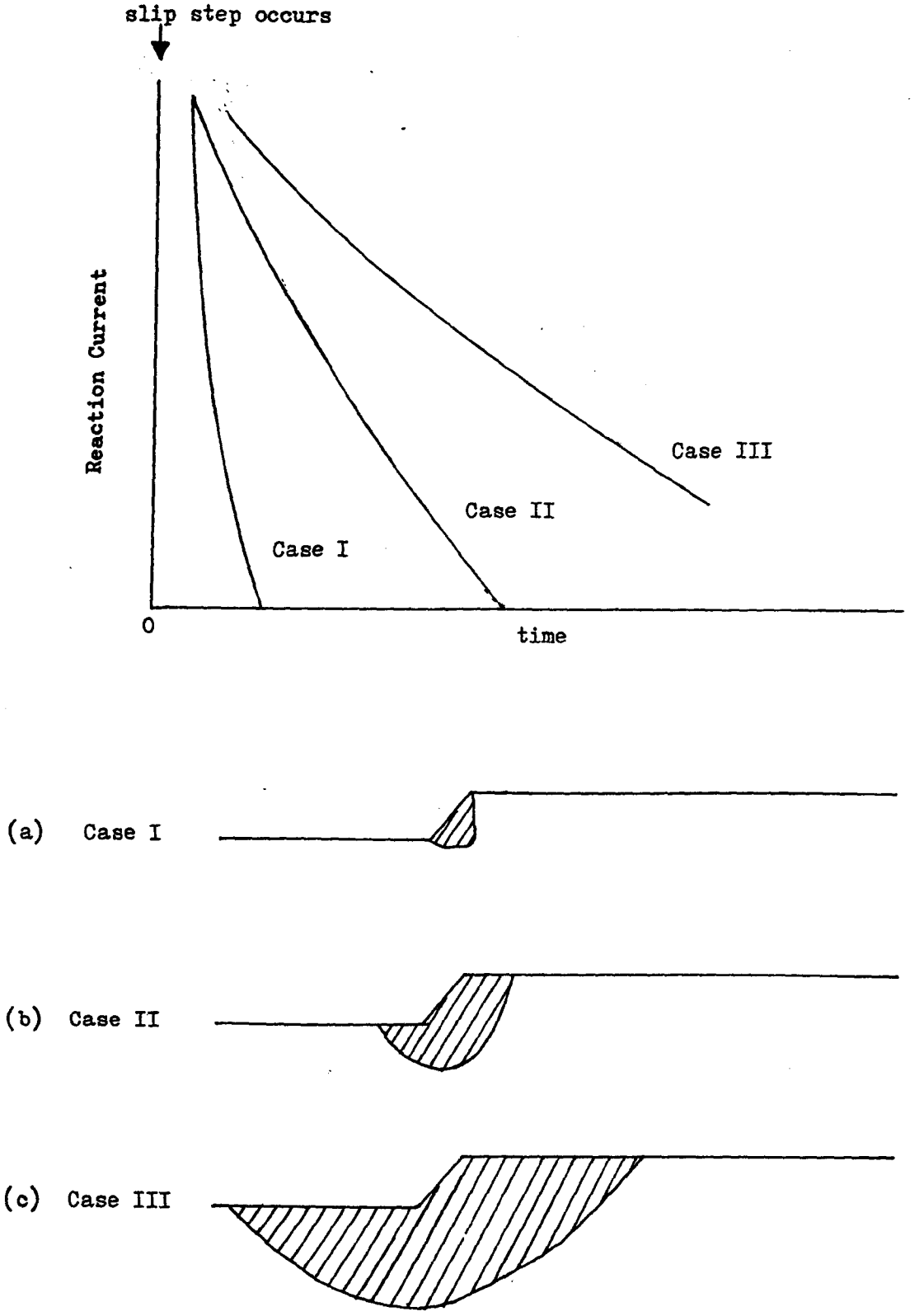

Figure 5.8 Effect of the rate of repassivation on the amount of transient dissolution. Shaded areas on (a) to (c) correspond to the metal dissolved during repassivation.

(From reference 188)

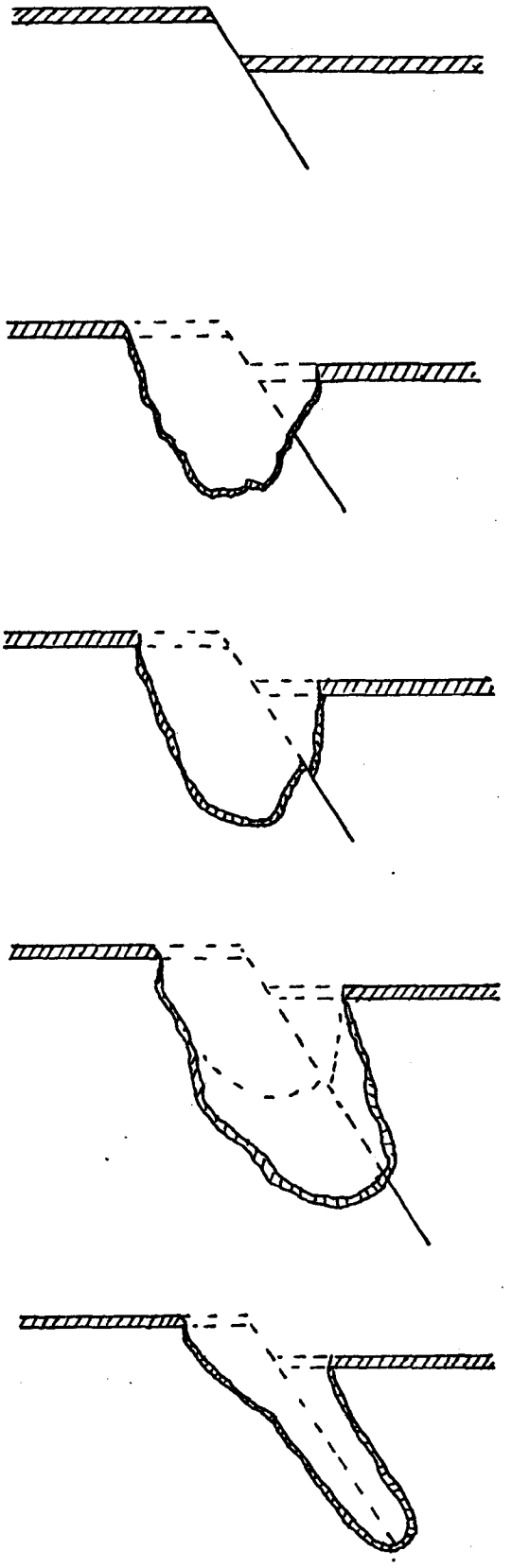

Figure 5.9 Schematic diagrams to show how transient dissolution can propagate deeply into the metal producing a dissolution trench.

Figure A.1 Calibration curve for type AISI 316 stainless steel test-pieces on the reverse-bend fatigue rig